

UNIVERSITY OF SOUTHERN QUEENSLAND



**RICE CROP MONITORING USING NEW GENERATION
SYNTHETIC APERTURE RADAR (SAR) IMAGERY**

A Dissertation submitted by
Nguyen Lam-Dao, *M Eng.*

For the award of
Doctor of Philosophy

2009

To my parents

ABSTRACT

Rice cultivation systems in various countries of the world have been changing in recent years. These changes have been observed in the Mekong River Delta, Vietnam, specifically in An Giang province. The changes in rice cultural practices have impacts on remote sensing methods developed for rice monitoring, in particular, methods using new generation radar data. The objectives of the study were a) to understand the relationship between radar backscatter coefficients and selected parameters (e.g. plant age and biomass) of rice crops over an entire growth cycle, b) to develop algorithms for mapping rice cropping systems, and c) to develop a rice yield prediction model using time-series Envisat (Environmental Satellite) Advanced Synthetic Aperture Radar (ASAR) imagery.

Ground data collection and *in situ* measurement of rice crop parameters were conducted at 35 sampling fields in An Giang province, Mekong River Delta, Vietnam. The average values of the radar backscattering coefficients that corresponded to the sampling fields were extracted from the ASAR *Alternative Polarisation Precision* (APP) images (C band, spatial resolution of 30 m, and swath width of 100 km). The temporal rice backscatter behaviour during the cropping seasons, including *Winter Spring* (WS), *Summer Autumn* (SA), and *Autumn Winter* (AW), were analysed for HH (Horizontal transmit and Horizontal receive), VV (Vertical transmit and Vertical receive), and polarisation ratio data. In addition, the relationships between rice biomass and backscattering coefficient of HH, VV, and polarisation ratio were established.

The methods were examined for rice identification and mapping in the study area by using ASAR APP and Wide Swath (WS) imagery. ASAR APP data were firstly used to determine the best method with high accuracy for rice delineation. Then, the proposed method was applied for ASAR WS data (C band, 150 m spatial resolution, and 450 km swath width), covering the entire agricultural region of the An Giang province. Based on the discovered relationships between rice parameters and radar backscattering, a *thresholding* method applied for polarisation ratio and VV polarisation values of single-date ASAR APP data acquired in the middle of

crop season was found to be the best method among various classification methods. Another threshold, i.e. the “*normalised difference polarisation ratio (NDRa) index*”, where $NDRa = (\sigma_{HH}^0 \text{ in dB} - \sigma_{VV}^0 \text{ in dB}) / (\sigma_{HH}^0 \text{ in dB} + \sigma_{VV}^0 \text{ in dB})$, was formulated in this study for mapping the rice crops using ASAR APP image. The classification accuracy was assessed on the basis of the existing land use data and the published statistical data.

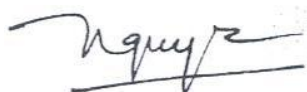
By using multiple regression analysis (rather than using an agrometeorological model found unsuitable for modern rice cultural practices), the correlation between backscattering coefficients of multi-date ASAR APP images acquired during the crop season and the *in situ* measured yield was derived. The distribution maps of estimated rice yield were then produced based on that relationship. Consequently, rice production was finally estimated from these maps.

This study showed that the radar backscattering behaviour was much different from that of the traditional rice reported in previous studies, due to changes brought by modern cultural practices. HH, VV and HH/VV radar values were not significantly related to biomass (maximum $r^2 = 0.494$) due to the effect of water management, plant density and structure. Using the polarisation ratio and VV data of rice fields during a long period of the rice season, the thresholding method based on empirical relationships demonstrated a relatively simple but effective tool to accurately derive the rice/non-rice classes. The results using Envisat ASAR APP data acquired at a single date have provided the highest accuracy (99%) of provincial planted rice areas. To generate map of the rice area planted using three-date or two-date ASAR WS data, the integrated method (based on the temporal variation of the radar response and thresholding) yielded the highest accuracies of 99% and 95%, respectively, at the provincial scale. This study developed a method to generate an accurate map of rice growing area before the end of crop season using single-date ASAR APP image taken in the middle of the rice cropping season. During this period, the difference between the HH and VV values is the highest. On the other hand, the predictive model based on multiple regression analysis between *in situ* measured yield and polarisation ratios attained good results (97% accuracy) and thus proved to be a potential tool for rice yield prediction.

This study concluded that time-series Envisat ASAR imagery can generate accurate maps of rice planted areas. Since radar backscattering coefficients were found uncorrelated with plant biomass in the study area, the use of SAR imagery for agro-meteorological (crop growth) modelling for rice yield prediction will be less reliable. Conversely, the use of statistical modelling (regression approach) was found highly accurate to generate rice production forecasts. Further work is needed to examine and validate the rice mapping algorithm and statistical model-based method for rice yield estimation at other regions in the Mekong River Delta.

CERTIFICATION OF DISSERTATION

I certify that my ideas, experimental work, results, analyses, software and conclusions reported in this dissertation are entirely my own effort, except where otherwise acknowledged. I also certify that the work is original and has not been previously submitted for any other award, except where otherwise acknowledged.



23rd November 2009

Signature of Candidate

Date

ENDORSEMENT



24th November 2009

Signature of Principal Supervisor

Date

PUBLICATIONS PRODUCED FROM THIS DISSERTATION AND OTHER RELATED WORKS

Refereed Journals

1. BOUVET, A., LE-TOAN, T. and LAM-DAO, N., (2009). Monitoring of the rice cropping system in the Mekong delta using Envisat/ASAR dual polarization data. *IEEE Transaction on Geoscience and Remote Sensing*, Vol. 47, No. 2, pp. 517-526.
2. LAM-DAO, N., LE-TOAN, T., BOUVET, A., APAN, A., YOUNG, F., and LE-VAN, T., (2009). Effects of changing rice cultural practices on C-band SAR backscatter using Envisat ASAR data in the Mekong River Delta, *Journal of Applied Remote Sensing*, Vol. 3, Iss. 1.
3. LAM-DAO, N., APAN, A., LE-TOAN, T., BOUVET, A., YOUNG, F., and LE-VAN, T., (under revision). Rice crop monitoring and mapping in the Mekong Delta using Envisat ASAR APP and WS data, *Asian Journal of Geoinformatics*.

Conference Proceedings

1. LAM-DAO, N., APAN, A., YOUNG, F., LE-VAN, T., LE-TOAN, T. and BOUVET, A. (2007). Rice Monitoring Using ENVISAT ASAR Data: Preliminary results of a Case Study in the Mekong River Delta, Vietnam. Proceedings of “*The 28th Asian Conference on Remote Sensing*”, Kuala Lumpur, Malaysia, November 2007 (ISBN 978-983-43550-0-5).
2. LAM-DAO, N., LE-TOAN, T., BOUVET, A., APAN, A., YOUNG, F., and LE-VAN, T., (2008). Effects of changing rice cultural practices on C-band SAR backscatter using ENVISAT ASAR data in the Mekong Delta. Proceedings of the Conference “*GeoInformatics for Spatial-Infrastructure*

Development in Earth and Allied Sciences (GIS-IDEAS)”, Ha Noi, Vietnam, December 2008 (ISBN 978-4-901668-37-8).

3. LAM-DAO, N., APAN, A., LE-TOAN, T., YOUNG, F., LE-VAN, T., and BOUVET, A., (2009). The use of Envisat ASAR APP Data for rice yield estimation – A case study of Mekong River Delta, Vietnam. *8th Annual Asian Conference and Exhibition on Geospatial Information, Technology and Applications*, Singapore, August 2009.
4. LAM-DAO, N., APAN, A., LE-TOAN, T., BOUVET, A., YOUNG, F., and LE-VAN, T., (2009). Rice crop mapping using radar imagery: Comparison of classification accuracy of different Envisat ASAR modes and classifiers. *Spatial Sciences Institute Biennial International Conference*, Adelaide, Australia, September 2009 (**Refereed paper**).
5. LAM-DAO, N., APAN, A., LE-TOAN, T., YOUNG, F., LE-VAN, T., and BOUVET, A., (2009). Towards an Operational System for Rice Crop Inventory in the Mekong River Delta, Vietnam Using Envisat ASAR Data. *7th FIG Regional Conference*, Ha Noi, Vietnam, October 2009.

ACKNOWLEDGEMENTS

First of all, I would like to thank the Vietnamese Government, Ministry of Education and Training of Vietnam (MOET), and the Vietnam Academy of Science and Technology (VAST) for giving me the opportunity to participate in the doctoral research programme.

My research work included monthly field trips in 2007 to measure and collect rice parameters at the sampling fields across the An Giang province in Vietnam. I wish to thank staff and students of the Faculty of Agriculture and Natural Resources, An Giang University for their help with the field work.

I thank the European Space Agency (ESA) for providing the Envisat ASAR satellite data I used in this study.

I would like to express my gratitude to my Principal Supervisor, Associate Professor Armando Apan, for his valuable advice and guidance during the four years of my study. I also appreciate the support of my Associate Supervisors: Associate Professor Frank Young (USQ) and Associate Professor Trung Le-Van of the HoChiMinh City University of Technology (HCMUT), Vietnam National University - HoChiMinh City (VNU-HCM).

I would like to thank Dr. Thuy Le-Toan for her enthusiasm and worthy advice, and her colleagues (particularly Alexandre Bouvet), for giving me a friendly environment during my three-month research period at the *Centre d'Etudes Spatiales de la Biosphère* (CESBIO), Toulouse, France.

I wish to thank all the lecturers and staff of the Faculty of Engineering and Surveying, USQ, and the Department of Geomatics, HCMUT, for their academic and administrative assistance. I thank my colleagues at the GIS and Remote Sensing Research Center, HoChiMinh City Institute of Resources Geography, VAST, for their support in GIS data preparation and field work.

Last but not the least, my sincere thanks to my parents, Ly Lam-Minh and Nhut Duong-Thi, my wife Hue-Nhan, and sons Dat, Minh and Nghia, for their continuing support and patience during this period. Thank you for their encouragement and believing in me, which helped me to pursue my research study towards the end.

TABLE OF CONTENTS

ABSTRACT.....	iv
CERTIFICATION OF DISSERTATION.....	vii
PUBLICATIONS PRODUCED FROM THIS DISSERTATION.....	viii
ACKNOWLEDGEMENTS.....	x
LIST OF FIGURES.....	xv
LIST OF TABLES.....	xx
LIST OF ABBREVIATIONS.....	xxiii
Chapter 1 INTRODUCTION.....	1
1.1 Introduction.....	1
1.2 Statement of the Problem.....	2
1.3 Research Objectives.....	3
1.4 Significance of the Study.....	4
1.5 Conceptual Framework.....	5
1.6 Thesis Outline.....	5
Chapter 2 LITERATURE REVIEW.....	7
2.1 Physics of Radar Backscattering.....	7
2.1.1 Frequency.....	9
2.1.2 Polarisation.....	10
2.1.3 Incidence angle.....	11
2.1.4 Surface roughness characteristics.....	12
2.1.5 Electrical characteristics and moisture content.....	13
2.1.6 Target interaction.....	15
2.2 Radar Image Properties.....	16
2.2.1 Spatial resolution.....	16
2.2.2 Speckle.....	18
2.2.3 Radar image distortions.....	19
2.3 Vegetation Response to Microwave Energy.....	20
2.3.1 Scattering mechanism for vegetation.....	20
2.3.2 Penetration depth and frequency.....	22

2.3.3 Radar backscatter and biomass	22
2.4 Rice Crop Monitoring	24
2.4.1 Rice crop discrimination and monitoring.....	24
2.4.2 Rice yield prediction models.....	29
2.5 Summary	31
Chapter 3 METHODS.....	32
3.1 Overview	32
3.2 Study Area.....	33
3.3 Description of Rice Growing and Rice Cropping Systems.....	39
3.3.1 Rice growing stages	39
3.3.2 Rice cropping systems in the Mekong River Delta.....	42
3.4 Data Acquisition	43
3.4.1 Imagery used	43
3.4.2 Ground truth and survey data.....	51
3.4.3 Climatic data and maps	55
3.4.4 Data processing software	56
Chapter 4 ANALYSIS OF RADAR BACKSCATTER OF RICE	
FIELDS	58
4.1 Introduction	58
4.2 Methods.....	60
4.3 Results and discussion	62
4.3.1 Rice parameters.....	62
4.3.2 Analysis of temporal radar backscatter as a function of rice parameters..	67
4.3.3 Effect of plant structure and rice varieties	74
4.3.4 Radar backscatter and rice biomass	76
4.4 Conclusion	79
Chapter 5 RICE MAPPING	81
5.1 Introduction.....	81
5.2 Methods.....	82
5.2.1 ASAR APP image classification.....	84

5.2.2 ASAR WS image classification	93
5.3 Results and discussion	94
5.3.1 Rice mapping from ASAR APP data	94
5.3.2 Rice mapping using ASAR WS data	107
5.4 Conclusion	125
Chapter 6 RICE YIELD ESTIMATION	128
6.1 Introduction	128
6.2 Methods	131
6.2.1 Statistical model-based method	131
6.3 Results and discussion	135
6.3.1. Regression analysis between rice biomass and yield	135
6.3.2. Regression analysis between HH, VV, HH/VV and sample rice yield .	136
6.3.3 Distribution map of estimated rice yield	141
6.4 Conclusion	150
Chapter 7 CONCLUSIONS	152
7.1 Summary of Findings	152
7.1.1 Analysis of rice backscatter	152
7.1.2 Rice mapping	153
7.1.3 Yield estimation	154
7.2 Conclusions	155
7.3 Recommendations	157
REFERENCES	159
APPENDICES	164
A. ASAR APP images used	164
B. Backscattering coefficient and yield of sampling fields, and their regression models	172
B.1 A case of Summer Autumn 2007 crop	172
B.2 A case of Winter Summer 2007 crop	174

LIST OF FIGURES

Figure 1.1 Conceptual framework used in this study	5
Figure 2.1. An example of active sensor	8
Figure 2.2. The microwave portion of the electromagnetic spectrum	9
Figure 2.3. Horizontal and vertical polarisation	11
Figure 2.4. Incidence angle (left) and local incidence angle (right)	12
Figure 2.5. The effect of surface roughness on radar backscatter	13
Figure 2.6. Irrigation / soil moisture influences	14
Figure 2.7. Volume scattering, surface scattering, and corner reflection	15
Figure 2.8. Slant range and ground range plane	17
Figure 2.9. Azimuth resolution	18
Figure 2.10. Example of speckle in a radar image	19
Figure 3.1. Overview of methods for the study	32
Figure 3.2. Equipment of row seeding	34
Figure 3.3. A technology for water saving in rice production	35
Figure 3.4. The An Giang province: Location of the frame of ENVISAT ASAR APP scene on the study site (a) and Administrative boundary map of An Giang province, with locations (red dots) of the sampling areas (b)	36
Figure 3.5. An example of rice field in the study area	38
Figure 3.6. Field trip on the Mekong River	38
Figure 3.7. Rice growing stages (crop cycle length of 120 days)	39
Figure 3.8. Photographs of rice growing stages	40
Figure 3.9. ASAR antenna	44
Figure 3.10. Envisat sensor coverage	45
Figure 3.11. Colour composite ASAR APP image acquired on 13 Jan. 2007 (R=HH, G=VV, B=HH), provincial boundary in yellow polyline	46
Figure 3.12. Colour composite ASAR APP image acquired on 17 Feb. 2007 (R=HH, G=VV, B=HH), provincial boundary in yellow polyline	47
Figure 3.13. Colour composite ASAR APP image acquired on 24 Mar. 2007	48

(R=HH, G=VV, B=HH), provincial boundary in yellow polyline	
Figure 3.14. Colour composite ASAR WS image (R=5 Dec. 06, G=20 Feb. 07, B=24 Apr. 07), provincial boundary in yellow polyline	50
Figure 3.15. Colour composite ASAR WS image (R=1 May 07, G=5 Jun. 07, B=23 Aug. 07), provincial boundary in yellow polyline	51
Figure 3.16. Photographs of drying the rice plant	55
Figure 3.17. Land use map in 2005 of An Giang province (rice in yellow colour)	56
Figure 4.1. Temporal variation of σ^0 by plant age (a), height (b), and biomass (c)	59
Figure 4.2. Methods for the analysis of radar backscatter of rice fields	60
Figure 4.3. Percentage of rice varieties grown in WS, SA, and AW 2007 crops of the sampling fields	63
Figure 4.4. Temporal variation of plant height (a) and biomass (b)	64
Figure 4.5. Average plant density of sampling fields at the middle of the WS, SA, AW crop seasons and of traditional practiced rice fields	65
Figure 4.6. Temporal variation of plant height (a) and biomass (b) in SA crop of Jasmine and IR 50404	66
Figure 4.7. An example of field samples a week after sowing (no-water, very wet soil with surface roughness)	67
Figure 4.8. Field sample with standing water at about 20-day after sowing	68
Figure 4.9. Backscatter temporal variation of HH (a) and VV (b) in WS, SA and AW 2007 crops of the fields with water and without water	70
Figure 4.10. Temporal variation of HH/VV ratio in WS, SA and AW 2007 crops of the fields with water and without water	71
Figure 4.11. Backscatter temporal variation of HH (a), VV (b), and HH/VV ratio (c) of the traditional practiced rice fields	73
Figure 4.12. Temporal variation of HH/VV ratio of Jasmine (a) and IR 50404 varieties (b) in WS, SA and AW 2007 crops	74
Figure 4.13. Sampling fields with plants in quasi-vertical structure (a) and lodging (b) at the end of SA crop	75
Figure 4.14. Radar backscattering of Radarsat and ERS data vs. plant wet	76

biomass in traditional practiced rice	
Figure 4.15. Radar backscattering of HH (a) and VV (b) vs. plant wet biomass in WS, SA and AW 2007 crops	77
Figure 4.16. Polarisation ratio vs. plant wet biomass in WS, SA and AW 2007 crops	78
Figure 4.17. Polarisation ratio vs. plant wet biomass in traditional practiced rice	79
Figure 5.1. Methods for rice mapping	83
Figure 5.2. Polarisation ratio HH/VV and normalised difference ratio index (NDRa) of the sampling rice planted in WS (a), SA (b), AW 2007 (c), and WS 2008 crops (d) extracted from the images taken in the mid-season	86
Figure 5.3. Backscattering coefficients of HH and VV data of sampling fields in WS (a), SA (b), AW 2007 (c), and WS 2008 crops (d)	89
Figure 5.4. Rice and non-rice maps (rice in green) of WS (a), SA (b), AW 2007 (c), and WS 2008 crops (d)	105
Figure 5.5. Rice cropping system map of An Giang province in 2007	106
Figure 5.6. A colour composite MODIS image (Red=band 7, Green= band 2, and Blue= band 1) acquired on 9 October 2007	107
Figure 5.7. Backscatter temporal variation of the land use samples from ASAR WS ascending mode data collected during the period of Jan. - Aug. 2007	109
Figure 5.8. Backscatter temporal variation of the rice samples from ASAR WS ascending mode data in WS and SA 2007 crops	110
Figure 5.9. Rice and non-rice map (rice in green) of WS 2007 crop produced by using three-date ASAR WS images taken in ascending mode	111
Figure 5.10. ASAR WS colour composite image (Red=May image, Green=June image, and Blue=July image) of the Mekong River Delta (District boundaries of An Giang province in blue polylines)	113
Figure 5.11. Rice and non-rice maps (rice in green) of SA 2007 crop produced by using three-date (a) and two-date (b) ASAR WS image taken in ascending mode	114

Figure 5.12. Backscatter temporal variation of the rice samples from ASAR WS descending mode data in WS and SA 2007 crops	116
Figure 5.13. Rice and non-rice maps (rice in green) of WS 2007 crop produced by using three-date (a) and two-date (b) ASAR WS image taken in descending mode	118
Figure 5.14. Rice and non-rice maps (rice in green) of SA 2007 crop produced by using three-date (a) and two-date (b) ASAR WS image taken in descending mode	120
Figure 5.15. Backscatter temporal variations of the rice samples from ASAR WS ascending and descending mode data in WS and SA 2007 crops	122
Figure 5.16. Rice and non-rice map (rice in green) of WS (a) and SA 2007 (b) crop produced by using two-date ASAR WS image taken in ascending and descending modes	124
Figure 6.1. Agro-meteorological model of rice yield prediction	129
Figure 6.2. Methods used for rice yield estimation	131
Figure 6.3. Statistical model of rice yield prediction	132
Figure 6.4. A distribution map of estimated rice yield in SA 2007 crop at Cho Moi district using three-date polarisation ratio and LINEST regression analysis	143
Figure 6.5. A distribution map of estimated rice yield of SA crop in Cho Moi district using three-date polarisation ratio and LOGEST regression analysis	145
Figure 6.6. A distribution map of estimated rice yield of WS crop in Cho Moi district using three-date polarisation ratio and LINEST regression analysis	147
Figure A.1. Colour composite ASAR APP image acquired on 28 Apr. 2007 (R=HH, G=VV, B=HH), provincial boundary in yellow polyline	164
Figure A.2. Colour composite ASAR APP image acquired on 02 Jun. 2007 (R=HH, G=VV, B=HH), provincial boundary in yellow polyline	165
Figure A.3. Colour composite ASAR APP image acquired on 07 Jul. 2007 (R=HH, G=VV, B=HH), provincial boundary in yellow polyline	166

Figure A.4. Colour composite ASAR APP image acquired on 15 Sep. 2007 (R=HH, G=VV, B=HH), provincial boundary in yellow polyline	167
Figure A.5. Colour composite ASAR APP image acquired on 20 Oct. 2007 (R=HH, G=VV, B=HH), provincial boundary in yellow polyline	168
Figure A.6. Colour composite ASAR APP image acquired on 24 Nov. 2007 (R=HH, G=VV, B=HH), provincial boundary in yellow polyline	169
Figure A.7. Colour composite ASAR APP image acquired on 29 Dec. 2007 (R=HH, G=VV, B=HH), provincial boundary in yellow polyline	170
Figure A.8. Colour composite ASAR APP image acquired on 02 Feb. 2008 (R=HH, G=VV, B=HH), provincial boundary in yellow polyline	171

LIST OF TABLES

Table 3.1. Area, population and population density by district of An Giang province in 2007	37
Table 3.2. Main rice-based cropping systems in the Mekong River Delta	42
Table 3.3. Main rice seasons in An Giang, Mekong River Delta	43
Table 3.4. Technical summary of Envisat sensors ASAR and MERIS	44
Table 3.5. List of Envisat ASAR APP data used	45
Table 3.6. List of Envisat ASAR WS data used	49
Table 3.7. Size and area of sampling fields	52
Table 3.8. List of rice parameters collected from this study	53
Table 3.9. Rice crop calendar in 2007	54
Table 4.1 Effect of water on radar backscattering at early stage in WS 2007 crop	68
Table 5.1. Percentage errors between planted rice acreage of An Giang province in WS, SA, AW 2007 and WS 2008 crops produced by ASAR data and statistical data using various threshold combinations	95
Table 5.2. Percentage errors between planted rice acreage produced by ASAR APP data using different classifiers and statistical data	96
Table 5.3. Percentage errors between planted rice acreage in WS 2007 crop produced by ASAR APP data and statistical data	98
Table 5.4. Percentage errors between planted rice acreage in SA 2007 crop produced by ASAR APP data and statistical data	99
Table 5.5. Percentage errors between planted rice acreage in AW 2007 crop produced by ASAR APP data and statistical data	100
Table 5.6. Percentage errors between planted rice acreage in WS 2008 crop produced by ASAR APP data and statistical data	100
Table 5.7. A confusion matrix of rice/non-rice map in WS 2007 crop	101
Table 5.8. A confusion matrix of rice/non-rice map in SA 2007 crop	102
Table 5.9. A confusion matrix of rice/non-rice map in WS 2008 crop	102
Table 5.10. Backscattering coefficients of land use samples extracted from	108

ASAR WS ascending mode data	
Table 5.11. Backscattering coefficients of rice samples extracted from ASAR WS ascending mode data	109
Table 5.12. Percentage errors between planted rice acreage in WS crop produced by ASAR WS data acquired on 16 Jan., 20 Feb., and 1 May 2007 and statistical data	112
Table 5.13. Percentage errors between planted rice acreage in SA crop produced by ASAR WS data acquired on 1 May, 5 Jun. and 10 Jul. 2007 and statistical data	115
Table 5.14. Backscattering coefficients of rice samples extracted from ASAR WS descending mode data	116
Table 5.15. Percentage errors between planted rice acreage in WS 2007 crop produced by ASAR WS data acquired on 5 Dec. 2006, 13 Feb. and 1 Mar. 2007 and statistical data	119
Table 5.16. Percentage errors between planted rice acreage in SA crop produced by ASAR WS data acquired on 24 Apr., 14 Jun., and 7 Aug. 2007 and statistical data	121
Table 5.17. Percentage errors between planted rice acreage in WS crop produced by ASAR WS data acquired on 5 Dec. 2006, and 20 Feb. 2007 and statistical data	123
Table 5.18. Percentage errors between planted rice acreage in SA crop produced by ASAR WS data acquired on 5 Apr., and 5 Jun. 2007 and statistical data	123
Table 6.1. Correlation between sample rice yield and dry biomass in WS 2007 crop	135
Table 6.2. Correlation between sample rice yield and dry biomass in SA 2007 crop (n=10)	136
Table 6.3. Correlation between sample rice yield and HH, VV, HH/VV by village in SA 2007 crop using LINEST function (n=5)	137
Table 6.4. Correlation between sample rice yield and HH, VV, HH/VV by district in SA 2007 crop using LINEST function (n=10)	138
Table 6.5. Correlation between sample rice yield and HH, VV, HH/VV by	138

district in SA 2007 crop using LOGEST function (n=10)	
Table 6.6. Correlation between sample rice yield and HH, VV, HH/VV by village in WS 2007 crop using LINEST function (n=5)	140
Table 6.7. Correlation between sample rice yield and HH, VV, HH/VV by district in WS 2007 crop using LINEST function (n=9)	140
Table 6.8. Yield estimation for SA crop in Cho Moi district using three-date polarisation ratio and LINEST regression analysis	142
Table 6.9. Percentage error between rice production in SA 2007 crop at Cho Moi district derived from three-date polarisation ratio data using LINEST function and statistical data	143
Table 6.10. Yield estimation for SA 2007 crop at Cho Moi district using three-date polarisation ratio and LOGEST regression analysis	144
Table 6.11. Percentage error between rice production in SA 2007 crop at Cho Moi district derived from three-date polarisation ratio data using LOGEST function and statistical data	145
Table 6.12. Yield estimation for WS 2007 crop at Cho Moi district using three-date polarisation ratio and LINEST regression analysis	146
Table 6.13. Percentage error between rice production in WS 2007 crop at Cho Moi district derived from three-date polarisation ratio data using LINEST function and statistical data	147
Table 6.14. Yield estimation for SA crop in Thoai Son district using three-date polarisation ratio and LINEST regression analysis	148
Table 6.15. Percentage error between rice production in SA 2007 crop at Thoai Son district derived from three-date polarisation ratio data using LINEST function and statistical data	149
Table 6.16. Difference between ground data and statistical data	150

LIST OF ABBREVIATIONS

AGDARD	Department of Agriculture and Rural Development of An Giang province
AGSO	Statistical Office of An Giang province
ALOS	Advanced Land Observing Satellite
ASAR	Advanced Synthetic Aperture Radar
ASAR APP	Advanced Synthetic Aperture Radar Alternative Polarisation Precision
ASAR WS	Advanced Synthetic Aperture Radar Wide Swath
AW	Autumn Winter (crop)
CCRS	Canada Centre for Remote Sensing
dB	Decibel
DGPS	Differential Global Positioning System
Envisat	Environmental Satellite
ERS	European Remote Sensing Satellite
ESA	European Space Agency
FAO	Food and Agriculture Organization
GIS	Geographic Information System
GPS	Global Positioning System
GSO	General Statistics Office of Vietnam
HH	horizontal transmit and horizontal receive
HV	horizontal transmit and vertical receive
IS	Image Swath
JERS	Japanese Earth Resources Satellite
LAI	Leaf Area Index
MODIS	Moderate Resolution Imaging Spectroradiometer
NOAA/AVHRR	National Oceanic and Atmospheric Administration/ Advanced Very High Resolution Radiometer
PALSAR	Phased Array type L-band Synthetic Aperture Radar
PCA	Principle Component Analysis
RADAR	Radio Detection And Ranging
RISAT	Radar Imaging Satellite

SA	Summer Autumn (crop)
SAM	Spectral angle mapping
SAR	Synthetic Aperture Radar
SPOT	Systeme Probatoire d'Observation de la Terre
VH	vertical transmit and horizontal receive
VV	vertical transmit and vertical receive
WS	Winter Summer (crop)

Chapter 1

INTRODUCTION

1.1 Introduction

Rice (*Oryza sativa*) is one of the world's major agricultural crops and is the staple food for more than half of the world population. In Asia, more than 2,000 million people obtain 60 to 70 percent of their calories from rice and its products (FAO, 2004). Food security has become a key global issue due to the Asian region's rapid population growth, extensive conversion of arable lands, and declining overall productivity in some areas because of climate effects (floods, water shortage, low or high temperature) and plant diseases. To maintain a close balance between rice production and food demand, effective rice monitoring programs are necessary at regional, national and global levels. In particular, there is a need to develop spatio-temporal monitoring system that can accurately assess rice cultivated area, crop vigour and health, and can predict crop yield.

In the past years, many research projects on rice crop monitoring have been carried out using remote sensing data (e.g. Le-Toan et al., 1989, Aschbacher et al., 1995). Among them, space-borne *Synthetic Aperture Radar* (SAR) data was used as main data source. Since the 1990s, a new era of wide-scale availability of radar imagery data has emerged, particularly those collected from earth observation satellites, such as ERS-1 and 2, JERS-1, and Radarsat-1 (e.g. Kurosu et al., 1995, Liew et al., 1998, Rosenqvist, 1999). This trend continued into the new century with the most advanced satellite radar systems launched as Envisat in 2002, ALOS in 2006, Radarsat-2 and TerraSAR in 2007, and RISAT-2 in 2009 (e.g. Stankiewicz, 2006).

More sophisticated radar remote sensing systems are scheduled for deployment in the near future, for example Sentinel-1. Thus, the field of space-borne radar

remote sensing continues to provide technological advances, an expanding range of data sources, and new opportunities for research on rice monitoring.

1.2 Statement of the Problem

As new investments in irrigation, flood control and drainage management infrastructure are being developed, the rice cropping systems in many parts of the world have been undergoing rapid changes in recent years. Traditionally, estimates of rice planting area and productivity are based on ground survey data. While ground collection of data has some merits, it is often time-consuming and expensive. In addition, the information collected is often imprecise and unreliable, leading to inaccurate crop yield forecasts and subsequent difficulties for agriculture planners and managers in both regional and national scales.

Earth observation from space allows regular and timely monitoring of rice cultivated areas and can provide accurate information about the status of rice growth. Hence, the use of satellite remote sensing data acquired at the appropriate time can be expected to help in producing synoptic rice field maps and predicting crop yield. Optical remote sensing satellites that have high revisit capability, such as NOAA/AVHRR, SPOT/Vegetation or TERRA and AQUA/MODIS, may be considered for such purpose (e.g. Sakamoto et al., 2006, Xiao et al., 2006). However, their spatial resolutions are regarded as too coarse for accurate estimation of crop growth and extent.

On the other hand, the moderate resolution Landsat and SPOT satellites could also be considered (e.g. Oguro et al., 2001). Still, their temporal resolutions (repeat cycle) have significant limitation for rice monitoring in the tropical and sub-tropical regions. Additionally, a large part of rice crop growing cycle coincides with rainy season, resulting in only a limited number of cloud-free images being possible. Weather independent systems utilising medium resolution microwave sensor such as synthetic aperture radar are therefore potentially best suited for rice field mapping and yield estimation in the tropical and sub-tropical areas.

Past studies using SAR data acquired from the ERS-1 and 2 and Radarsat-1 satellites focused on the use of temporal variation of the backscattering coefficient at single polarisation for rice mapping and monitoring (e.g. Le-Toan et al., 1997, Takeuchi et al., 1999, Holecz et al., 2000, Lam-Dao et al., 2005). With the launch of Envisat and ALOS, the use of *multi-dimensional* (multi-polarised, multi-incidence angle and multi-date) radar imagery is expected to offer new capabilities for monitoring rice crops (e.g. Choudhury et al., 2007). Therefore, pioneering studies are needed to assess these new generation SAR imagery.

1.3 Research Objectives

One of the primary advantages of microwave remote sensing is its low dependence on atmospheric conditions and therefore is best suited for monitoring rice crop in the tropical and sub-tropical regions. In addition, previous results on mapping rice cropping systems and predicting the crop yield using old generation SAR data were demonstrated to have some limitations. Therefore, the goal of the study was to evaluate the use of new generation SAR data in monitoring the growth and yield of rice crops. The specific objectives of the research were:

- to establish correlations between radar backscatter coefficients and selected parameters (e.g. plant age and biomass) of rice crops over an entire growth cycle;
- to develop algorithms for mapping and monitoring rice cropping systems for one year cycle using time-series SAR imagery; and
- to develop a rice yield prediction model over various cropping systems using new generation SAR imagery.

This study has the following hypotheses:

- Backscatter coefficients from the new generation SAR data will produce high correlations with selected rice plant parameters (e.g. plant age, biomass, etc.).

- New algorithms or image processing techniques of time-series radar data can be developed to accurately (>70%) map and monitor rice cropping systems.
- A functional rice yield prediction model, over various cropping systems, can be developed using new generation SAR imagery.

1.4 Significance of the Study

Previous research studies on rice monitoring were carried out using different kinds of SAR data (e.g. ERS-SAR, Radarsat, JERS-SAR, and Envisat-ASAR) in different geographical sites particularly in tropical and temperate regions (e.g. Aschbacher et al., 1995, Bakar et al., 1997, Le-Toan et al., 1997, Frei et al., 1999, Panigrahy et al., 1999, Li et al., 2004, Lam-Dao et al., 2005, Liew et al., 1998). Most of these were conducted to understand the temporal change of backscattering coefficient, interpret the theoretical model, define the classification method, retrieve the rice parameters, and estimate the rice yield. Among them, the research study conducted by Liew et al. (1998) reported the use of ERS-SAR images in delineating and mapping areas under different rice cropping systems using two methods, namely, human visual inspection and semi-automatic hierarchical clustering algorithm.

The new generation SAR instruments, such as the Advanced Synthetic Aperture Radar (ASAR) on Envisat and Phased Array type L-band Synthetic Aperture Radar (PALSAR) on ALOS, have important new capabilities that may provide better results for mapping and monitoring rice crops. These include beam steering for acquiring images with different incidence angles, dual polarization, and wide swath coverage (ESA, 2007). The mapping of rice cropping systems and crop yield estimation from data acquired by these relatively new SAR instruments have been rarely reported in the scientific literature. This present study attempts to contribute to developing SAR-based monitoring system for rice crops.

1.5 Conceptual Framework

This study was anchored on the premise (as supported by literature in Chapter 2) that radar backscatter coefficients and selected rice parameters are correlated. Consequently, innovative techniques can be developed to map and monitor rice plant and rice cropping systems, including the prediction of yield, using new generation radar imagery.

From Envisat ASAR dual polarisation data and *in situ* rice data, the relationships between radar backscatter coefficients and rice parameters (e.g. plant age and biomass) of crop over an entire growth cycle were established. This constitutes the “analysis of rice backscatter” component. Based on these relationships, the rice mapping method (“rice cropping system mapping”) was developed. Yield estimation model (“rice yield prediction”) was examined for rice cultivated areas and then rice production was computed based on rice growing acreage and predicted yield (Figure 1.1).

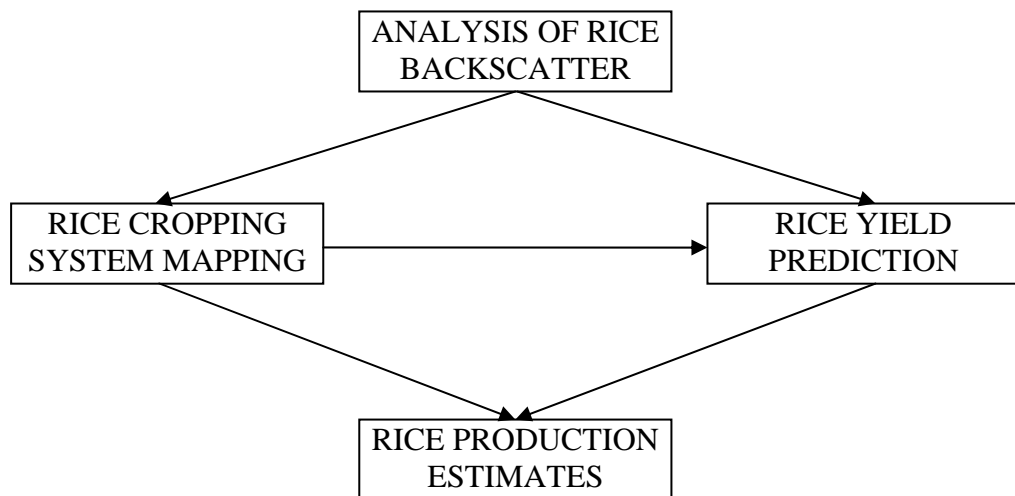


Figure 1.1 Conceptual framework used in this study.

1.6 Thesis Outline

Chapter 1 highlights the need to develop a spatio-temporal rice monitoring system using radar remote sensing. The goal and specific objectives, research hypotheses, and significance of the study are addressed. To achieve the above goal,

chapter 2 reviews the physics of radar backscattering, properties of radar imagery, vegetation response to microwave energy, and the results of previous research studies on rice crop monitoring using radar remotely sensed data. This highlights the knowledge gaps, as well as the potential contribution of this dissertation. In chapter 3, the selection of the study area, description of rice growing and rice cropping system, data acquisition are discussed.

As mentioned in the first objective, radar backscatter of rice fields is analysed in chapter 4. This includes image pre-processing techniques, the analysis of rice parameters, effects of plant structure, rice varieties and water management in the field, and the relationship between radar backscatter and rice biomass. Chapter 5 presents the methods and results of rice mapping (second objective). ASAR APP and ASAR WS data analysis for rice mapping using thresholding algorithms were developed. Classification accuracies assessed from various classifiers was compared.

The agro-meteorological model-based and statistical model-based methods are addressed in chapter 6. The multiple regression analysis between *in situ* measured yield and backscattering coefficients derived from time-series ASAR APP data was discussed. The distribution maps of rice yield estimated from these relationships were demonstrated. The production of rice area was then estimated (third objective). Finally, the findings of the research and further recommendations are summarised in chapter 7.

Chapter 2

LITERATURE REVIEW

This chapter reviews the existing theory and the results of the previous studies in relation with the research topic. The physics of radar backscattering, image properties and radar response of vegetation are introduced to give the background information. The research problems are discussed on the basis of the previous investigations into rice crop monitoring using radar imagery. This chapter highlights the knowledge gaps related to the study, as well as the potential contribution of this work.

2.1 Physics of Radar Backscattering

The microwave portion of the electromagnetic spectrum commonly used for remote sensing of land surfaces covers the range from approximately 1 cm to 1 m in wavelength. Because of their long wavelengths (compared to the visible and infrared regions), microwaves have the following special properties that are important for remote sensing (FAO/ESA, 1993):

- small dependence on atmospheric conditions,
- control of the emitted (for active remote sensing) and received electromagnetic radiation: power, frequency, polarisation,
- ability to choose an incidence angle and an azimuth angle to meet the objectives of the study, and
- possibility to obtain information on subsurface features, when low soil density and moisture permit.

These are the primary advantages of radar remote sensing. Moreover, it is also important to understand that radar and optical data can be complementary to one another as they offer different perspectives of the earth's surface providing different information content.

The sensor transmits a microwave signal towards the target and detects the backscattered portion of the signal (Figure 2.1). The power scattered back toward the radar antenna is represented by the *radar equation* (2.1) (Henderson and Lewis, 1998):

$$P_R = P_T (\sigma^0 A) \left(\frac{G^2 \lambda^2}{(4\pi)^3 R^4} \right) \quad (2.1)$$

where

P_R : the power received,

P_T : the power transmitted toward the target,

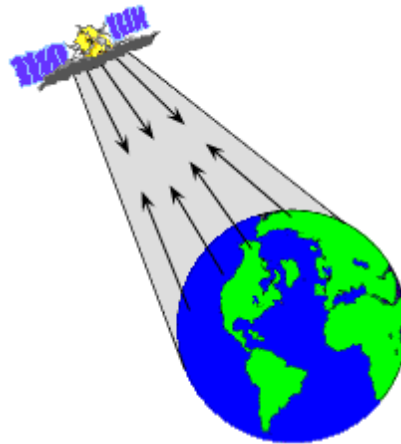
G : the gain of the antenna,

R : the range distance from the transmitter to the target,

σ^0 : the radar scattering coefficient,

λ : the wavelength of the radar system,

A : an area on the ground.



Source: CCRS (2007a)

Figure 2.1. An example of active sensor.

The *radar backscattering coefficient* determines the percentage of electromagnetic energy reflected back to the radar from within a resolution cell. It depends on (FAO/ESA, 1993):

- radar observation parameters (frequency, polarisation and incidence angle of the electromagnetic waves emitted);

- terrain parameters (surface roughness, geometric shape and dielectric properties of the target).

2.1.1 Frequency

There are several wavelength ranges or frequency bands (Figure 2.2) commonly used in radar remote sensing (Henderson and Lewis, 1998):

- Ka (0.75 - 1.18 cm), K (1.18 - 1.67 cm), Ku (1.67 - 2.40 cm) bands;
- X-band (2.40 - 3.75 cm);
- C-band (3.75 - 7.5 cm): used on many space-borne systems (ERS-1 and 2, ASAR onboard Envisat, and Radarsat);
- S-band (7.5 - 15 cm);
- L-band (15 - 30 cm): used onboard Japanese JERS-1, ALOS (PALSAR) satellites;
- P-band (77 - 136 cm).

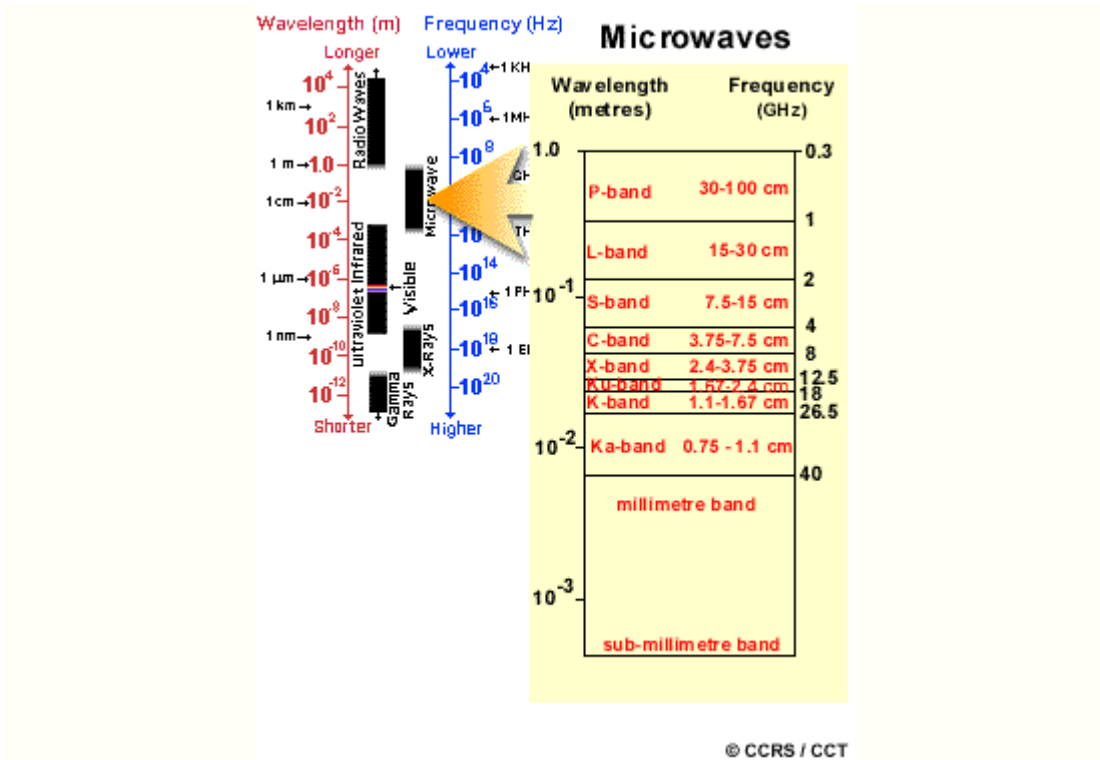


Figure 2.2. The microwave portion of the electromagnetic spectrum.

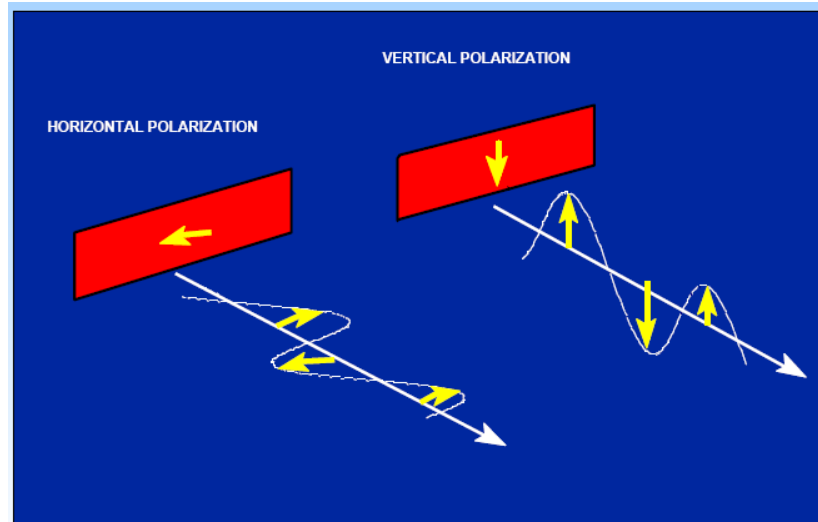
The frequency of the incident radiation determines what would be the major *scattering mechanism*; it has an impact on the penetration depth and the scales of roughness of the surfaces. The penetration depth tends to be longer with longer wavelengths and is also related to the moisture content of the target. For this study, Envisat ASAR data acquired in C-band frequency, i.e. 5.6 cm, was used. This frequency band is considered more appropriate for rice crop monitoring (Huadong et al., 2006).

2.1.2 Polarisation

Polarisation refers to the orientation of the electric field. Most radars are designed to transmit microwave radiation either horizontally polarised (H) or vertically polarised (V). Similarly, the antenna receives either the horizontally or vertically polarised backscattered energy, while some radars can receive both (Figure 2.3). These two polarisation states are designated by the letters H for horizontal, and V for vertical. Thus, there can be the four combinations of both transmit and receive polarisations as follows.

- HH - for horizontal transmit and horizontal receive,
- VV - for vertical transmit and vertical receive,
- HV - for horizontal transmit and vertical receive, and
- VH - for vertical transmit and horizontal receive.

The first two polarisation combinations are referred to as like-polarised because the transmit and receive polarisations are the same. The last two combinations are referred to as cross-polarised because the transmit and receive polarisations are orthogonal of one another.



Source: CCRS (2002)

Figure 2.3. Horizontal and vertical polarisation.

In certain cases, polarisation can provide information on different layers of the target, for example flooded vegetation. The penetration depth of the radar wave varies with the polarisation chosen. Polarisation may provide information on the form and the orientation of small scattering elements that compose the surface or target.

The ERS and Radarsat-1 sensors provide radar images with one specific polarisation, i.e. VV and HH, respectively. On the other hand, the new Envisat-ASAR system includes image acquisitions with *dual polarisation* (HH/VV, HH/HV, and VV/VH), which can open up new possibilities in land observations. This research study used HH and VV polarisation imagery of ASAR as a main data source for rice monitoring in the Mekong River Delta.

2.1.3 Incidence angle

Incidence angle (Figure 2.4) is the angle between the direction of the incident radiation and the perpendicular to the imaged surface, which increases across the swath from near to far range. For most natural targets, backscatter coefficient varies with the incidence angle (FAO/ESA, 1993).

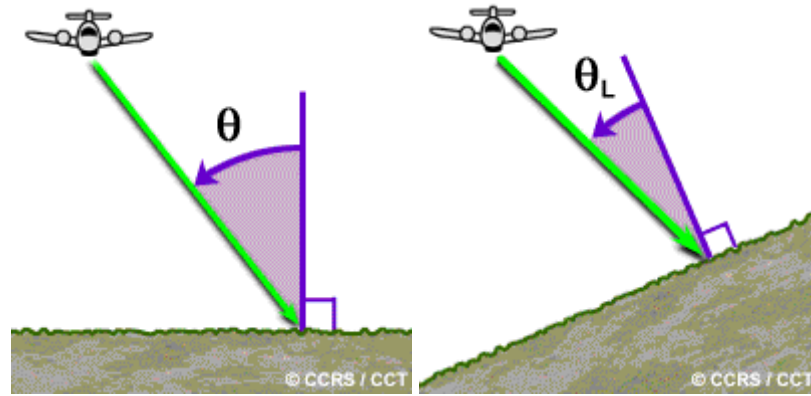


Figure 2.4. Incidence angle (left) and local incidence angle (right).

In relation to surface geometry and its effect on target interaction and image appearance, the *local incidence angle* is a more appropriate and relevant concept. The local incidence angle (Figure 2.4) is the angle between the radar beam and a line perpendicular to the slope of the imaged surface at the point of incidence. Thus, local incidence angle takes into account the local slope of the terrain in relation to the radar beam. With flat terrain, the local incidence angle is the same as the look angle of the radar. For terrain with any type of relief, this is not the case. Generally, slopes facing towards the radar will have small local incidence angles, causing relatively strong backscattering to the sensor, which results in a bright-toned appearance in an image.

ERS-SAR system operates with the incidence angle of 23° at the mid swath. The new capability of Envisat-ASAR includes beam steering for acquiring images in one of the seven swaths with different incidence angles spanning 15° to 45° . In this study, ASAR AP data with IS2 incidence angle (19.2° - 26.7°) and ASAR WS imagery with incidence angle range from 15° to 37° were utilised.

2.1.4 Surface roughness characteristics

The effect of *surface roughness* on radar backscatter (Figure 2.5) depends on wavelength and look angle. According to the Rayleigh criterion, a surface is (Henderson and Lewis, 1998):

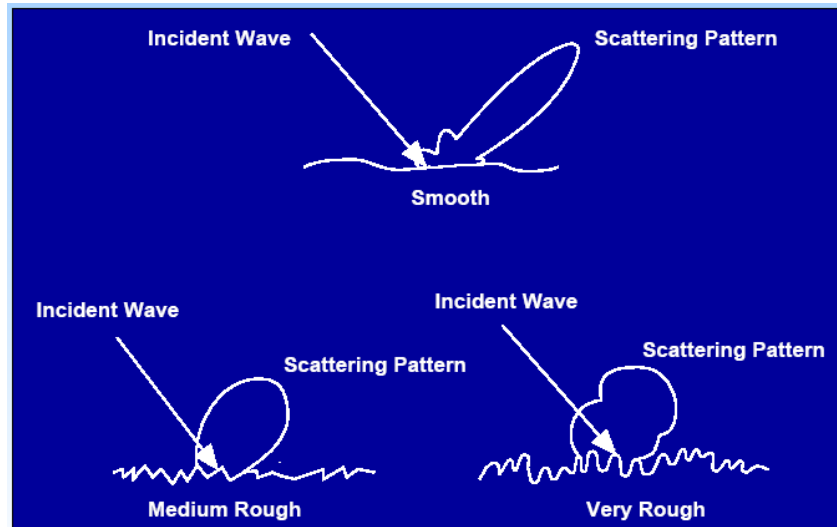
- rough if:
$$h_{rms} > \frac{\lambda}{8 \cos \phi} \quad (2.2)$$

where

h_{rms} : average height variations

λ : radar wavelength

ϕ : look angle (is defined as the angle between the vertical of the antenna to the ground and the transmitted ray at the point of incidence (Henderson and Lewis, 1998)).



Source: CCRS (2002)

Figure 2.5. The effect of surface roughness on radar backscatter.

An example of the effect of surface roughness can be observed in the zones of contact between land and water. In the absence of wind, inland water bodies tend to be relatively smooth with most energy being reflected away from the radar and only slight backscatter towards the radar. On the contrary, surrounding land surfaces tend to have a higher roughness and greater backscatter.

2.1.5 Electrical characteristics and moisture content

The complex *dielectric constant* is a measure of the electric properties of surface materials. It consists of two parts (permittivity and conductivity) that are both highly dependent on the moisture content of the material considered (FAO/ESA, 1993). At C-band, most natural materials have a permittivity around 3 to 8 in the dry condition. Water has a high permittivity of approximately 80, at least 10

times higher than for dry soil. As a result, a change in moisture content generally provokes a significant change in the electric properties of natural materials. The electromagnetic wave penetration in an object is an inverse function of water content. Increasing moisture is associated with an increased radar reflectivity and hence the advantage of using radar for determining moisture content (Figure 2.6).

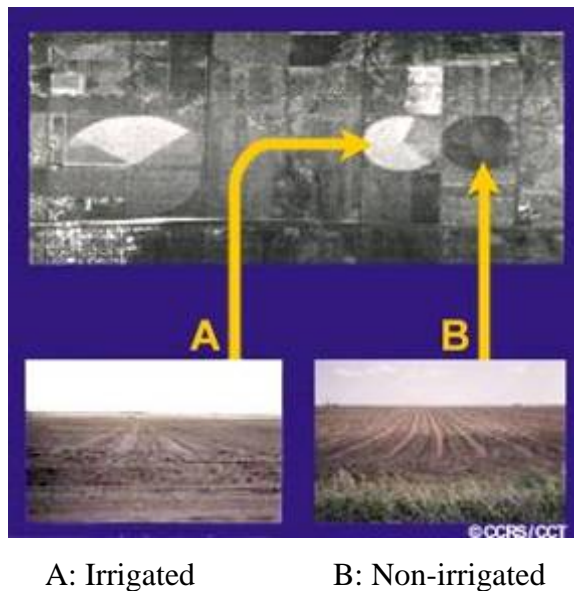


Figure 2.6. Irrigation / soil moisture influences.

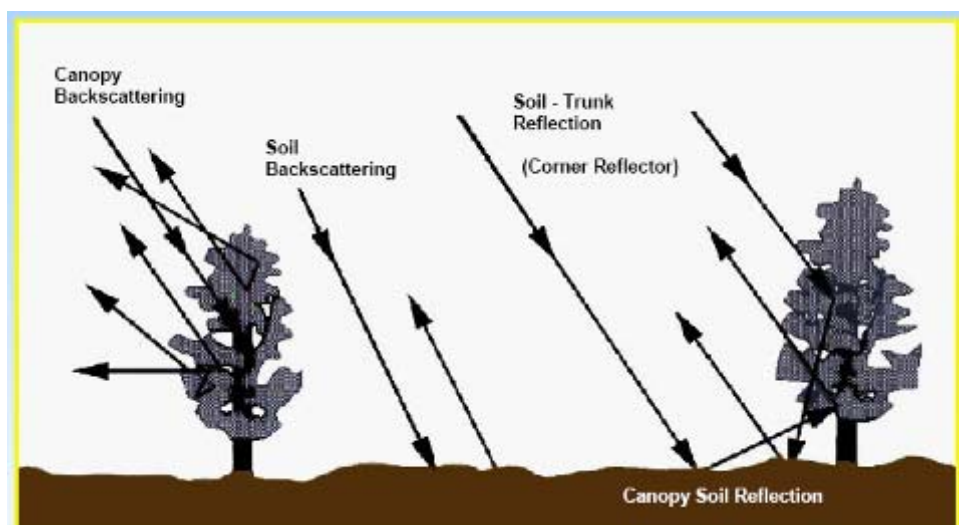
Changes in the electrical properties influence the absorption, transmission, and reflection of microwave energy. Thus, the moisture content will influence how targets and surfaces reflect energy from radar and how they will appear on an image.

Moist soils reflect more radar energy than dry soils, which absorb more of the radar wave, depending on the dielectric constant of the soil material. Radar images may be used to estimate bare ground soil moisture content when the terrain is devoid of most other material such as plants and rocks and has uniform surface roughness. If the soil has a high surface soil moisture content, then the incident energy will only penetrate a few centimetres into the soil and be scattered more at the surface producing a stronger, brighter return. In the specific case of vegetation, penetration depth into a canopy depends on moisture, density and geometric structure of the plants (leaves and branches). In this current study, an analysis on the effects of the surface roughness and soil moisture of rice fields for radar response at the beginning of crop cycle was discussed in chapter 4.

2.1.6 Target interaction

The look direction or aspect angle of the radar describes the orientation of the transmitted radar beam relative to the direction or alignment of linear features on the surface. The look direction can significantly influence the appearance of features on a radar image, particularly when ground features are organised in a linear structure (such as agricultural crops). Look direction is important for enhancing the contrast between features in an image. By acquiring imagery from different look directions, it may be possible to enhance identification of features with different orientations relative to the radar (CCRS, 2007a).

Features, which have two or more surfaces (usually smooth) at right angles to one another, may cause *corner reflections* (Figure 2.7) to occur if the 'corner' faces the general direction of the radar antenna. The orientation of the surfaces at right angles causes most of the radar energy to be reflected directly back to the antenna due to the double bounce reflection. Corner reflectors with complex angular shapes are common in urban environments (e.g. buildings and streets, bridges, other man-made structures). Naturally occurring corner reflectors may include upright vegetation standing in water, e.g. rice plants in this research study. In all cases, corner reflectors show up as very bright targets in an image (CCRS, 2007a).



Source: CCRS (2002)

Figure 2.7. Volume scattering, surface scattering, and corner reflection.

When a surface is moist or wet, scattering from the topmost portion (*surface scattering*) is the dominant process taking place (Figure 2.7). The type of reflection (ranging from specular to diffuse) and the magnitude will depend on how rough the material appears to the radar. If the target is very dry (in terms of “free water”) and the surface appears smooth to the radar, the radar energy may be able to penetrate below. For a given surface, longer wavelengths are able to penetrate further than shorter wavelengths (CCRS, 2007a).

If the radar energy does manage to penetrate through the topmost surface, then *volume scattering* may occur (Figure 2.7). Volume scattering is the scattering of radar energy within a volume or medium, and usually consists of multiple bounces and reflections from different components within the volume. For example, in a forest, scattering may come from the leaf canopy at the tops of the trees, the leaves and branches further below, and the tree trunks and soil at the ground level. Volume scattering may serve to decrease or increase image brightness, depending on how much of the energy is scattered out of the volume and back to the radar (CCRS, 2007a).

Scattering mechanism in the case of rice crop during its growth cycle includes all of corner reflection, surface scattering, and volume scattering as described above.

2.2 Radar Image Properties

2.2.1 Spatial resolution

To determine the spatial resolution at any point in a radar image, it is necessary to compute the resolution in two dimensions: the range and azimuth resolution.

Range resolution

The *range resolution* (in the across-track direction) is proportional to the length of the microwave pulse. The shorter the pulse length, the finer the range

resolution. The equation for computing the ground range (Figure 2.8) resolution G_r is (Henderson and Lewis, 1998):

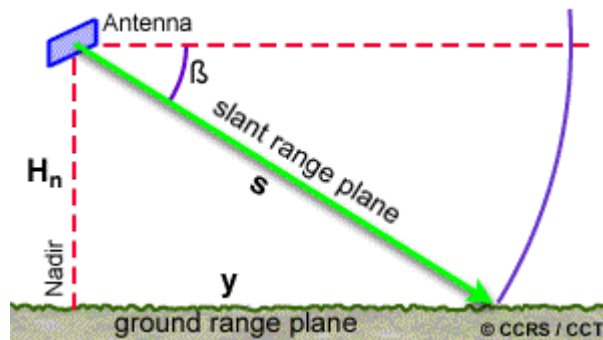
$$G_r = \frac{c\tau}{2\sin\phi} \quad (2.3)$$

with

c : speed of light

τ : pulse length

ϕ : look angle



H_n = flying height β = depression angle

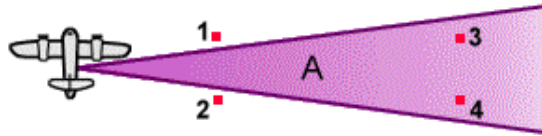
Figure 2.8. Slant range and ground range plane.

Azimuth resolution

The equation for the optimal *azimuth or along-track resolution* A_s (Figure 2.9) for a point target in a synthetic aperture radar is (Henderson and Lewis, 1998):

$$A_s = \frac{l}{2} \quad (2.4)$$

where l is antenna length.



► Resolution in the flight or azimuth direction

- A = antenna beam
- 1, 2, = two targets that can be resolved as being separate
- 3, 4, = two targets that cannot be resolved as being separate

Source: CCRS, (2007b)

Figure 2.9. Azimuth resolution.

The coherent nature of the SAR signal produces *speckle* in the image. To remove the speckle, the image is usually processed using several looks, i.e. an averaging takes place. This improves the interpretability of the SAR image data. However, the azimuth resolution must be adjusted by the equation (Henderson and Lewis, 1998):

$$A_s = (N) \frac{l}{2} \quad (2.5)$$

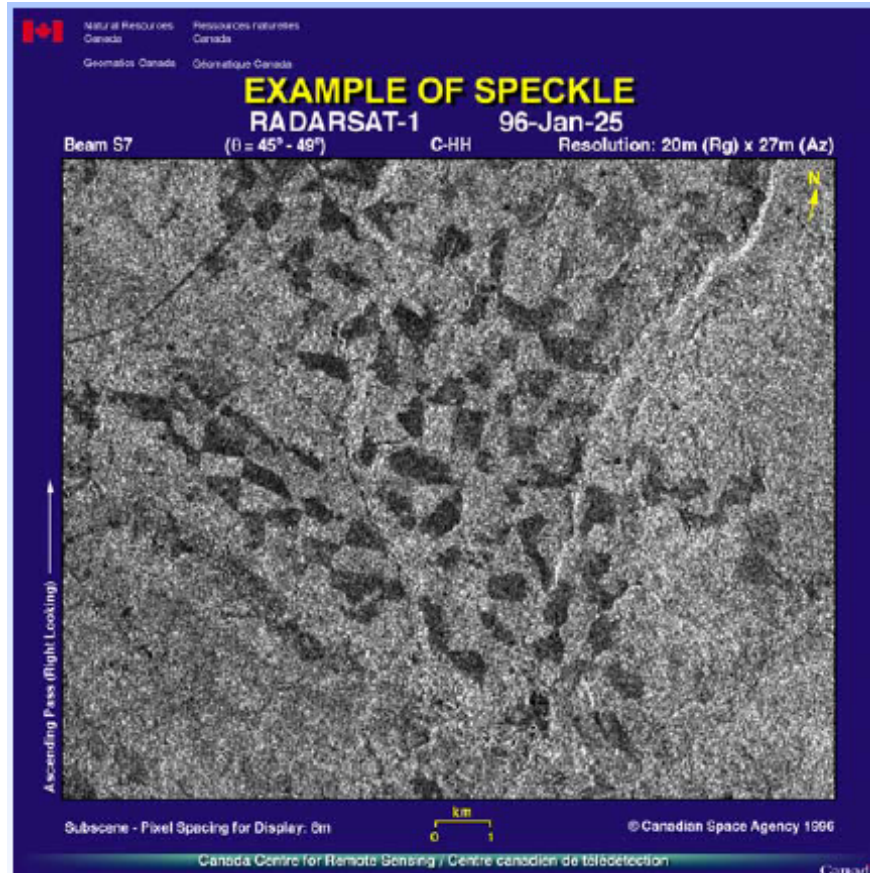
where N is number of looks.

The ASAR AP and WS mode data with 30m and 150m spatial resolution, respectively, were collected for this research study. The investigation on these imagery for rice monitoring, mapping and yield estimation was conducted to meet the research goal.

2.2.2 Speckle

All radar images appear with some degree of what is termed radar speckle, a grainy “salt and pepper” texture in an image (Figure 2.10). This is caused by random constructive and destructive interference from the multiple scattering returns that will occur within each resolution cell. Speckle degrades the quality of an image and may make interpretation (visual or digital) more difficult. Thus, it is generally desirable to reduce speckle prior to interpretation and analysis by either multi-look

processing or filtering techniques. While multi-looking processing is usually done before the delivery of the data product, speckle reduction by temporal and spatial filtering is performed on the output image in a digital image analysis environment.



Source: CCRS (2002)

Figure 2.10. Example of speckle in a radar image.

2.2.3 Radar image distortions

Geometric distortions, such as *foreshortening*, *layover*, and *shadowing*, exist in almost all radar imagery. In radar relief displacement, the horizontal displacement of an object in the image caused by the object's elevation is in a direction towards the radar antenna. Because the radar image is formed in the range direction, the higher the object, the closer it is to the radar antenna, and therefore the sooner (in time) it is detected on the radar image. The elevation-induced distortions in the radar imagery are referred to as foreshortening and layover. Radar shadow occurs when the radar beam is not able to illuminate the ground surface (CCRS, 2007a). Some

processing techniques exist that can partly correct or minimise these effects. Whereas, in this study area, rice crop are mainly cultivated in the flat plain of An Giang province. Therefore, geometric distortions of this area on radar imagery did not exist.

2.3 Vegetation Response to Microwave Energy

Synthetic aperture radar imagery may provide some of the following vegetation biophysical parameters (Jensen, 2007):

- canopy water content,
- vegetation type,
- biomass by component (foliage, higher-order stems and main stem),
- canopy structure (including green leaf area index), leaf orientation, main stem (trunk) geometry and spatial distribution, stem, branch size, and angle distributions.

Any plant canopy (forest, agriculture, grassland, etc.) may be thought of as a seasonally dynamic three-dimensional water-bearing structure consisting of the foliage components (leaves) and woody components (stem, trunk, stalks, and branches). Active microwave energy can penetrate the canopy to varying depths depending upon the frequency, polarisation, and incidence angle of the radar system. It is useful to identify the relationship between the canopy components and how they influence the radar backscattering (Jensen, 2007).

2.3.1 Scattering mechanism for vegetation

For wetlands containing shrubs and trees there are three distinct layers to consider: a) a canopy layer that consists of small branches and foliage (leaves); b) a trunk layer that consists of large branches and trunks or boles; and c) a surface layer, that may or may not be covered by water if wetland is present. The backscattering coefficient σ_w^0 of a woody vegetation canopy towards the radar system can be expressed as (Jensen, 2007):

$$\sigma_w^0 = \sigma_c^0 + \tau_c^2 \tau_t^2 (\sigma_m^0 + \sigma_t^0 \sigma_s^0 + \sigma_d^0) \quad (2.6)$$

where

σ_c^0 : the backscatter coefficient of the canopy layer of smaller woody

branches and foliage (i.e., surface scattering),

τ_c : the transmission coefficient of the vegetation canopy,

τ_t : the transmission coefficient of the trunk layer,

σ_m^0 : the multiple-path scattering between the ground and canopy layer,

σ_t^0 : direct scattering from the tree trunks,

σ_s^0 : direct surface backscatter from the ground,

σ_d^0 : the double-bounce scattering between the trunks and the ground.

By eliminating all terms associated with the trunk layer, it is possible to determine the total radar backscattering coefficient from terrain with non-woody, herbaceous vegetation, σ_h^0 (Jensen, 2007):

$$\sigma_h^0 = \sigma_c^0 + \tau_c^2 (\sigma_m^0 + \sigma_s^0) \quad (2.7)$$

The terms in equations are dependent on: a) the type of vegetation present as well as the roughness of the ground surface; b) the wavelength and polarisation of the incident microwave energy; c) the dielectric constant of the vegetation; and d) the dielectric constant of the ground surface. Live vegetation, with a higher water content has a higher dielectric constant than drier or dead vegetation. The presence of dew or moisture acts to increase the dielectric constant of vegetated surfaces.

The condition of the ground layer is also very important in microwave scattering from vegetated surfaces. There are two properties of this layer that are important: a) the micro- and meso-scale surface roughness (relative to the radar wavelength); and b) the soil moisture (dielectric constant). In general, a greater surface roughness increases the amount of microwave energy backscattered (σ_s^0) and decreases the amount of energy scattered in the forward direction (σ_m^0 and σ_d^0). The reflection coefficient is dependent on the dielectric constant of the ground layer. Given a constant surface roughness, as the soil dielectric constant increases, so does

both amount of backscattered and forward scattered microwave energy (resulting in increases in σ_m^0 , σ_s^0 , and σ_d^0).

If there is a layer of water over the ground surface of a vegetated landscape such as in rice paddy fields of this study, two things can happen: a) it eliminates any surface roughness; and b) it increases the reflection coefficient. In terms of microwave scattering, the elimination of any surface roughness means that all the energy is forward scattered, eliminating the surface backscattering (σ_s^0), and the increased forward scattering and higher reflection coefficient lead to significant increases in the ground-trunk (σ_d^0) and ground-canopy interaction (σ_m^0).

2.3.2 Penetration depth and frequency

The longer the microwave wavelength, the greater the penetration into the plant canopy. Surface scattering takes place at the top of the canopy as the energy interacts with the leaves and stems. Volume scattering by the leaves, stems, branches and trunk takes place throughout the stand, and surface scattering can occur at the soil surface. The shorter wavelength X-band energy is more attenuated by the top of the canopy (by foliage and small branches). The C-band energy experiences scattering at the top of the canopy as well as some volume scattering in the heart of the stand. Little energy reaches the ground. L-band microwave energy penetrates farther into the canopy, where volume scattering among the leaves, stems, branches, and trunk cause the beam to become depolarised. Also, some energy may be transmitted to the ground, where surface scattering from the soil-vegetation boundary layer may take place. Longer wavelength P-band radar would afford the greatest penetration through the vegetation and mainly reflect off large stems and the soil surface (Jensen, 2007).

2.3.3 Radar backscatter and biomass

Radar backscatter increases with increasing biomass until it saturates at a biomass level that depends on the radar frequency. In the case of forest, generally, backscatter at lower frequencies (P- and L-band) is dominated by scattering

processes involving the major woody biomass components (trunks and branches), while scattering at high frequencies (C- and X-band) is dominated by scattering processes in the top crown layer of branches and foliage. Radar canopy measurements have also been found to be correlated with leaf-area-index (LAI) measurements. Some general observations about SAR vegetation interpretation include (Jensen, 2007):

- vertically polarised energy is highly attenuated by the vertically oriented canopy components (leaves, stems, branches, and trunk) such as rice plants in this research while horizontally polarised energy is not;
- the brighter the return on like-polarised radar images (HH or VV) in comparison to (HV), the greater the contribution from surface scattering.
- the brighter the return on cross-polarised radar images (HV or VH), the greater the contribution from volume (internal canopy) scattering;
- when the radar wavelength is approximately the same size as the canopy components (C- or X-band), substantial canopy surface and volume scattering will take place and little energy may reach the ground. Consequently, shorter wavelength radars (2 – 6 cm) may be preferred when monitoring crop canopies and tree leaves. Longer wavelength radars (9 – 30 cm) exhibit substantial volume scattering as incident energy interacts with larger trunk and branch components. Considerable surface scattering from the underlying soil may also occur which can cause confusion;
- cross-polarised images (HV or VH) are less sensitive to slope variations. This suggests vegetation monitoring in mountainous areas may best be performed using cross-polarisation techniques. Also, the same row crop planted in different directions can produce like-polarised images that are difficult to interpret. This ambiguity may be reduced when cross-polarised images are available in addition to like-polarised images;
- the more moisture in the vegetation canopies, the greater the dielectric constant and the higher the radar backscatter return. Active microwave remote sensing is capable of sensing canopy (or leaf) water content in certain instances;

- radar imagery can provide some information on landscape-ecology patch size and canopy gaps that are of value when monitoring ecosystem fragmentation and health.

2.4 Rice Crop Monitoring

2.4.1 Rice crop discrimination and monitoring

Several studies have been carried out on rice mapping and rice monitoring since the launch of the first European remote sensing satellite (ERS-1) in 1991, driven by earlier successes of using airborne SAR (Le-Toan et al., 1989) and ground-based scatterometer data. These studies covered sites in Indonesia (Le-Toan et al., 1997, Ribbes and Le-Toan, 1999a), Japan (Kurosu et al., 1995, Le-Toan et al., 1997, Ogawa et al., 1998), Vietnam (Liew et al., 1998, Kajalainen et al., 2000, Lam-Dao et al., 2005), China (Li et al., 2003, Ling et al., 2005, Quegan et al., 2005, Bingbai et al., 2005), Sri Lanka (Frei et al., 1999), India (Choudhury and Chakraborty, 2006), Philippines (Chen and McNairn, 2006), and other countries. These studies reported results, most of them based on C-band (frequency = 5.3 GHz, wavelength = 5.6 cm) SAR data, on various aspects including a) experimental SAR data analysis as a function of rice biophysical parameters and their temporal change, b) interpretation of the observations by theoretical modelling, c) development and application of classification methods, d) retrieval of biophysical parameters, and e) interface with rice growth models for crop yield prediction.

Experimental studies: Kurosu et al. (1995), Le-Toan et al. (1997), (2005), Ribbes and Le-Toan (1999a), Shao et al. (2001), (2002), Bingbai et al. (2005), and Chen and McNairn (2006) related SAR data to crop parameters (height, biomass, and age). Similar variations of the radar backscattering coefficients were observed at the two different areas when expressed as a function of rice biomass (Le-Toan et al., 1997). The experimental results have shown that the radar backscattering coefficients of rice fields have a characteristic increasing temporal behaviour (Bingbai et al., 2005, Chen and McNairn, 2006, Le-Toan et al., 1997, Liew et al., 1998, Ogawa et al., 1998). Most studies were implemented in the areas with

traditional rice cultivation system, whereas no previous literature was reported for modern cultivated rice fields.

Interpretation by modelling: Le-Toan et al. (1997) used a coherent cluster model, where a good agreement was obtained between the theoretical modelling and the ERS-1 measurements. On the other hand, Shao et al. (2002) used a radiative transfer microwave backscatter model. They attributed the backscatter signal to the multiple interactions between wave-plant-water, and that explained the relationship with rice biomass. Based on field measured rice biophysical parameters, rice paddy backscatter was simulated by a continuous canopy microwave backscatter model (Li et al., 2004). They reported that both ASAR data and model simulation was strongly correlated with rice parameters. On the other hand, Chen and Lin (2005) proposed a semi-empirical backscattering model. The results showed that the model can be used to extract LAI of rice in growing season using ASAR APP data with certain accuracy when optical remote sensing data can not be acquired.

Classifiers: In case of uniform rice cropping system, i.e. same crop calendar (China), absolute backscatter can work, but not for non-uniform cropping system (Indonesia, Vietnam). In this case, the ratio of temporal backscatter is found more relevant in image classification. An algorithm for rice field mapping using the temporal change of the radar backscatter as a classifier was implemented by Le-Toan et al. (1997).

Classification method: Classification of the rice cropping systems was based on thresholding the change indices (CIs), the thematic categories of rice cropping systems, using two methods: human visual inspection and semiautomatic hierarchical clustering algorithm (Liew et al., 1998). Le-Toan et al. (1997) developed a method of rice/non rice mapping based on the temporal variation of the radar response. This method was used in several research works (Ribbes and Le-Toan, 1998, Liew et al., 1998, Holecz et al., 2000, Chen and Mcnairn, 2006, Lam-Dao et al., 2005, Takeuchi et al., 1999). As expected, the maximum likelihood classifier was applied for classification in many research studies (Aschbacher et al., 1995, Frei et al., 1999, Holecz et al., 2000, Ouchi et al., 2002, Li et al., 2003, Li et al., 2004,

Phoompanich et al., 2005, Chen and McNairn, 2006, Takeuchi et al., 1999, Chakraborty and Panigrahy, 2000, Wooding and Zengyuan, 2000).

In order to differentiate rice fields from other land cover types, some research projects (Chakraborty et al., 1997, Panigrahy et al., 1999, Shao et al., 1999, Wooding and Zengyuan, 2000, Chen and McNairn, 2006) used a neural network classification. Another approach of a decision-rule based classifier has been used to classify a pixel as rice or not in several studies (Chakraborty and Panigrahy, 2000, Chakraborty et al., 2005, Choudhury and Chakraborty, 2006). An objected-oriented classifier has been applied for the studies of Wang et al. (2005) and Ling et al. (2005). Several recent studies proposed new algorithms for classification, such as principal component analysis (PCA) based method (Quegan et al., 2005) or single-date mapping algorithm for ASAR APP data (Bouvet et al., 2005). In the study of Kajalainen et al. (2000), the actual rice identification was done using unsupervised classification, the so-called ISODATA algorithm.

In the study of Le-Toan et al. (1997), a synthesis of experimental results at two different geographic locations was first conducted, and then followed by the development of a theoretical model to interpret the observations. They investigated the temporal behaviour of ERS-1 SAR backscatter from rice crops in relation to the rice growing conditions for a tropical test site in Indonesia and a temperate site in Japan. They observed similar relations between radar backscatter and plant biomass for rice plants in these two different areas. The results of theoretical modelling were compared with experimental data. Good agreement was obtained between the modelling and the observations.

Le-Toan et al. (1997) determined standard classification to identify rice fields was inappropriate. One possibility would be to use the temporal curve of the radar backscatter coefficient as the classifier, but the ERS-1 and ERS-2 35-day cycle would only enable a few (a maximum of three or four data points) data points that could be acquired during a rice crop cycle. They used the temporal change between any pair of data acquired during the crop cycle or between the end of one cycle and the beginning of the following cycle. Based on this principle, they developed an

algorithm for rice/non rice mapping using the temporal change of the radar backscatter as classifier.

Classification of the rice cropping systems based on thresholding the change indices using the series of multi-temporal ERS-2 SAR images was done by Liew et al. (1998). A two-step approach was employed. First, a visual inspection of the time series of radar backscattering coefficient for each change class associated with rice cropping was interpreted in relation with known crop calendars and local knowledge of the general geographical pattern of the various rice-based cropping systems. Second, a semiautomatic, hierarchical clustering algorithm was devised to group the change classes based on the similarity of their CI time series. This was based on the assumption that change classes with similar change pattern in their backscatter time series were likely to represent similar cropping systems. The limitation of this method is the use of human interpretation for the radar backscatter time series, together with the knowledge of field conditions and crop calendars.

A study examining the backscatter behaviour of rice as a function of time using Radarsat data (Shao et al., 2001) produced a rice-type distribution map showing four types of rice with different life spans ranging from 80 days to 120-125 days. By applying a neural net classifier the accuracy of the rice classification was found to be 91% (97% after post-classification filtering). Then, an empirical growth model was established and applied to the results of the rice classification, which related radar backscatter values to rice life spans. Although different varieties and life spans of rice crop generate different backscatter behaviour, the form of the relationship is the same, allowing this model to be applied to other types of rice.

Choudhury and Chakraborty (2006) found that the knowledge-based decision rule classifier is an optimum classifier for classification of rice and non-rice areas in the case of multi-temporal Radarsat SAR data that has large signature variability. The overall accuracy was found to be more than 98% in the case of rice class.

The above projects reported the use of single polarisation SAR data, e.g. VV polarised ERS-SAR data or HH polarised Radarsat data, for rice mapping and monitoring. This study emphasized the need of a radar remote sensing system that

has a dual polarisation, i.e. HH and VV to enable accurate discrimination between different rice-based cropping systems within a one-year growth cycle.

The use of HH/VV, HH and VV at low incident angle IS2 attained good classifiers for rice/non-rice mapping algorithm based on thresholding using Envisat ASAR APP (alternating polarisation precision) data acquired at a single date (Bouvet et al., 2005). One sample area of about one square kilometre was mapped with a DGPS (differential global positioning system) in order to validate and improve the mapping algorithms. The results produced an accuracy of approximately 88% for the classified rice and non-rice pixels.

In another research project (Ling et al., 2005), the strategy of rule base development using fuzzy sets and fuzzy logic was used for classification. For comparison, unsupervised classification and supervised classification were carried out with the same Envisat ASAR data. The classification results were aggregated into 2 classes, rice and non-rice to simplify the accuracy assessment. The classification accuracy at confidence level of 95% and kappa coefficient of the class rice was 0.943.

A principal component analysis based method was used in the research (Quegan et al., 2005) to enhance the rice distribution information. PCA is a well-known tool for image information compression and enhancement of multi-spectral data. An experiment was implemented with the HH-VV Envisat ASAR data acquired on three dates by selecting two different areas, including and excluding the river. Similar results were obtained, both showing strong brightness of rice fields in PC2.

Le-Toan et al.'s (2005) mid-term report on the first phase of the rice monitoring "Dragon" project conducted in China developed a remote sensing methodology at selected test areas for rice mapping and retrieving of rice parameters. The results obtained using Envisat data in 2004 and 2005 indicated that it is possible to:

- map rice field at a single data using two polarisations of ASAR APP;

- retrieve rice biomass using the polarisation ratio;
- map the main rice varieties;
- achieve regional rice mapping using multi-date ASAR Wide Swath data;
and
- detect intermittent drainage.

These new findings still need to be validated and confirmed. It also showed that HH/VV ratio is highly correlated with rice wet biomass. This relationship differs according to the growth period: it was observed that there is a linear increase from the beginning of tillering to flowering, and then a decrease after flowering.

Leaf area index is a very important parameter in many model of crop yield estimate. Chen and Lin (2005) proposed the semi-empirical backscattering model to estimate LAI of the rice using Envisat ASAR data in experimental site. The results indicated that ASAR C-band VV and HH polarisation data are useful in estimating LAI of rice. When LAI of the rice is less than 2.5, estimated LAI from the model using VV and HH data have relatively high correlation.

These rice mapping and retrieving methods have been widely validated in the past ten years. However, in recent years, changes in rice cultural practices have been observed in different regions of the world. The changes are caused by the rice demand pressure and water shortage, and exacerbated by the progress in technology and the decrease of available manpower. This study was intended to develop an algorithm for mapping the rice cropping system with modern cultural practices and to examine the use of new generation SAR data that has advantages over the previous systems, e.g. dual polarisation and different modes of acquisition. None of the previous studies have focussed on discriminating between different rice cropping systems using new generation of SAR data.

2.4.2 Rice yield prediction models

Ribbes and Le-Toan (1999a) found that the radar backscattering coefficient measured by ERS and Radarsat is related to rice plant age, height and biomass. The

rice growth model ORYZA1 (Kropff et al., 1994) was used to simulate rice growth with sowing date and biomass values retrieved from ERS and Radarsat SAR data as input parameters. The simulated yields were found to lie within 10% of in-situ measured yield when ERS data were used and 15% with Radarsat data. The main factors determining the growth rate were light, temperature, and the various characteristics for phenological and morphological processes. The model calculated daily rates of dry matter production of the various plant organs, the rate of leaf area development, and the rate of phenological development. By integrating these rates over time, using a time step of one day, dry matter production of the crops was simulated throughout the growing season.

Kajalainen et al. (2000) reported the identification of rice fields from ERS-2 SAR images based on the temporal variation of SAR backscattering. The actual rice identification was done using unsupervised classification, implementing the ISODATA algorithm. The rice yield estimates were calculated using the CROPWATN crop growth model, which used meteorological data from the growing season, as well as soil data and information about different rice varieties.

A model was provided for rice yield estimation based on the relationship between the backscatter coefficient of multi-temporal Radarsat data and biomass of rice (Li et al., 2003). For the sake of validation, the estimation of errors was carried out using global positioning system (GPS) data. This achieved an accuracy of 95% for the rice mapping and 94% for the rice yield estimation. The detected rice fields need to be classified into nine yield levels through analysis of the relationship between the backscatter coefficient and rice biomass in each growing period on the ScanSAR narrow band (SNB) images. GPS ground data were used to verify the correlation between yield and backscatter coefficient. A multivariate regression model based on radar remote sensing was established to reveal the relationship between the backscatter coefficient of time-series SNB data and rice yield. Distribution maps of rice yields were obtained after the classification of rice fields on SNB images.

Chen and McNairn (2006) compared the results of the four methods for rice acreage mapping using Radarsat SAR data: change detection, neural network

classification, maximum likelihood classification, and an integrated change detection neural network approach. In the integrated method, the neural network training data were extracted from the change detection results without the requirement for significant ground data to train the network. A minimum mapping accuracy of 96% was achieved using this integrated method. This information was then used in a neural network-based yield model to predict rice yield on a regional basis. The predicted yield from the neural network Net1 is about 6% higher than the government statistics. Net2 yield predictions were about 3% lower than the government statistics.

The application of new generation SAR imagery for crop yield prediction of modern cultivated rice areas was not reported in the past research studies. Therefore, the potential integration of new generation SAR data with yield forecasting model could lead to rapid, objective and accurate production estimates.

2.5 Summary

Most studies were implemented in the areas with traditional rice cultivation system, whereas no previous literature was reported for modern cultivated rice fields. These rice mapping and retrieving methods have been widely validated in the past ten years. None of the previous studies focussed on discriminating between different rice cropping systems using new generation of SAR data. This study was intended a) to understand the relationship between radar backscatter coefficients and selected parameters (e.g. plant age and biomass) of rice crops over an entire growth cycle; and b) to develop an algorithm for mapping the rice cropping system with modern cultural practices and to examine the use of new generation SAR data that has advantages over the previous systems, e.g. dual polarisation and different modes of acquisition (i.e. AP and WS mode).

There was no report on the study of new generation SAR imagery for crop yield prediction of modern cultivated rice areas, on the previous literature materials. Therefore, this study was intended to examine new generation SAR data with yield forecasting model in order to provide accurate production estimates in the study area.

Chapter 3

METHODS

3.1 Overview

This chapter describes the following components of the research methods employed in this study (Figure 3.1): a) study area and reasons for site selection; b) rice growing stages and rice cropping systems of the area; c) satellite data and relevant data collected and used; and d) rice parameters observed and measured on the ground. Although shown in Figure 3.1 below, the following components of the methods were presented in other chapters: e) the alternative methods used for analysis of rice backscatter (Chapter 4), rice mapping (Chapter 5), and yield prediction (Chapter 6).

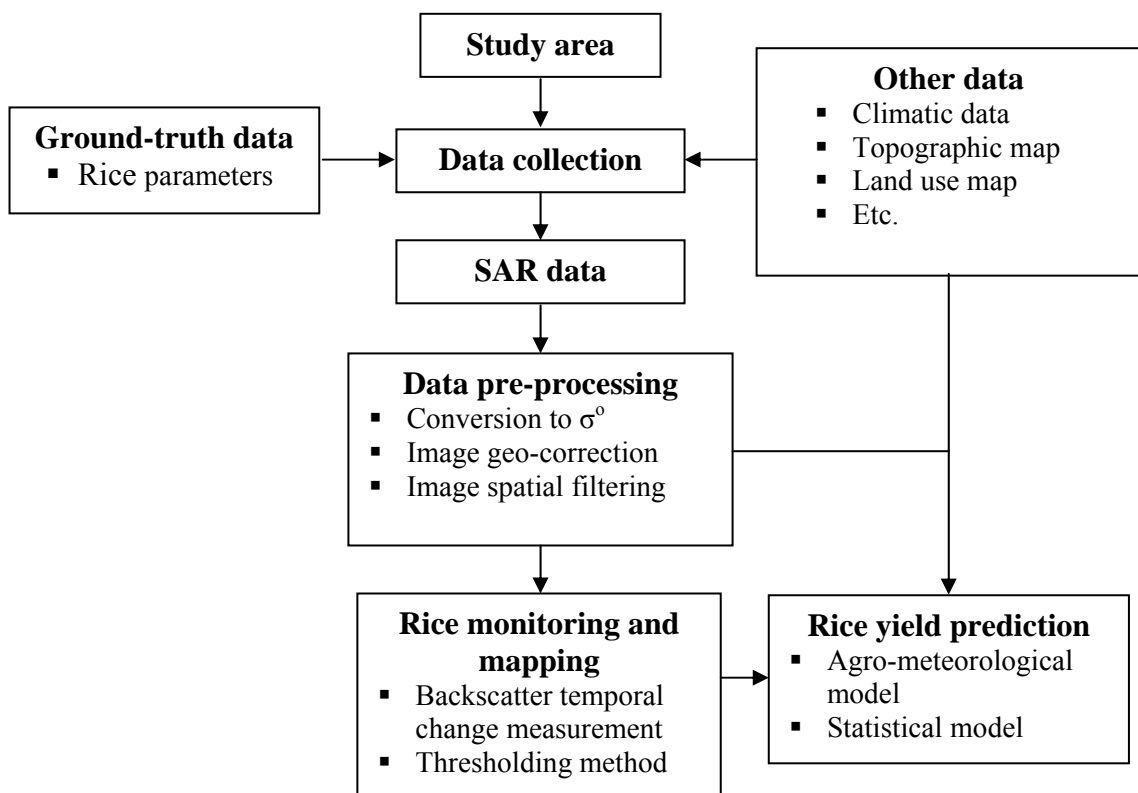


Figure 3.1. Overview of methods for the study.

3.2 Study Area

Vietnam is one of the world's largest rice exporting countries since the mid-1990s and the fifth producer country in the world with about 5.5% of the global production (FAOSTAT, 2007). The fertile Mekong River Delta at the southern tip of Vietnam accounts for more than half of the rice production in the country (GSO, 2007a). In addition, the Vietnamese are among the world top five rice consumers (FAO, 2004). This makes the rice growing areas of the Mekong River Delta a good example to study the changes from traditional to modern rice cultivation system gradually adopted in the last ten years. The changes consist of a) increasing the number of crops from 1 or 2, to 2 or 3 crops per year; b) changing from transplanting to direct sowing; c) using water-saving technology; d) using short-cycle rice varieties (85 to 105 days); and e) using fertilizer and pesticide more intensively. These changes in rice practices can have a significant impact on radar backscattering behaviour that may have an influence on remote sensing methods.

In the Mekong River Delta of Vietnam, the rainy season usually lasts for seven months from May to November, and floods annually occur starting from August. Dike system has been built and intensified in recent years to block the floodway into the fields during the flood season in order to increase the number of crops during the wet season from one crop to two crops of rain-fed rice, named *Summer Autumn* (SA) and *Autumn Winter* (AW) crops. In the dry season, an irrigated rice crop, *Winter Spring* (WS) has been grown. As a result, two or three rice crops in a year have been planted, resulting in an increase in rice production from 12.8 million tons in 1995 to 19.3 million tons in 2005, i.e. raising 51% in ten years (GSO, 2006). These multiple crops are made possible by the availability of short cycle rice varieties.

Besides increasing the number of crops a year, cultural practices have been changed in various ways. Rice farmers scarcely practice transplanting as they did few years ago, and today the conversion to direct sowing is almost fully achieved. Because of economic growth, increased labour demand puts upward pressure on wages or reduces the availability of labour for many farm operations. This has encouraged farmers to switch from transplanting, which requires 25-50 person-days

per hectare, to direct seeding or row seeding (Figure 3.2), which requires at most only about 5 person-days per hectare (Dawe, 2005).



Figure 3.2. Equipment of row seeding.

Concerning water management, the rice-based cultivation system is a major consumer of the freshwater resource. Saving water in the field is economically important for farmers and contributes to environmental protection. Therefore, a new water saving technology named *alternative wetting and drying* (AWD) was introduced and disseminated several years ago (Figure 3.3). AWD is also called ‘intermittent irrigation’ or ‘controlled irrigation’. The number of days of nonflooded soil in AWD before irrigation is applied can vary from one day to more than 10 days. A practical way to implement AWD is to monitor the depth of the water table on the field using a simple perforated ‘field water tube’. After an irrigation application, the field water depth will gradually decrease in time. When the water level (as measured in the tube) is 15 cm below the surface of the soil, it is time to irrigate and flood the soil with a depth of around 5 cm. Around flowering, from one week before to one week after the peak of flowering, ponded water should be kept at 5 cm depth to avoid any water stress that would result in potentially severe yield loss. The use of

AWD technique requires fewer water pumping operations where the crop is not continuously flooded.



Source: Tuong (2007)

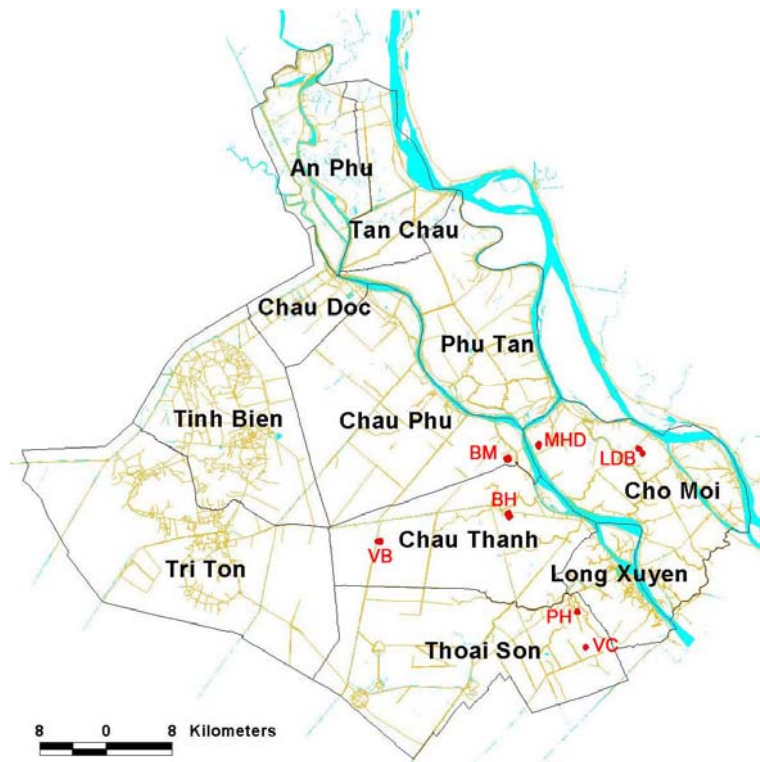
Figure 3.3. A technology for water saving in rice production.

The study area is the An Giang province (Figure 3.4), extending from 10° 12' to 10° 57' N latitude and 104° 46' to 105° 35' E longitude and is covered by the entire 100 x 100 km Envisat ASAR scene IS2 mode (Figure 3.4a). The province is located in the Mekong river plain, South of Vietnam and is surrounded by Kien Giang, Can Tho and Dong Thap provinces, and Cambodia. Located about 190 km from Ho Chi Minh City, An Giang has an area of 3,536.8 square kilometres, with a population of about 2,231,000 people (GSO, 2007b). Population and area of districts in the province are presented in Table 3.1.



Source: <http://www.crisp.nus.edu.sg/>

(a)



(b)

Figure 3.4. The An Giang province: Location of the frame of ENVISAT ASAR APP scene on the study site (a) and Administrative boundary map of An Giang province, with locations (red dots) of the sampling areas (b).

An Giang is located in a tropical monsoon climate with an average temperature of 26 to 28 °C. The temperature is 35 to 36 °C in April and May and 20 to 21 °C in December and January. A northerly wind blows from November to April and a south westerly wind from May to October. The annual rainfall is around 1,400 – 1,500

mm. There is a dry season from December to April and a rainy season from May to November with heavy rain in September (AGDPI, 2009).

Table 3.1. Area, population and population density by district of An Giang province in 2007.

District name	Area (km²)	Population (person)	Population density (pers./km²)
Phu Tan	328.06	243117	741
Chau Phu	451.01	252066	559
Tri Ton	600.40	127106	212
Tinh Bien	355.50	123948	349
Chau Doc	104.68	118615	1133
Long Xuyen	115.43	275519	2387
Thoai Son	468.72	191303	408
Tan Chau	17045	164548	965
An Phu	217.78	187767	862
Cho Moi	369.62	369443	1000
Chau Thanh	355.11	177630	500
Province	3536.76	2231062	631

Source: AGSO (2008b)

Thirty-seven kinds of soil are categorised into six main groups: alluvial soil (44.5%), alkaline alluvial soil (27.5%), ancient alluvial soil (7.3%), and other soil (20.70%). An Giang's land is mostly flat and suitable for tree cultivation. Land for forestry is 21,060 hectares; of which, mountainous area is 13,092 hectares and plain area is 7,968 hectares (AGDPI, 2009). In the provincial acreage, agricultural land covers the largest area (280,494 ha or 79.3% provincial acreage); of which is dominated (262,649 ha) by rice farms (AGDARD, 2007) (Figure 3.5 and 3.6).



Figure 3.5. An example of rice field in the study area.

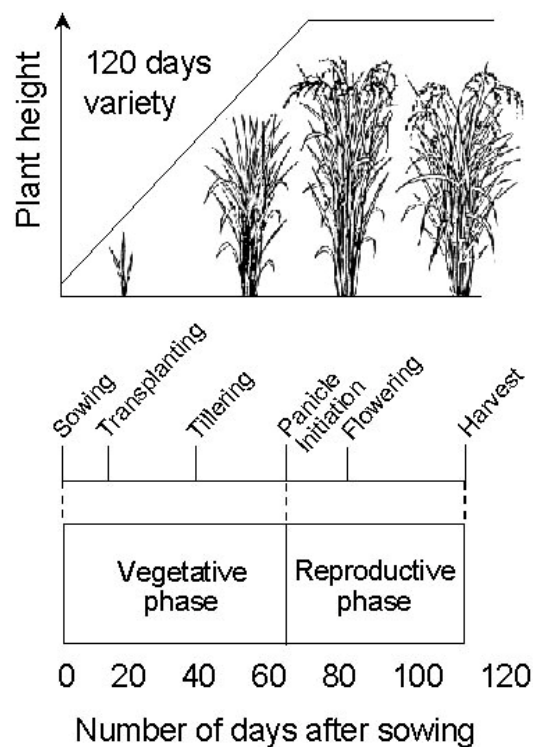


Figure 3.6. Field trip on the Mekong River.

3.3 Description of Rice Growing and Rice Cropping Systems

3.3.1 Rice growing stages

The temporal aspect of rice development is important to the understanding of the radar responses of rice fields at different growing stages. The rice plant usually takes 3-6 months from germination to maturity, depending on the variety and the environment under which it is grown. During this period, rice completes basically two distinct sequential growth stages: vegetative and reproductive (Figure 3.7). The reproductive stage is subdivided into preheading and postheading periods. The latter is better known as the ripening period. Agronomically, it is convenient to regard the life history of rice in terms of three growth stages: vegetative, reproductive, and ripening (Figure 3.8). A 120-day variety, when planted in a tropical environment, spent about 60 days in the vegetative stage, 30 days in the reproductive stage, and 30 days in the ripening stage (Yoshida, 1981).



Source: Le-Toan et al. (2003)

Figure 3.7. Rice growing stages (crop cycle length of 120 days).

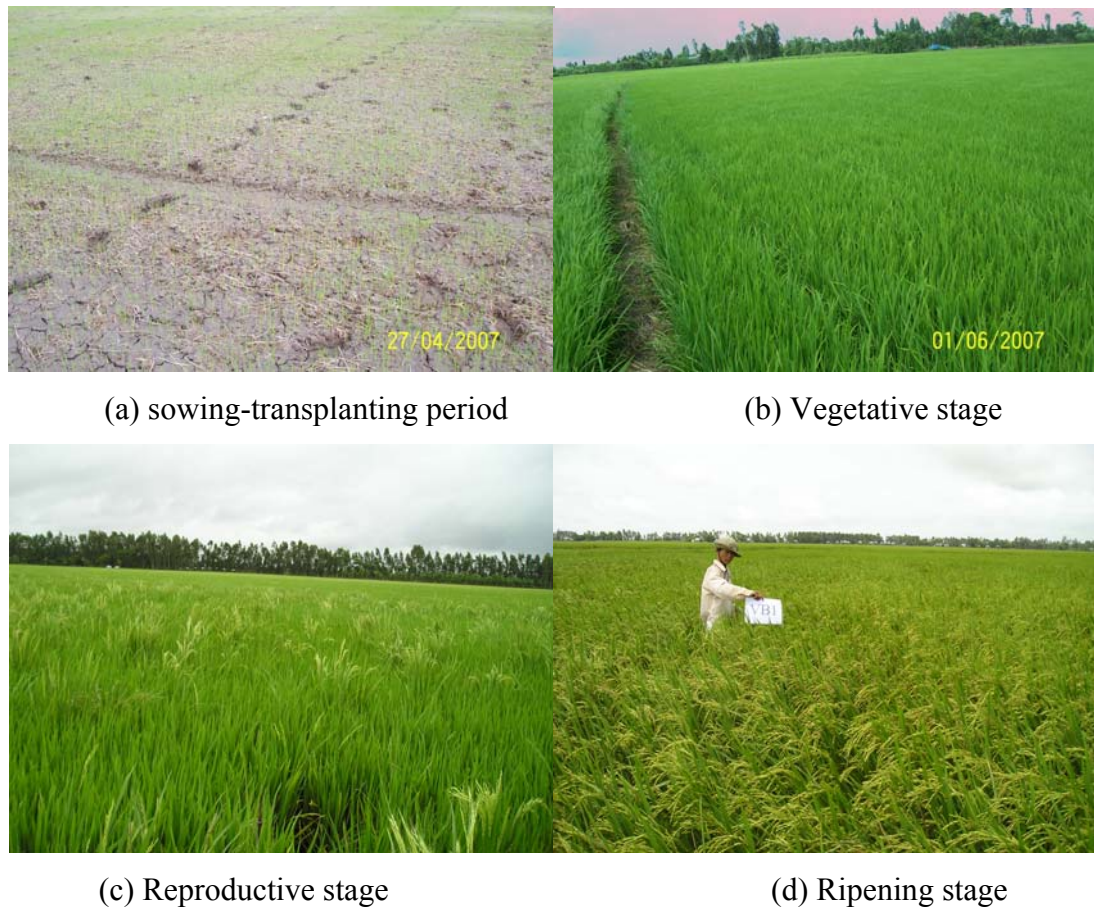


Figure 3.8. Photographs of rice growing stages.

a) Vegetative stage refers to a period from germination to the initiation of panicle primordia.

The sowing-transplanting period: At the onset of the rains or with the arrival of irrigation water, the fields are flooded in order to prevent weeds and pests. The water depth varies from 2 to 15 cm. The rice plants are sown in nurseries before transplantation. After 25 to 35 days depending upon labour availability, the plants are transplanted in clusters of one to ten plants and planted in line (approximately 10 to 20 clusters in a 1 m²). In recent plantation techniques, direct sowing can take place: the grains are sown at a high density, directly in flooded soil under 2-5 cm of water, or in most cases, in wet soil (Le-Toan et al., 2003).

The vegetative stage is characterized by active tillering, gradual increase in plant height, and leaf emergence at regular intervals. All contributes to the increasing of the leaf area that receives sunlight (Yoshida, 1981). Tillering starts about 15 days

after sowing and continues until flowering. About 50 to 60 days after transplantation, the clusters almost cover the area between plants. From sowing to heading, the plant structure remains mostly erectophile. The stems are quasivertical and the leaves have a small insertion angle (5-20°) (Le-Toan et al., 2003).

b) Reproductive stage refers to a period from panicle primordia initiation to heading.

The reproductive stage is characterized by stem elongation which increases plant height, decline in tiller number, emergence of the flag leaf, booting, heading, and flowering. Initiation of panicle primordia usually dates back to about 30 days before heading. The reproductive growth stage is sometimes called the internode elongation stage (Yoshida, 1981). After heading, the growth (height, biomass) stops and the leaves change their orientation to be no more erectophile (their insertion angles are typically 30-40°) (Le-Toan et al., 2003).

c) Ripening stage refers to a period from heading to maturity.

The length of ripening is largely affected by temperature that ranges from about 30 days in the tropics to 65 days in cool, temperate regions. Ripening follows fertilisation; and may be subdivided into milky, dough, yellow-ripe, and maturity stages. Ripening is characterized by leaf senescence and grain growth (Yoshida, 1981), with a decrease of leaf and stem moisture content, and a decrease of the number of leaves. In some systems, irrigation is stopped during the latter part of this period; in others, water may remain in field up to harvest (Le-Toan et al., 2003).

After harvest, fields can be either bare and dry at the end of the dry season or covered with weeds in wet conditions. In some areas, short cycle secondary crops (e.g. vegetable and bean) can take place between two rice crops.

3.3.2 Rice cropping systems in the Mekong River Delta

In general, the wetland rice production can be classified into *irrigated rice fields* and *rain-fed rice fields* (Le-Toan et al., 1997). For irrigated rice fields, the water is supplied artificially from a surface or underground source. One, two, even more crops of rice per year can be found depending on the water supply. The rain-fed rice fields are irrigated by rainfall, sometimes supplemented by localized runoff collection.

The Mekong River Delta has many advantages in climatic conditions, such as high solar radiation and favourable and stable high temperature. The Delta has a monsoon tropical semi-equatorial climate. Two seasons are distinguishable: the rainy season that constitutes approximately 90 percent of the total rainfall; and the dry season. The combination of hydrology, rainfall pattern, and availability of irrigation determines the variety of rice-based cropping systems practiced in the Mekong River Delta (Table 3.2).

Table 3.2. Main rice-based cropping systems in the Mekong River Delta.

Rice cropping system	Rice season
Single rice crop	Traditional rice (rain-fed)
Double rice crop	Summer Autumn – Autumn Winter (rain-fed)
	Winter Spring – Summer Autumn (irrigated)
Triple rice crop	Winter Spring – Summer Autumn - Autumn Winter

Table 3.2 summarises the major rice cropping systems practiced in the Mekong River Delta. The double cropping system may be the WS – SA or the SA – AW system. As the WS crop grows during the dry season, the WS – SA cropping system is practiced in areas that receive irrigation water. The SA – AW system is practiced under predominantly rain-fed conditions. The crop calendar varies each year, depending on the onset of the rainy season at the start of the Summer Autumn crop. The main rice seasons in 2007 in the An Giang province are tabulated below (Table 3.3).

Table 3.3. Main rice seasons in An Giang, Mekong River Delta.

Rice crop		Planting	Harvesting
English name	Local name		
Winter Spring		Nov/Dec	Mar/Apr
Summer Autumn		Apr/May	Jul/Aug
Rainy season	Autumn Winter	Jul/Sep	Oct/Dec
	Traditional rice	Jul/Sep	Nov/Jan

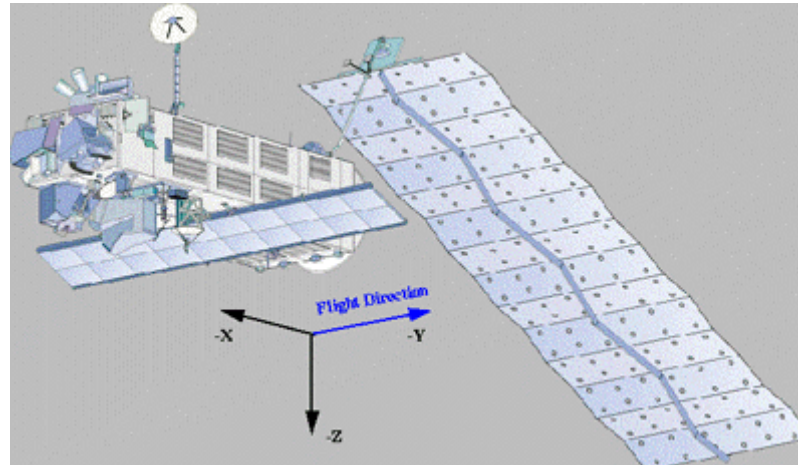
The complicated rice cropping systems in the Mekong River Delta are characterised by the following:

- size of rice field ranging from small (0.5 – 1 ha) to large;
- sowing dates are different from field to field (1 or 2 weeks);
- cultural practices (sowing, transplanting);
- rice varieties.

3.4 Data Acquisition

3.4.1 Imagery used

This study used the remote sensing data taken by the Environment Satellite (Envisat) ASAR sensor (Figure 3.9). ASAR is one of instruments on board the Envisat. Following on from the very successful ERS-1/2 SARs, ASAR is an all-weather, day-and-night, high resolution instrument that will provide radar backscatter measurements indicative of terrain structure, surface roughness, and dielectric constant. Important new capabilities of ASAR (Figure 3.10) include beam steering for acquiring images with different incidence angle, dual polarisation, and wide swath coverage (ESA, 2007). As two of ASAR modes (Table 3.4) were available and both can offer potential solutions, the rice monitoring in the Mekong River Delta using these modes of data was analysed.



Source: ESA (2007)

Figure 3.9. ASAR antenna.

Table 3.4. Technical summary of Envisat sensors ASAR and MERIS.

Sensor/Mode	Geometrical resolution (m)	Polarisation	Wavelength	Frequency range
ASAR Image Mode (IM)	30	VV or HH	C-band	5.331 GHz
ASAR Alternating Polarisation Mode (AP)	30	HH/HV VV/VH HH/VV	C-band	5.331 GHz
ASAR Wide Swath Mode (WS)	150	VV or HH	C-band	5.331 GHz
MERIS	300		Visible, Near-IR	390-1040nm (15 bands)

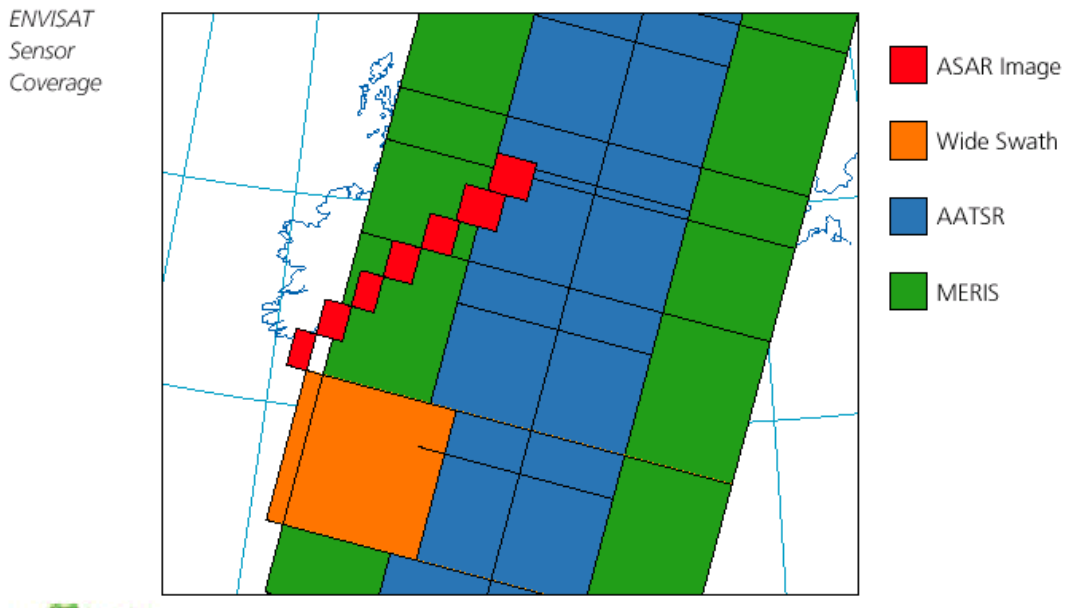


Figure 3.10. Envisat sensor coverage.

Table 3.5. List of Envisat ASAR APP data used.

ASAR mode	Observation date	Rice crop
ASAR APP	13/01/2007	Winter Spring 2007
	17/02/2007	
	24/03/2007	
	28/04/2007	Summer Autumn 2007
	02/06/2007	
	07/07/2007	
	15/09/2007	Autumn Winter 2007
	20/10/2007	
	24/11/2007	
	29/12/2007	Winter Spring 2008
	02/02/2008	

The Envisat ASAR APP data of C-band (5.3 GHz frequency and 5.6 cm wavelength), HH&VV polarisation, IS2 incidence angle (19.2° - 26.7°), and ascending mode were available at the following dates during the year 2007 and February 2008 (Table 3.5). APP images have a nominal spatial resolution of 30 m x 30 m and pixel size of 12.5 m x 12.5 m with a swath width of about 100 km. The

mosaic of two ASAR APP scenes covers most the study area. The total number of ASAR APP images used in this study is 22. Sample images taken at the beginning, middle of WS crop and harvest period are presented in Figures 3.11, 3.12, 3.13, respectively. Rice areas are showed as magenta pixels in the images. Appendix A presented the rest of the images listed in Table 3.5.

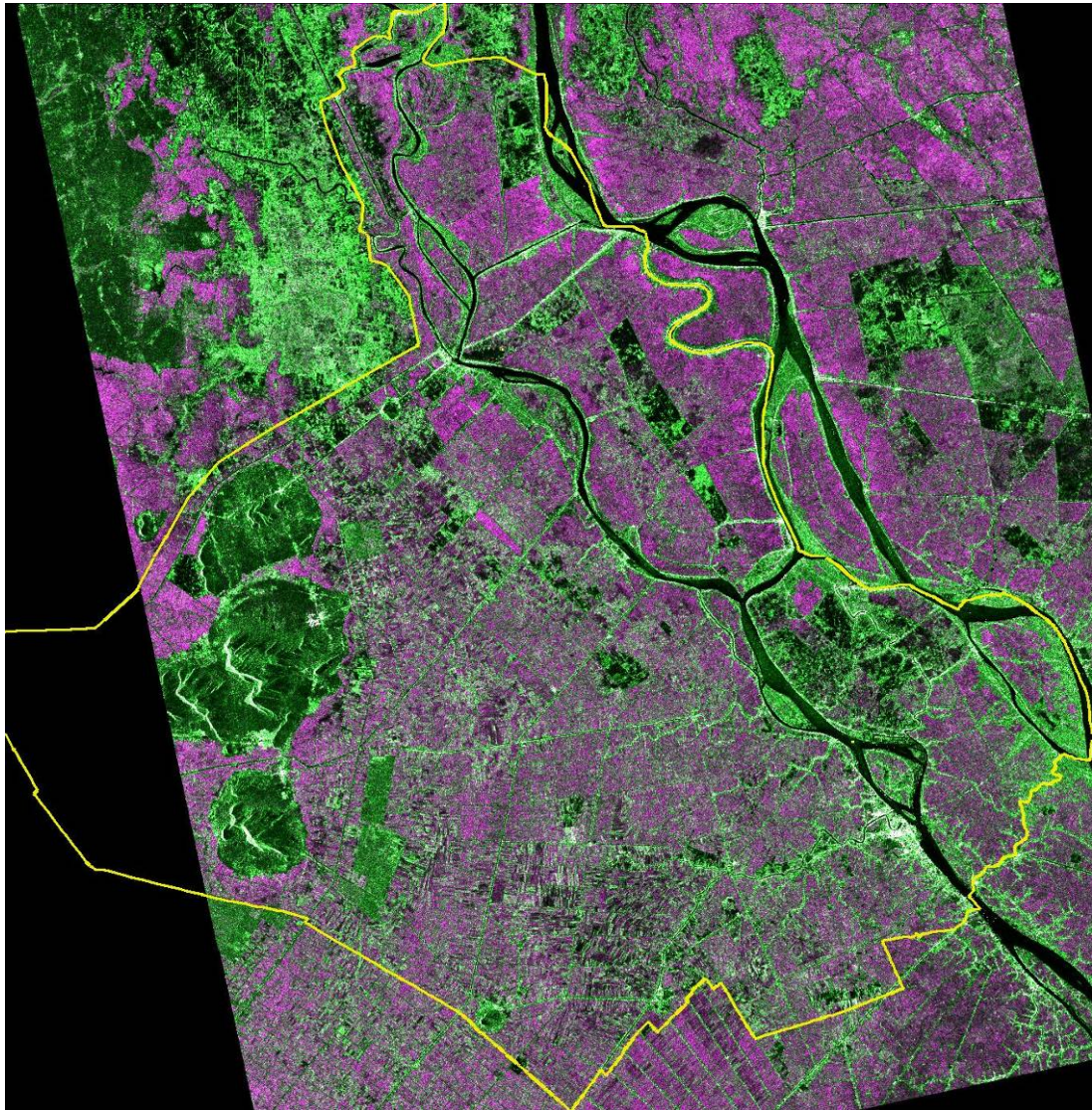


Figure 3.11. Colour composite ASAR APP image acquired on 13 Jan. 2007 (R=HH, G=VV, B=HH), provincial boundary in yellow polyline.

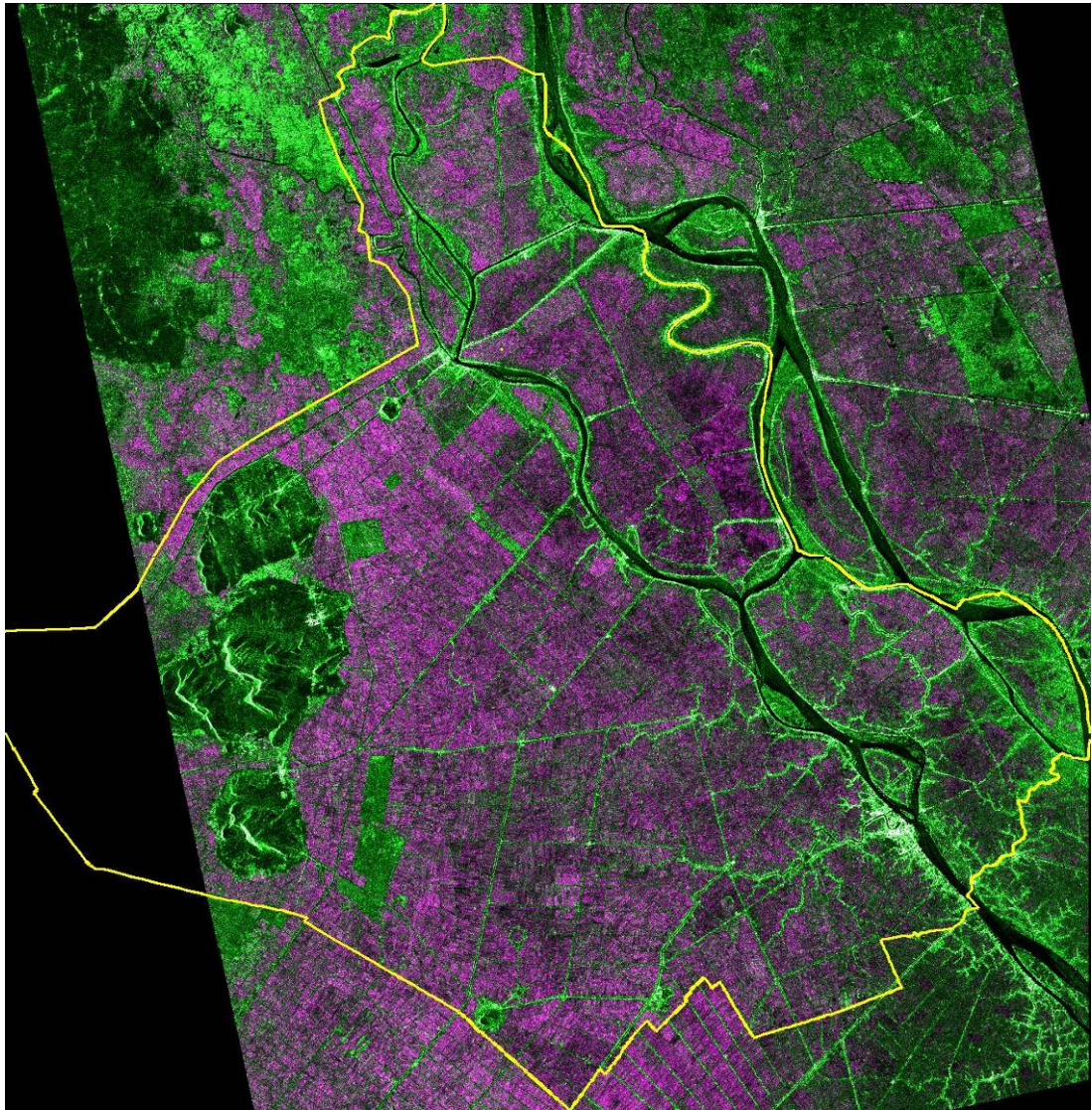


Figure 3.12. Colour composite ASAR APP image acquired on 17 Feb. 2007 (R=HH, G=VV, B=HH), provincial boundary in yellow polyline.

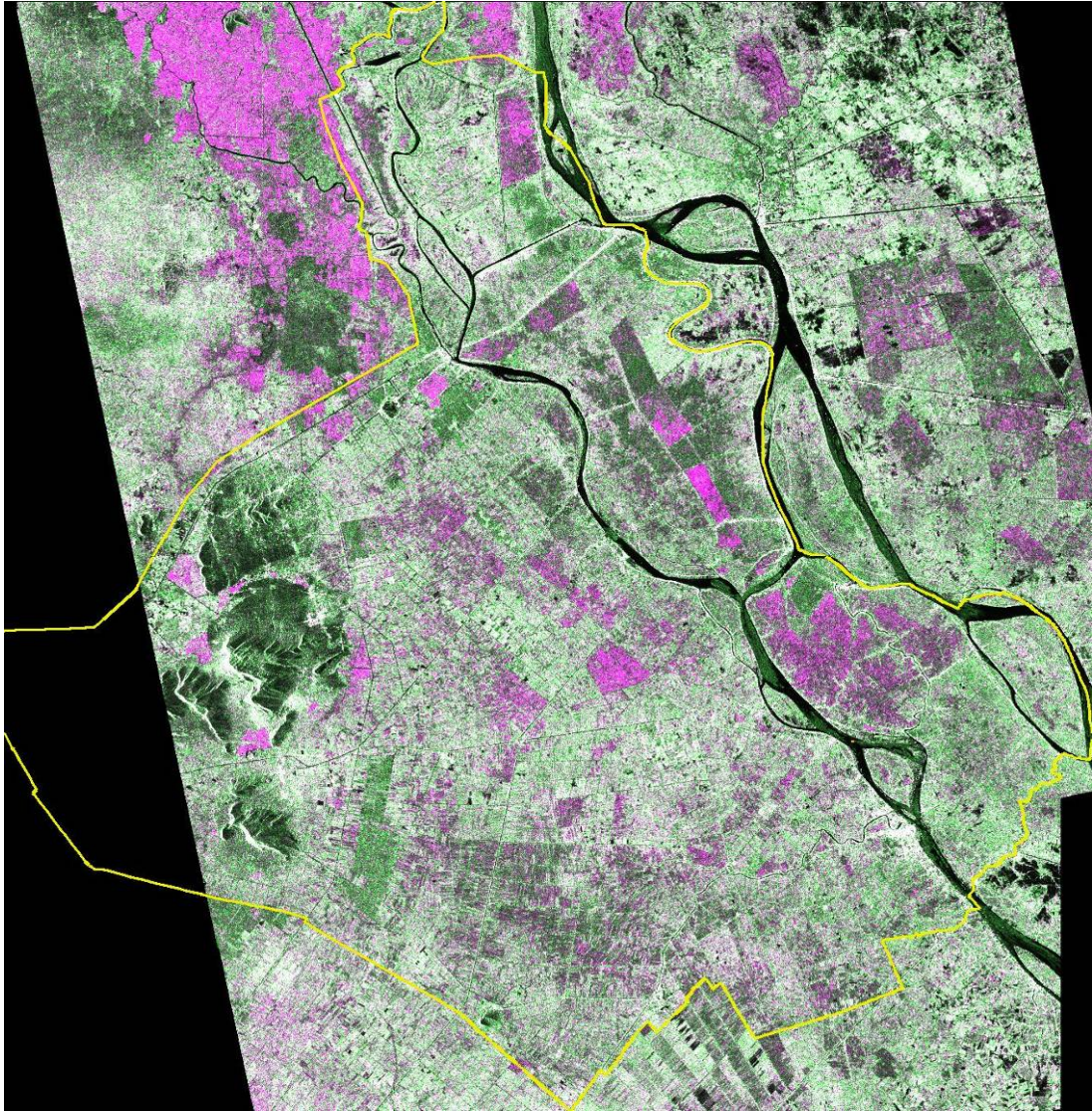


Figure 3.13. Colour composite ASAR APP image acquired on 24 Mar. 2007 (R=HH, G=VV, B=HH), provincial boundary in yellow polyline.

Another product of ASAR measurement modes used for rice mapping is ASAR WS mode data. The product provides greater swath width at reduced spatial resolution through the use of the ScanSAR technique. The standard product available for WS mode is a 150 m resolution image with the full 405 km swath width. The product contains VV or HH polarisation image (Table 3.4). In this case, only HH images were collected for the study, because HH polarisation is more sensitive to rice backscatter than VV does (Ribbes and Le-Toan, 1999b).

Table 3.6. List of Envisat ASAR WS data used.

ASAR mode	Observation date	Ascending mode	Descending mode	Rice crop
ASAR WS	05/12/06		D0	Winter Summer
	09/01/07		D1a	
	16/01/07	A1		
	25/01/07		D1b	
	13/02/07		D2	
	20/02/07	A2		
	01/03/07		D3a	
	20/03/07		D3b	
	27/03/07	A3		
	05/04/07		D4a	
	24/04/07		D4b	Summer Autumn
	01/05/07	A5		
	10/05/07		D5a	
	29/05/07		D5b	
	05/06/07	A6		
	14/06/07		D6	
	03/07/07		D7a	
	10/07/07	A7		
	19/07/07		D7b	
	07/08/07		D8a	
	14/08/07	A8		None
	23/08/07		D8b	Rainy season
	11/09/07		D9	
	18/09/07	A9		
	16/10/07		D10	
	23/10/07	A10		
	01/11/07		D11a	
	20/11/07		D11b	
	27/11/07	A11		
	06/12/07		D12	

This study utilised ten images in ascending mode and twenty images in descending mode. They were acquired from December 2006 to December 2007 covering three rice crops WS, SA and rainy season in the Mekong River Delta (Table 3.6). Some of them were utilised for testing of the rice mapping method during WS and SA 2007 crop seasons in An Giang province. Sample images were presented in Figures 3.14 and 3.15.

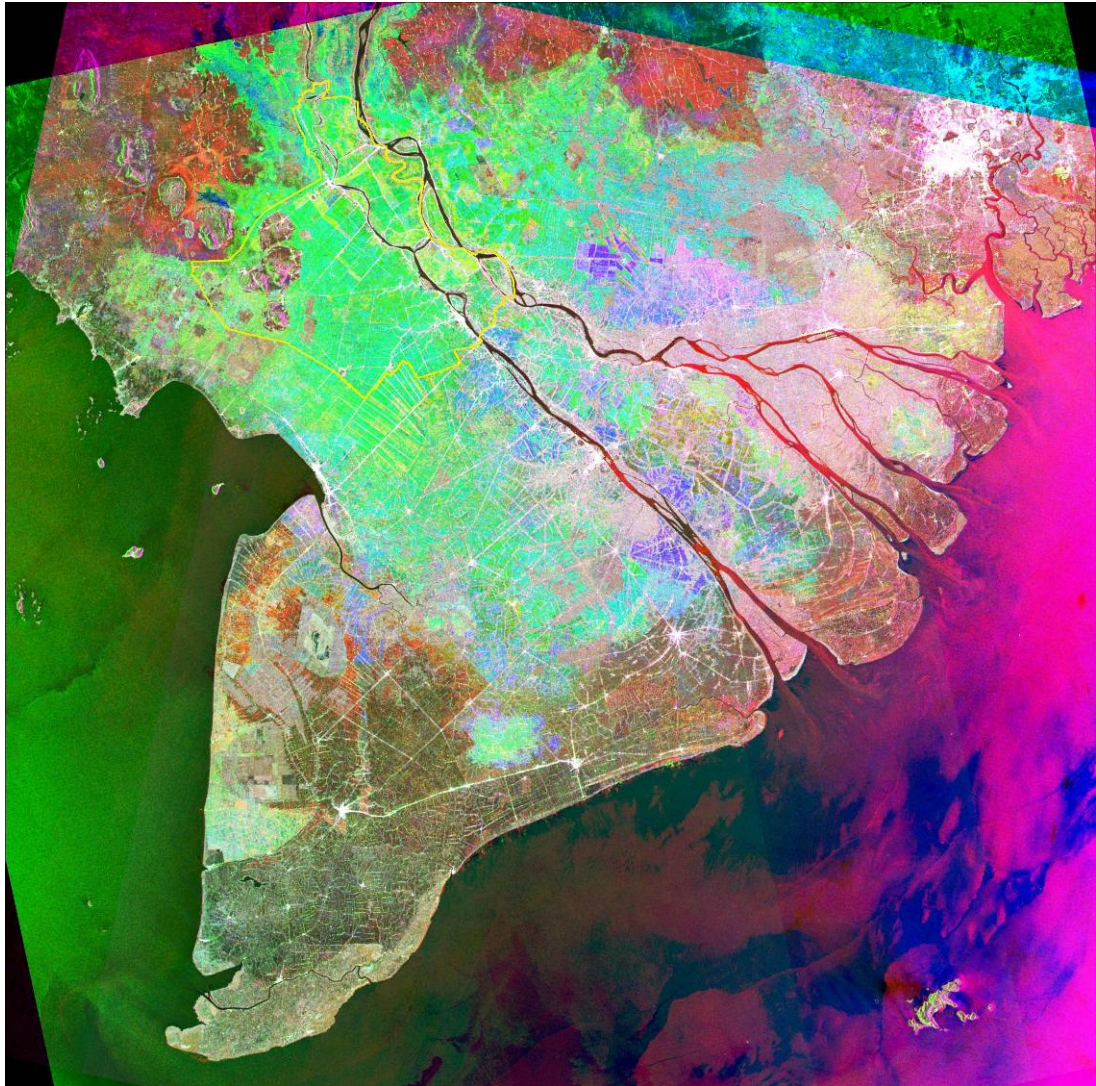


Figure 3.14. Colour composite ASAR WS image (R=5 Dec. 06, G=20 Feb. 07, B=24 Apr. 07), provincial boundary in yellow polyline.

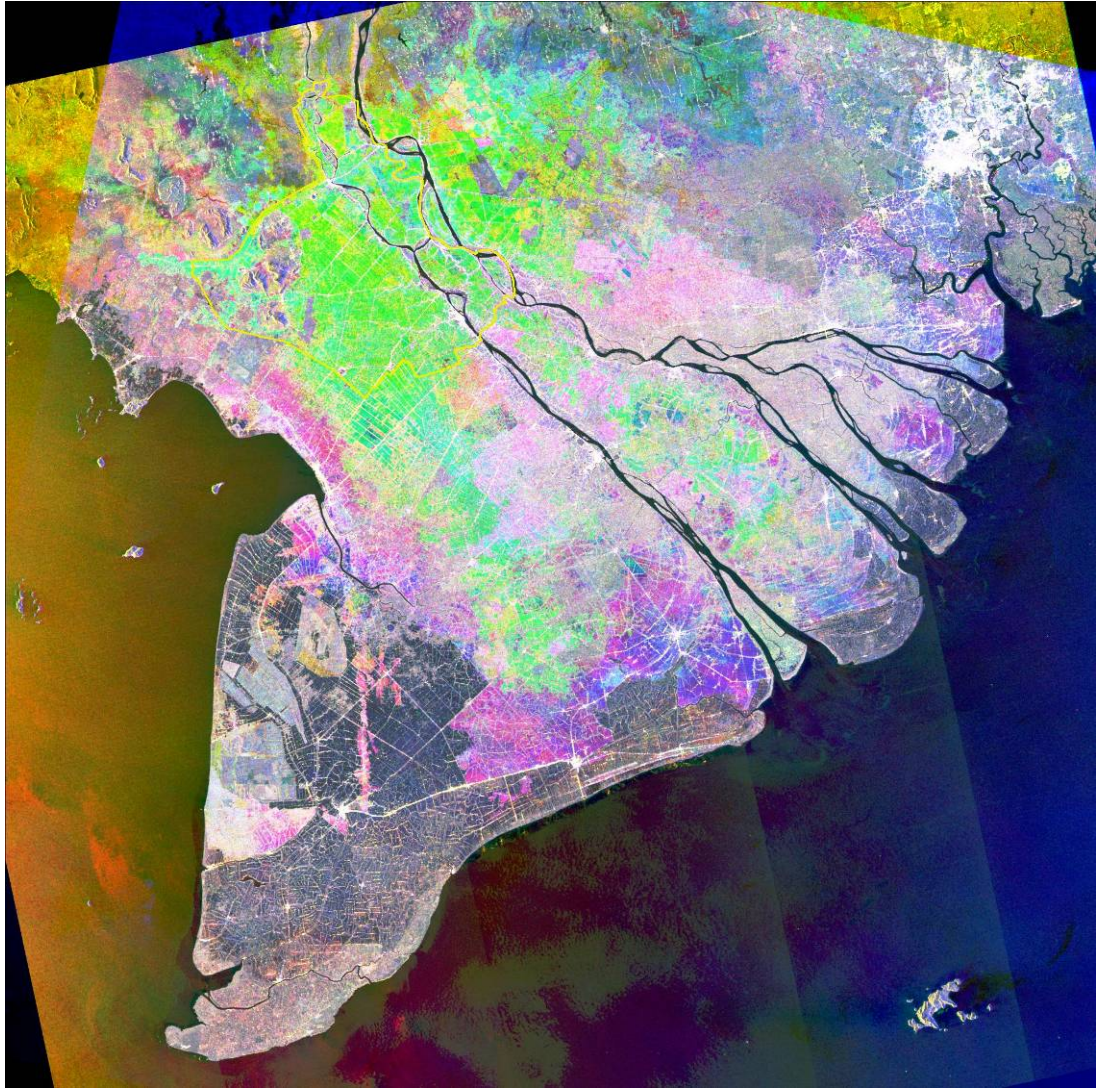


Figure 3.15. Colour composite ASAR WS image (R=1 May 07, G=5 Jun. 07, B=23 Aug. 07), provincial boundary in yellow polyline.

3.4.2 Ground truth and survey data

Seven sampling areas which were located in Binh My (BM) village of Chau Phu (CP) district, Binh Hoa (BH) and Vinh Binh (VB) village of Chau Thanh (CT) district, Vinh Chanh (VC) and Phu Hoa (PH) village of Thoai Son (TS) district, and Long Dien B (LDB) and My Hoi Dong (MHD) village of Cho Moi (CM) district were selected to meet the research objectives. Locations of these sampling areas were presented on the map in Figure 3.4b. The main criteria used for the selection of sampling areas were representativeness of rice growing regions in term of physiographic stratification, variety of crop type and cultural practices, and

accessibility of the area for ground data collection (Le-Toan, 2002). The measurements were done on five rice fields in each of the seven sampling areas (Table 3.7). The size of fields ranged from 0.2 to 1.7 ha. The parameters (Table 3.8) measured for each field include general parameters (rice variety, method of planting, sowing/transplanting and harvesting date (Table 3.9), plant phenological stage, water layer height, yield), plant parameters (number of plants per square meter, plant height, height uniformity, number of stems per plant, wet and dry biomass (see photographs of drying the rice plant in Figure 3.16)), leaf parameters (number of leaves per stem, leaf length and width) and panicle parameters (number of panicles per plant, number of grain per panicle and moist weight of panicle). Each parameter of plant, leaf or panicle was estimated over 3 to 5 sampling plots of 0.50 x 0.50 m within the fields (according to the field uniformity). The plots selected were not near the edge of the fields.

Table 3.7. Size and area of sampling fields.

Field	L (m)	W (m)	S (m ²)	Field	L (m)	W (m)	S (m ²)
BM1	85	31	2635	VC1	141	19	2679
BM2	140	77	10780	VC2	139	108	14688
BM3	76	74	5624	VC3	56	35	1960
BM4	132	43	5676	VC4	63	59	3717
BM5	125	47	5875	VC5	139	108	14688
VB1	330	52	17160	PH1	192	59	11328
VB2	321	54	17334	PH2	186	35	6510
VB3	199	51	10149	PH3	221	30	6630
VB4	109	34	3706	PH4	221	30	6630
VB5	89	29	2581	PH5	186	35	6510
BH1	77	40	3080	LDB1	130	24	3120
BH2	169	53	8957	LDB2	143	27	3861
BH3	110	101	11110	LDB3	84	63	5292
BH4	118	72	8496	LDB4	112	89	9968
BH5	286	31	8866	LDB5	50	38	1900
				MHD1	97	22	2134
				MHD2	186	22	4092

				MHD3	118	49	5782
				MHD4	88	71	6248
				MHD5	69	43	2967

Table 3.8. List of rice parameters collected from this study.

Rice parameters		Description	Equipment
General parameters	Paddy variety	Ex.: IR 64	
	Method of planting	direct sowing/ transplanting	
	Sowing date	date of sowing or number of days after sowing	
	Transplanting date	date of transplantation or the number of days after transplantation	
	Date of harvesting	if the rice is harvested	
	Plant phenological stage	Seeding, transplanting, tillering, heading, flowering, ripening, ready to harvest	
	Water level (cm)	if fields are flooded	stick
	Yield (kg/m ²)	if the rice is harvested	
Plant parameters	Planting x bunch distance (cm)	distance between 2 rows and between 2 bunches within the same row	tape
	Plant row direction (°)	orientation of the rows from the North	compass
	Number of bunch/m ²	make a square of 0.5x0.5m and count the number of bunches	tape
	Plant height (cm)	above water layer	tape
	Height uniformity		
	Number of stems per bunch		

	Wet weight per bunch (g)	above water biomass (moist weight by m ²) = moist weight/per bunch x number of bunch/m ²	cut all plants from defined areas (min 50 x 50 cm)
	Dry weight per bunch (g)	objective is to measure the bunch water content (= Dry weight per bunch / Moist weight per bunch * 100)	oven (105° during 24 hours)
Leaf parameters	Number of leaves per stem		
	Leaf length (cm)		
	Leaf width (cm)		
Panicle parameters	Number of panicles per bunch		
	Number of grain/pan.		
	Moist w. of a pan.		

Table 3.9. Rice crop calendar in 2007.

Crop	12	1	2	3	4	5	6	7	8	9	10	11	12
WS	←			→									
SA					←			→					
AW										←			→

← Seeding dates

→ Harvesting dates

All field works were accomplished during or near the time of the satellite pass. The location of rice fields were identified on the reference map scale of 1:50,000 and measured on the ground using hand-held GPS receivers with a location accuracy of approximately 10 meters.



Figure 3.16. Photographs of drying the rice plant.

3.4.3 Climatic data and maps

The following daily meteorological data at An Giang gauge station were collected during the year 2007: temperature (max, min); irradiance; vapour pressure; wind speed; precipitation. These parameters were intended to be used to predict the rice yield in the agro-meteorological model-based method if there is a good correlation between in situ rice biomass and radar backscattering coefficient.

Topographic maps with a scale of 1:50.000, published by the Department of Survey and Mapping of Ministry of Natural Resource and Environment, and their digital maps were used to establish base map GIS data layers, such as water bodies, road network, administrative boundaries, etc.

The existing land use map of An Giang province (Figure 3.17) prepared in the year 2005 was sourced from the An Giang Department of Natural Resources and Environment (AGDONRE, 2005). This map was used for setting up sample areas and as reference data for accuracy assessment of rice classified images.

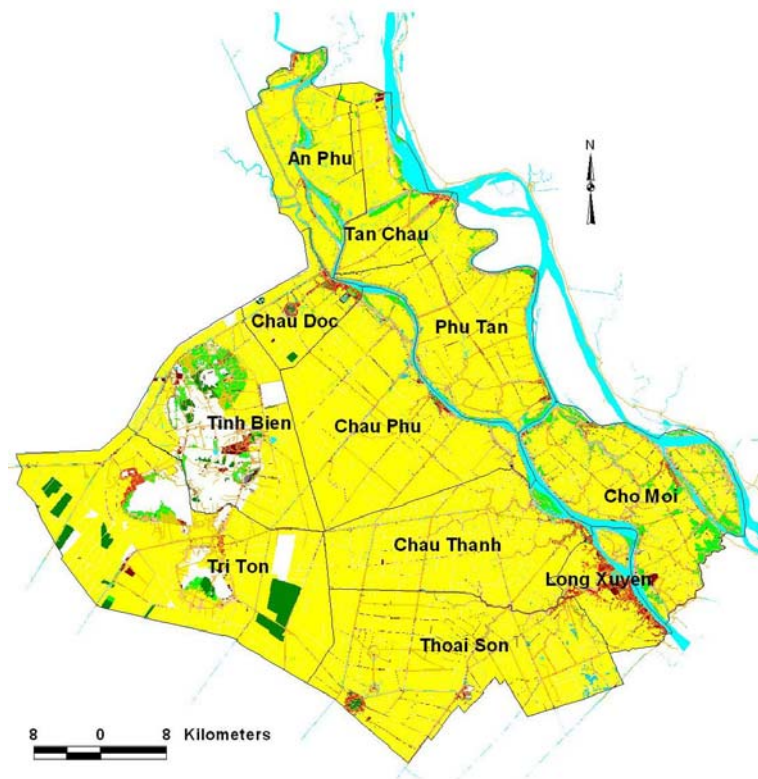


Figure 3.17. Land use map in 2005 of An Giang province (rice in yellow colour)

3.4.4 Data processing software

The use of specific software modules, e.g. the ESA software BEST (Basic Envisat SAR Toolbox) (ESA/ESRIN, 2009), was explored. This toolbox was used for the pre-processing steps implemented on Envisat ASAR AP and WS mode imagery as described in the Chapter 4.

ENVI (ITT Visual Solutions) digital image processing software and ArcGIS (ESRI) available at the USQ laboratory were used for the analysis of imagery and maps. ENVI software was used for manipulation and analysis of pre-processing images to map rice crop and estimate the rice yield. ArcGIS was used for GIS data analysis and management.

Chapter 4

ANALYSIS OF RADAR BACKSCATTER OF RICE FIELDS

4.1 Introduction

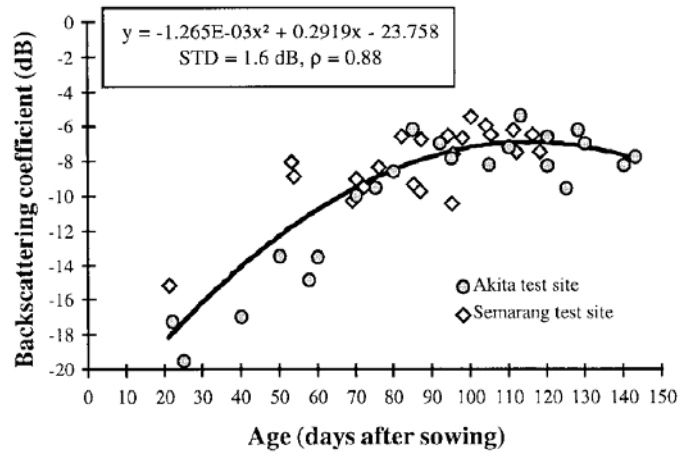
Results from previous experimental and theoretical research discussed in Chapter 2 showed that traditional rice fields presented a large variation in their temporal radar response. Therefore, in this study, the temporal variations of radar response were thoroughly examined with particular focus on understanding the effects of modern cultural practices on rice crop grown in the study site.

The objective of the study presented in this chapter was to analyse: a) the temporal variation of the rice parameters (e.g. plant age and biomass) and of radar backscatter of C-band (HH, VV and polarisation ratios) from ASAR APP data at different growing stages, b) the relationship between rice parameters and radar backscatter, and c) the effect of the cultural practices such as water management, plant structure and density, and rice variety on radar response.

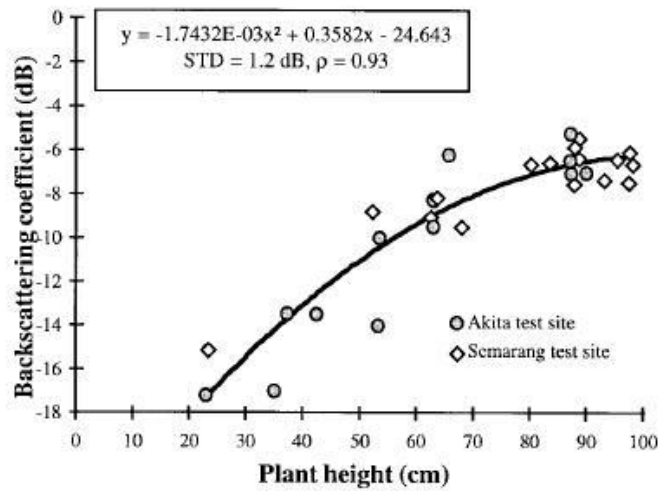
Data previously acquired by different space-borne radar systems provided some correlations with rice crop parameters. For instance, the radar backscattering coefficient at C band measured by ERS, Radarsat and Envisat ASAR was found to be related to rice plant age, height and biomass (an example in Figure 4.1) as reported in the literature (Aschbacher et al., 1995, Le-Toan et al., 1997, Ribbes and Le-Toan, 1998, Li et al., 2004, Bingbai et al., 2005, Chakraborty et al., 2005, Chen et al., 2007).

These parameters retrieved from SAR data were inputs in the rice growth model ORYZA. Two parameters can be derived from SAR imagery: sowing date (via the relationship between the backscattering coefficient and plant age) and plant biomass. The main factors determining the growth rate on a given day are light,

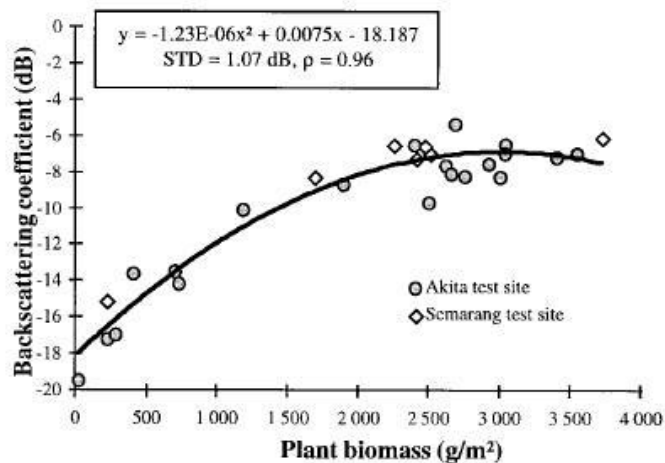
temperature and the variety characteristics for phenological and morphological processes (Le-Toan et al., 1997, Ribbes and Le-Toan, 1999a).



(a)



(b)



(c)

Figure 4.1. Temporal variation of σ^0 by plant age (a), height (b), and biomass (c) (Le-Toan et al., 1997).

The results of the study conducted by Chen et al. (2007) showed that the rice parameters (i.e. rice height and biomass) retrieved from HH and HV polarisation ASAR data had a relatively high correlation with field measurements, with correlation coefficients of 0.83, 0.89, 0.85, and 0.90, respectively. The reason that the correlation at HV is a little higher than at HH may be a saturation effect at HH.

4.2 Methods

Common research methods (i.e. study area selection, description of rice parameters and cropping system, imagery used, etc.) implemented in this study were detailed in Chapter 3. In chapter 4, the following methods were used for the analysis of radar backscatter of rice fields (Figure 4.2): a) collection and surveying at the sampling fields to measure rice parameters, such as plant age, height and biomass, etc.; b) extraction of average backscatter coefficient of sampling fields from pre-processed ASAR data; c) analysis of temporal variation of rice parameters; d) analysis of temporal variation of backscatter coefficient; and e) analysis of the relationship of rice biomass and backscatter coefficient.

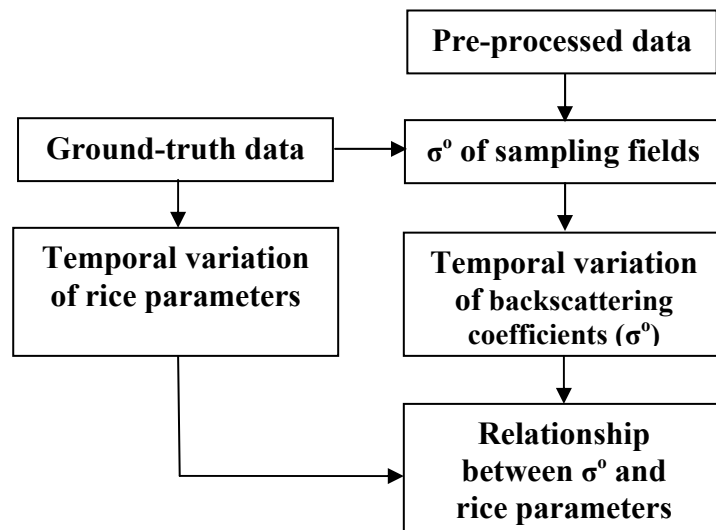


Figure 4.2. Methods for the analysis of radar backscatter of rice fields.

In order to understand the relationship between rice parameters measured from the study area and their radar backscatters, ground data collection were carried

out. In this work, 35 sampling fields were selected on the ground in An Giang province during the first field trip in November 2006. Data collection and measurement were also conducted at the same sampling fields in the year 2007. Methodologies and techniques used to collect rice-related data followed the “*Guidelines for ground data collection for rice monitoring experiments using radar data*” (Le-Toan, 2002) and described in Section 3.4.2 “Ground truth and survey data”. Different rice parameters, such as rice variety, density, plant height, and biomass, were analysed and the relationships between plant height, biomass and the age of rice were established.

Methods for measuring the plant height, rice biomass and yield, for example, are described as follows (Le-Toan, 2002):

- *Plant height*: Place a measuring stick vertically near selected plants. Take a sufficient number of measurements to obtain a representative height value from the ground to the top of the canopy. The ground level is the water air interface for flooded fields, and soil air interface for non flooded fields. A minimum of five measurements are recommended for relatively uniform canopies. This number should be increased as canopy variability and/or the area measured increase.
- *Rice biomass*: Cut all plants from a pre-defined area. (If plant density is known, it is preferable to randomly select a number of individual plants for biomass determination). If applicable, separate plants into components (stems, leaves, fruits) and place into separate containers (plastic bags, etc.). Weigh each component within a few hours. Dry the plants at 70°C until constant weight is reached and weigh again. From the two masses and the known sampled area, wet and dry biomass can be calculated.
- *Yield*: When the rice is harvested, the rice yield information can be collected from the farmer. Unit: kg/m²

Concerning the pre-processing of ASAR data, it consisted of a) image calibration or conversion to the radar backscattering coefficient sigma nought (σ^0); b) image geo-correction; and c) image spatial filtering.

Image calibration consists of correcting SAR images for incidence angle effect and for replica pulse power variations to derive physical values. This transformed SAR precision images into intensity images expressed in σ^0 . *Image geo-correction* was performed to reproject the calibrated images to the selected cartographic projection, i.e. UTM, ellipsoid WGS-84. *Spatial filtering* was then done to reduce the speckle effect in the image. In this work, the enhanced Frost spatial filter was applied to each image due to its known ability to reduce speckle and preserve texture information (Lopes et al., 1990, Shi and Fung, 1994, Li et al., 2003, Thiel et al., 2007). The software BEST - Basic Envisat SAR Toolbox (ESA/ESRIN, 2009) and ENVI (ITT Visual Solutions) were used for these processing steps.

The value of the radar backscattering coefficient for the sampling field was derived from pixels' average values extracted from the pre-processed ASAR APP images. Then, the polarisation ratio (Ra) was computed on the basis of the following formula (4.1):

$$Ra = \sigma_{HH}^0 - \sigma_{VV}^0 \quad (4.1)$$

where: σ_{HH}^0 is backscattering coefficient of HH data in dB

σ_{VV}^0 is backscattering coefficient of VV data in dB.

The temporal rice backscatter behaviour during crop seasons in the year 2007, such as WS, SA, and AW, were analysed for HH, VV, and polarisation ratio data. The effects of water management, rice varieties, plant structure and density (which were observed on the ground during the satellite pass) on radar response, were taken into account. Finally, the relationships between rice biomass and backscattering coefficient of HH, VV, and polarisation ratio were established.

4.3 Results and discussion

4.3.1 Rice parameters

For the WS, SA and AW 2007 crops in the study area, the farmers used various rice varieties (e.g. Jasmine, IR 50404, OM 2514, OM 2517, OMTH1, CS 2000, etc.) of short cycle ranging from 86 to 106 days with the mean of 97 days. In

the sampling fields, the dominant varieties grown were Jasmine (34%) and IR 50404 (21%) (Figure 4.3). Direct seedling method was dominant at about 80% of the selected fields. In each sampling area, the sowing/transplanting dates differ between the sampling fields from 0 to a maximum of 9 days.

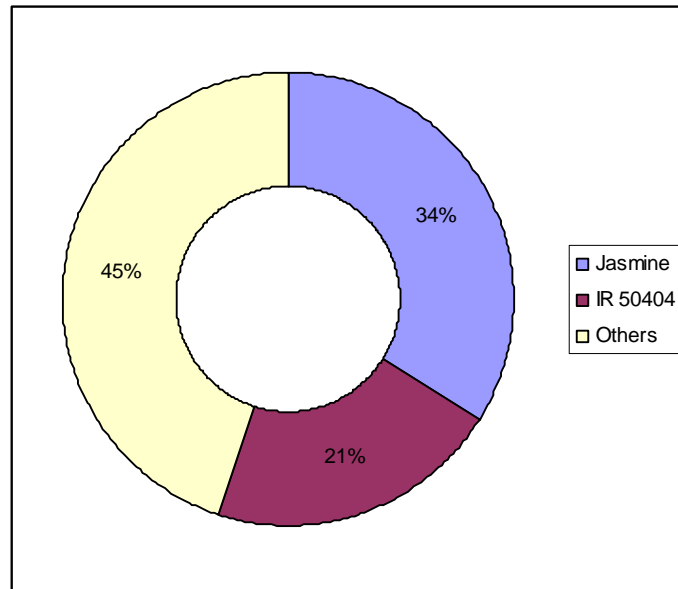
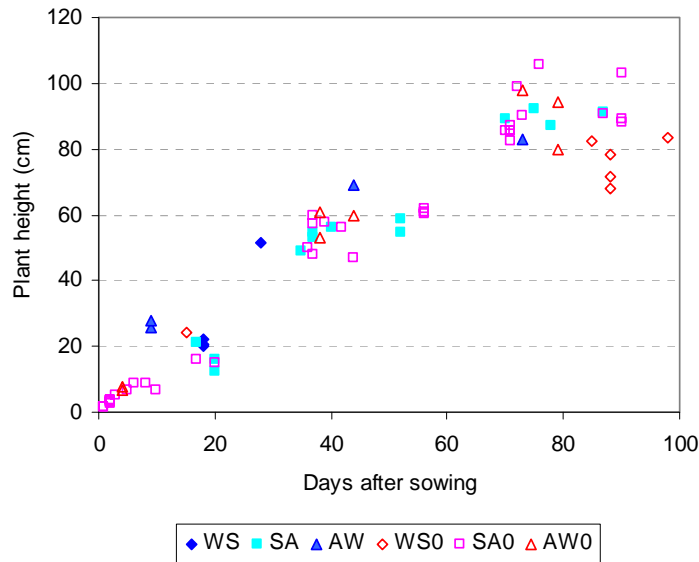


Figure 4.3. Percentage of rice varieties grown in WS, SA, and AW 2007 crops of the sampling fields.

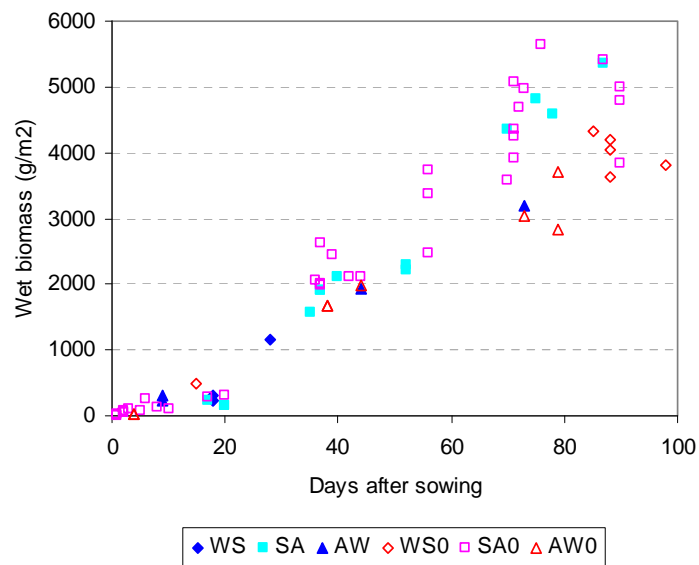
Among the sampling rice fields, five fields grown in WS, 16 in SA, and four in AW crop were selected for the analysis of their radar backscatter in the year 2007. The other fields were not chosen because: a) the radar response of some fields was not homogenous in terms of backscatter; and b) the sampling fields grown in AW crop were only in Cho Moi district (i.e. ten fields).

The height of rice plant was measured at the SAR acquisition date and plotted in Figure 4.4a. Two categories were distinguished: fields with standing water (indicated as WS, SA and AW), and fields without standing water (indicated as WS0, SA0, and AW0). The height was measured from the top of the plant to the ground or water level. Since the water layer (when present) ranged from 1 to 9 cm thick (with an average of 3.2 cm), the difference between plant height in fields with and without water does not seem significant. The plant height increases up to 80 –

100 cm, at about 70 days, where it started at 100 days for long cycle rice (Le-Toan et al., 1997).



(a)



(b)

Figure 4.4. Temporal variation of plant height (a) and biomass (b).

There were no readings taken for WS crop during the first 18 days of growth. This is because the rice parameters need to be measured as close as possible to each imaging date (i.e. in many cases, 1 or 2 days are acceptable) and satellite pass, and to acquire an APP image every 35 days.

The plant densities of sampling fields measured at the middle of the season have average values of 928, 850, and 750 stems per square meter in WS, SA and AW crops, respectively (Figure 4.5). In comparison, the plant density of 200 stems per square meter was observed in traditional practiced rice fields at the same stage (Le-Toan et al., 1997). Therefore, the average plant density in the study area, where direct seeding dominated, was about four times higher than that of traditional transplanting rice.

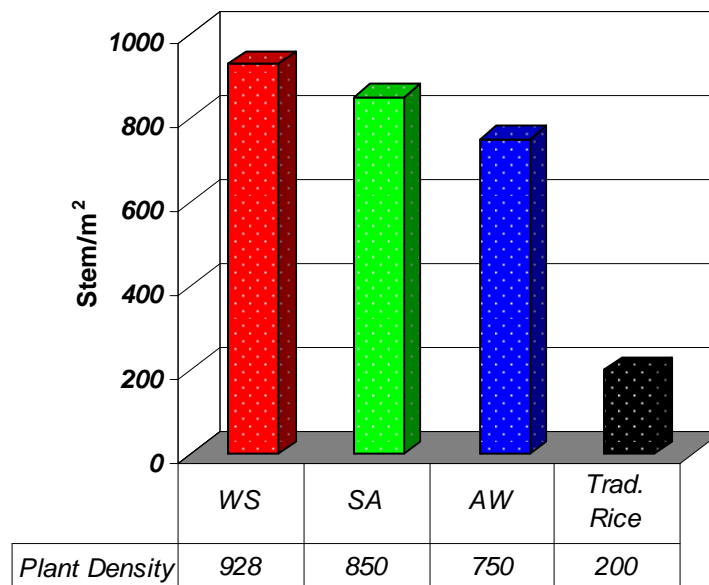
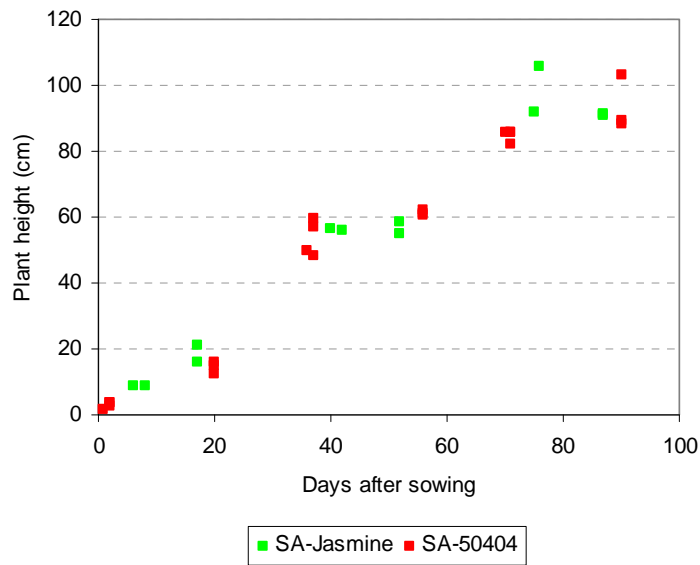


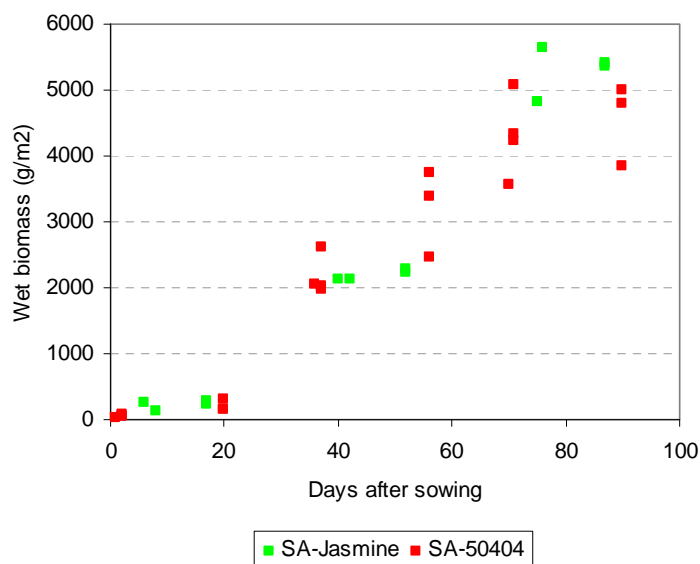
Figure 4.5. Average plant density of sampling fields at the middle of the WS, SA, AW crop seasons and of traditional practiced rice fields.

In the SA crop, the rice biomass increased steadily during the growing stage (vegetative stage and continue at the reproductive stage) and reached the maximum values of about 5000 g/m² or more at the final stage (harvest). For the WS and AW rice crops, a maximum value of 4000 g/m² was observed (Figure 4.4b). In comparison, the plant wet biomass in Akita, Japan (Kurosu et al., 1995) and in Semarang, Indonesia (Le-Toan et al., 1997) showed an increase until the reproductive phase. The maximum biomass value obtained by these previous studies was around 3500 g/m², which was lower than that of the fields cultivated by modern practices. This could be explained by the higher plant density of the modern cultivated rice fields as explained in the above paragraph, the use of fertilizer, and the rice varieties of higher yield.

The plant height and rice biomass of the two dominant rice varieties, i.e. Jasmine and IR 50404, in the same crop season SA were analysed (Figure 4.6). While the temporal increase of the height was similar, the rice biomass showed some differences between the two varieties. Overall, Jasmine attained more than 5000 g/m² while IR 50404 was lower than 5000 g/m² at the final stage of the SA season.



(a)



(b)

Figure 4.6. Temporal variation of plant height (a) and biomass (b) in SA crop of Jasmine and IR 50404.

4.3.2 Analysis of temporal radar backscatter as a function of rice parameters

With the traditional method, the fields are flooded at the onset of the rains or with the arrival of irrigation water, in order to prevent weeds and pests. The water depth varies from 2 to 15 cm, with an average of 10 cm. The rice plants are sown in nurseries before transplantation. After 25 to 35 days depending upon labour availability, the plants are transplanted in clusters of one to ten plants and planted in line (ten to 20 clusters per m²) (Le-Toan et al., 1997).



Figure 4.7. An example of field samples a week after sowing (no-water, very wet soil with surface roughness).

With the present technique of direct sowing, the grains were sown at a high density directly in wet soil (Figure 4.7). At the early stage of the rice crop cycle, the fields in the test area were wet soil. After 10-20 days, the fields were filled with water. Table 4.1 showed values of backscatter at HH and VV at the dates around 15-20 days. For fields not yet irrigated, such as field WS01, the radar backscattering coefficient was high, with values ranging from -7 dB to -2 dB in both HH and VV polarisation (Figure 4.9). This high backscatter resulted from wet and rough soil surface. When the fields were flooded as seen in Figure 4.8 (e.g. fields WS1, WS2, WS3), the backscatter decreased significantly, with HH ranging from -7 to -9 dB and

VV from -11 to -15 dB. The low backscatter resulted from the backscattering from water surface, attenuated by the plant. VV was more attenuated by vertical stem and has lower values than HH.

Table 4.1 Effect of water on radar backscattering at early stage in WS 2007 crop.

Sample name	Age (day)	Water height (cm)	σ°_{HH} (dB)	σ°_{VV} (dB)
WS1	19	7.0	-9.1	-14.9
WS2	19	5.0	-9.1	-13.6
WS3	19	2.0	-7.2	-11.6
WS01	16	no-water	-3.3	-6.3



Figure 4.8. Field sample with standing water at about 20-day after sowing.

Backscatter temporal variations of HH and VV polarisation data for the three rice crops WS, SA, and AW in the year 2007 were presented in Figure 4.9 and described as follows:

- 1) At the beginning of the rice season (<20 days after sowing), i.e. the first half of the vegetative stage, flooded and non-flooded rice fields had low and high backscatter, respectively (with the exception of two data points, most likely due to field observation performed before the exact flooding time),

2) During the period of 20-70 days, i.e. the second half of the vegetative stage and the reproductive stage, flooded and non-flooded fields had similar high backscatter response.

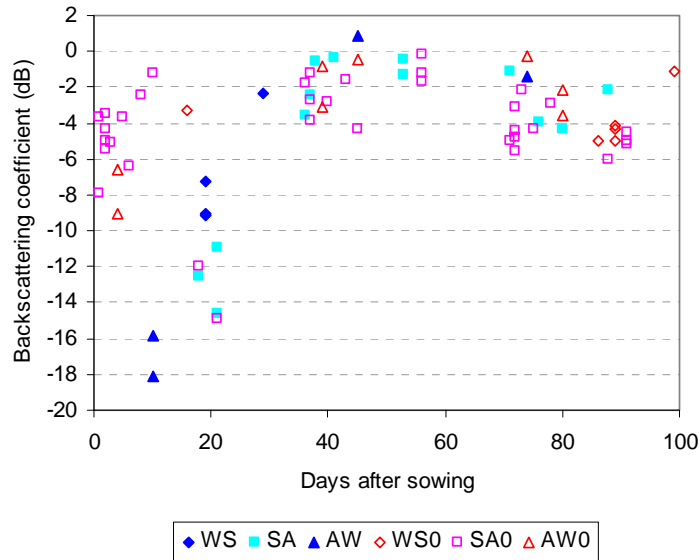
It was expected that in flooded fields, the plant-water double bounce interaction should be dominant, thus the backscatter of flooded fields should be higher than that of drained fields. A possible explanation could be due to the high density of the plants (as explained in Section 4.3.1 “Rice parameters”), or the contribution of volume scattering and multiple plant-ground scattering become important. $HH > VV$ was as expected, linked to attenuation of the waves by the vertical plant elements. However, the most surprising feature was the very high value of HH (0 to -2 dB), not often seen in natural surfaces.

3) During the period from 0 to 70 days, i.e. from sowing to heading, the plant structure remained mostly erectophile. The stems were quasivertical and the leaves had a small insertion angle (5-20°) (Le-Toan et al., 2003). The temporal increase of SAR backscatter at two consecutive data acquisition dates (e.g. 35 days with Envisat) was high if the fields were flooded at both dates, i.e. 18 dB at HH and 11 dB at VV as the maxima observed, if the fields were flooded and without much vegetation at the first date. In contrast, if the field was not flooded at the first date, a variable increase was observed at HH (0 to 8 dB), and a variable decrease (0 to 6 dB) at VV . Consequently, the backscatter temporal change was not considered a robust rice classifier.

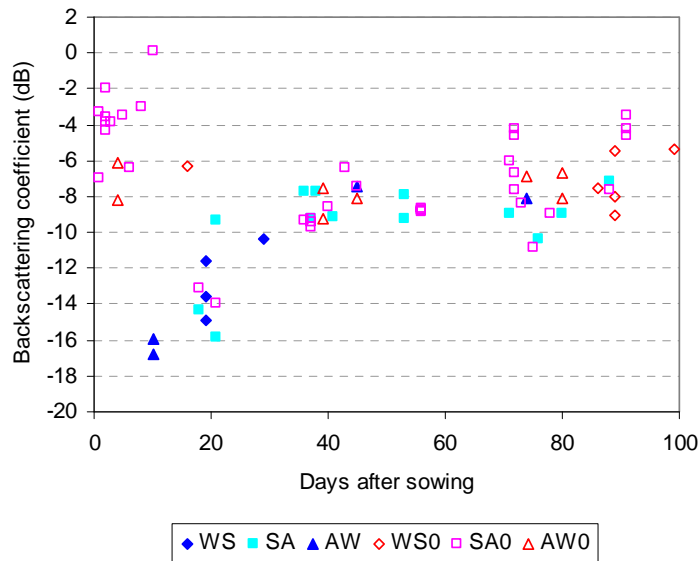
4) After the age of 70 days, i.e. the ripening stage, the growth (height and biomass) stopped and the leaves changed their orientation to be no more erectophile (i.e. their insertion angles were typically 30-40°) (Le-Toan et al., 2003). Most backscattering coefficient values of the rice fields without water were slightly lower (around 2 dB) in HH and higher (around 2 dB) in VV compared to that of fields with standing water (Figure 4.9).

5) The polarisation ratio was presented in Figure 4.10. In general, the ratio increased until the period 30-70 days, then decreased until harvest. The most striking

observation was the high value of the ratio (4.6 to 7.8 dB for flooded fields). However, fields without water at the SAR overpass had large dispersion of the ratio values, varying from -1.4 to 6.5 dB.



(a) HH



(b) VV

Figure 4.9. Backscatter temporal variation of HH (a) and VV (b) in WS, SA and AW 2007 crops of the fields with water and without water.

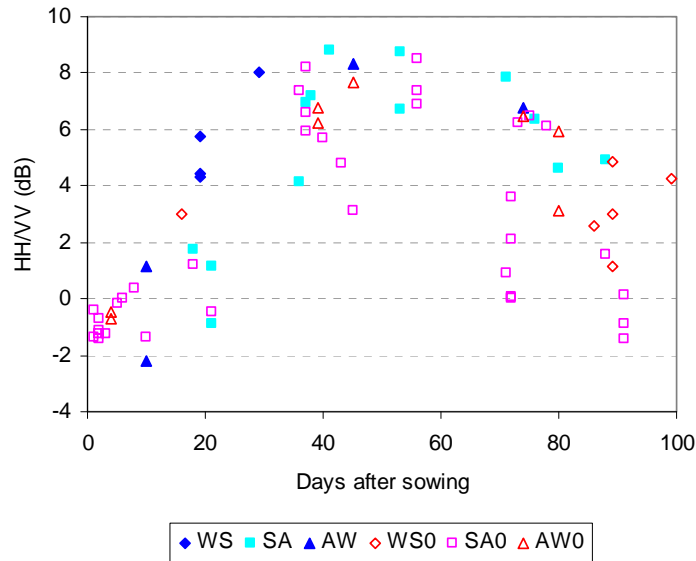
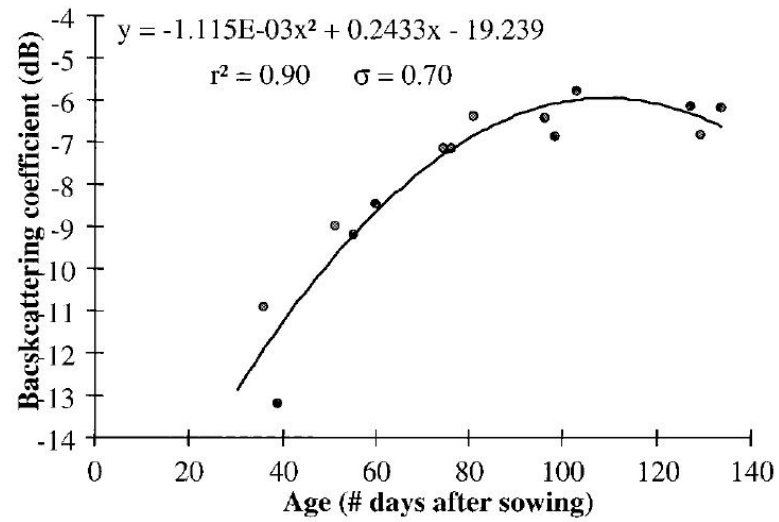
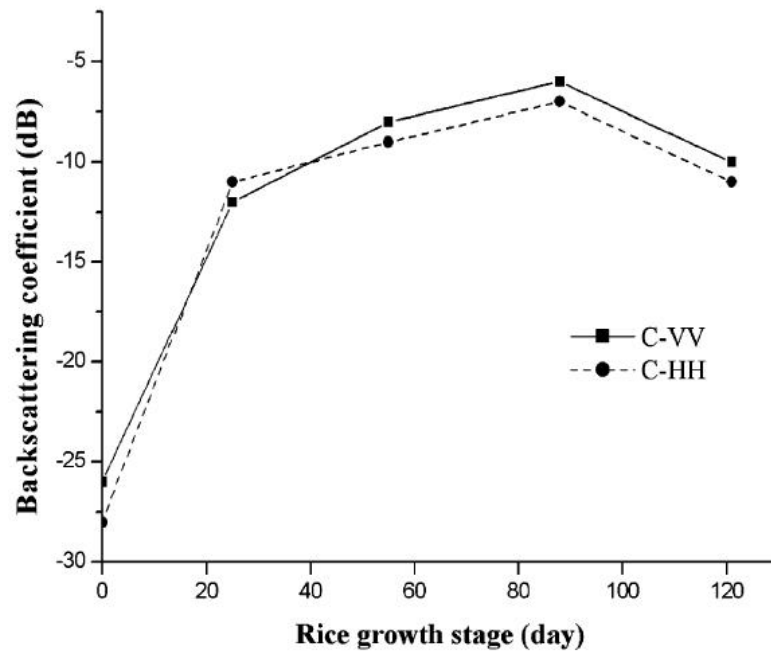


Figure 4.10. Temporal variation of HH/VV ratio in WS, SA and AW 2007 crops of the fields with water and without water.

In this study, HH, VV and HH/VV radar values were not significantly related to modern practiced rice fields with coefficients of determination r^2 of 0.229, 0.161, and 0.645, respectively. In contrast, previous studies on traditional practiced rice fields reported that the backscattering coefficient (analysed as a function of age), such as (Ribbes and Le-Toan, 1999b), showed a coefficient of determination of 0.90 for the case of Radarsat HH data (Figure 4.11a). The maximum backscattering coefficient -6 dB of HH data of traditional cultivated rice fields was observed for the cases of Radarsat (Ribbes and Le-Toan, 1999b) and Envisat ASAR (Chen et al., 2006). In contrast, after the age of 20 days, the minimum backscattering coefficient of HH data of modern cultivated rice was -6 dB.



(a) HH



(b) HH, VV

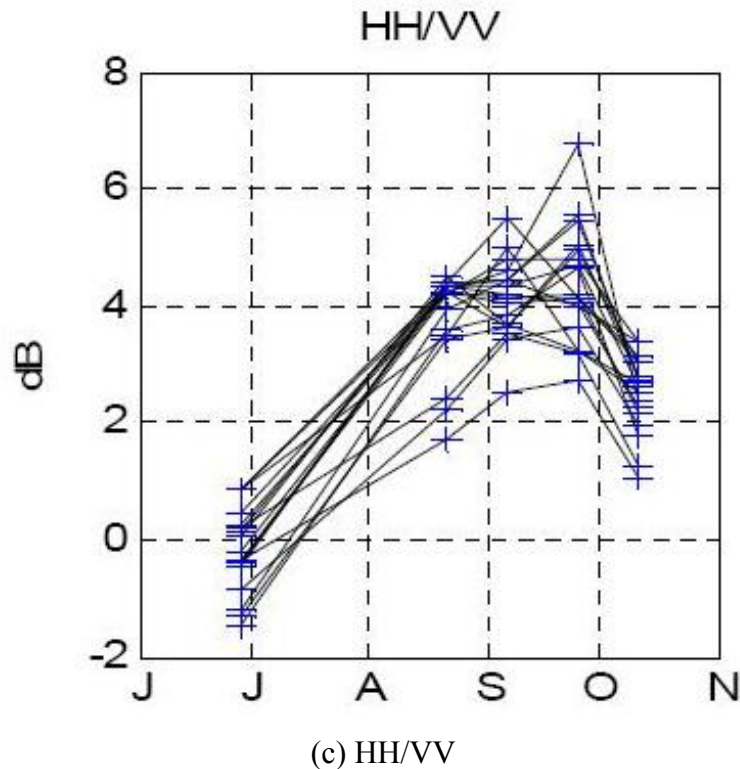
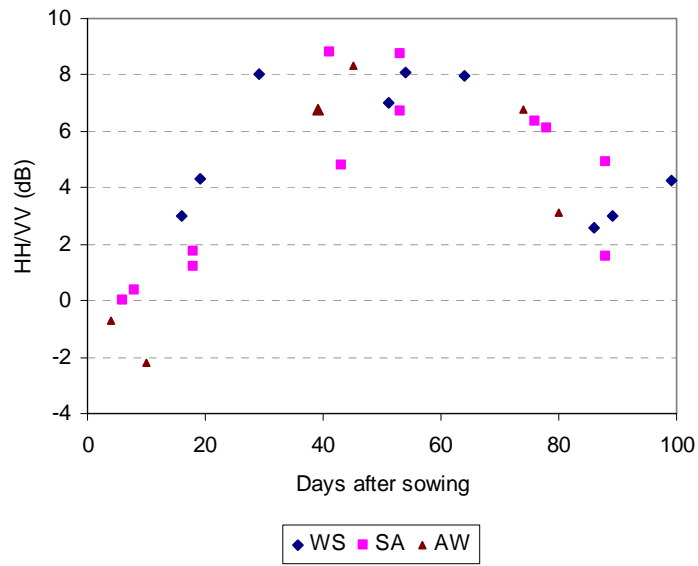


Figure 4.11. Backscatter temporal variation of HH (a), VV (b), and HH/VV ratio (c) of the traditional practiced rice fields (Ribbes and Le-Toan, 1999b, Bouvet et al., 2005, Chen et al., 2006).

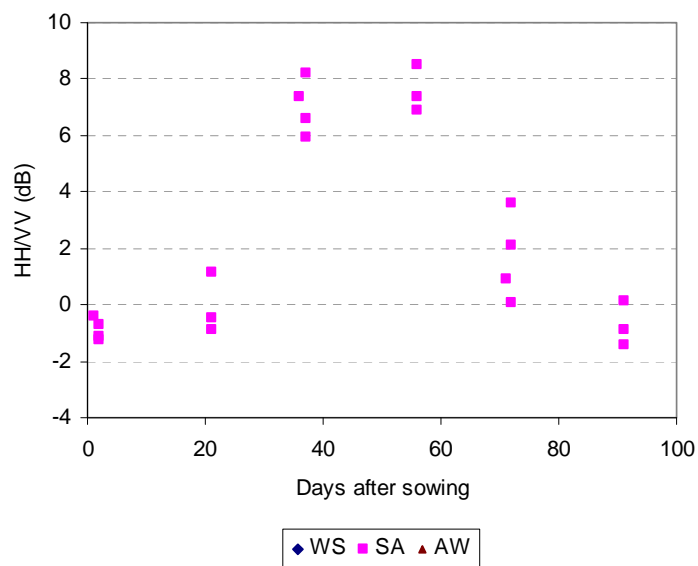
The causes of the difference between radar backscatter of traditional practiced rice fields and of modern practiced rice fields may be due to flooding condition and plant density (as explained in the above paragraphs), plant structure and rice variety (as discussed in Section 4.3.3 below).

In fact, since 2005, the Water-Saving Work Group of the Irrigated Rice Research Consortium (IRRC), in collaboration with Vietnam's Plant Protection Department, established activities on water management and water-saving in rice in the Mekong River Delta (Mendoza et al., 2007). The farmers have, on average, two fewer pumping operations during the season to irrigate their fields than the past regular practice of continuous flooding.

4.3.3 Effect of plant structure and rice varieties



(a)



(b)

Figure 4.12. Temporal variation of HH/VV ratio of Jasmine (a) and IR 50404 varieties (b) in WS, SA and AW 2007 crops.

Plant structure and different rice varieties can have an impact on radar response (CCRS, 2007a). The polarisation ratio can have lower values when the plant structure deviates from vertical. For example, for plants affected by wind, the decrease could be 2 dB (see Figure 4.12a and 4.12b at the ripening stage). This could be due to plants in lodging (rice plants falling over) as recorded in field samples. In

fact, nine sampling fields grown from IR 50404 variety in Vinh Chanh and Phu Hoa villages were measured with stem inclination of $10^{\circ} - 45^{\circ}$ (28° in average value) at the ripening stage (Figure 4.13b). In comparison, stem inclinations ranging from 5° to 15° (with mean of 9°) were observed at the same stage from seven other fields where Jasmine seed were planted (Figure 4.13a). The radar response of those plants decreased in comparison with vertical rice plants in HH (below -4.5 dB), and increased in VV polarisation (above -6.0 dB) (see Figure 4.9) because rice stems were not vertical at the maturation stage.



(a) Jasmine



(b) IR 50404

Figure 4.13. Sampling fields with plants in quasi-vertical structure (a) and lodging (b) at the end of SA crop.

The differences in plant structure were also related to rice varieties. As plotted in Figure 4.12b, most of IR 50404 rice variety (grown in SA crop only) was characterised by a very low HH/VV (0 dB or less) at the end of the rice crop, whereas Jasmine species with a quasi-vertical structure had higher ratio (Figure 4.12a) at the same stage of the rice season.

4.3.4 Radar backscatter and rice biomass

In traditional rice cultivation system, radar backscatter was found to be strongly correlated to several rice parameters (Le-Toan et al., 1997), e.g. a coefficient of determination r^2 of 0.81 between Radarsat HH backscatter and rice biomass in Figure 4.14 (Ribbes and Le-Toan, 1999b). Backscatter of rice fields increased steadily during the growing stage and then reaches a saturation level. This temporal variation of radar response had proved to be effective for rice crop monitoring. Radar backscatter can increase by more than 10 dB from the beginning of the crop (flooded fields) to the saturation level (Kurosu et al., 1995, Le-Toan et al., 1997, Inoue et al., 2002, Choudhury et al., 2007).

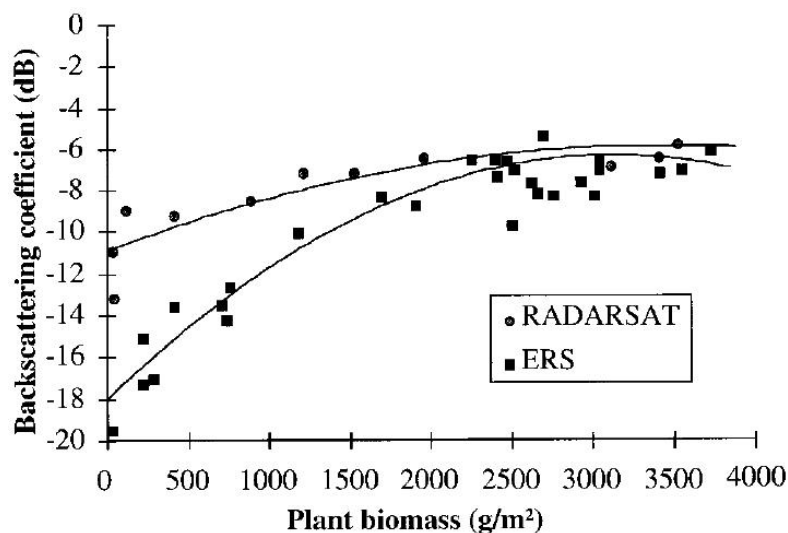
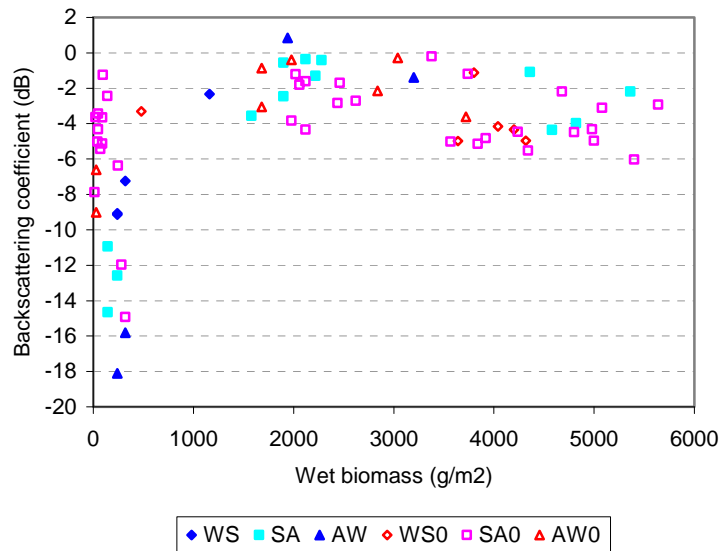


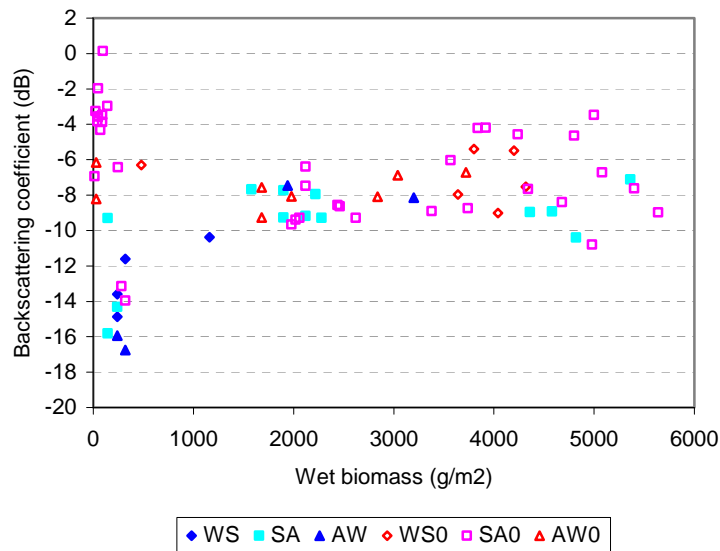
Figure 4.14. Radar backscattering of Radarsat and ERS data vs. plant wet biomass in traditional practiced rice (Ribbes and Le-Toan, 1999b).

In the study of Ribbes and Le-Toan, (1999a), the rice growth model ORYZA1 was used to simulate rice growth with the sowing date and rice biomass values retrieved from ERS and Radarsat SAR data as input parameters. The coupling of

SAR data and ORYZA model gave good results for rice yield estimation. Choudhury et al., (2007) recently used dual polarisation ASAR data. A linear relation between polarisation ratio (HV/HH) and fresh biomass was found in the case of regular practice in the Bardhaman, India, even though Envisat data were acquired during vegetative stage, rice biomass could be retrieved with less uncertainty as HH alone shows saturation before maturity stage.



(a) HH



(b) VV

Figure 4.15. Radar backscattering of HH (a) and VV (b) vs. plant wet biomass in WS, SA and AW 2007 crops.

For this present study, an analysis of the relationship between radar backscatter and rice biomass in the study site of An Giang was carried out. Figure 4.15 showed the HH and VV data as a function of biomass with a coefficient of determination of 0.374 and 0.019, respectively. HH and VV polarisation data increased strongly until the plant fresh biomass reached 1000 g/m² (at 30 days after seeding). However, for non-flooded fields, the increase in HH was smaller and VV even decreased. A saturation level of backscatter was reached at around 2000 g/m² at the middle of crop cycle. After saturation level, radar backscatter remains stable and slightly reduced for HH and rose for VV until biomass gets to maximum values.

Figure 4.16 shows the polarisation ratio (HH/VV) as a function of rice biomass having a coefficient of determination of 0.494. Only the increase of HH/VV at the beginning of the season was clearly observed, however, this increase was restricted to the first month or a limit of 1000g/m². After this date, the backscatter of non-flooded fields had a large dispersion (no correlation) with respect to biomass. Figure 4.15 and 4.16 showed that HH, VV and HH/VV were not strongly related to plant biomass as in the reported traditional rice results (Figure 4.17), and thus retrieving rice biomass using HH, VV or HH/VV was not applicable to modern rice practices.

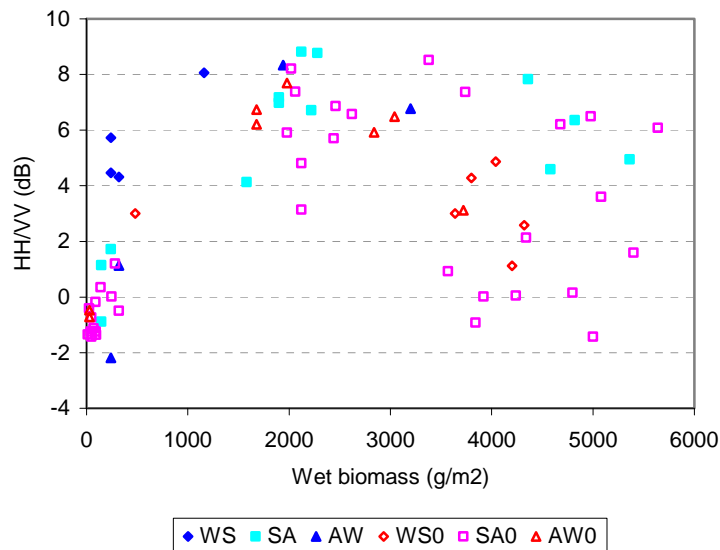


Figure 4.16. Polarisation ratio vs. plant wet biomass in WS, SA and AW 2007 crops.

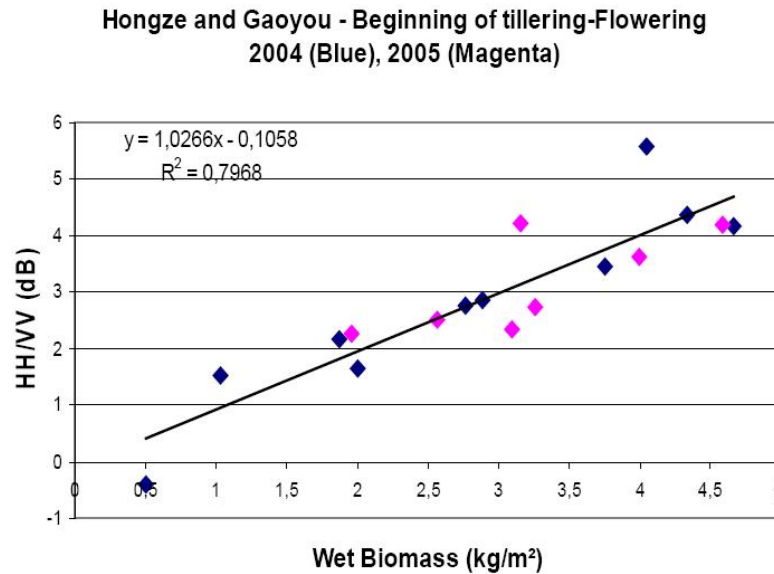


Figure 4.17. Polarisation ratio vs. plant wet biomass in traditional practiced rice (Le-Toan et al., 2005).

4.4 Conclusion

As a consequence of changes brought by modern cultural practices, such as direct seedling, high plant density, short cycle rice varieties, high rice biomass, and water management, the radar backscattering behaviour was much different from that of the traditional rice plant previously reported in scientific literature. At the early stage of the season, direct sowing on fields with rough and wet soil surface provided very high backscattered values for both HH and VV data (about -7 to -2 dB). Around 10 – 20 days after sowing, rice plants attained more or less 20 cm high and field flooding decreased dramatically the backscatter to -18 to -12 dB. The backscatter then increased and reached a saturation level (-2 to 1 and -9 to -7 for HH and VV, respectively) in the middle of crop cycle. The very high value of HH and the similar response of flooded and non-flooded fields were explained by the high plant density. At the end of crop season, radar backscattering of the rice fields without water was slightly lower in HH and higher in VV when compared to that of fields with standing water.

As a result, methods using the temporal change of HH and VV will not work for fields which are not inundated at the beginning of the season. However, the polarisation ratio HH/VV was found to be a potentially good rice classifier during

the period of 30 days to 60 days after seeding in the study area, i.e. during the second half of the vegetative stage and the first half of the reproductive stage for 100-day rice variety.

HH, VV and HH/VV were not strongly related to plant biomass (coefficient of determination of 0.374, 0.019, and 0.494, respectively) as in the reported results for traditional rice. This is explained by the effect of water management, plant density and structure. As a result, retrieving rice biomass using HH, VV or HH/VV was not applicable to modern rice growing practices that prevailed in the study area. Consequently, the use of agro-meteorological model and SAR data for yield prediction will not work in this case.

Chapter 5

RICE MAPPING

5.1 Introduction

To identify and map rice fields in traditional cropping system (as reviewed in Chapter 2), a method can be adopted that uses the temporal change between any pair of data required during the crop cycle or between the end of one cycle and the beginning of the following cycle. For modern practiced rice fields in the study area, the previous chapter pointed out that the radar backscattering behaviour is much different from that of the traditional rice plant. Therefore, the methods previously developed for rice mapping may not be adapted to modern rice cropping.

This chapter examined the methods for rice identification and mapping in the study area by using ASAR APP and WS datasets. Based on the discovered relationships between rice parameters and radar backscattering of ASAR APP data in Chapter 4, a *thresholding* method was applied and compared with the different classification methods, such as minimum-distance-to-means, maximum likelihood, spectral angle mapping (SAM), ISODATA, and K-means. The classification accuracies assessed from these methods were compared in order to select the best one for delineating various rice crops in the year 2007 and WS 2008. In addition, the method and results of rice mapping using ASAR Wide Swath (WS) imagery were also discussed.

In the study of Chen et al. (2007), the HH and HV polarisation ASAR dataset of two dates, i.e. April 4 and July 4, 2006, gave the biggest difference of radar backscatter variation between rice and other targets. In these two images, the change of backscattering response of rice field ranged from 8 to 13 dB, while other main ground types were less than 7 dB. Therefore, the ratio image was segmented by a threshold of 7 dB to highlight the rice field. The study showed that the mapping results of the three datasets had a promising high accuracy of a) 77% for the HH in

July and HH in April, b) 81% for the HH in July and HV in April, and c) 80% for the HV in July and HV in April dataset.

Some other recent studies using dual polarisation ASAR data focused on the use of polarisation ratio of single-date image for rice mapping (Bouvet et al., 2005). To assess quantitatively the mapping algorithm, four values of the HH/VV threshold were tested: 1 dB, 1.5 dB, 2 dB, and 2.5 dB. The value of 1.5 dB proved to be the best threshold with about 88% well classified pixels. In another study in China, the threshold classification method was used (Yang et al., 2008). Validation of classification accuracy was implemented by using differential GPS sampling records. The rice identification accuracy was found to be about 84%.

5.2 Methods

Chapter 3 detailed the common research methods implemented in this study. For this present chapter, Figure 5.1 presents the methods examined for rice identification and mapping in the study area by using two ASAR APP and WS datasets. ASAR APP data were firstly used to determine the best method with high accuracy for rice delineation. Then, the proposed method was applied for ASAR WS data, covering the entire agricultural region of the An Giang province.

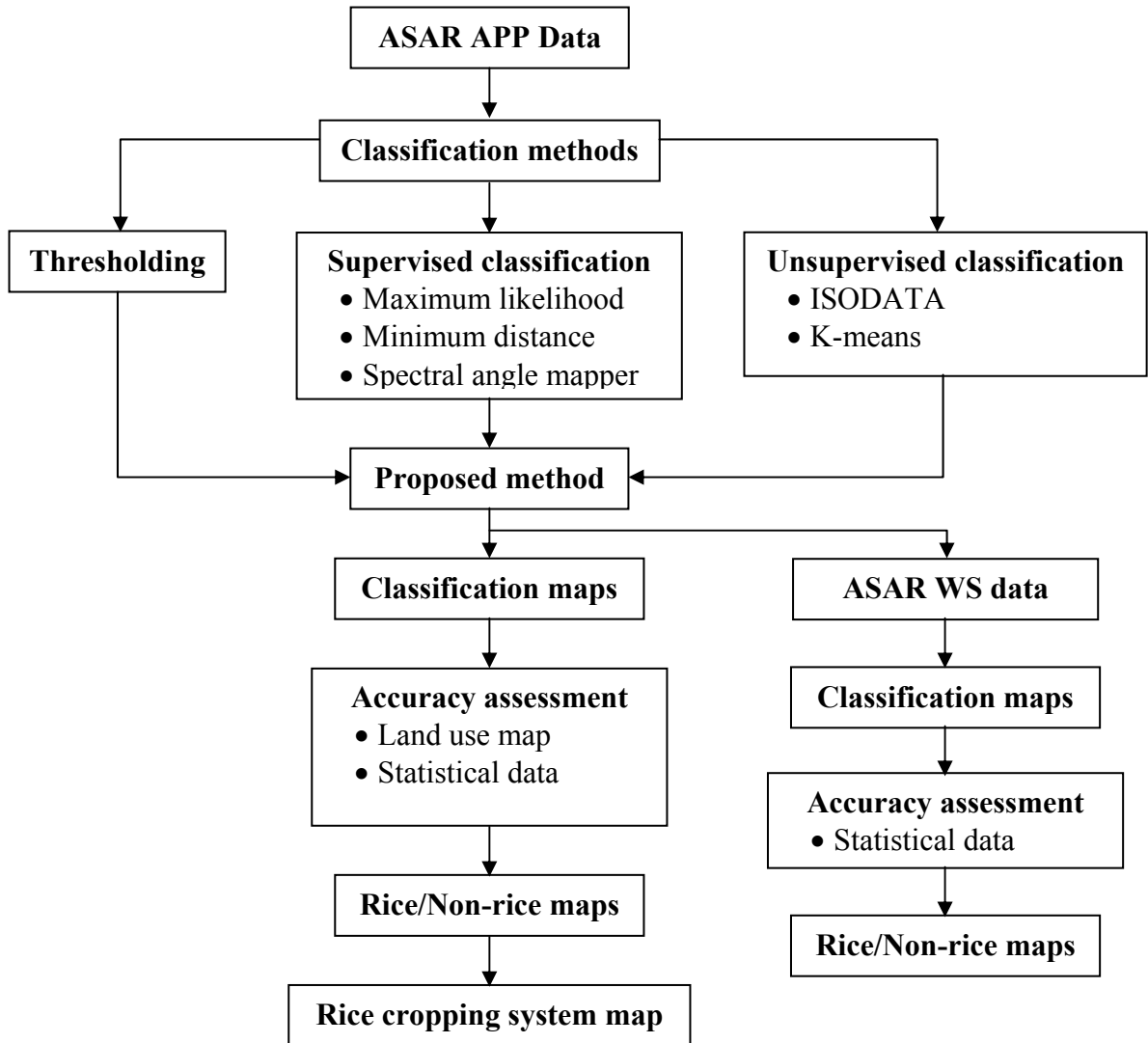


Figure 5.1. Methods for rice mapping.

In previous investigations (Ribbes and Le-Toan, 1998, Liew et al., 1998, Holecz et al., 2000, Chen and Mcnairn, 2006, Lam-Dao et al., 2005, Takeuchi et al., 1999, Le-Toan et al., 1997), the temporal change of the SAR signal was estimated by dividing the intensity values of each pixel between two dates. In order to maximise the intensity ratio (the temporal change), the maximum temporal change (MTC) was calculated using the following equation (5.1) (CESBIO/MATRA-SYSTEMS, 1999):

$$MTC_{i,j} = \frac{Max(I_{i,j,k})}{Min(I_{i,j,k})} \quad (5.1)$$

with

I: intensity value of pixel,

i and j: pixel column and line coordinates respectively,

k: number of the image.

The principle was to threshold the maximum temporal change image to identify image pixels that change by more than x dB in order to produce a rice/non-rice image map. Another approach was to use temporal change behaviour in order to produce monthly harvested rice maps. Combinations of these maps based on crop calendar was used to map the different rice cropping systems (Lam-Dao et al., 2005).

5.2.1 ASAR APP image classification

5.2.1.1 Thresholding method

In many image processing applications, the grey levels of pixels belonging to the object are quite different from the levels belonging to the background. Thresholding becomes then a simple but effective tool to separate objects from the background. This segmentation tool is being used in many research and operational applications (e.g. Bouvet et al., 2005, Yang et al., 2008), so attempts to automate thresholding have been a permanent area of interest. However, several difficulties impede to achieve the desired results for all situations, thus different techniques will have to be tested in order to select those providing the best performance (Javier Marcello, 2004).

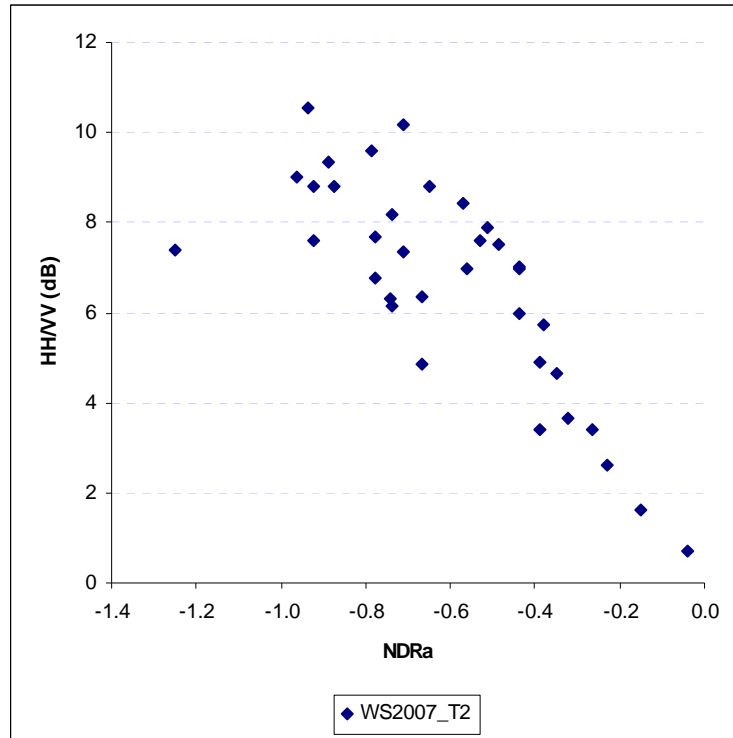
In the context of SAR image processing for mapping the rice area planted in the study site, the thresholding method was applied. The previous results in chapter 4 had shown that: a) methods using the temporal change of HH and VV will not work for fields which are not inundated at the beginning of the season, and b) the ratio HH/VV is a good classifier during the middle period of the rice season, i.e. 30 days to 60 days after seeding, during a second half of the vegetative stage, and the first half of the reproductive stage for 100-day rice variety.

The principle inherent in this method was to threshold the maximum or minimum values of the HH, VV, and HH/VV image to identify image pixels that

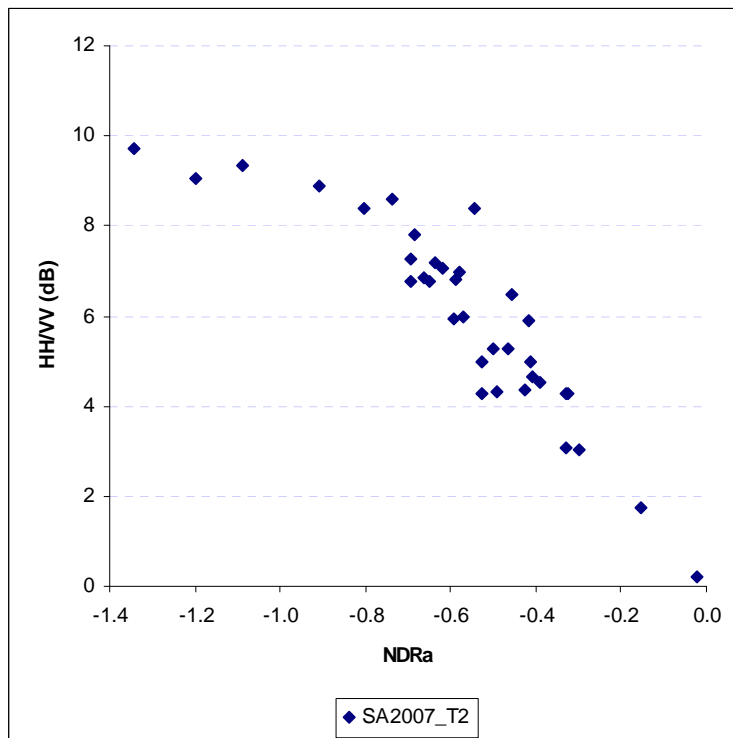
satisfy by more or less than x dB. The following algorithm (5.2) serves as an example:

$$DN_{i,j} = \text{Rice if } \sigma^0 \geq x \text{ dB else } DN_{i,j} = \text{Non-rice} \quad (5.2)$$

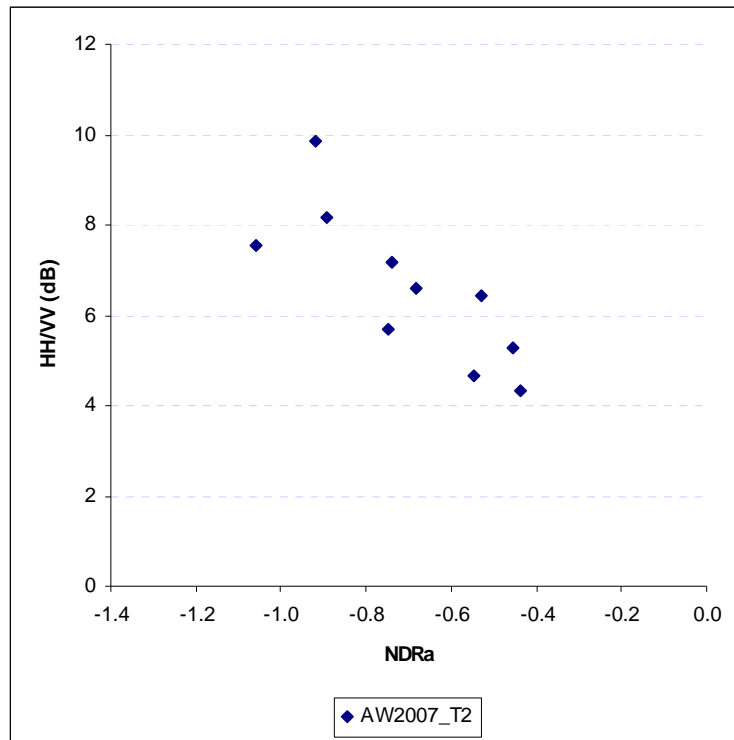
where $DN_{i,j}$ is pixel value of output image.



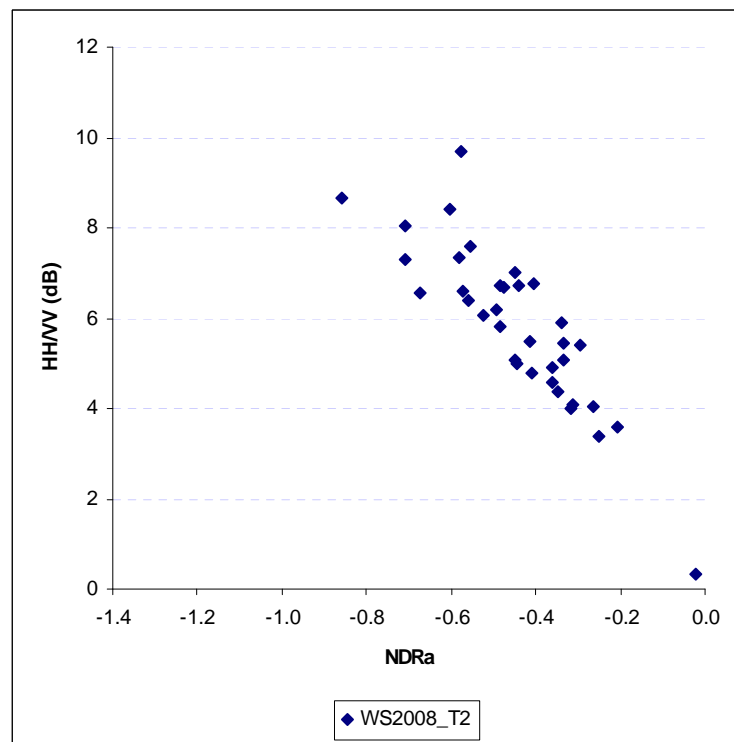
(a) WS 2007 crop



(b) SA 2007 crop



(c) AW 2007 crop

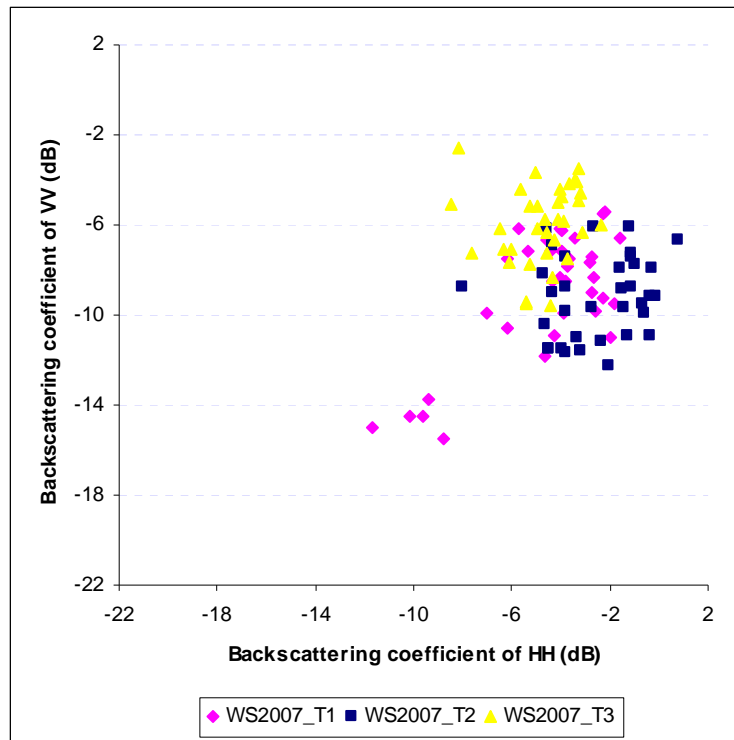


(d) WS 2008 crop

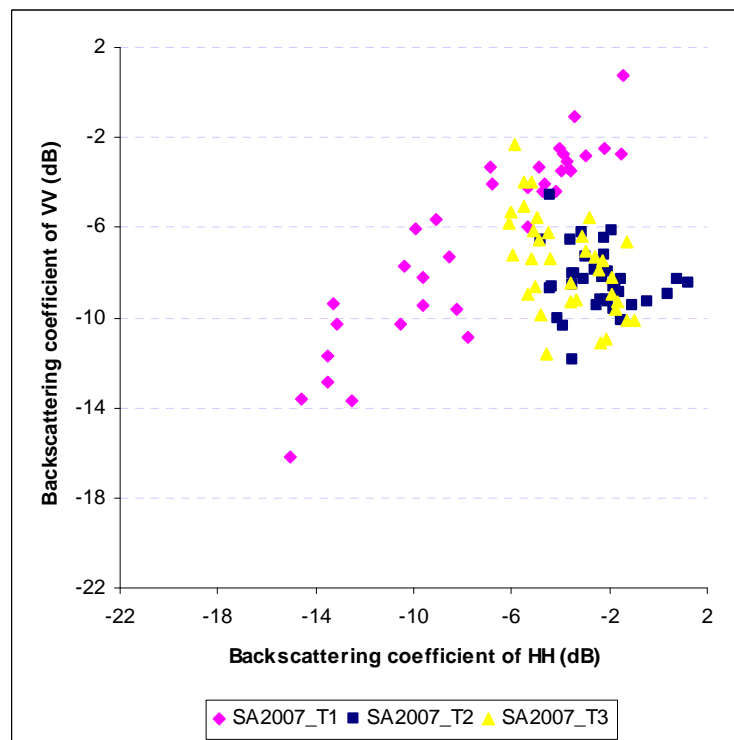
Figure 5.2. Polarisation ratio HH/VV and normalised difference ratio index (NDRA) of the sampling rice planted in WS (a), SA (b), AW 2007 (c), and WS 2008 crops (d) extracted from the images taken in the mid-season.

The polarisation ratios of sampling rice fields derived from the images acquired in the middle of crop seasons (i.e. Feb, Jun, Oct. 2007, and Feb. 2008 images for WS, SA, AW 2007, and WS 2008 crops, respectively, see Table 3.5) were plotted in a Figure 5.2. In most cases, the ratio values of the fields were over 3 dB, except for few points. In WS 2007 crop, five sampling fields located at Vinh Binh village of Chau Thanh district were early sown at the end of November 2006, whereas the image was acquired on 17th Feb. 2007, i.e. more than 70 days after seeding. Therefore, their HH/VV ratio values were around 3 dB or lower (see Figure 5.2a). In contrast, five sampling fields at Long Dien B village of Cho Moi district were started at the beginning of May (SA 2007 crop), whereas the image was taken on 2nd June 2007. Thus, the image was acquired just one month after seeding and four of them consequently obtained the ratio values of 3 dB or less (Figure 5.2b). As a result, an optimum threshold value of 3 dB of HH/VV ratio was determined to segment the rice and non-rice classes using an ASAR APP image collected in the middle of crop season.

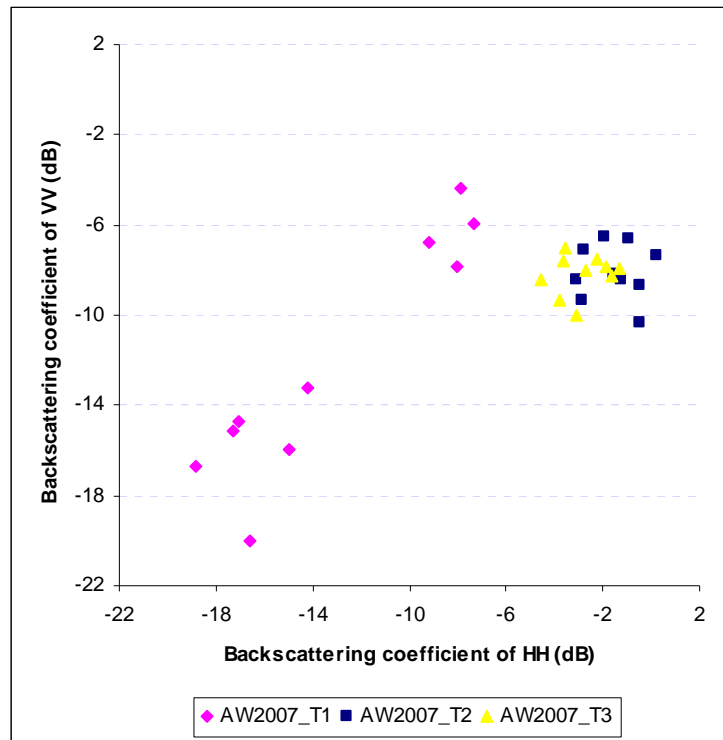
Additionally, thresholds from HH and VV polarisation data were analysed. Figure 5.3 showed that during the middle period of crop season, most radar backscattering coefficients of sampling rice obtained values of -6 dB or less in VV polarisation and higher than -7 or -6 dB in HH polarisation (blue dots with symbol T2 of 35 sampling fields in WS and SA crops and of ten fields in AW crop). Another threshold formulated in this study, i.e. the “*normalised difference polarisation ratio index*” (NDRa), where $NDRa = (\sigma_{HH}^0 \text{ in dB} - \sigma_{VV}^0 \text{ in dB}) / (\sigma_{HH}^0 \text{ in dB} + \sigma_{VV}^0 \text{ in dB})$, were also considered. The NDRa value of -0.2 in the middle of crop season strongly demonstrated that it was an optimum threshold for most sampling fields (see Figure 5.2).



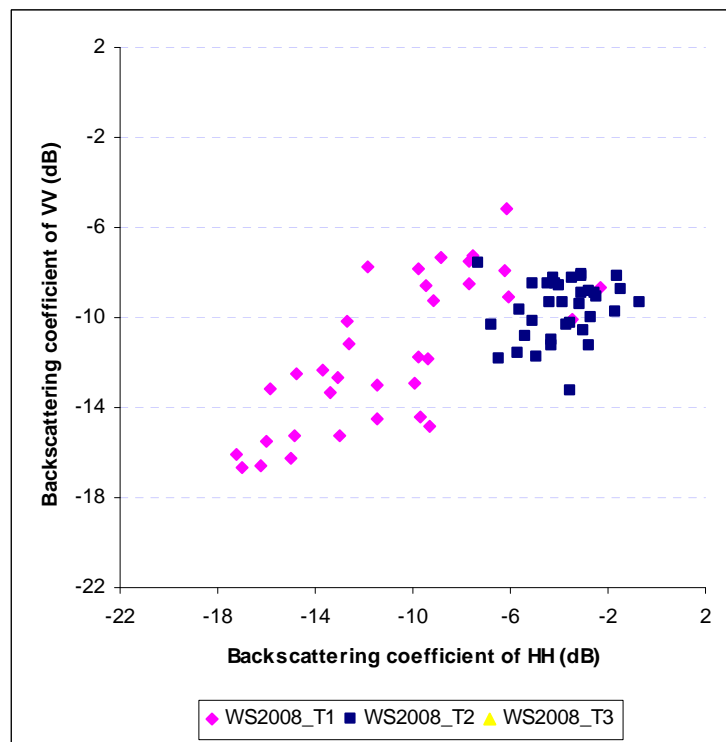
(a) WS 2007 crop



(b) SA 2007 crop



(c) AW 2007 crop



(d) WS 2008 crop

Figure 5.3. Backscattering coefficients of HH and VV data of sampling fields in WS (a), SA (b), AW 2007 (c), and WS 2008 crops (d).

5.2.1.2 Supervised and unsupervised classification methods

There are three basic steps involved in a typical supervised classification procedure: training stage, classification stage, and output stage (Lillesand et al., 2004). In the training stage, the analyst identifies representative training areas and develops a numerical description of the spectral attributes of each land use type of interest in the scene. In the classification stage, each pixel in the image data set is categorised into the land cover class it most closely resembles. After the entire data set has been categorised, the results are presented in the output stage.

Unsupervised classifiers do not utilise training data as the basic classification. Rather, the classifiers involve algorithms that examine the unknown pixels in an image and aggregate them into a number of classes based on the natural groupings or clusters present in the image values. The basic premise is that values within a given cover type should be close together in the measurement space, whereas data in different classes should be comparatively separated. The classes that result from unsupervised classification are spectral classes. The analyst must compare the classified data with some form of reference data to determine the identity and informational value of the spectral classes (Lillesand et al., 2004, Richards and Jia, 2006).

In this work, a number of supervised and unsupervised classifiers were selected for ASAR APP image classification in order to compare their classification accuracies with those derived from the thresholding method. In the case of supervised classification, one-, two- or three-date image taken during the crop growth were used as input data. The principal component (PC) analysis was first applied to three-date image, and PC1, PC2, and PC3 data were then selected for classification. A set of training data (rice and other non-rice classes, e.g. annual plant, perennial plant, forest, rural area, urban area, water bodies) were delineated from the images based on the existing land use map. The selected classifiers were minimum-distance-to-means, maximum likelihood, and spectral angle mapper. Similarly, two clustering algorithms, K-means and ISODATA, were also examined. To reduce the processing time, a subset of three districts in An Giang province (Phu Tan (PT), Chau Phu (CP) and Chau Doc (CD)) was included.

In the case of the minimum-distance-to-means classifier, first the mean (or average) spectral value in each band for each category is determined. Then a pixel of unknown identity may be classified by computing the distance between the value of the unknown pixel and each of the category means. The minimum-distance-to-means strategy is mathematically simple and computationally efficient, but it has certain limitations. Most importantly, it is insensitive to different degrees of variance in the spectral response data (Lillesand et al., 2004, Campbell, 2007).

Maximum likelihood classifier quantitatively evaluates both the variance and covariance of the category spectral response patterns when classifying an unknown pixel. To do this, an assumption is made that the distribution of the cloud of points forming the category training data is Gaussian (normally distributed). This assumption of normality is generally reasonable for common spectral response distributions. Under this assumption, the distribution of a category response pattern can be completely described by the mean vector and the covariance matrix. Given these parameters, we may compute the statistical probability of a given pixel value being a member of a particular land cover class (Lillesand et al., 2004, Jensen, 1996).

In this work, spectral angle mapping (SAM) was also examined. It is a classification approach that examines multispectral or hyperspectral data by evaluating the relationships between pixel values projected in multispectral data space. Envision a pixel projected into multispectral data space: its position can be described by a vector with an angle in relation to the measurement axes. Its position relative to another pixel (or perhaps a set of reference or training data) can be evaluated by assessing the difference between the angles of the two vectors. Small angles indicate a close similarity, large angles indicate lower similarity. SAMs differ from the usual classification approaches because they compare each pixel in the image with each spectral class, then assign a value between 0 (low resemblance) and 1 (high resemblance) to each pair (Campbell, 2007).

There are numerous clustering algorithms. The K-means algorithm locates a number of clusters in the multidimensional measurement space. Each pixel in the

image is then assigned to the cluster whose arbitrary mean vector is closest. After all pixels have been classified in this manner, revised mean vectors for each of the clusters are computed. The revised means are then used as the basis to reclassify the image data. The procedure continues until there is no significant change in the location of class mean vectors between successive iterations of the algorithm. A widely used variant of the K-means method for unsupervised clustering is the ISODATA algorithm. This algorithm permits the number of clusters to change from one iteration to the next, by merging, splitting, and deleting clusters (Lillesand et al., 2004).

5.1.2.3 Classification accuracy assessment

Classified data often manifest a salt-and-pepper appearance due to the inherent spectral variability encountered by a classifier when applied on a pixel-by-pixel basis. In such situations, it is often desirable to smooth the classified output to show only the “dominant” classes. The output from an image classification is an array of pixel locations containing numbers serving the function of labels, not quantities. Therefore, post-classification smoothing algorithms must operate on the basis of logical operation, such as majority filter (Lillesand et al., 2004). In the study, all classified images from ASAR APP data were smoothed by using the majority filter of 5x5 window size, whereas those from ASAR WS imagery, the filter size of 3x3 were applied before assessing the classification accuracy.

The actual quality of image classification results i.e. rice/non-rice maps should be assessed. This work was performed on the basis of the reference data, i.e. the statistical data published and existing land use map.

Method based on the published statistical data

In this work, assessing the accuracy was based on the official statistics (planted area, yield and production of rice by crop season) provided by the Statistical Office of An Giang province (AGSO, 2008a, AGSO, 2008b). Using this set of data, the accuracy of classification was calculated as follows: let the true value of a

quantity be x and the measured or inferred value x_0 . Then the relative error (5.3) is defined as follows (Weisstein, 2009).

$$\delta x = \frac{\Delta x}{x} = \frac{x_0 - x}{x} = \frac{x_0}{x} - 1 \quad (5.3)$$

where Δx is the absolute error. The percentage error is 100% times the relative error.

Method based on the existing land use map

This was done by a sampling approach in which a number of pixels were selected and both the classification result and the reference data were compared. The recommended sampling strategy in the context of rice cropping systems is stratified random sampling (McCoy, 2005). The choice of the testing set of pixels for accuracy assessment is an important consideration. In practice, one may wish to choose between 30 and 60 samples per category (Richards and Jia, 2006). Comparison is done by creating an error matrix from which widely used accuracy measures can be calculated, such as the overall accuracy and kappa statistics.

The official statistics used were planted area, yield and production of rice by crop season. This data has been systematised, readjusted and additionally completed from new statistical surveys, of which the data are estimated. Data has been collected and calculated in accordance with the methods currently stipulated by Vietnam Statistical branch (AGSO, 2008b). The official statistics by season for each district were used for accuracy assessment of classified results from Envisat ASAR images. On the other hand, the existing land use map was published by the An Giang Department of Natural Resources and Environment. This data was prepared in accordance with the methods prescribed by Vietnam Ministry of Natural Resources and Environment. Because of limited funding, the ground data was only used for method development purpose.

5.2.2 ASAR WS image classification

In the context of ASAR WS data used for rice mapping, the integrated method of backscatter temporal change and thresholding was applied by using two-date and three-date image. This is because the collected WS data had single

polarisation HH. The thresholds were determined on the basis of the temporal variation of radar backscattering from sampling rice fields. Finally, the classification accuracy of rice/non-rice maps was evaluated against the published agency statistical data.

5.3 Results and discussion

5.3.1 Rice mapping from ASAR APP data

5.3.1.1 Thresholding method

From the findings in the previous chapter, the rice classification was examined based on HH/VV ratio of the ASAR APP images acquired in the middle of crop season, i.e. February, June, October 2007, and February 2008, to map the rice planted of the WS, SA, AW 2007, and WS 2008 crops, respectively. The results of rice mapping using the optimum threshold of polarisation ratio (i.e. 3 dB) in most rice crops were very good, except in AW 2007 crop. The percentage error of the classified rice acreage at provincial scale in this crop was 12.7% when compared with the information published in the Statistical Yearbook 2007 of An Giang province (AGSO, 2008b) (see Table 5.1). Therefore, to reduce the confusion of rice with other non-rice classes having high HH/VV ratio values (e.g. reed or marshland with vertical structure of the plants, other crops, etc.), some threshold combinations of HH, VV and HH/VV data as presented in Table 5.1 were considered. Then, their classification accuracies at the provincial scale were assessed and compared. An additional criterion was finally determined: $\sigma_{VV}^0 \leq -6$ dB. In this case, the percentage error of the classified rice area at provincial scale in AW 2007 crop was reduced from 12.7% to 3.8% when compared with the statistical data. Similarly, threshold combinations using NDRa were also examined. The combination of thresholds “NDRa ≤ -0.2 and $\sigma_{VV}^0 \leq -6$ dB and $-6 \leq \sigma_{HH}^0 \leq 2$ dB” was found to produce good results in most cases.

Table 5.1. Percentage errors between planted rice acreage of An Giang province in WS, SA, AW 2007 and WS 2008 crops produced by ASAR data and statistical data using various threshold combinations.

Algorithm	Percentage error (%)			
	WS 2007	SA 2007	AW 2007	WS 2008
$Ra \geq 3$	3.4	2.4	12.7	-2.8
$Ra \geq 3$ and $\sigma_{VV}^0 \leq -6\text{dB}$	1.3	-1.6	3.8	-6.6
$Ra \geq 3$ and $-7 \leq \sigma_{HH}^0 \leq 2\text{dB}$	2.1	0.8	8.1	-4.9
$Ra \geq 3$ and $-6 \leq \sigma_{HH}^0 \leq 2\text{dB}$	0.0	-0.5	6.6	-6.8
$Ra \geq 3$ and $\sigma_{VV}^0 \leq -6\text{dB}$ and $-7 \leq \sigma_{HH}^0 \leq 2\text{dB}$	0.0	-3.1	-0.7	-8.6
$Ra \geq 3$ and $\sigma_{VV}^0 \leq -6\text{dB}$ and $-6 \leq \sigma_{HH}^0 \leq 2\text{dB}$		-4.5	-2.2	-10.5
$NDRa \leq -0.2$	8.4	10.4		4.9
$NDRa \leq -0.2$ and $\sigma_{VV}^0 \leq -6\text{dB}$	3.4	1.1	6.2	-3.5
$NDRa \leq -0.2$ and $-7 \leq \sigma_{HH}^0 \leq 2\text{dB}$	7.1			3.4
$NDRa \leq -0.2$ and $-6 \leq \sigma_{HH}^0 \leq 2\text{dB}$		8.0		
$NDRa \leq -0.2$ and $\sigma_{VV}^0 \leq -6\text{dB}$ and $-7 \leq \sigma_{HH}^0 \leq 2\text{dB}$	2.4	0.2	3.5	-4.7
$NDRa \leq -0.2$ and $\sigma_{VV}^0 \leq -6\text{dB}$ and $-6 \leq \sigma_{HH}^0 \leq 2\text{dB}$	0.6	-1.0	2.1	-6.5

Note: Lowest percentage errors in bold font.

5.3.1.2 Comparison of classification accuracy between different classifiers

As mentioned above, different classification methods were utilised, such as minimum-distance-to-means, maximum likelihood, spectral angle mapper, ISODATA, and K-means in order to compare the classification accuracy of the rice area mapped by these methods with published statistical data (Table 5.2).

Table 5.2. Percentage errors between planted rice acreage produced by ASAR APP data using different classifiers and statistical data.

Classifier	Data used	Percentage error (%)					
		WS crop			SA crop		
		PT	CP	CD	PT	CP	CD
Thresholding	Feb or Jun image ($Ra \geq 3$ and $\sigma_{VV}^0 \leq -6$)	6	6	-2	-2	2	1
	Feb or Jun image ($NDRa \leq -0.2$ and $\sigma_{VV}^0 \leq -6dB$ and $-6 \leq \sigma_{HH}^0 \leq 2dB$)	4	6	-3	-1	3	2
Minimum- distance-to- means	PC1, PC2, and PC3	6	8	6	8	6	11
	Jan+Feb or Apr+Jun images	8	8	7	9	10	10
	Feb+Mar or Jun+Jul images	3	7	4	12	9	4
	Jan or Apr image	0	-8	-14	-27	-27	-33
	Feb or Jun image	9	11	8	13	13	15
	Mar or Jul image	-32	-36	-41	-11	-15	-54
Maximum likelihood	PC1, PC2, and PC3	-4	-10	-7	-5	-5	-2
	Jan+Feb or Apr+Jun images	-8	-13	-42	-17	-17	-31
	Feb+Mar or Jun+Jul images	-11	-9	-18	-30	-41	-76
	Jan or Apr image	2	-4	-13	-18	-25	-35
	Feb or Jun image	11	10	3	12	13	14
	Mar or Jul image	-17	-16	-22	-8	-12	-49
Spectral angle mapper	PC1, PC2, and PC3	-12	-16	-19	-3	-3	0
	Jan+Feb or Apr+Jun images	10	9	7	12	12	11
	Feb+Mar or Jun+Jul images	8	10	8	9	7	-1
	Jan or Apr image	2	-4	-13	Bad	Bad	Bad
	Feb or Jun image	11	11	8	8	10	11
	Mar or Jul image	Bad	Bad	Bad	-5	-7	-43
ISODATA	PC1, PC2, and PC3 (No. of classes: 30)	-4	0	6	-27	-21	-28
	PC1, PC2, and PC3 (No. of classes: 10)	-41	-27	-24			
	Jan+Feb+Mar or Apr+Jun+Jul images (No. of classes: 30)	Bad	Bad	Bad			

K-means	PC1, PC2, and PC3 (No. of classes: 30)	-21	-9	-9	-33	-31	-22
	Jan+Feb or Apr+Jun images (No. of classes: 30)	-52	-37	-31			

Note: Lowest percentage errors in bold font.

Apart from thresholding method, the minimum-distance-to-means and SAM methods provided good results when the following datasets were used: a) the three first principal components of three-date ASAR APP images taken during the crop season, b) two consecutive images, and c) single-date image acquired in the middle of crop season. In the case of single-date image, the maximum percentage errors were observed for the minimum-distance-to-means and SAM classifiers, i.e. 15% and 11%, respectively (Table 5.2).

In relation to the maximum likelihood classifier, the method provided rather good results for rice mapping when PC1, PC2, and PC3 of three-date image or single image in the mid-season were used. Conversely, two-date image or other single-date image yielded rather low accuracies.

Compared with supervised classification, unsupervised classification methods produced low accuracy or bad results (i.e. percentage error more than 50%). Therefore, unsupervised classifiers such as ISODATA and K-means could not be effective for rice mapping using Envisat ASAR APP images in this case study.

By comparing the obtained accuracy, the classified results using thresholding algorithm provided higher and consistent accuracies between districts and seasons (percentage errors ranging from -2 to 6% or -3 to 6% for WS crop and from -2 to 2% or -1 to 3% for SA crop in the case of polarisation ratio or normalised difference polarisation ratio index used, respectively). Other classification methods did not improve classification accuracy despite their sophisticated algorithm basis.

5.3.1.3 Accuracy assessment of the thresholding method

As analysed above, the thresholding algorithm using single-date ASAR APP image taken in the middle of crop season was considered as an effective tool for rice mapping in the study area. Thus, in this section, the accuracy assessment based on statistical data and reference data of images classified from the thresholding method using polarisation ratio and VV data is discussed.

Accuracy assessment based on the official statistics

The accuracy assessment results of the classified rice pixels by the thresholding method were produced based on the statistical data published by An Giang province for the WS, SA, and AW crops planted in 2007 (Tables 5.3, 5.4, and 5.5) and WS crop planted in 2008 (Table 5.6) (AGSO, 2008a, AGSO, 2008b).

Table 5.3. Percentage errors between planted rice acreage in WS 2007 crop produced by ASAR APP data and statistical data.

District name	Statistical data (Ha)	Rice from ASAR (Ha)	Percentage error (%)
Phu Tan	23041	24546	6.5
Chau Phu	34383	36556	6.3
Tri Ton (*)			
Tinh Bien	14952	14999	0.3
Chau Doc	7148	6965	-2.6
Long Xuyen	5591	5244	-6.2
Thoai Son	36691	39112	6.6
Tan Chau	11420	10114	-11.4
An Phu	14443	12377	-14.3
Cho Moi	17887	17235	-3.6
Chau Thanh	27686	28702	3.7
Province	193242	195850	1.3

(*) Outside of the SAR image coverage

Table 5.4. Percentage errors between planted rice acreage in SA 2007 crop produced by ASAR APP data and statistical data.

District name	Statistical data (Ha)	Rice from ASAR (Ha)	Percentage error (%)
Phu Tan	22968	22471	-2.2
Chau Phu	33959	34612	1.9
Tri Ton (*)			
Tinh Bien	15164	14689	-3.1
Chau Doc	7123	7220	1.4
Long Xuyen	5433	5227	-3.8
Thoai Son	35990	35223	-2.1
Tan Chau	10908	9687	-11.2
An Phu	12856	11699	-9.0
Cho Moi	16324	16827	3.1
Chau Thanh	27629	27659	0.1
Province	188354	185314	-1.6

(*) Outside of the SAR image coverage

The difference between rice area planted by district from classified images and the government statistics ranged from -14.3 to 6.6% (Table 5.3), -11.2 to 3.1% (Table 5.4) and 10.8 to 0.6% (Table 5.6) for WS and SA 2007, and WS 2008 crops, respectively. In contrast, the percentage errors of rice area planted in the AW 2007 crop obtained for several districts (e.g. Long Xuyen, An Phu, and Chau Thanh) were quite high, possibly due to small rice acreage planted for that season (Table 5.5). In fact, the statistical planted rice area of these three districts in AW 2007 was 100, 143, 646 Ha, respectively, occupied only 1.34% of provincial rice acreage. The differences of provincial rice grown area, however, were 1.8% in WS crop, -1.3% in SA crop, 3.8% in AW crop 2007, and -6.6% in WS crop 2008.

Table 5.5. Percentage errors between planted rice acreage in AW 2007 crop produced by ASAR APP data and statistical data

District name	Statistical data (Ha)	Rice from ASAR (Ha)	Percentage error (%)
Phu Tan	11963	12873	7.6
Chau Phu	6389	6514	2.0
Tri Ton (*)			
Tinh Bien	5636	6315	12.1
Chau Doc	3530	3633	2.9
Long Xuyen	100	174	73.5
Thoai Son	15115	15262	1.0
Tan Chau	6355	5857	-7.8
An Phu	143	289	101.8
Cho Moi	13224	13661	3.3
Chau Thanh	646	917	41.9
Province	63101	65494	3.8

(*) Outside of the SAR image coverage

Table 5.6. Percentage errors between planted rice acreage in WS 2008 crop produced by ASAR APP data and statistical data.

District name	Statistical data (Ha)	Rice from ASAR (Ha)	Percentage error (%)
Phu Tan	23041	21306	-7.5
Chau Phu	34376	33406	-2.8
Tri Ton (*)			
Tinh Bien	15020	14162	-5.7
Chau Doc	7063	7103	0.6
Long Xuyen	5505	5101	-7.3
Thoai Son	36516	34554	-5.4
Tan Chau	11253	10313	-8.4
An Phu	14382	13423	-6.7
Cho Moi	17364	15625	-10.0
Chau Thanh	29525	26338	-10.8
Province	194045	181332	-6.6

(*) Outside of the SAR image coverage

Accuracy assessment based on the existing land use map

The reference data available in the study area was the land use map prepared in 2005 by the Department of Natural Resources and Environment of An Giang province. Considering the “rice” class in the map, it implies that this class may be the single, double or triple crop rice, although they were not categorised at that level as such.

The classification accuracy was determined by randomly selecting a testing set of 174 pixels from the rice/non-rice maps and checking their labels against classes determined from the reference data. The classification accuracy of the resulting maps of WS, SA 2007, and WS 2008 crop seasons were presented in the classification error (or confusion) matrices (Tables 5.7, 5.8, and 5.9). The accuracy assessment of rice map in AW 2007 crop was not implemented because most rice fields in the province have been growing two crops (WS and SA) during a year, and only few do triple rice. As mentioned above, the land use map was not presented where triple rice was planted.

Table 5.7. A confusion matrix of rice/non-rice map in WS 2007 crop.

Classification data	Reference data (Pixels)		
	Rice	Non-rice	Total
Rice	120	3	123
Non-rice	7	44	51
Total	127	47	174

Producer's accuracy

$$\text{Rice} = 120/127 = 94\%$$

$$\text{Non-rice} = 44/47 = 94\%$$

$$\text{Overall accuracy} = 164/174 = 94\%$$

$$\text{Kappa coefficient} = 0.86$$

User's accuracy

$$\text{Rice} = 120/123 = 98\%$$

$$\text{Non-rice} = 44/51 = 86\%$$

The values listed in the confusion matrices represented the number of testing pixels, in each case, correctly and incorrectly labelled by the classifier. The overall classification accuracies were 94 and 93% for WS crops in 2007 and 2008, respectively, whereas 87% for SA 2007 crop season.

Table 5.8. A confusion matrix of rice/non-rice map in SA 2007 crop.

Classification data	Reference data (Pixels)		
	Rice	Non-rice	Total
Rice	113	8	121
Non-rice	14	39	53
Total	127	47	174

Producer's accuracy	User's accuracy
Rice = $113/127 = 89\%$	Rice = $113/121 = 93\%$
Non-rice = $39/47 = 83\%$	Non-rice = $39/53 = 74\%$
Overall accuracy = $152/174 = 87\%$	
Kappa coefficient = 0.69	

Table 5.9. A confusion matrix of rice/non-rice map in WS 2008 crop.

Classification data	Reference data (Pixels)		
	Rice	Non-rice	Total
Rice	116	1	117
Non-rice	11	46	57
Total	127	47	174

Producer's accuracy	User's accuracy
Rice = $116/127 = 91\%$	Rice = $116/117 = 99\%$
Non-rice = $46/47 = 98\%$	Non-rice = $46/57 = 81\%$
Overall accuracy = $93\% (162/174)$	
Kappa coefficient = 0.84	

It is important to understand that different indications of class accuracies will result according to whether the number of correct pixels for a class is divided by the

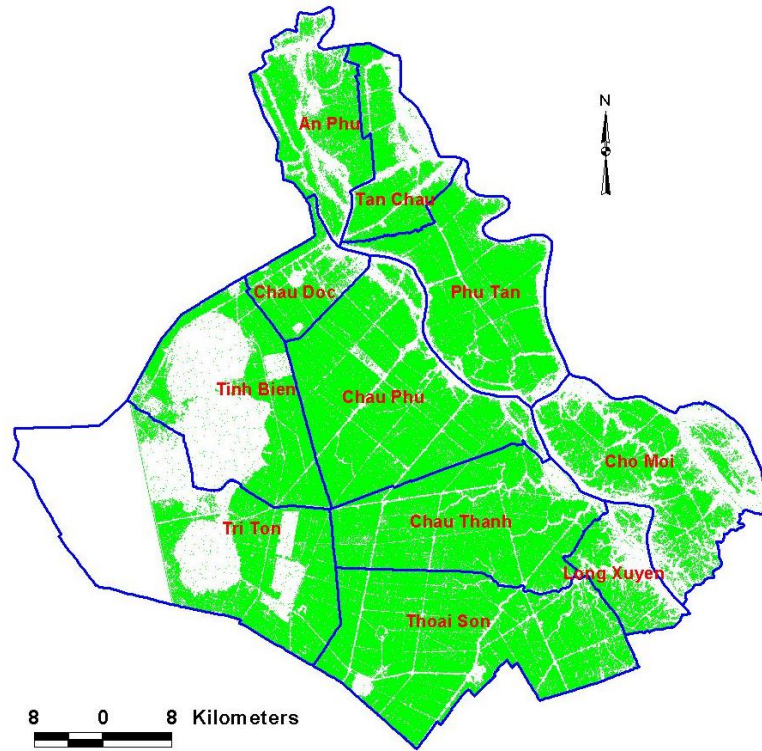
total number of reference pixels for the class (the column sum) or the total number of pixels the classifier attributes to the class (the row sum). The former refer to the *Producer's accuracy*, whereas the latter refer to the *User's accuracy*. This distinction is important and one believes that the User's accuracy is the figure that should most often be adopted (Richards and Jia, 2006). In the case, the User's accuracies of rice class attained the very high accuracies of 98, 93, and 99% for WS, SA 2007, and WS 2008, respectively.

Whereas the overall accuracy only includes the data along the major diagonal and excludes the errors of omission and commission, *the kappa (KHAT) statistic* incorporates the nondiagonal elements of the error matrix as a product of the row and column marginal (Lillesand et al., 2004). The kappa coefficients of the classified rice/non-rice images were 0.86, 0.69, and 0.84 for WS, SA 2007, and WS 2008 crop, respectively.

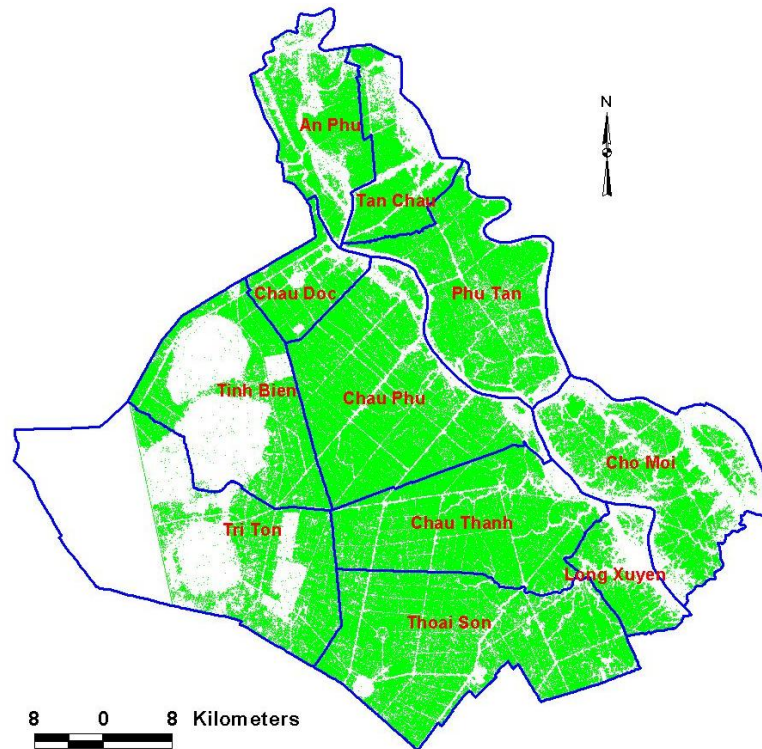
On the basis of the existing land use map for assessing the classification accuracy, the overall accuracies obtained were mostly lower than those which were assessed based on the statistics. This can be explained by the information content provided by the land use map where rice cropping systems were not explicitly identified. Therefore, several testing pixels labelled as "rice" in the reference map were classified as "non-rice" in the classified maps (7/51, 14/53, and 11/57 pixels in WS, SA 2007, and WS 2008 crop, respectively). However, the accuracy results are acceptable for practical applications on rice crop inventory. Most classification accuracies obtained for various rice crop seasons planted in the 2007 and 2008 in this study were higher than those of the previous studies (Li et al., 2003, Yang et al., 2008, Bouvet et al., 2009).

5.3.1.4 Rice maps from thresholding method

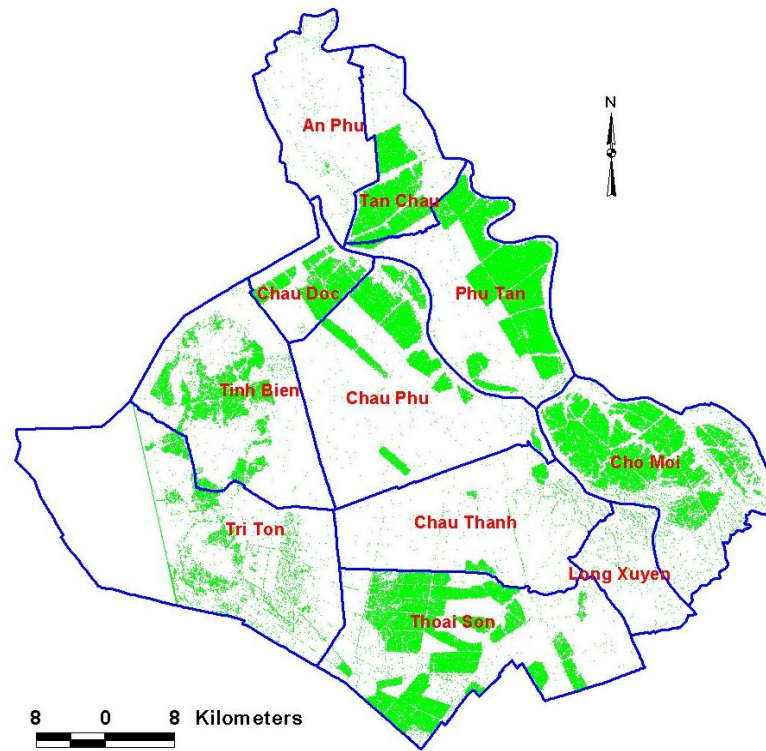
The thresholding algorithm for accurate rice/non-rice mapping across the seasons was finally used. Figure 5.4 shows the pixel based mapping results of WS, SA, AW 2007, and WS 2008 crops using the optimum thresholds, i.e. $R_a \geq 3$ and $\sigma_{VV}^0 \leq -6\text{dB}$.



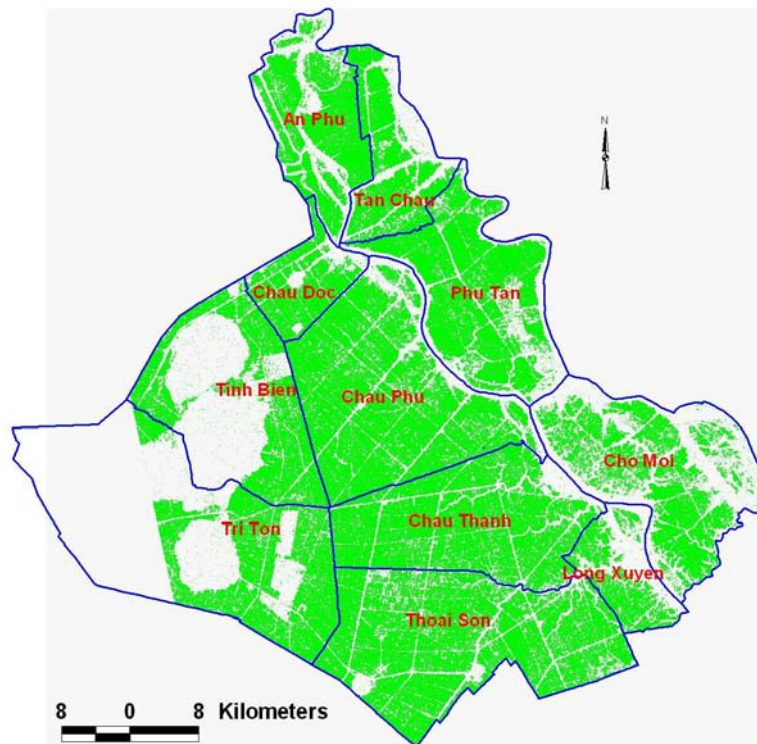
(a) WS 2007 crop



(b) SA 2007 crop



(c) AW 2007 crop



(d) WS 2008 crop

Figure 5.4. Rice and non-rice maps (rice in green) of WS (a), SA (b), AW 2007 (c), and WS 2008 crops (d).

The rice cropping system map of An Giang province in 2007 (Figure 5.5) were then produced by combining three rice/non-rice maps of WS, SA and AW 2007 crops. Special attention has been paid to the Cho Moi district, which is located in the south-east of the province. With the extensive dyke network established in recent years, almost the entire rice area of the district has been growing with triple crop rice.

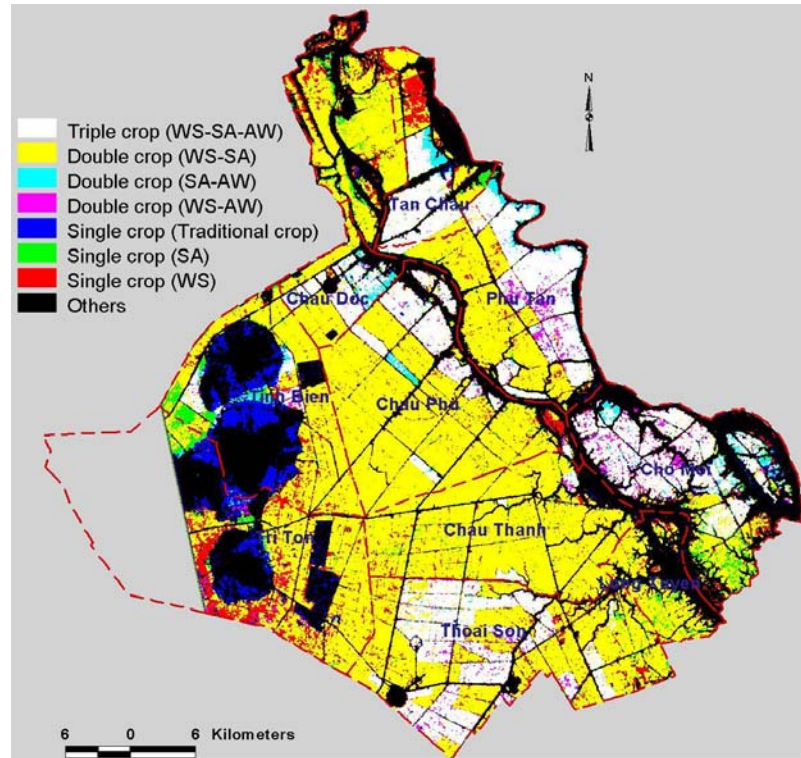
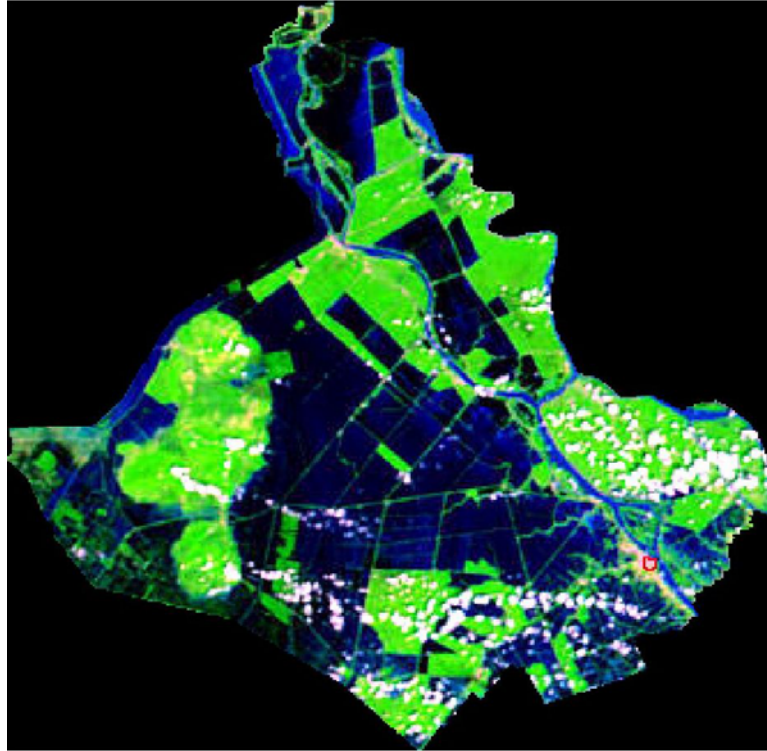


Figure 5.5. Rice cropping system map of An Giang province in 2007.

The colour composite MODIS image (Figure 5.6) was collected on 9th October 2007, i.e. in the middle of AW2007 rice crop season. The image presented rice fields grown in green pixels, except forest and mountainous areas in the western part, whereas inundated regions in the flood season in blue pixels. Based from qualitative visual interpretation, the rice fields in this image had good agreement with the classified rice results from ASAR APP data (Figure 5.4c and Figure 5.5).



Source: <http://rapidfire.sci.gsfc.nasa.gov/>

Figure 5.6. A colour composite MODIS image (Red=band 7, Green= band 2, and Blue= band 1) acquired on 9 October 2007.

5.3.2 Rice mapping using ASAR WS data

Although the spatial resolution of ASAR WS data is lower than that of the ASAR APP products, it may have the advantages for rice monitoring due to its wide area coverage. The possibility of ASAR WS data utilisation is not only reducing the cost of data acquisition and processing time but also increasing the area coverage and repeat pass. Because there is not much literature on rice/non-rice mapping using multi-temporal ASAR WS data, a test was done based on the temporal variation of radar response (Le-Toan et al., 1997) and thresholding method as analysed in the section 5.2 “Methods”. As introduced in section 3.4.1 “Imagery used”, the HH polarisation WS images were used in this case of study.

5.3.2.1 Image analysis of ASAR WS data in ascending mode

Seven images in ascending mode taken during the WS and SA crop growth from January to August 2007 were used for data analysis. A number of represented samples of different land use classes in the study site were delineated on the basis of the existing land use map in order to analyse their backscatter temporal variation. It consisted of annual plant (AP); perennial plant (PP); forest (Fo); rural area (Ru); urban area (Ur); water bodies (Wa); and rice paddy (Rice). The temporal change of their radar backscattering was then presented in Table 5.10 and plotted in Figure 5.7.

Table 5.10. Backscattering coefficients of land use samples extracted from ASAR WS ascending mode data.

LU code	Backscattering coefficient (dB)						
	Date of image acquisition						
	16/01/07	20/02/07	27/03/07	01/05/07	05/06/07	10/07/07	14/08/07
AP1	-5.8	-6.5	-6.4	-6.8	-6.5	-5.5	-6.2
AP2	-3.7	-4.7	-4.5	-4.6	-2.8	-3.2	-3.6
PP	-5.4	-5.8	-4.5	-4.3	-3.8	-3.3	-3.5
Fo1	-6.8	-8.4	-7.9	-7.8	-7.8	-7.0	-5.9
Fo2	-6.0	-6.7	-6.3	-6.8	-6.8	-6.8	-6.0
Ru1	-3.6	-3.9	-3.0	-3.3	-3.5	-2.5	-2.4
Ru2	-6.1	-6.7	-5.8	-5.8	-4.7	-4.9	-5.8
Ru3	-4.6	-4.9	-4.9	-4.5	-4.6	-4.8	-4.1
Ur1	-1.3	-1.9	-1.2	-1.7	-1.4	-1.5	-1.7
Ur2	1.1	0.0	0.8	-0.4	-0.6	-0.5	0.7
Wa1	-18.5	-17.4	-17.9	-16.5	-16.8	-15.0	-15.0
Wa2	-16.0	-15.9	-14.7	-14.8	-14.0	-14.3	-14.4
Wa3	-18.2	-17.5	-18.2	-16.0	-18.2	-17.2	-16.9
Rice	-7.0	-4.1	-7.7	-11.5	-3.5	-5.0	-5.7

As expected, the radar backscattering of water bodies was always very low, ranged between -18.5 dB and -14 dB. In contrast, high backscatter (around -2 to 1 dB) was observed from urban settlement, due to scattering mechanism of their corner reflectors. In general, backscatter temporal change of most land use samples was quite stable with the exception of the rice backscatters.

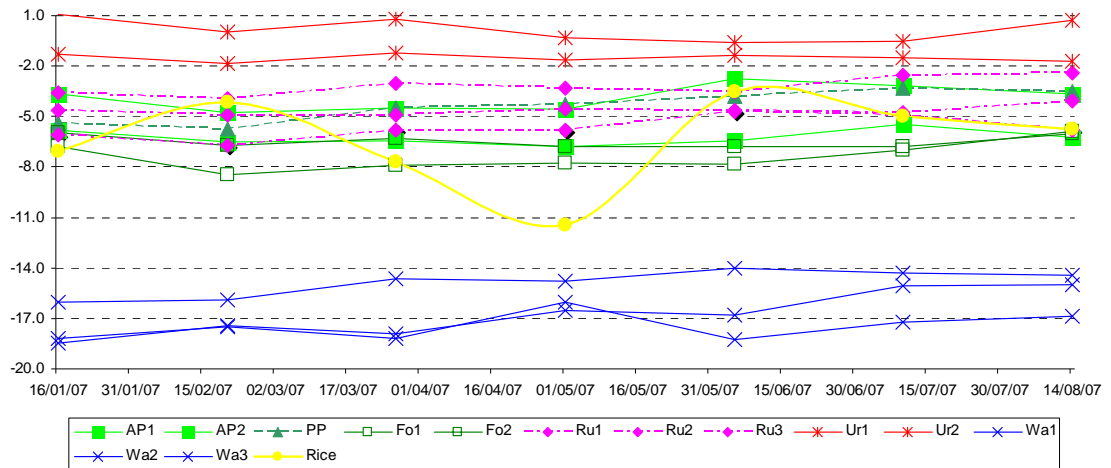


Figure 5.7. Backscatter temporal variation of the land use samples from ASAR WS ascending mode data collected during the period of Jan. - Aug. 2007.

Backscatter temporal change of rice sampling areas, which were selected on the ground for ASAR APP data analysis, was also interpreted for ASAR WS data (Figure 5.8). Since the size of rice fields in the area is usually quite small, more or less one ha, and the spatial resolution of ASAR WS imagery is more than two ha ($150 \times 150 \text{ m}^2$), therefore, the mean value of sigma nought from five sampling fields in each sampling area was used (Table 5.11).

Table 5.11. Backscattering coefficients of rice samples extracted from ASAR WS ascending mode data.

Site code	Backscattering coefficient (dB)						
	Date of image acquisition						
	16/01/07	20/02/07	27/03/07	01/05/07	05/06/07	10/07/07	14/08/07
BM	-5.1	-3.9	-6.1	-9.5	-4.1	-5.4	-10.2
VB	-4.2	-5.1	-5.9	-9.2	-2.3	-6.1	-9.4
BH	-4.8	-4.4	-4.7	-9.5	-3.3	-5.0	-7.5
VC	-4.8	-5.2	-7.0	-9.8	-4.7	-6.2	-11.0
PH	-4.6	-3.8	-6.1				
LDB	-7.0	-4.1	-7.7	-11.5	-3.5	-5.0	-5.7
MHD	-6.9	-3.2	-7.5	-7.3	-4.0	-3.8	-8.1
Mean	-5.3	-4.2	-6.4	-9.5	-3.6	-5.3	-8.6

Note: BM: Binh My, VB: Vinh Binh, BH: Binh Hoa, VC: Vinh Chanh, PH: Phu Hoa, LDB: Long Dien B, MHD: My Hoi Dong.

Figure 5.8 depicted the backscatter temporal change of rice sampling areas in WS and SA 2007 crops. In the middle period of the crop seasons, i.e. February for WS and June for SA crop, the high radar response from the rice plants were recorded on the images and their backscattering coefficients more than -6 dB were extracted. This explanation agreed with the previous analysis on the high resolution ASAR APP data (Section 4.3.2).

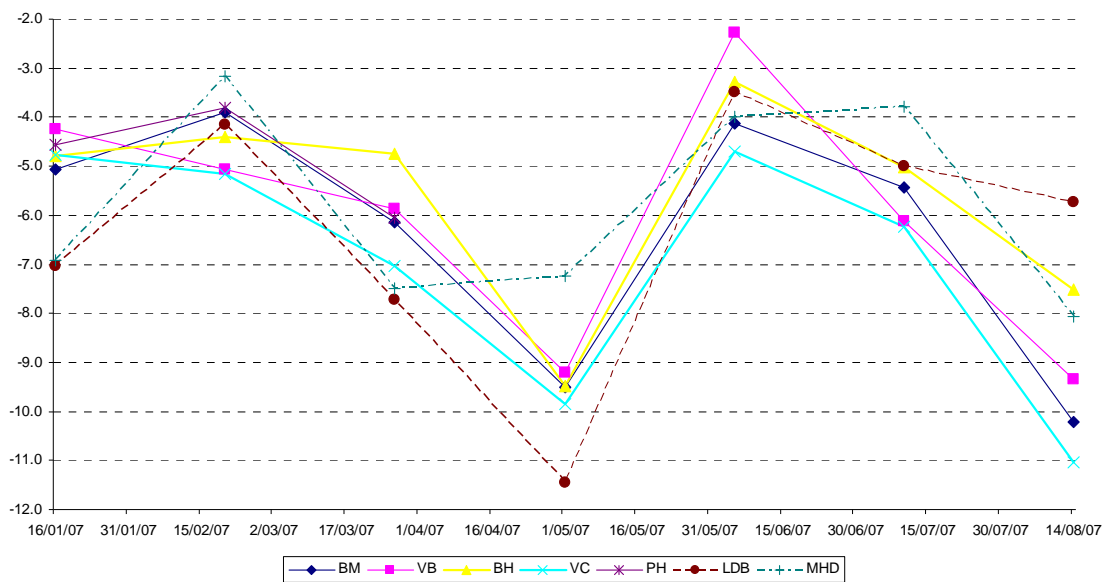


Figure 5.8. Backscatter temporal variation of the rice samples from ASAR WS ascending mode data in WS and SA 2007 crops.

In order to map the rice by using multi-temporal ASAR WS data, the “integrated method” based on the temporal variation of the radar response and thresholding was proposed. In the case of three-date image used, they should be: a) first image taken before seeding or at the first period of vegetative stage, b) second image acquired in the middle of crop season, and c) third image collected in the reproductive stage or after harvest. Two first images were applied in the case of two-date image used. The threshold of 3 dB was appropriate for backscatter temporal change of rice, whereas sigma nought of HH data acquired in the middle of crop

season was thresholded using -7 dB (see Table 5.11, Figure 5.8, and Table 5.14, Figure 5.12 for a case of descending mode).

In case of WS 2007 crop, two images taken during the crop season (16 Jan and 20 Feb) and one image taken after harvest period (1 May) were utilised. The pixels were segmented as rice class if they conformed to the following thresholds (5.4):

$$(\sigma_{A2}^0 - \sigma_{A1}^0 \geq 3dB) \cup (\sigma_{A2}^0 - \sigma_{A5}^0 \geq 3dB) \cap (\sigma_{A2}^0 \geq -7dB) \quad (5.4)$$

where

σ_{A1}^0 : backscattering coefficient of ASAR WS image taken on 16 Jan. 2007,

σ_{A2}^0 : backscattering coefficient of ASAR WS image taken on 20 Feb. 2007,

σ_{A5}^0 : backscattering coefficient of ASAR WS image taken on 1 May. 2007.

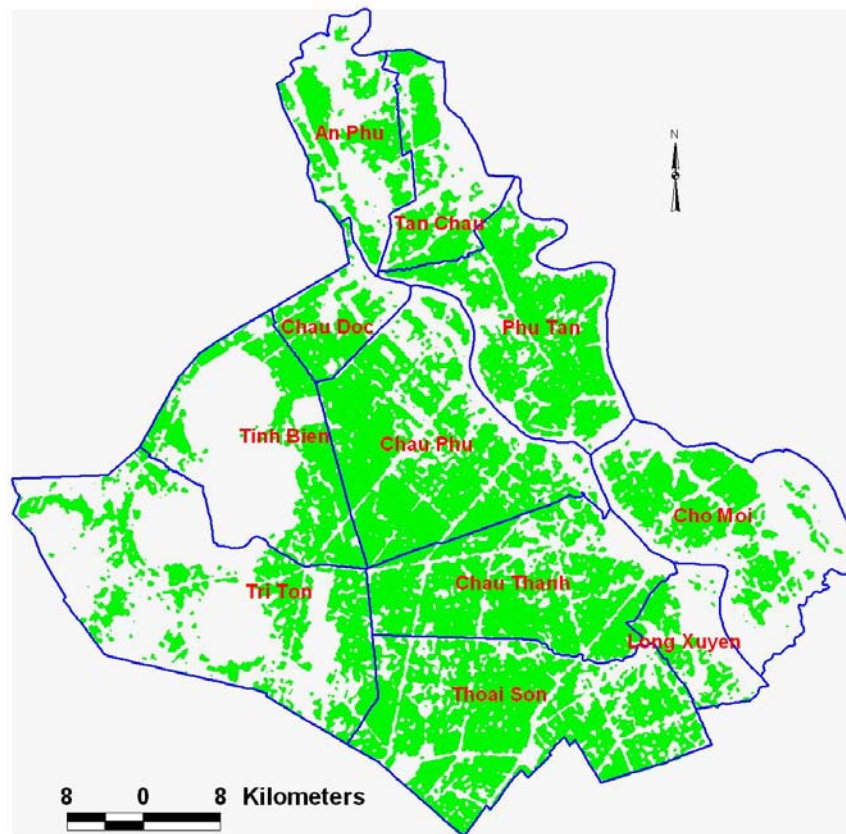


Figure 5.9. Rice and non-rice map (rice in green) of WS 2007 crop produced by using three-date ASAR WS images taken in ascending mode.

Afterwards, the classified image of rice/non-rice was created (Figure 5.9). The percentage errors between planted rice area produced by ASAR WS data and the official statistics were presented in Table 5.12. The classified rice layer was underestimated for most districts and consequently the percentage error at the provincial scale was of -23.9%. This may be due to: a) the first date image was collected about one month after seeding for almost rice fields, thus the radar response was quite high at that time and the backscatter temporal change of some of rice fields derived from first and second date images was less than 3 dB, b) the one-month shift in crop calendar took place between various rice fields in the province, and c) additionally, no kind of terrain relief was considered, since most areas are flat, except those mountainous parts located in Tri Ton and Tinh Bien districts.

Table 5.12. Percentage errors between planted rice acreage in WS crop produced by ASAR WS data acquired on 16 Jan., 20 Feb., and 1 May 2007 and statistical data.

District name	Statistical data (ha)	Rice from ASAR (ha)	Percentage error (%)
Phu Tan	23041	20674	-10.3
Chau Phu	34382	30066	-12.6
Tri Ton	37373	17017	-54.5
Tinh Bien	14952	12505	-16.4
Chau Doc	7148	5889	-17.6
Long Xuyen	5591	3368	-39.8
Thoai Son	36691	32267	-12.1
Tan Chau	11420	7702	-32.6
An Phu	14443	8236	-43.0
Cho Moi	17887	13105	-26.7
Chau Thanh	27686	24574	-11.2
Province	230614	175403	-23.9

In the Summer Autumn 2007 crop, three-date image (1 May, 5 June, and 10 July 2007) collected during the crop season were used for segmentation of the rice and non-rice. The colour composite image (May image in Red, June image in Green, and July image in Blue) was created (Figure 5.10). The district boundaries of An

Giang province were in blue polylines, where most rice pixels in green colour were interpreted because high backscatters from rice in the middle of crop season, i.e. June 2007 took place. On the other hand, urban settlements of Ho Chi Minh City could be easily recognised with the bright pixels in the north western part of the image. Furthermore, the algorithm was also tested for the utilisation of two-date image taken during the first period of the vegetative stage and in the middle of crop season. The thresholds were applied in the case of three-date image (5.5) and two-date image used (5.6) as follows:

$$(\sigma_{A6}^0 - \sigma_{A5}^0 \geq 3dB) \cup (\sigma_{A6}^0 - \sigma_{A7}^0 \geq 3dB) \cap (\sigma_{A6}^0 \geq -7dB) \quad (5.5)$$

$$(\sigma_{A6}^0 - \sigma_{A5}^0 \geq 3dB) \cap (\sigma_{A6}^0 \geq -7dB) \quad (5.6)$$

where

σ_{A5}^0 : backscattering coefficient of ASAR WS image taken on 1 May. 2007,

σ_{A6}^0 : backscattering coefficient of ASAR WS image taken on 5 Jun. 2007,

σ_{A7}^0 : backscattering coefficient of ASAR WS image taken on 10 Jul. 2007.

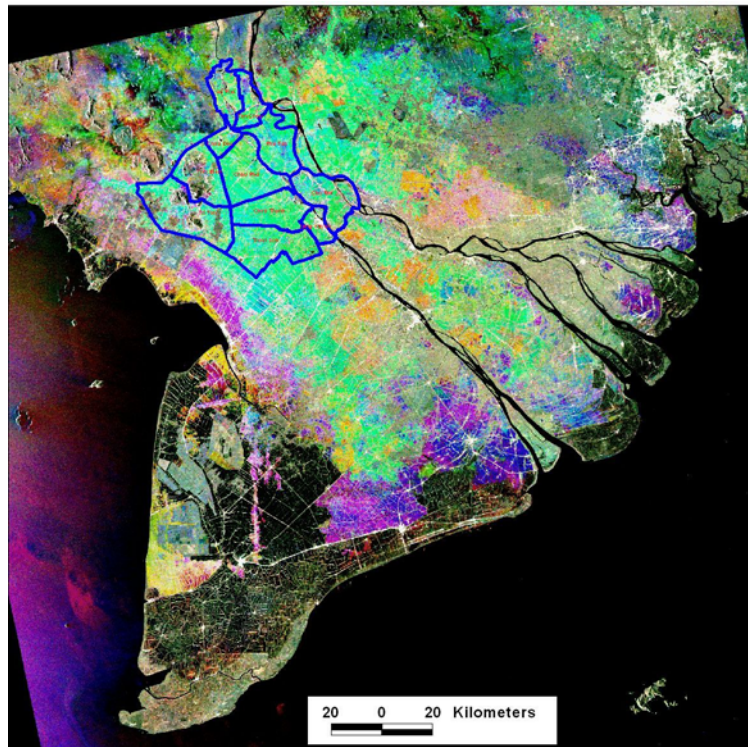
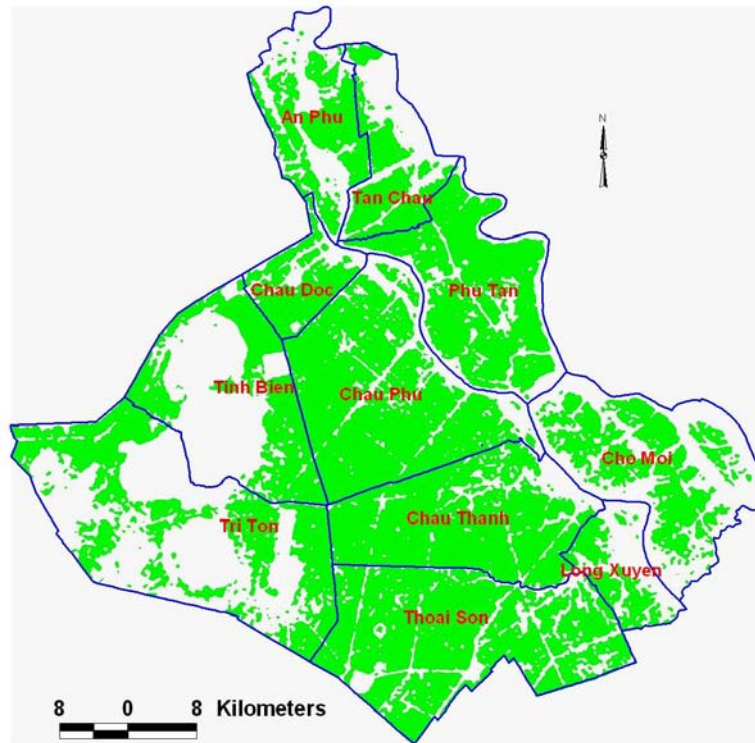
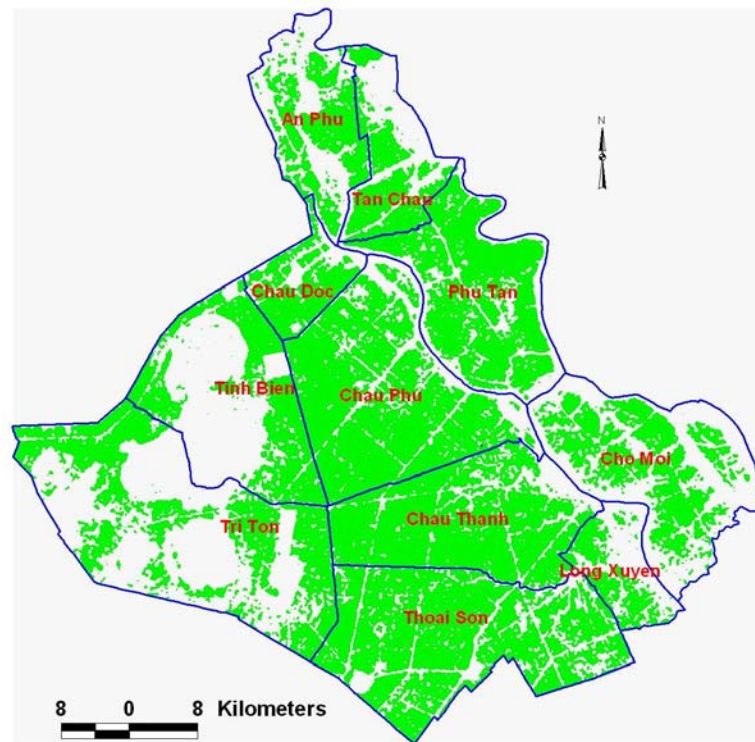


Figure 5.10. ASAR WS colour composite image (Red=May image, Green=June image, and Blue=July image) of the Mekong River Delta (District boundaries of An Giang province in blue polylines).



(a)



(b)

Figure 5.11. Rice and non-rice maps (rice in green) of SA 2007 crop produced by using three-date (a) and two-date (b) ASAR WS image taken in ascending mode.

In this case, we can estimate the rice acreage planted of each district, as well as for the whole province before harvest. While three-date image were used, the accuracies of classified rice pixels (Figure 5.11a) for most districts were rather good: the percentage errors by district range from -16 to 7%, except for Tri Ton district. The error of -3.1% was finally observed for the provincial rice grown acreage in the SA 2007 crop season extracted from ASAR WS data when compared to the statistical data (Table 5.13) . On the other hand, the percentage error was slightly lower in the case of two-date ASAR WS data for rice segmentation (Figure 5.11b), i.e. an error of -6.4%.

Table 5.13. Percentage errors between planted rice acreage in SA crop produced by ASAR WS data acquired on 1 May, 5 Jun. and 10 Jul. 2007 and statistical data.

District name	Statistical data (ha)	Using 3-date images		Using 2-date images	
		Rice (ha)	Percentage error (%)	Rice (ha)	Percentage error (%)
Phu Tan	22968	24134	5.1	23380	1.8
Chau Phu	33959	36436	7.3	35019	3.1
Tri Ton	35242	25050	-28.9	24518	-30.4
Tinh Bien	15164	15163	0.0	14774	-2.6
Chau Doc	7123	7549	6.0	7219	1.3
Long Xuyen	5433	4829	-11.1	4772	-12.2
Thoai Son	35990	38024	5.7	36456	1.3
Tan Chau	10908	9119	-16.4	8950	-18.0
An Phu	12856	11075	-13.9	10199	-20.7
Cho Moi	16324	15677	-4.0	15492	-5.1
Chau Thanh	27629	29512	6.8	28618	3.6
Province	223596	216568	-3.1	209397	-6.4

5.3.2.2 Image analysis of ASAR WS data in descending mode

There were 14 ASAR WS images in descending mode acquired in the Mekong River Delta during the period of December 2006 to August 2007, double those collected in ascending mode. The backscatter temporal change of sampling rice was presented in Table 5.14 and depicted in Figure 5.12. Two rice crops WS and SA were separated by low radar backscatter in the April image because the first crop was fully harvested in March. A maximum one-month shift in the calendar was observed in the plots (Figure 5.8 and 5.12) and agreed with the ground truth data collected.

Table 5.14. Backscattering coefficients of rice samples extracted from ASAR WS descending mode data.

Site code	Backscattering coefficient (dB)													
	Date of image acquisition													
	5/12	9/1	13/2	1/3	20/3	5/4	24/4	10/5	29/5	14/6	3/7	19/7	7/8	23/8
BM	-11.1	-5.3	-4.9	-6.2	-5.6	-9.0	-9.0	-11.2	-5.3	-4.2	-6.5	-8.8	-7.3	-12.1
VB	-10.6	-5.5	-5.9	-9.1	-8.2	-9.0	-10.4	-5.4	-4.3	-5.0	-8.6	-9.6	-8.0	-12.5
BH	-13.9	-6.3	-6.5	-6.3	-6.0	-8.3	-11.1	-11.1	-5.7	-4.7	-5.4	-7.3	-7.0	-11.6
VC	-11.3	-6.1	-5.7	-8.1	-8.0	-9.8	-9.1	-7.7	-6.1	-5.1	-8.8	-8.0	-9.2	-10.2
PH	-14.8	-9.5	-5.6	-7.0	-6.3	-7.5								
LDB	-6.9	-11.4	-4.3	-5.5	-5.8	-7.5	-11.7	-9.0	-5.4	-4.5	-5.3	-5.7	-8.0	-10.9
MHD	-8.2	-10.3	-4.2	-5.4	-6.5	-6.5	-10.1	-12.2	-8.4	-5.4	-4.4	-6.8	-7.3	-16.4
Mean	-11.0	-7.8	-5.3	-6.8	-6.6	-8.2	-10.2	-9.4	-5.9	-4.8	-6.5	-7.7	-7.8	-12.3

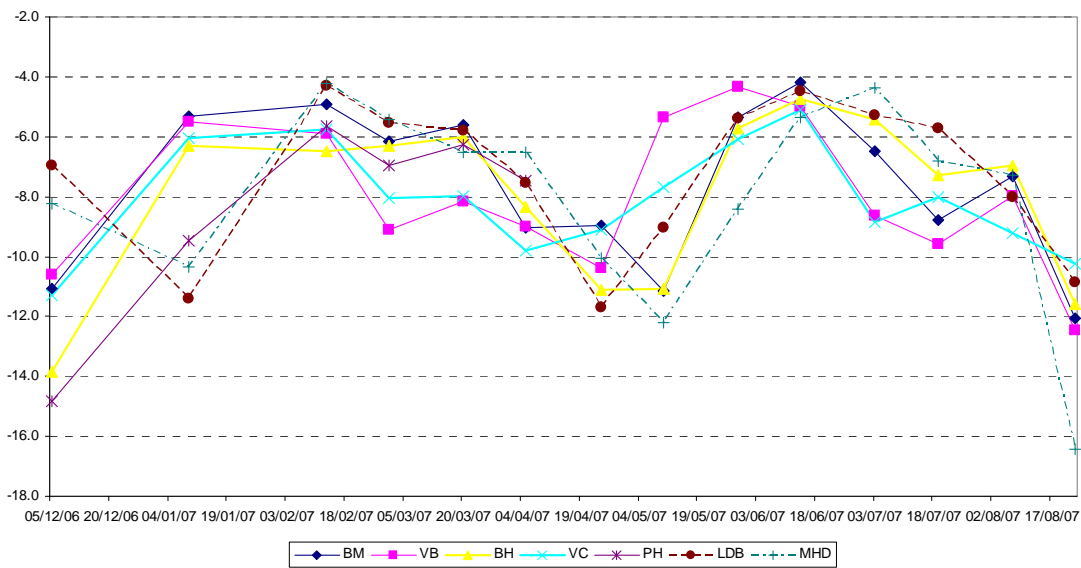


Figure 5.12. Backscatter temporal variation of the rice samples from ASAR WS descending mode data in WS and SA 2007 crops.

As discussed above, to estimate the rice area planted for the WS crop, the following thresholding algorithm (5.7) was proposed by using three-date image collected before or during the rice crop growth (5 Dec. 2006, 13 Feb., and 1 Mar. 2007). The result of classified image (Figure 5.13a) showed relatively good percentage errors of planted rice area when compared to the statistical data published in the Statistical Yearbook 2007 An Giang province (Table 5.15). In most districts, the percentage errors were between -14.3% and 14.7%, except Tri Ton and Tan Chau having the error of -23.7 and -20.4% respectively. However, the percentage error of the provincial scale was 0.7%.

$$(\sigma_{D_2}^0 - \sigma_{D_0}^0 \geq 3dB) \cup (\sigma_{D_2}^0 - \sigma_{D_{3a}}^0 \geq 3dB) \cap (\sigma_{D_2}^0 \geq -7dB) \quad (5.7)$$

$$(\sigma_{D_2}^0 - \sigma_{D_0}^0 \geq 3dB) \cap (\sigma_{D_2}^0 \geq -7dB) \quad (5.8)$$

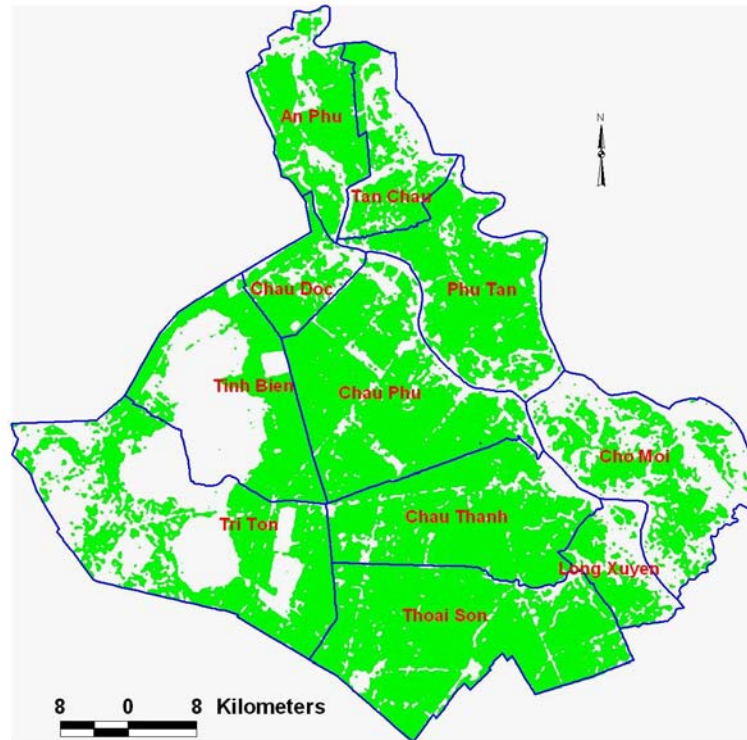
where

$\sigma_{D_0}^0$: backscattering coefficient of ASAR WS image taken on 5 Dec. 2006,

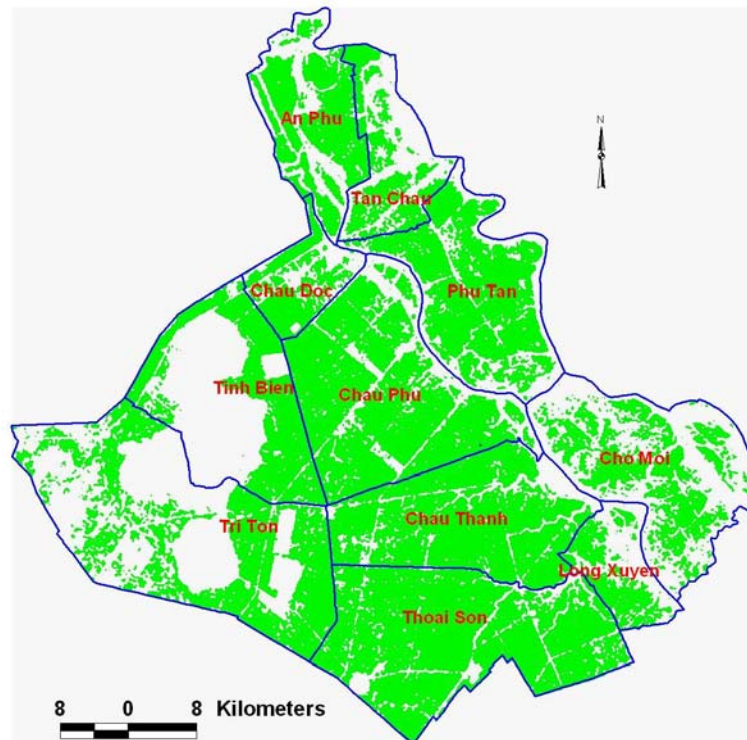
$\sigma_{D_2}^0$: backscattering coefficient of ASAR WS image taken on 13 Feb. 2007,

$\sigma_{D_{3a}}^0$: backscattering coefficient of ASAR WS image taken on 1 Mar. 2007.

In the case of two-date ASAR WS data utilisation (5.8), the percentage errors by district were slightly lower than that of three-date image used. At provincial level, the error of the rice classified (Figure 5.13b) was acceptable with an accuracy of 95%.



(a)



(b)

Figure 5.13. Rice and non-rice maps (rice in green) of WS 2007 crop produced by using three-date (a) and two-date (b) ASAR WS image taken in descending mode.

Table 5.15. Percentage errors between planted rice acreage in WS 2007 crop produced by ASAR WS data acquired on 5 Dec. 2006, 13 Feb. and 1 Mar. 2007 and statistical data.

District name	Statistical data (ha)	Using 3-date images		Using 2-date images	
		Rice (ha)	Percentage error (%)	Rice (ha)	Percentage error (%)
Phu Tan	23041	24480	6.2	22828	-0.9
Chau Phu	34382	37238	8.3	35261	2.6
Tri Ton	37373	28534	-23.7	26902	-28.0
Tinh Bien	14952	16312	9.1	15662	4.7
Chau Doc	7148	7398	3.5	6556	-8.3
Long Xuyen	5591	5884	5.2	5510	-1.5
Thoai Son	36691	42100	14.7	40634	10.7
Tan Chau	11420	9093	-20.4	8024	-29.7
An Phu	14443	15342	6.2	13849	-4.1
Cho Moi	17887	15323	-14.3	14411	-19.4
Chau Thanh	27686	30629	10.6	29449	6.4
Province	230614	232333	0.7	219086	-5.0

Similarly, the thresholds proposed for SA crop by using three-date (5.9) and two-date image (5.10) were as follows:

$$(\sigma_{D6}^0 - \sigma_{D4b}^0 \geq 3dB) \cup (\sigma_{D6}^0 - \sigma_{D8a}^0 \geq 3dB) \cap (\sigma_{D6}^0 \geq -7dB) \quad (5.9)$$

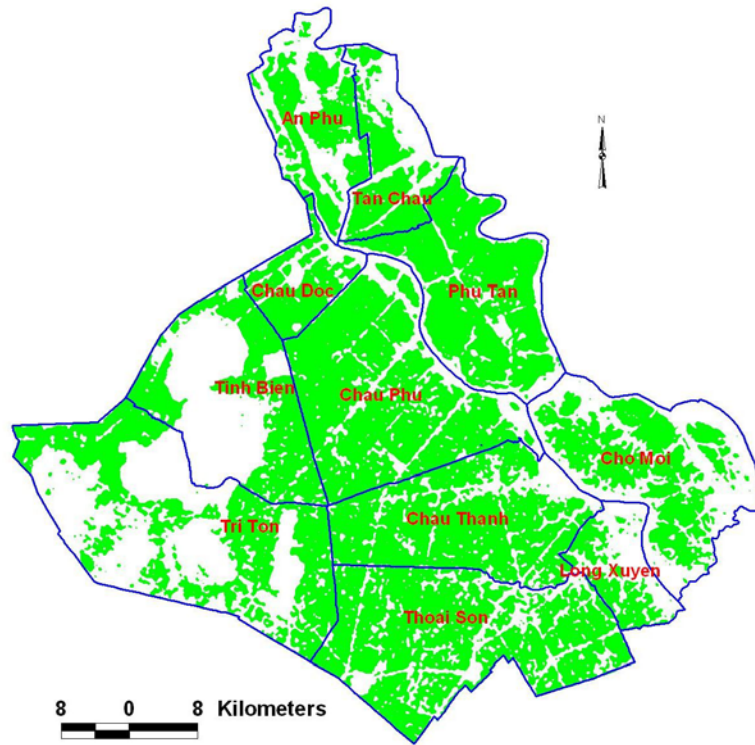
$$(\sigma_{D6}^0 - \sigma_{D4b}^0 \geq 3dB) \cap (\sigma_{D6}^0 \geq -7dB) \quad (5.10)$$

where

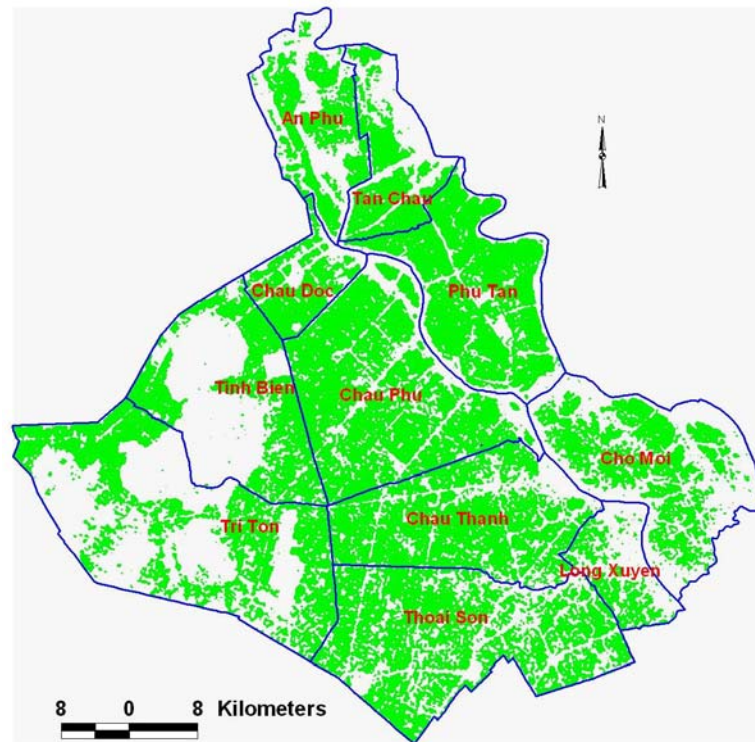
σ_{D4b}^0 : backscattering coefficient of ASAR WS image taken on 24 Apr. 2007,

σ_{D6}^0 : backscattering coefficient of ASAR WS image taken on 14 Jun. 2007,

σ_{D8a}^0 : backscattering coefficient of ASAR WS image taken on 7 Aug. 2007.



(a)



(b)

Figure 5.14. Rice and non-rice maps (rice in green) of SA 2007 crop produced by using three-date (a) and two-date (b) ASAR WS image taken in descending mode.

Again, Tri Ton district obtained a percentage error of -24.1%, lower than that of the other districts, when three-date image were utilised. At the provincial scale, the classified image (Figure 5.14a) attained a good accuracy with the percentage error of -4.5% and -11.3% in the case of three-date and two-date image used, respectively, when compared with existing statistical data (Table 5.16, Figure 5.14b).

Table 5.16. Percentage errors between planted rice acreage in SA crop produced by ASAR WS data acquired on 24 Apr., 14 Jun., and 7 Aug. 2007 and statistical data.

District name	Statistical data (ha)	Using 3-date images		Using 2-date images	
		Rice (ha)	Percentage error (%)	Rice (ha)	Percentage error (%)
Phu Tan	22968	24769	7.8	23948	4.3
Chau Phu	33959	35129	3.4	33010	-2.8
Tri Ton	35242	26748	-24.1	25126	-28.7
Tinh Bien	15164	15585	2.8	14623	-3.6
Chau Doc	7123	7315	2.7	6936	-2.6
Long Xuyen	5433	4566	-16.0	4195	-22.8
Thoai Son	35990	34843	-3.2	30151	-16.2
Tan Chau	10908	9383	-14.0	9223	-15.4
An Phu	12856	11295	-12.1	10576	-17.7
Cho Moi	16324	16943	3.8	15686	-3.9
Chau Thanh	27629	26865	-2.8	24826	-10.1
Province	223596	213441	-4.5	198300	-11.3

5.3.2.3 Image analysis of ASAR WS data in ascending and descending mode

The temporal backscatter of rice was recorded by 21 ASAR WS images collected in ascending and descending modes (Figure 5.15). In this case, only two-date image were used to segment rice and non-rice by the following thresholds for WS (5.11) and SA (5.12) 2007 crop season. One was acquired before seeding and the other in the middle of crop season, i.e. 5 Dec. 2006, 20 Feb. 2007, and 5 Apr., 5 June 2007 for WS and SA crops, respectively.

$$\text{For WS: } (\sigma_{A2}^0 - \sigma_{D0}^0 \geq 3dB) \cap (\sigma_{A2}^0 \geq -7dB) \quad (5.11)$$

$$\text{For SA: } (\sigma_{A5}^0 - \sigma_{D6}^0 \geq 3dB) \cap (\sigma_{A5}^0 \geq -7dB) \quad (5.12)$$

where

σ_{D0}^0 : backscattering coefficient of ASAR WS image taken on 5 Dec. 2007.

σ_{A2}^0 : backscattering coefficient of ASAR WS image taken on 20 Feb. 2007,

σ_{A5}^0 : backscattering coefficient of ASAR WS image taken on 1 May. 2007,

σ_{D6}^0 : backscattering coefficient of ASAR WS image taken on 14 Jun. 2007.

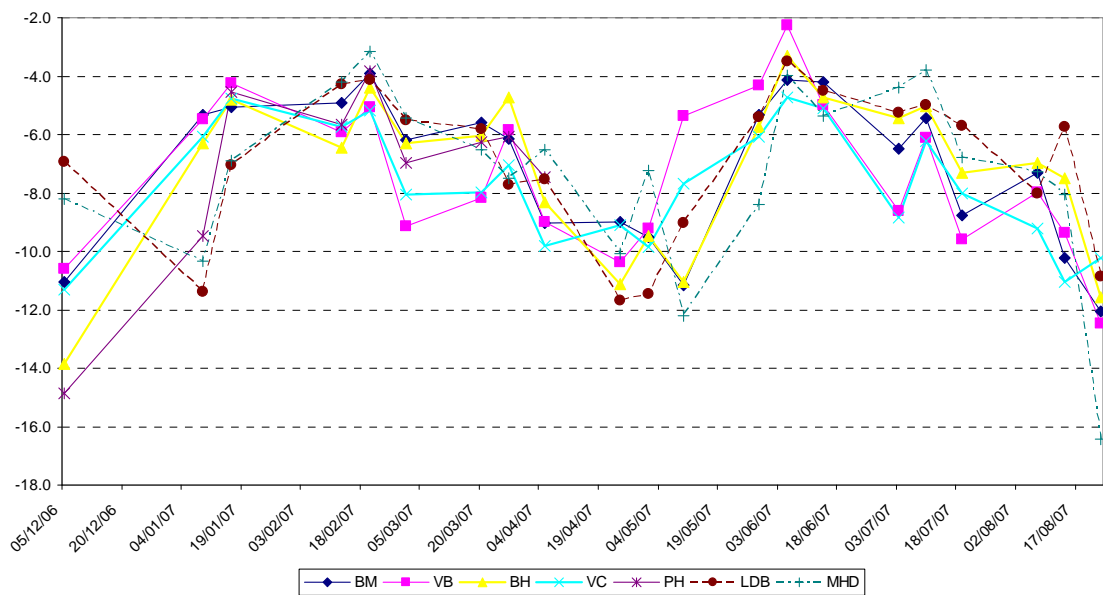


Figure 5.15. Backscatter temporal variations of the rice samples from ASAR WS ascending and descending mode data in WS and SA 2007 crops.

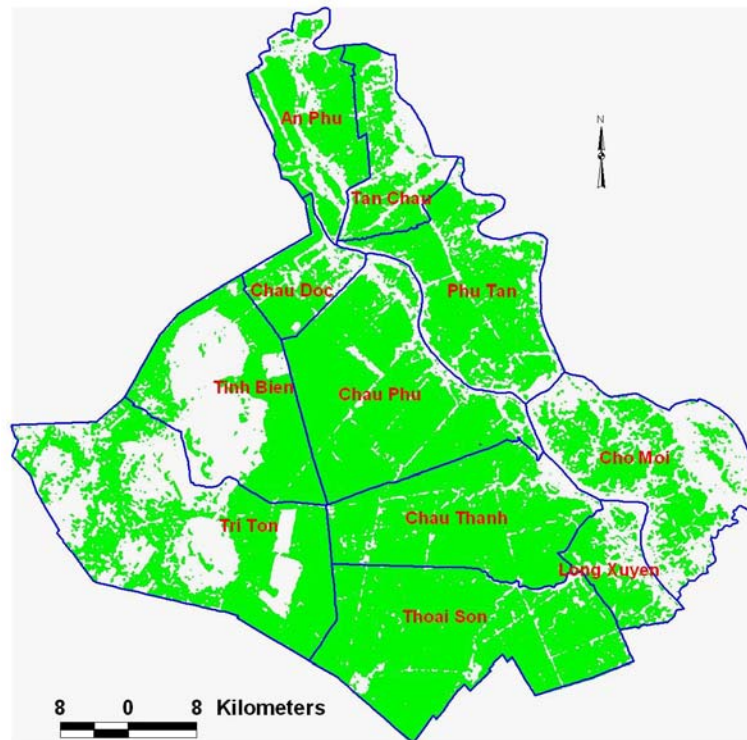
By using ascending and descending mode images, Tri Ton district obtained better results in both WS and SA crops. But Tinh Bien district had, in contrast, lower accuracy with the percentage error of 70% in SA 2007 crop. Considering the provincial level, the algorithm yielded a rather low error with a difference of 5.1% and 14.4% between planted rice area extracted from two ASAR WS images and that from the statistical agency for WS and SA crop, respectively (Tables 5.17 and 5.18). The rice and non-rice classes were displayed in the result maps (Figure 5.16).

Table 5.17. Percentage errors between planted rice acreage in WS crop produced by ASAR WS data acquired on 5 Dec. 2006, and 20 Feb. 2007 and statistical data.

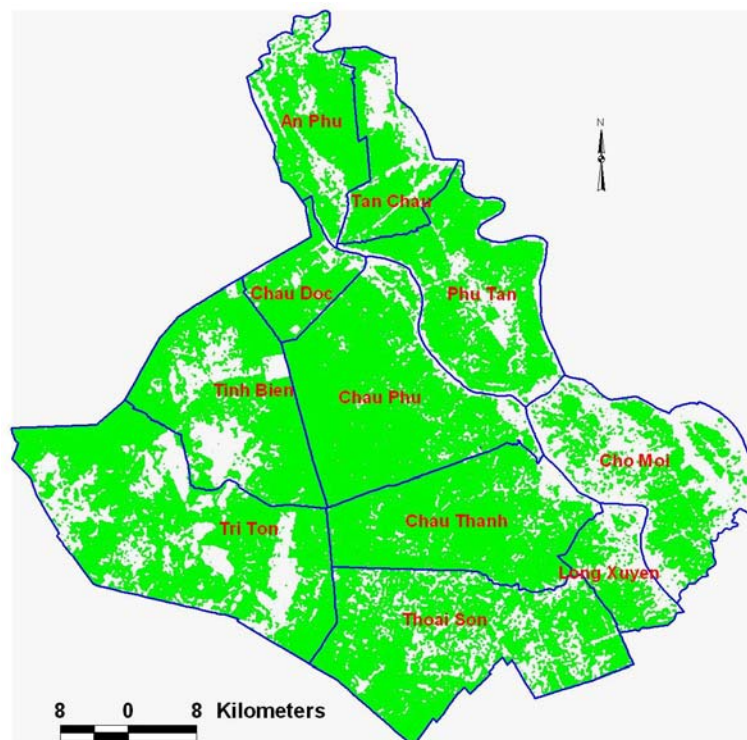
District name	Statistical data (ha)	Rice from ASAR (ha)	Percentage error (%)
Phu Tan	23041	23840	3.5
Chau Phu	34382	38807	12.9
Tri Ton	37373	33330	-10.8
Tinh Bien	14952	17961	20.1
Chau Doc	7148	7379	3.2
Long Xuyen	5591	6290	12.5
Thoai Son	36691	43637	18.9
Tan Chau	11420	9656	-15.4
An Phu	14443	14827	2.7
Cho Moi	17887	15404	-13.9
Chau Thanh	27686	31345	13.2
Province	230614	242476	5.1

Table 5.18. Percentage errors between planted rice acreage in SA crop produced by ASAR WS data acquired on 5 Apr., and 5 Jun. 2007 and statistical data.

District name	Statistical data (ha)	Rice from ASAR (ha)	Percentage error (%)
Phu Tan	22968	23942	4.2
Chau Phu	33959	39854	17.4
Tri Ton	35242	42216	19.8
Tinh Bien	15164	25774	70.0
Chau Doc	7123	8770	23.1
Long Xuyen	5433	6406	17.9
Thoai Son	35990	34839	-3.2
Tan Chau	10908	11051	1.3
An Phu	12856	15543	20.9
Cho Moi	16324	16316	0.0
Chau Thanh	27629	31155	12.8
Province	223596	255866	14.4



(a) WS 2007 crop



(b) SA 2007 crop

Figure 5.16. Rice and non-rice map (rice in green) of WS (a) and SA 2007 (b) crop produced by using two-date ASAR WS image taken in ascending and descending modes.

In brief, the classified results of rice layer by using HH polarisation WS data provided inconsistent accuracies between districts and crop seasons. Several districts such as Tri Ton, Tinh Bien, Tan Chau, and An Phu had low accuracies in some cases, possibly due to their location in the northwestern part of the province and hence, to be influenced by flood season on crop calendar of these districts during the year. However, in most cases, the ASAR WS data yielded low relative errors of planted rice area at provincial scale when compared to the published statistics, except for the case of WS crop season using ascending mode data.

Comparing ASAR APP and WS datasets used for rice mapping in the study area, APP data yielded rice maps with better accuracies at the district level. On the other hand, WS imagery with lower resolution proved as an effective data source for rice mapping at the provincial scale.

5.4 Conclusion

The following conclusions were reached on the proposed method for rice mapping using ASAR APP data:

- Applying a thresholding algorithm for polarisation ratio and VV values of single-date ASAR APP data acquired in the middle of crop season, the classified images showed only a maximum of 14% difference at the district level, with the exception of several districts in AW 2007 crop, when compared to the estimates from the agency statistical data. On the basis of the existing land use map, the User's accuracies of rice class assessed were very high, i.e. more than 93% for WS, SA 2007, and WS 2008 crops;
- A thresholding algorithm applied for polarisation ratio and VV data yielded higher classification accuracies when compared to that applied for polarisation ratio data alone.
- The supervised classification methods applied to single-date image taken in the middle period of crop season gave good accuracies when compared to the existing agency data. Thresholding method provided higher accuracy than the

others methods such as minimum-distance-to-means, maximum likelihood, and SAM;

- The thresholding algorithm provided consistent accuracies between districts (percentage errors ranging from -14 to 7% for WS 2007 crop and from -11 to 3% for SA 2007 crop) and between seasons across the province (from -7 to 4% percentage errors). Other classification methods did not improve classification accuracy despite their sophisticated algorithm formulation;
- A threshold formulated in this study, i.e. the “normalised difference polarisation ratio index” proved to produce high accuracies of mapping for most rice crops, when ASAR APP image acquired in the middle of crop season was used.
- Three acquisition dates of ASAR data are sufficient to accurately determine rice acreage planted for triple crop rice during the year, if the rice crop calendar is not much different among rice growing areas in the province;
- Radar backscattering coefficient is physical values (like reflectance in optical data). Therefore, methods formulated in this study can be adapted for other SAR sensor data.
- The method for rice crop inventory in the province before harvest was developed by using a single-date ASAR APP data taken in the mid-crop season. For operational purposes, this rice mapping algorithm needs to be further investigated for other crops and at other provinces in the Mekong River Delta.

In the case of ASAR WS data used for mapping rice, the following conclusions were drawn:

- The classified results of rice/non-rice by using multi-date ASAR WS images provided inconsistent accuracies between districts and crop seasons. However, it yielded low relative errors of planted rice area at the provincial scale when compared to the official statistics, except for the case of WS crop season using ascending mode data.

- By using two-date image in ascending or descending mode acquired on the first half of crop season, the classified images of rice and non-rice yielded acceptable accuracies.
- Overall, the use of ASAR WS data for rice mapping is appropriate at the regional level with its low cost and wide-area coverage.

In this work, a novel method was developed for accurately mapping rice area planted using single-date ASAR APP image taken in the middle of the rice cropping season. This is briefly described as follows:

1. An ASAR APP image acquired in the middle of the crop season is selected;
2. Image pre-processing steps were implemented: a) image calibration or conversion to the radar backscattering coefficient sigma nought (σ^0), b) image geo-correction, and c) image spatial filtering;
3. A polarisation ratio image was created;
4. Thresholding method was applied to the polarisation ratio and VV images in order to segment rice and non-rice classes;
5. A post-classification step was conducted by using majority filter to the classified image; and
6. A rice and non-rice map was finally produced.

In the case of changing cultural practices in the future, this method for rice mapping can also be used by paying attention to the threshold values of polarisation ratio and VV. These values need to be examined before applying the method.

Chapter 6

RICE YIELD ESTIMATION

6.1 Introduction

The overall objective of rice monitoring is rice yield estimation. Accurate crop production estimates can provide important information for agricultural planners and managers in both regional and national scales. This information can be computed on the basis of an estimated yield and rice acreage. For this dissertation, the latter was conducted in the previous chapter.

Traditionally, estimates of rice area planted and productivity are based on ground survey data. It is often time-consuming and expensive. In the early 1980s, much attention was paid to using optical remote sensing for crop yield estimation all over the world. Remarkable achievements were obtained after many studies were carried out (Li et al., 2003). Nevertheless, because of the limitations of the data acquisition for optical remote sensing, it was very difficult to carry out real-time monitoring of crop growth and estimate rice yield promptly based on these methods. Hence, radar remote sensing is the obvious choice as the most appropriate data source for agricultural monitoring and crop yield estimation in large areas in the tropical and sub-tropical regions (e.g. Ribbes and Le-Toan, 1999, Li et al., 2003, Chen and McNairn, 2006).

In previous research, experiments were carried out to show the effectiveness of Radarsat ScanSAR data for rice yield estimation in the whole Guangdong, South China (Li et al., 2003). A methodology was developed to deal with a series of issues in extracting rice information from the ScanSAR data, such as topographic influences, levels of agro-management, irregular distribution of paddy fields and different rice cropping systems. A model was provided for rice yield estimation based on the relationship between the backscatter coefficient of the multi-temporal SAR data and the biomass of rice.

Accurate statistics within each rice cycle can be generated by analysing space-borne earth observation data to determine rice acreage. On the other hand, rice yield, production and harvest time are estimated in a predictive way using an approach based on *agro-meteorological* and a statistical model. The agro-meteorological model (AMM) (Figure 6.1), which is built around a crop growth model, can determine crop yield (ton/ha) based on the parameters for soil characteristics and the rice crop variety. This also includes a full series of daily meteorological data (i.e. minimum/maximum/average temperature, sun radiation, relative humidity, wind speed, sun illumination hours, and precipitation) and the transplanting dates based on satellite data. The production estimate is simply calculated by combining yield estimation and the acreage.

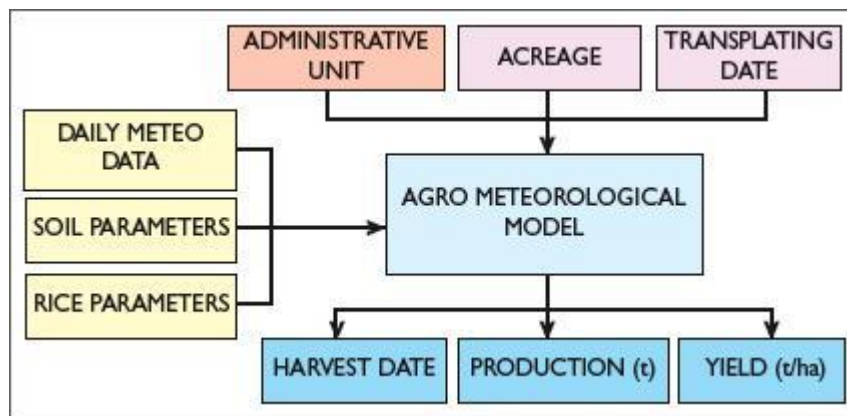


Figure 6.1. Agro-meteorological model of rice yield prediction (ESA/EOMD, 2006).

A methodology for rice yield estimation using agro-meteorological model and radar data was developed by Ribbes and Le Toan (1999). The approach consisted of coupling ERS-SAR data and the ORYZA rice production model (Le-Toan et al., 1999) in order to simulate plant growth and thus the final yield. Seeding date and plant biomass as a function of time were key parameters that could be both retrieved from SAR data and were necessary inputs to production models.

In order to estimate the rice yield of a field, the following operations were performed (MATRA-SYSTEMS, 2000):

- calculate the radar backscattering coefficient of the selected rice fields within the SAR images;
- retrieve, from SAR data, selected plant variables necessary to parameterise the rice growth model; and
- simulate rice growth using ORYZA model parameterised with input data retrieved from SAR data and climatic data.

In traditional rice cultivation system, radar backscatter was found to be strongly correlated to rice parameters, i.e. plant height and biomass (Le-Toan et al., 1997). Backscatter of rice fields increases steadily during the growing stage and then reaches a saturation level.

In this study, an analysis of the relationship between radar backscatter and modern cultivated rice biomass in the study site of An Giang was carried out as described in Chapter 4. HH and VV polarisation data increased strongly until the plant fresh biomass reaches 1000 g/m^2 (about 30 days after seeding). Nevertheless, for non-flooded fields, the increase in HH was smaller and VV even decreased. A saturation level of backscatter was reached at around 2000 g/m^2 at the middle of crop cycle. After saturation level, radar backscatter remains stable and slightly reduced for HH and rose for VV until biomass got to maximum values.

Concerning the polarisation ratio (HH/VV), only the increase of HH/VV at the beginning of the season was clearly observed, however, this increase was restricted to the first month or a limit of 1000 g/m^2 . After this date, the backscatter of non-flooded fields had a large dispersion with respect to biomass. Thus, retrieving rice biomass using HH, VV or HH/VV was not applicable to modern rice practices that prevailed in the study area. Consequently, the use of agro-meteorological model was not pursued due to the poor radar-biomass relationships discovered in the previous chapter. Instead, this study implemented the statistical model (ESA/EOMD, 2006).

6.2 Methods

6.2.1 Statistical model-based method

By using multiple regression analysis, the correlation between backscattering coefficients σ^0 of multi-date ASAR APP images acquired during the crop season and the in situ measured yield was derived. The distribution maps of estimated rice yield were then produced on the basis of that relationship. Consequently, rice production was finally estimated on the basis of these yield maps and rice/non-rice maps (Figure 6.2).

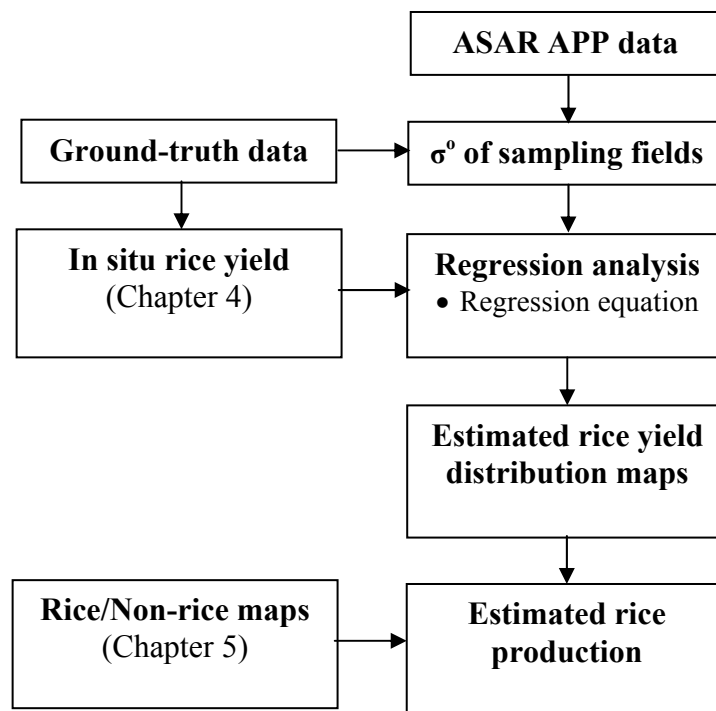


Figure 6.2. Methods used for rice yield estimation.

A statistical model-based approach (ESA/EOMD, 2006) for rice yield prediction is presented in Figure 6.3. It is followed in order to get a) rice production estimates by combining historical yield figures or in situ measurements and acreage measurements; and b) harvest date estimates by integrating crop calendar information and actual transplanting dates. In situ sample measurements are additionally considered to validate, at harvest time, the predicted production figures. Rice acreage measurements and transplanting dates are extracted from satellite SAR data.

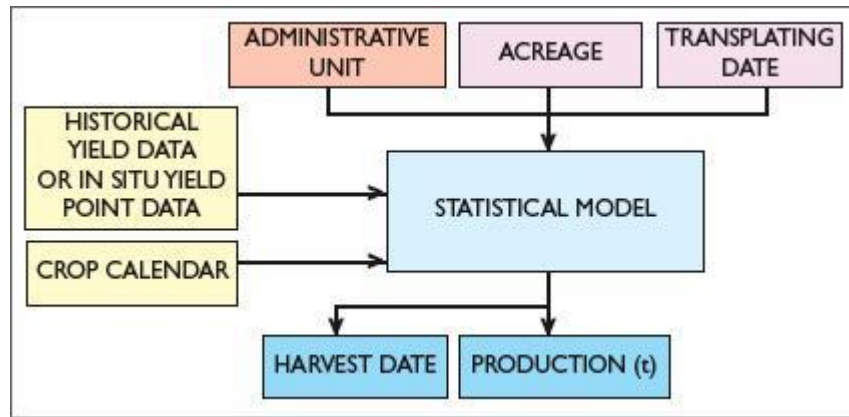


Figure 6.3. Statistical model of rice yield prediction (ESA/EOMD, 2006).

Previous studies reported their results on rice yield estimation from old generation radar imagery (i.e. Radarsat and ERS-SAR data). Some of them used the statistical model-based method. In the study site of Guangdong, South China, for example, an analysis of the relationship between the backscatter coefficient and rice biomass in each growing period on the Radarsat images was implemented (Li et al., 2003). A multivariate regression model based on radar remote sensing was established to reveal the relationship between the backscatter coefficient of time-series Radarsat data and rice yield. The accuracies of the yield estimation were over 94%.

In another study conducted in the Philippines (Chen and McNairn, 2006), a neural network-based yield model was used for predicting rice yield on a region by using multi-temporal Radarsat-1 data. The result was a prediction accuracy of 94% when the yields predicted by the neural network were compared with government statistics.

In this present work, rice yield and crop calendar of the sampling fields collected on the ground and the new generation dual-polarisation Envisat ASAR data were used. Multiple linear and non-linear regression analysis was implemented using in situ rice yield and biomass data. There were two villages selected for rice parameter collection from each of three districts: Chau Thanh (CT), Thoai Son (TS), and Cho Moi (CM), except one village for Chau Phu (CP) district. In each village, the measurements were done on five sampling fields.

During the rice crop season with 100-day rice varieties used, three ASAR APP images can be, in principle, collected in most cases. However, in the WS 2007 crop, most sampling fields were collected and measured at only two times, except nine sampling fields in Cho Moi district where three data collection times were done. Therefore, on the basis of regression analysis, some districts were chosen for examining rice yield estimation: a) Cho Moi district in WS 2007 season, and b) Cho Moi and Thoai Son districts in SA 2007 season.

Regression analysis between rice yield and radar backscattering coefficients derived from three-date ASAR APP images was performed using the line- and curve-fitting functions “LINEST” and “LOGEST” on Microsoft Excel[®]. A description of each function is provided below:

a) LINEST function

- Calculates the statistics for a line by using the “least squares” method to calculate a straight line that best fits the data, and returns an array that describes the line.
- The equation for the line is:
 - $y = mx + b$ (Simple linear regression) or
 - $y = m_1x_1 + m_2x_2 + \dots + b$ (Multiple linear regression if there are multiple ranges of x-values)

where the dependent y-value is a function of the independent x-values. The m-values are coefficients corresponding to each x-value, and b is a constant value. Note that y, x, and m can be vectors. The array that LINEST returns is $\{m_n, m_{n-1}, \dots, m_1, b\}$. LINEST can also return additional regression statistics.

b) LOGEST function

- Calculates an exponential curve that fits the data and returns an array of values that describes the curve.

- The equation for the curve is:
 - $y = b * m^x$ or
 - $y = (b * (m_1^{x_1}) * (m_2^{x_2}) * \dots)$ (if there are multiple x-values)where the dependent y-value is a function of the independent x-values. The m-values are bases corresponding to each exponent x-value, and b is a constant value. Note that y, x, and m can be vectors. The array that LOGEST returns is $\{m_n, m_{n-1}, \dots, m_1, b\}$. LOGEST can also return additional regression statistics.

The additional regression statistics are as follows:

- se_1, se_2, \dots, se_n : The standard error values for the coefficients m_1, m_2, \dots, m_n .
- se_b : The standard error value for the constant b ($se_b = \#N/A$ when const is FALSE).
- r^2 : The coefficient of determination. Compares estimated and actual y-values, and ranges in value from 0 to 1. If it is 1, there is a perfect correlation in the sample— there is no difference between the estimated y-value and the actual y-value. At the other extreme, if the coefficient of determination is 0, the regression equation is not helpful in predicting a y-value.
- se_y : The standard error for the y estimate.
- F: The F statistic, or the F-observed value. Use the F statistic to determine whether the observed relationship between the dependent and independent variables occurs by chance.
- df : The degrees of freedom. Use the degrees of freedom to help finding F-critical values in a statistical table. Compare the values finding in the table to the F statistic returned by LINEST to determine a confidence level for the model.
- ss_{reg} : The regression sum of squares.
- ss_{resid} : The residual sum of squares.

The rice production by district of each crop season in the study site was then estimated based on the relationship between sampling rice yield (y-value) and backscattering coefficients (multiple x-values), and rice acreage derived from ASAR

APP data as discussed in Chapter 5. The accuracy of the estimated rice production was finally assessed against the official statistics published in the Statistical Yearbook 2007 An Giang province (AGSO, 2008b).

6.3 Results and discussion

In this section, regression analysis was discussed to understand the correlation between rice yield, biomass, and radar backscattering coefficients. The rice production was then estimated for several districts where ground data collection was carried out during the satellite overpass in the year 2007.

6.3.1. Regression analysis between rice biomass and yield

As discussed in Section 6.2.1 “Statistical model-based method”, multiple linear regression analysis between in situ rice yield and biomass was performed for Cho Moi district in WS 2007 crop season (Table 6.1). The coefficient of determination between rice yield and dry biomass was 0.913. It proved a very good correlation between rice biomass and yield within the samples.

Table 6.1. Correlation between sample rice yield and dry biomass in WS 2007 crop.

District name	r²
CP	
CT	
TS	
CM (9 samples)	0.913

In SA 2007 crop, regression analysis was done for most districts and also for the province. Correlation between rice yield and biomass was different from district to district. The coefficient of determination in the cases of Chau Phu, Chau Thanh, and Thoai Son districts ranged from 0.558 to 0.778 for dry biomass. Cho Moi district

had a highest correlation of 0.998. This high correlation may be attributed to only one-week maximum difference in sowing date between sampling fields observed in Cho Moi. In contrast, the correlation at the provincial level (i.e. all sampling fields used) was very poor—less than 0.1 (Table 6.2). This can be due to: a) a maximum one-month shift in crop calendar took place between areas, b) difference in rice varieties used, and c) cultural practices were different from area to area.

Table 6.2. Correlation between sample rice yield and dry biomass in SA 2007 crop (n=10).

District name	r²
CP	0.558
CT	0.778
TS	0.732
CM	0.998
Province	0.078

6.3.2. Regression analysis between HH, VV, HH/VV and sample rice yield

In order to predict the rice production in the study area, a multiple linear regression analysis between rice yield with HH, VV backscattering coefficients, and polarisation ratios was firstly implemented for the sampling fields in SA 2007 crop. This was due to the availability of three-date ASAR APP images during the 2007 crop season (see appendix B1 “*Backscattering coefficient and yield of sampling fields, and their regression models - A case of Summer Autumn 2007 crop*”). A distribution map of estimated rice yield was then produced based on a good relationship. Rice production by district was finally estimated.

The correlation between sample rice yield with HH, VV, and polarisation ratio by village (five sampling fields) was analysed (Table 6.3). The coefficients of determination r^2 attained were very high for most villages. However, a few areas had

very low r^2 values, such as in the case of HH data of BH (0.044) or VV data of BM village (0.345). An explanation may be due to three different varieties (Jasmine, 2517, and 1490-55) used by farmers for five sampling fields selected in BH village. When the coefficient was computed for all of fields (provincial level), it showed that the correlation was very low (~ 0.1). The reason for that can be explained by the same explanation provided in Section 6.3.1 “Regression analysis between rice biomass and yield”.

Table 6.3. Correlation between sample rice yield and HH, VV, HH/VV by village in SA 2007 crop using LINEST function (n=5).

District name	Village name	r^2		
		HH	VV	HH/VV
CP	BM	0.977	0.345	0.976
CT	VB	0.882	1.000	0.588
	BH	0.044	0.991	0.689
TS	VC	0.839	0.659	0.977
	PH	1.000	0.994	0.767
CM	LDB	0.934	0.997	0.927
	MHD	0.830	0.658	0.978
Province		0.088	0.062	0.145

In order to derive the relationship for predicting the rice yield by district, a multiple linear regression analysis using LINEST function at the district level was done. In three districts (i.e. Chau Thanh, Thoai Son and Cho Moi), which had 10 sampling rice fields in two villages, the coefficients of determination between yield and polarisation ratios of Cho Moi and Thoai Son were higher than that of the others (i.e. 0.833 and 0.772, respectively) (Table 6.4). This difference can be explained by the following factors: a) only one-week maximum difference in seedling date between ten sampling fields observed in Cho Moi, and b) nine of the ten sampling fields in Thoai Son were planted with the same seed of 50404 variety. Whereas in Chau Thanh district, the sampling fields were grown with various rice varieties and the area has more than two weeks shift in crop calendar between field to field.

Therefore, the rice yield was estimated on the basis of the regression models of Cho Moi and Thoai Son cases.

Table 6.4. Correlation between sample rice yield and HH, VV, HH/VV by district in SA 2007 crop using LINEST function (n=10).

District name	r^2		
	HH	VV	HH/VV
CP	0.977	0.375	0.976
CT	0.096	0.762	0.321
TS	0.522	0.669	0.772
CM	0.653	0.328	0.833
Province	0.088	0.062	0.145

On the other hand, a non-linear regression analysis using LOGEST function was tested for Cho Moi district to compare its relationship with that of the linear regression model. The results showed that the coefficients of determination in both cases were nearly the same (Tables 6.4 and 6.5).

Table 6.5. Correlation between sample rice yield and HH, VV, HH/VV by district in SA 2007 crop using LOGEST function (n=10).

District name	r^2		
	HH	VV	HH/VV
CP			
CT			
TS			
CM	0.659	0.326	0.834
Province			

The regression equation between rice yield and polarisation ratios of sampling fields at Cho Moi district in SA 2007 crop using LINEST function was determined as follows (6.1):

$$Y_{Ra} = 0.072 Ra_1 - 0.017 Ra_2 - 0.002 Ra_3 + 0.503 \quad (6.1)$$

$$r^2 = 0.833, se_y = 0.11 \text{ ton/ha}$$

where

Y_{Ra} : rice yield (kg/m²),

Ra_1 : polarisation ratio of first date image,

Ra_2 : polarisation ratio of second date image,

Ra_3 : polarisation ratio of third date image,

r^2 : the coefficient of determination,

se_y : the standard error for the y estimate.

The values of r^2 and se_y were 0.833 and 0.11 ton/ha, respectively. It indicates that the relationship is positive and can be consequently used to predict the yield for all rice fields planted in SA 2007 crop season of the Cho Moi district.

The regression equation between rice yield and polarisation ratios of sampling fields planted in SA 2007 crop at Cho Moi district using LOGEST function (6.2) was formulated follows:

$$Y_{Ra} = 1.16^{Ra_1} * 0.965^{Ra_2} * 0.995^{Ra_3} * 0.503 \quad (6.2)$$

$$r^2 = 0.834, se_y = 0.22 \text{ ton/ha}$$

where

Y_{Ra} : rice yield (kg/m²),

Ra_1 : polarisation ratio of first date image,

Ra_2 : polarisation ratio of second date image,

Ra_3 : polarisation ratio of third date image,

r^2 : the coefficient of determination,

se_y : the standard error for the y estimate.

Subsequent to Cho Moi district, the regression analysis using LINEST function between rice yield and polarisation ratio of sampling fields in SA 2007 crop at Thoai Son district was derived as follows:

$$Y_{Ra} = -0.124 Ra_1 - 0.034 Ra_2 + 0.114 Ra_3 + 0.704 \quad (6.3)$$

$$r^2 = 0.772, se_y = 0.54 \text{ ton/ha}$$

where

Y_{Ra} : rice yield (kg/m²),

Ra_1 : polarisation ratio of first date image,

Ra_2 : polarisation ratio of second date image,

Ra_3 : polarisation ratio of third date image,

r^2 : the coefficient of determination,

se_y : the standard error for the y estimate.

In WS 2007 crop season, multiple linear regression analysis was only examined for the case of sampling fields grown at LDB village and Cho Moi district (see appendix B2 “*Backscattering coefficient and yield of sampling fields, and their regression models - A case of Winter Spring 2007 crop*”). The relationship between rice yield and polarisation ratios was presented in Tables 6.6 and 6.7.

Table 6.6. Correlation between sample rice yield and HH, VV, HH/VV by village in WS 2007 crop using LINEST function (n=5).

Field name	r^2		
	HH	VV	HH/VV
BM			
VB			
BH			
VC			
PH			
LDB	0.935	0.780	0.134
MHD			
Province			

Table 6.7. Correlation between sample rice yield and HH, VV, HH/VV by district in WS 2007 crop using LINEST function (n=9).

District name	r^2		
	HH	VV	HH/VV
CP			
CT			
TS			
CM	0.575	0.661	0.675
Province			

The regression equation between rice yield and polarisation ratio of nine sampling fields in WS 2007 crop at Cho Moi district using LINEST function (6.4) was formulated as follows:

$$Y_{Ra} = -0.033 Ra_1 + 0.017 Ra_2 + 0.019 Ra_3 + 0.628 \quad (6.4)$$
$$r^2 = 0.675, se_y = 0.38 \text{ ton/ha}$$

where

Y_{Ra} : rice yield (kg/m^2),

Ra_1 : polarisation ratio of first date image,

Ra_2 : polarisation ratio of second date image,

Ra_3 : polarisation ratio of third date image,

r^2 : the coefficient of determination,

se_y : the standard error for the y estimate.

The coefficients of determination and the standard errors for the rice yield estimated in the cases of Cho Moi in WS 2007 were 0.675 and 0.38, and of Thoai Son in SA 2007 crop were 0.772 and 0.54, respectively. The values of 0.833 and 0.11, respectively, were found for Cho Moi in SA 2007. The two cases of Cho Moi in WS 2007 and Thoai Son in SA 2007 crop obtained lower correlation between in situ rice yield and polarisation ratio. It maybe due to a) seven various rice varieties were grown in ten sampling fields of Cho Moi in WS 2007, and b) in the case of Thoai Son in SA 2007 crop, about three-week shift in crop calendar was observed from sampling fields between Vinh Binh and Phu Hoa villages.

6.3.3 Distribution map of estimated rice yield

The detected rice fields was classified into 17 yield levels, ranging from 0.5 to 10 ton/ha, through analysis of the relationship between rice yield and backscattering coefficients of three-date ASAR APP images acquired over the rice growing period.

The yield of rice fields planted in SA 2007 crop at Cho Moi district was estimated on the basis of the correlation between in situ rice yield and polarisation

ratios (Equation 6.1). The rice fields with estimated yield levels ranging from four to six ton per hectare were dominated and occupied 89.8% total of rice area planted in this crop season (Table 6.8), whereas the statistical average yield of rice in SA 2007 crop at the district was 4.86 ton/ha (AGSO, 2008b). Consequently, there was a good agreement between rice production estimated from ASAR APP and the official statistics with the difference of 3.2% between them (Table 6.9). This accuracy of yield estimation was higher than those reported in the previous studies (e.g. Ribbes and Le-Toan, 1999, Li et al., 2003, Chen and Mcnairn, 2006).

Table 6.8. Yield estimation for SA crop in Cho Moi district using three-date polarisation ratio and LINEST regression analysis.

Level	Rice area (Ha)	Estimated yield (Ton/Ha)	Estimated production (Ton)	Percentage (%)
1	5.4	0.5	2.7	0.0
2	21.1	1.5	31.7	0.0
3	120.8	2.5	302.1	0.4
4	1033.0	3.5	3615.3	4.4
5	2621.6	4.25	11141.7	13.6
6	6476.5	4.75	30763.6	37.6
7	4614.0	5.25	24223.5	29.6
8	1279.9	5.75	7359.3	9.0
9	374.9	6.25	2343.0	2.9
10	132.3	6.75	893.2	1.1
11	58.5	7.25	424.2	0.5
12	28.1	7.75	217.5	0.3
13	15.0	8.25	123.8	0.2
14	10.0	8.75	87.2	0.1
15	6.7	9.25	62.1	0.1
16	4.8	9.75	46.8	0.1
17	18.2	10	182.0	0.2
Sum	16820.8		81819.7	100

Table 6.9. Percentage error between rice production in SA 2007 crop at Cho Moi district derived from three-date polarisation ratio data using LINEST function and statistical data.

District name	Agency data (Ton)	Estimated Production (Ton)	Percentage error (%)
Cho Moi	79256	81819.7	3.2

A distribution map of estimated yield of the rice fields planted in SA 2007 crop at Cho Moi district using three-date polarisation ratios and LINEST regression analysis was plotted in Figure 6.4. Most of the rice fields with yield ranging from four to six ton /ha was distributed throughout the district.

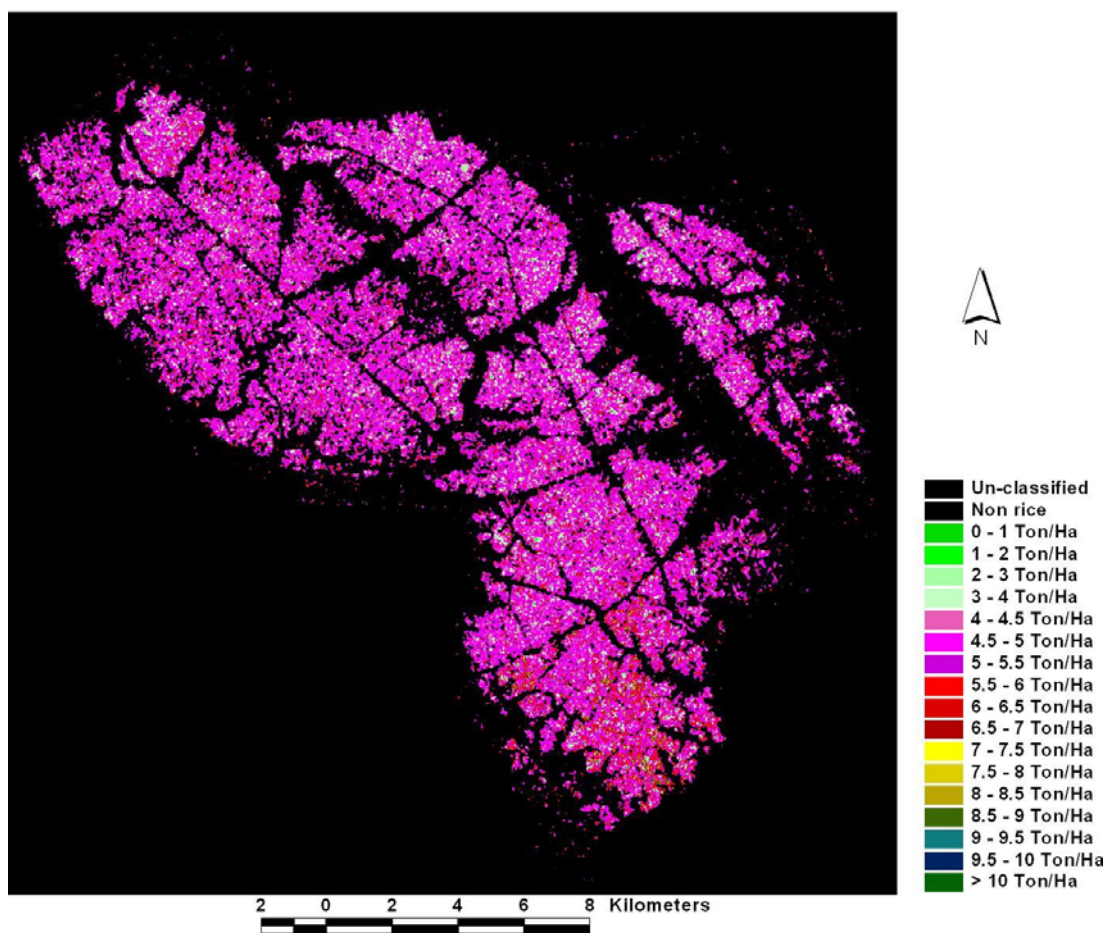


Figure 6.4. A distribution map of estimated rice yield in SA 2007 crop at Cho Moi district using three-date polarisation ratio and LINEST regression analysis.

Similarly, non-linear regression equation (6.2) was used to estimate the yield of the rice fields in SA 2007 crop of Cho Moi district. The total area of rice fields which had the estimated yield of four to six ton/ha was 88.9% of rice acreage planted in SA 2007 crop at Cho Moi district (Table 6.10). The percentage error between rice production estimated from ASAR APP data and that from statistical yearbook 2007 was 3.4% (Table 6.11). A distribution map of the estimated rice yield of the fields grown in SA 2007 crop was presented in Figure 6.5

Table 6.10. Yield estimation for SA 2007 crop at Cho Moi district using three-date polarisation ratio and LOGEST regression analysis.

Level	Rice area (Ha)	Estimated yield (Ton/Ha)	Estimated production (Ton)	Percentage (%)
1	2.1	0.5	1.1	0.0
2	6.4	1.5	9.6	0.0
3	68.6	2.5	171.6	0.2
4	1015.6	3.5	3554.7	4.3
5	2934.2	4.25	12470.5	15.2
6	6609.8	4.75	31396.7	38.3
7	4184.2	5.25	21967.2	26.8
8	1226.9	5.75	7054.6	8.6
9	398.2	6.25	2488.6	3.0
10	161.4	6.75	1089.6	1.3
11	75.1	7.25	544.2	0.7
12	42.4	7.75	328.4	0.4
13	25.2	8.25	208.1	0.3
14	15.5	8.75	135.9	0.2
15	10.8	9.25	100.0	0.1
16	7.3	9.75	70.8	0.1
17	37.7	10	376.9	0.5
Sum	16821.5		81968.4	100

Table 6.11. Percentage error between rice production in SA 2007 crop at Cho Moi district derived from three-date polarisation ratio data using LOGEST function and statistical data.

District name	Agency data (Ton)	Estimated Production (Ton)	Percentage error (%)
Cho Moi	79256	81968.4	3.4

The results of the above analysis using linear or non-linear regression equation proved that the statistical model-based method worked very well in the case of SA 2007 crop at Cho Moi district where the relationship between in situ yield point data and polarisation ratio data was positive with the high correlation coefficient of 0.913.

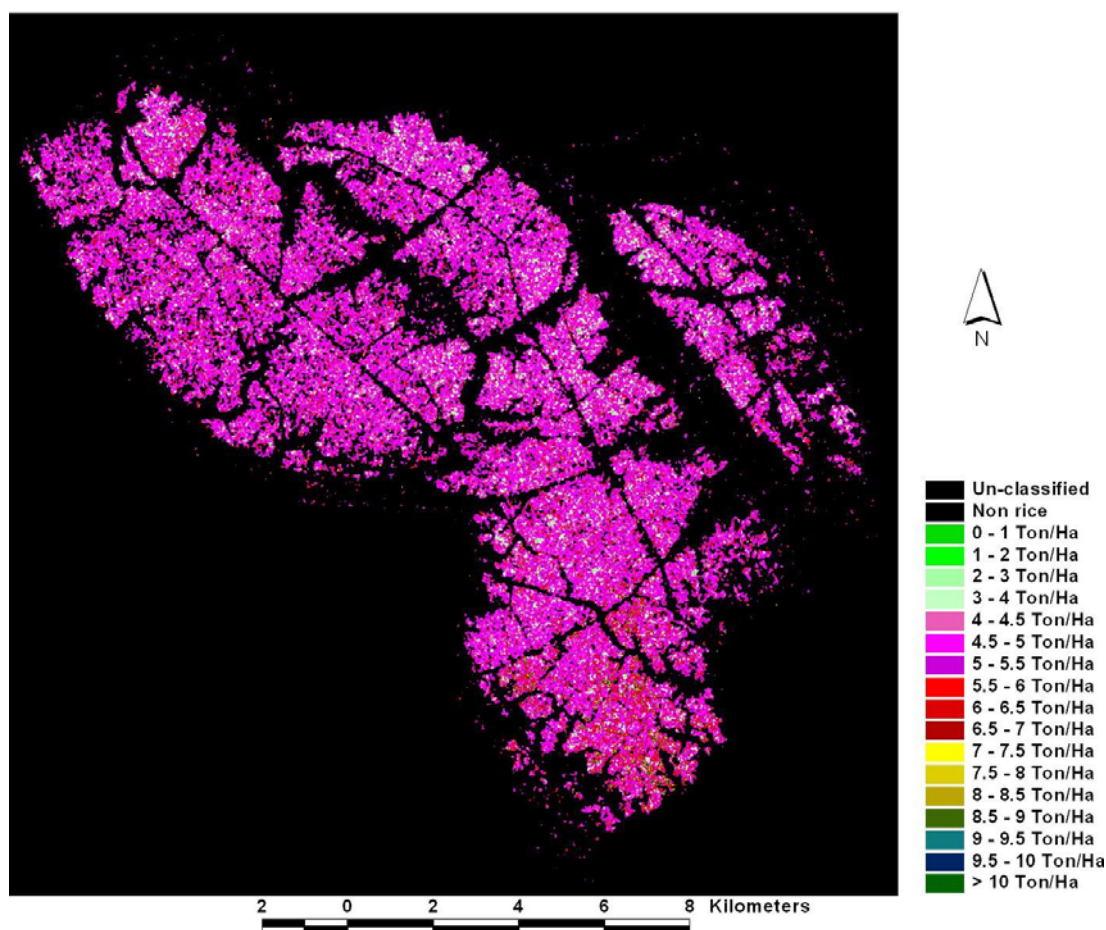


Figure 6.5. A distribution map of estimated rice yield of SA crop in Cho Moi district using three-date polarisation ratio and LOGEST regression analysis.

The same method was also applied in order to estimate rice production in WS 2007 crop at Cho Moi district. The rice yield of the same sampling fields was collected for the various crops in the year 2007. Using regression equation (6.4) rice production was estimated (Table 6.12). About 80% of total rice area planted had the estimated yield from 4.5 to 8 ton/ha, whereas the statistical mean yield of the district was 7.36 ton/ha. Consequently, the rice production in WS 2007 crop of Cho Moi district was underestimated, i.e. 19.4% lower than the agency statistics (Table 6.13).

Table 6.12. Yield estimation for WS 2007 crop at Cho Moi district using three-date polarisation ratio and LINEST regression analysis.

Level	Rice area (Ha)	Estimated yield (Ton/Ha)	Estimated production (Ton)	Percentage (%)
1	1.8	0.5	0.9	0.0
2	4.7	1.5	7.1	0.0
3	25.0	2.5	62.4	0.1
4	225.8	3.5	790.1	0.7
5	632.5	4.25	2688.1	2.5
6	2166.8	4.75	10292.4	9.7
7	3482.7	5.25	18284.3	17.2
8	2957.8	5.75	17007.3	16.0
9	2213.0	6.25	13831.1	13.0
10	1620.2	6.75	10936.2	10.3
11	1155.5	7.25	8377.6	7.9
12	811.8	7.75	6291.8	5.9
13	573.8	8.25	4734.0	4.5
14	401.0	8.75	3508.6	3.3
15	279.1	9.25	2581.9	2.4
16	194.5	9.75	1896.1	1.8
17	483.8	10	4838.4	4.6
Sum	17229.8		106128.2	100

Table 6.13. Percentage error between rice production in WS 2007 crop at Cho Moi district derived from three-date polarisation ratio data using LINEST function and statistical data.

District name	Agency data (Ton)	Estimated Production (Ton)	Percentage error (%)
Cho Moi	131595	106128.2	-19.4

Figure 6.6 presented a map of rice yield distribution in WS 2007 crop. The rice area planted that had estimated yield from eight ton/ha or more was 16.6% of the total. These areas were mostly distributed in the south western parts of the district.

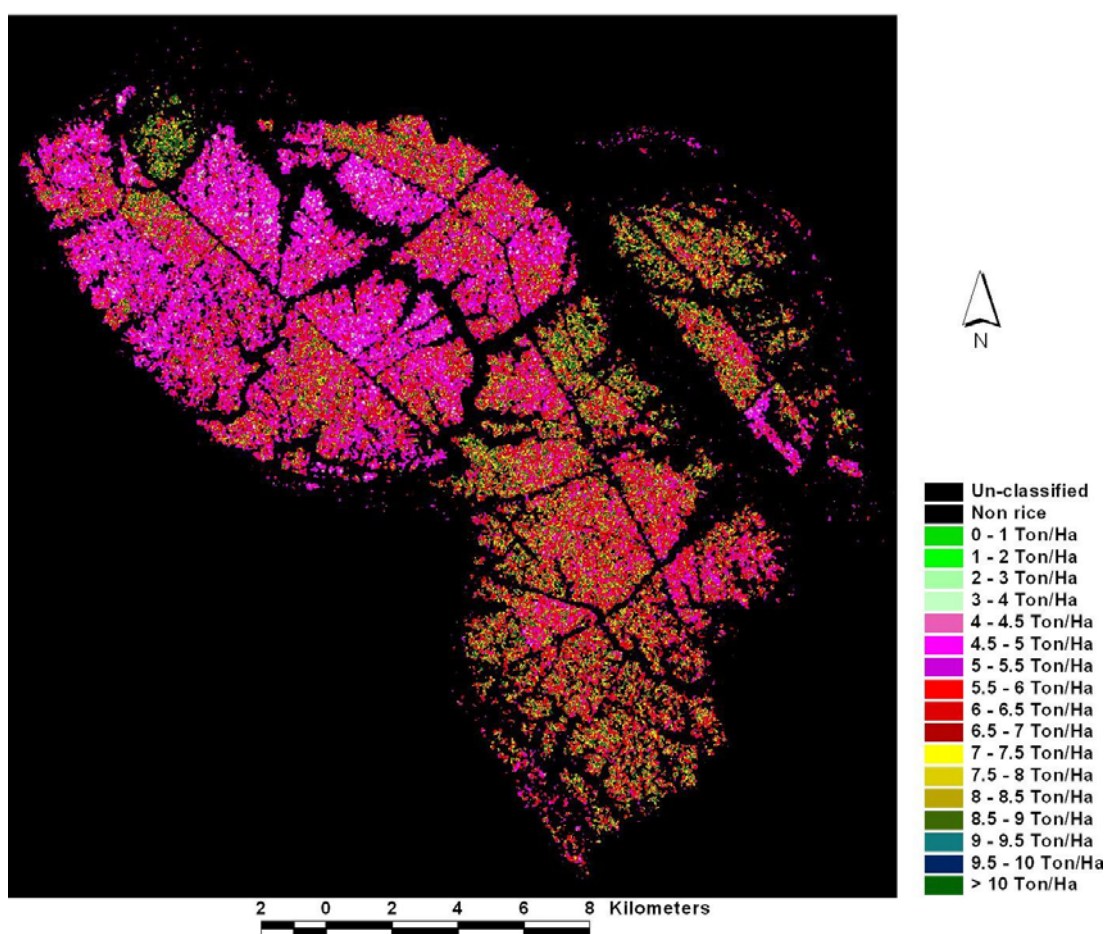


Figure 6.6. A distribution map of estimated rice yield of WS crop in Cho Moi district using three-date polarisation ratio and LINEST regression analysis.

Another district (Thoai Son) was chosen for estimating the rice yield in SA 2007 crop. The multiple linear regression equation (6.3) was utilised in rice yield estimation. In the total rice area planted in SA crop, nearly 90% had the estimated

yield from 5 ton/ha or more (Table 6.14), whereas the mean value of statistical yield of Thoai Son district was 5.07 ton/ha. Thus, rice production was estimated at about 30% higher than the statistics (Table 6.15). It means that the accuracies of estimated rice production for the cases of Cho Moi in WS 2007 and Thoai Son in SA 2007 crop were lower than those reported by previous research (Ribbes and Le-Toan, 1999, Li et al., 2003, Chen and Mcnairn, 2006).

Table 6.14. Yield estimation for SA crop in Thoai Son district using three-date polarisation ratio and LINEST regression analysis.

Level	Rice area (Ha)	Estimated yield (Ton/Ha)	Estimated production (Ton)	Percentage (%)
1	148.9	0.5	74.4	0.0
2	315.6	1.5	473.3	0.2
3	711.8	2.5	1779.4	0.8
4	1669.6	3.5	5843.7	2.5
5	1535.9	4.25	6527.5	2.8
6	2265.9	4.75	10762.9	4.5
7	3115.3	5.25	16355.5	6.9
8	3745.5	5.75	21536.8	9.1
9	3742.1	6.25	23388.0	9.9
10	3179.2	6.75	21459.7	9.1
11	2561.6	7.25	18571.9	7.8
12	2068.8	7.75	16032.8	6.8
13	1677.4	8.25	13838.9	5.8
14	1372.4	8.75	12008.7	5.1
15	1126.2	9.25	10416.9	4.4
16	925.4	9.75	9022.3	3.8
17	4870.8	10	48707.5	20.6
Sum	35032.3		236800.3	100

Table 6.15. Percentage error between rice production in SA 2007 crop at Thoai Son district derived from three-date polarisation ratio data using LINEST function and statistical data.

District name	Agency data (Ton)	Estimated Production (Ton)	Percentage error (%)
Thoai Son	182469	236800.3	29.8

In order to explain why lower accuracies of rice yield estimation occurred in the cases of Cho Moi in WS 2007 and Thoai Son in SA 2007 crop, Table 6.16 presented the difference between the statistical data (AGSO, 2008b) and the yield data collected during the ground campaigns in those districts. The comparison demonstrated that in SA crop at Cho Moi district, the mean yield (0.494 kg/m²) collected from ten sampling fields was nearly the same with the statistical yield data of Cho Moi (0.486 kg/m²) and the estimated rice production was consequently not much different from the statistics (error of 3.2%). In contrast, in two other cases with higher percentage errors (errors of -19.4% and 29.8%), it may be due to the rice yield of fields investigated on the ground (0.668 and 0.593 kg/m²) was not representative of the yield of entire rice area in the district (0.736 and 0.507 kg/m²). Additional research should be done to find out the real reasons for these cases.

Because different districts in the case study had different correlations and accuracies, therefore there was a need to design a mapping strategy that will first employ a “stratification approach”. It means that mapping should be done by district rather than the entire province. Stratification approach should be used to classify rice fields in the province separately into areas (by district) with the same cultural practices. Subsequently, multiple regression analysis between in situ rice yield and polarisation ratios of sampling fields can be examined. A rice yield map can be finally produced based on a regression equation.

Table 6.16. Difference between ground data and statistical data.

Sampling field N ^o	In situ measured rice yield		
	WS07_CM	SA07_CM	SA07_TS
S1	0.650	0.520	0.617
S2	0.650	0.520	0.571
S3	0.650	0.500	0.386
S4	0.600	0.480	0.540
S5	0.600	0.500	0.571
S6	0.700	0.500	0.617
S7	0.700	0.500	0.710
S8	0.760	0.500	0.602
S9	0.700	0.460	0.602
S10		0.460	0.710
Average in situ yield (kg/m ²)	0.668	0.494	0.593
Statistical yield by district (kg/m ²)	0.736	0.486	0.507
Percentage difference in yield (%)	-9.3	1.6	16.9
Estimated production by district (ton)	106128	81820	236800
Statistical production by district (ton)	131595	79256	182469
Percentage error of estimated production (%)	-19.4	3.2	29.8

6.4 Conclusion

The agro-meteorological model-based method for rice yield prediction will not work in Vietnam's Mekong Delta because retrieving rice biomass using HH, VV or polarisation ratio data was not applicable to modern rice growing practices prevailing in the area.

The statistical model-based method worked very well in the case of Cho Moi district where there is a strong positive relationship between in situ measured yield point data and polarisation ratio data derived from three-date ASAR APP images. The sampling rice fields chosen were represented for the entire region. The high accuracy of 97% was found when the rice production estimated from ASAR APP data was compared to the government statistics. This accuracy result is better than that of other previous studies (ranging from 85% to 94%).

The rice yield estimation model varies from region to region, where the cultural practices and crop calendar were significantly different in the study site. Therefore, the yield mapping strategy using time series ASAR APP data is proposed as follows:

- a) Stratification approach should be firstly used in order to separately classify rice fields in the province into areas with the same cultural practices in the districts;
- b) Multiple regression analysis between polarisation ratio data and in situ rice yield is implemented for each district;
- c) Based on this correlation, rice yield map is established; and
- d) Rice production is estimated on the basis of the yield map and rice/non-rice map.

Further research should be done to improve and validate the statistical model-based method for predicting rice production using dual polarisation ASAR data.

Chapter 7

CONCLUSIONS

7.1 Summary of Findings

This section summarises the results discovered from the research work on: a) the relationship between radar backscatter coefficients and the in situ measured parameters (e.g. age and biomass) of rice crops over an entire growth cycle, b) algorithms for mapping the rice cropping systems for one year cycle, and c) a rice yield prediction model using new generation ASAR imagery.

7.1.1 Analysis of rice backscatter

As a consequence of changes brought by modern cultural practices, the radar backscattering behaviour was much different from that of the traditional rice plant. At the early stage of the season, direct sowing on fields with rough and wet soil surface provided very high backscatter values for both HH and VV data (about -7 to -2 dB). Around 10 – 20 days after sowing, rice plants attained more or less 20 cm high and field flooding decreases dramatically the backscatter to -18 to -12 dB. The backscatter then increases and reaches a saturation level (-2 to 1 and -9 to -7 for HH and VV, respectively) in the middle of crop cycle. The very high value of HH and the similar response of flooded and non-flooded fields were explained by the high plant density. At the end of crop season, radar backscattering of the rice fields without water was slightly lower in HH and higher in VV when compared to that of fields with standing water.

HH, VV and HH/VV were not strongly related to plant biomass as in the reported results for traditional rice. This is explained by the effect of water management, plant density and structure.

7.1.2 Rice mapping

The following results were generated when ASAR APP imagery was utilised for rice mapping:

- Using a thresholding algorithm for the single-date ASAR APP data acquired in the middle of crop season, the classified images showed only a maximum of 14% difference at the district level, with the exception of several districts in AW 2007 crop, when compared to the estimates from the agency statistical data. On the basis of the existing land use map, the User's accuracies of rice class assessed were very high, i.e. more than 93% for WS, SA 2007, and WS 2008 crops. In this case, the thresholds of polarisation ratio and VV data were applied;
- The classification results using thresholding algorithm provided consistent accuracies between districts (percentage errors ranging from -14 to 7% for WS 2007 crop and from -11 to 3% for SA 2007 crop) and between seasons across the province (percentage errors from -7 to 4%). Other classification methods, i.e. minimum-distance-to-means, maximum likelihood, and spectral angle mapping did not improve classification accuracy despite their sophisticated algorithm formulation;
- Another threshold, i.e. the "normalised difference polarisation ratio index", was originally developed in this study. When applied, the percentage error of the provincial rice area planted between seasons ranged from -6 to 2% when compared to the official agency statistics.
- Radar backscattering coefficient is a physical value (like reflectance in optical data). Therefore, similar methods as conducted in this research can be used for other SAR sensor data.
- In this work, a method was developed for accurately mapping rice growing area using single-date ASAR APP image taken in the middle of the rice cropping season. This is briefly described as follows:
 1. An ASAR APP image acquired in the middle of the crop season is selected;

2. Image pre-processing steps were implemented: a) image calibration or conversion to the radar backscattering coefficient sigma nought (σ^0), b) image geo-correction, and c) image spatial filtering;
3. A polarisation ratio image was created;
4. Thresholding method was applied to the polarisation ratio and VV images in order to segment rice and non-rice classes;
5. A post-classification step was conducted by using majority filter to the classified image; and
6. A rice and non-rice map was finally produced.

In the case of ASAR WS data used for mapping rice, the following results are highlighted:

- The integrated method based on the temporal variation of the radar response and thresholding was proposed to map the rice area planted using multi-temporal ASAR WS data.
- The classification results of rice/non-rice by using multi-date ASAR WS images provided inconsistent accuracies between districts and crop seasons. However, the method yielded low relative errors of planted rice area at the provincial scale when compared to the official statistics (i.e. ranging from -4% to 1%, and from -11% to 14% when 3-date and 2-date image used, respectively), except for the case of WS crop season using ascending mode data.

7.1.3 Yield estimation

The statistical model-based method worked very well in the case of Cho Moi district where the relationship between in situ measured yield point data and polarisation ratio data derived from three-date ASAR APP images was very positive with a high correlation coefficient ($r = 0.913$). The sampling rice fields chosen were well represented for the entire region in term of rice yield. The accuracy of estimated rice production of SA 2007 crop was 97% when compared to the official agency statistics.

However, in the case of WS crop in Cho Moi and SA 2007 crop in Thoai Son district, the estimated accuracies of rice production were 81 and 70%, respectively. This may be due to the significant difference between the in situ measured yields and the average yield of the district.

7.2 Conclusions

Based on the results and discussion analysed in the previous chapters and above summaries, significant conclusions can be drawn from this research.

The radar backscattering behaviour of rice in the study site is much different from that of the traditional rice plant. Therefore, methods using the temporal change of HH and VV for rice mapping will not work for fields which are not inundated at the beginning of the season. However, the polarisation ratio HH/VV of the single ASAR APP image acquired in the middle period of the crop season (i.e. during the second half of the vegetative stage and the first half of the reproductive stage) is a good rice classifier.

Retrieving rice biomass using radar backscattering coefficient of HH and VV data or polarisation ratio data is not applicable to modern rice growing practices that prevailed in the study area.

The use of Envisat ASAR data was assessed for rice mapping in An Giang province, Mekong River Delta, where the complicated cropping systems have been taking place. In the case of ASAR APP mode, it was demonstrated that:

- The supervised classification methods applied to single-date image taken in the middle period of crop season gave good accuracies when compared to the existing agency data. Thresholding method provided higher accuracy than other methods such as minimum-distance-to-means, maximum likelihood, and SAM;

- A threshold formulated in this study, i.e. the “normalised difference polarisation ratio index”, produced high accuracies for rice mapping, when ASAR APP image acquired in the middle of crop season was used;
- Three acquisition dates of dual polarisation ASAR data are sufficient to accurately determine rice acreage planted during the year, if the rice crop calendar is not much different among rice growing areas in the province;
- In the case of changing cultural practices in the future, this method for rice mapping can also be used by paying attention to the threshold values of polarisation ratio and VV. These values need to be examined before applying the method.

Concerning the use of multi-temporal ASAR WS data for rice mapping, the following conclusions were drawn:

- Using three- or two-date ASAR WS data acquired in ascending, descending, or both modes, the integrated method based on the temporal variation of the radar response and thresholding was appropriate to map the rice area planted.
- The classification results of rice and non-rice by using multi-date ASAR WS images provided inconsistent accuracies between districts and crop seasons when compared to the statistical data published. However, using two-date ASAR WS images in ascending or descending mode acquired on the first half of crop season, the integrated method yielded the rice/non-rice classification images with acceptable accuracies at the provincial scale. As a whole, the use of ASAR WS data for rice mapping is appropriate at the regional level with its low cost and wide-area coverage.

The Agro-meteorological model-based method for rice yield prediction could not work in the study area, because retrieving rice biomass using HH, VV or HH/VV data was not applicable to modern rice growing practices in the Mekong River Delta.

The statistical model-based method for rice yield estimation worked very well in the case of Cho Moi district. The relationship between the in situ measured yield and polarisation ratios extracted from the three-date ASAR APP images taken

during the crop growth was extracted from the multiple regression analysis. Then, pixel-based rice yield was estimated on the basis of this relationship, and the production of rice area was finally computed.

The rice yield estimation model varies from region to region, where the cultural practices and crop calendar were significantly different in the study site. Therefore, the yield mapping strategy using time series ASAR APP data is proposed as follows: a) stratification approach should be firstly used in order to separately classify rice fields in the province into areas with the same cultural practices in the districts; b) multiple regression analysis between polarisation ratio data and in situ rice yield is implemented for each district; c) based on this correlation, rice yield map is established; and d) rice production is estimated on the basis of the yield map and rice/non-rice map.

7.3 Recommendations

Based on the results and discussion analysed in the previous chapters and the conclusions of the research study, the following are recommended for further investigation:

- The method for rice crop inventory in the province before harvest was developed by using a single-date ASAR APP data taken in the mid-crop season. For operational purposes, this rice mapping algorithm needs to be further investigated for other crops and at other provinces in the Mekong River Delta, where the cultivation systems may be different.
- Further research should be conducted to test Envisat ASAR WS data utilisation for mapping the rice cropping system of the entire Mekong River Delta. The method needs to be improved and the algorithm validated for each province, where flood season has been taking place annually and consequently prompting changes in the rice crop calendar and practices.
- Concerning rice production estimation in the study site and the Mekong River Delta, the statistical model-based method using multi-temporal dual polarisation ASAR data was found appropriate. However, more sampling rice

fields represented for various cultivation systems in the region need to be set up. Consequently, multiple regression analysis should be further examined to improve and validate the model.

- The ASAR WS imagery is a potential data source for rice crop monitoring in the tropical and subtropical regions, because cloud-free products provide greater swath width and higher repeat pass. Thus, multi-date ASAR WS data should be investigated for rice yield estimation.

REFERENCES

- AGDARD (2007) Statistical data of the agriculture, forest and aquatic land of An Giang Province. An Giang Department of Agriculture and Rural Development.
- AGDONRE (2005) Land use map of An Giang province, scale of 1:50,000. An Giang Department of Natural Resources and Environment.
- AGDPI (2009) Natural conditions of An Giang province. An Giang Department of Planning and Investment.
- AGSO (2008a) Report on Socio-Economic statistical data of the year 2008. An Giang, Vietnam, An Giang Statistical Office.
- AGSO (2008b) *Statistical Yearbook An Giang Province 2007*, An Giang, Vietnam, An Giang Statistical Office.
- ASCHBACHER, J., PONGSRIHADULCHAI, A., KARNCHANASUTHAM, S., RODPROM, C., PAUDYAL, D. R. & LE-TOAN, T. (1995) Assessment of ERS-1SAR data for rice crop mapping and monitoring. *IEEE Trans. Geosci. Remote Sensing*, 2183-2185.
- BAKAR, S. B. B. A., SHAARI, A. T. B., CHUAH, H. T. & EWE, H. T. (1997) SAR backscatter response of various growth stages of wetland rice paddy in Malaysia. *The Asian Conference on Remote Sensing*.
- BINGBAI, L., PINGPING, Z., LE-TOAN, T., BOUVET, A., BINGXIANG, T., ZENGYUAN, L. & WEI, H. (2005) Rice mapping and parameters retrieval using ASAR data in Jiangsu province, China. *The 2005 Dragon Symposium "Mid-Term results"*. Santorini, Greece.
- BOUVET, A., LE-TOAN, T., BINGXIANG, T., BINGBAI, L., WEI, H. & PINGPING, Z. (2005) Assessment of ENVISAT ASAR alternating polarisation data for rice mapping in Jiangsu province, China. IN CHINA (Ed.) *The 2005 Dragon Symposium "Mid-Term results"*. Santorini, Greece.
- BOUVET, A., LE-TOAN, T. & LAM-DAO, N. (2009) Monitoring of the rice cropping system in the Mekong delta using Envisat/ASAR dual polarization data. *IEEE Trans. Geosci. Remote Sensing*, 47, 517-526.
- CAMPBELL, J. B. (2007) *Introduction to remote sensing*, New York, London, The Guilford Press.
- CCRS (2002) GlobeSAR-2 radar remote sensing training package. Canada Centre for Remote Sensing - Natural Resources Canada.
- CCRS (2007a) Fundamentals of Remote Sensing. Ottawa, Canada Centre for Remote Sensing - Natural Resources Canada.
- CCRS (2007b) Tutorial: Radar and Stereoscopy. Canada Centre for Remote Sensing - Natural Resources Canada.
- CESBIO/MATRA-SYSTEMS (1999) RISAR project, Technical data package, ESA contract No 13201/98/NL/SB. CESBIO and MATRA SYSTEMS.
- CHAKRABORTY, M., MANJUNATH, K. R., PANIGRAHY, S., KUNDU, N. & PARIHAR, J. S. (2005) Rice crop parameter retrieval using multi-temporal, multi-incidence angle Radarsat SAR data. *ISPRS Journal of Photogrammetry & Remote Sensing*, 59, 310-322.
- CHAKRABORTY, M. & PANIGRAHY, S. (2000) A processing and software system for rice crop inventory using multi-date Radarsat ScanSAR data. *ISPRS Journal of Photogrammetry & Remote Sensing*, 55, 119-128.
- CHAKRABORTY, M., PANIGRAHY, S. & SHARMA, S. A. (1997) Discrimination of rice crop grown under different cultural practices using

References

- temporal ERS-1 synthetic aperture Radar data. *ISPRS Journal of Photogrammetry & Remote Sensing*, 52, 183-191.
- CHEN, C. & MCNAIRN, H. (2006) A neural network integrated approach for rice crop monitoring. *International Journal of Remote Sensing*, 27, 1367-1393.
- CHEN, J. & LIN, H. (2005) The application of Envisat Asar data for rice growth monitoring based on semi-empirical backscattering model. *The 26th Asian Conference on Remote Sensing*. Ha Noi, Vietnam.
- CHEN, J., LIN, H., LIU, A., SHAO, Y. & YANG, L. (2006) A semi-empirical backscattering model for estimation of leaf area index (LAI) of rice in southern China. *International Journal of Remote Sensing*, 27, 5417-5425.
- CHEN, J., LIN, H. & PEI, Z. (2007) Application of ENVISAT ASAR data in mapping rice crop growth in Southern China. *IEEE Geoscience and Remote Sensing Letters*, 4, 431-435.
- CHOUDHURY, I. & CHAKRABORTY, M. (2006) SAR signature investigation of rice crop using Radarsat data. *International Journal of Remote Sensing*, 27, 519-534.
- CHOUDHURY, I., CHAKRABORTY, M. & PARIHAR, J. S. (2007) Estimation of rice growth parameter and crop phenology with conjunctive use of Radarsat and Envisat. *Envisat Symposium 2007*. Montreux, Switzerland.
- DAWE, D. (2005) Increasing water productivity in rice-based systems in Asia – Past trends, current problems, and future prospects. *Plant Production Science*, 8, 221-230.
- ESA (2007) Envisat ASAR Product Handbook. European Space Agency.
- ESA/EOMD (2006) Rice Mapping. <http://www.eomd.esa.int/>
- ESA/ESRIN (2009) BEST Basic Envisat SAR Toolbox -User Manual Ver. 4.2.2.
- FAO (2004) International Year of Rice 2004.
<http://www.fao.org/rice2004/en/p12.htm>
- FAO/ESA (Ed.) (1993) *Radar imagery: Theory and interpretation*, Rome, Food and Agriculture Organization of the United Nations.
- FAO (2007) FAOSTAT.
<http://faostat.fao.org/site/567/DesktopDefault.aspx?PageID=567#ancor>.
- FREI, U., SPORRI, S., STEBLER, O. & HOLECZ, F. (1999) Rice field mapping in Sri Lanka using ERS SAR data. *Earth Observation Quarterly*, 63, 30-35.
- GSO (2006) Statistical data of annual rice production by province. General Statistics Office of Vietnam.
- GSO (2007a) Statistical data of annual rice production by province in the year 2007. General Statistical Office of Vietnam.
- GSO (2007b) Statistical data of population and area by province in the year 2007. General Statistics Office of Vietnam.
- HENDERSON, F. M. & LEWIS, A. J. (Eds.) (1998) *Principles and Applications of Imaging Radar*, New York, John Wiler & Sons, Inc.
- HOLECZ, F., DWYER, E., MONACO, S., SCHMID, B., FREI, U. & FISCHER, R. (2000) An operational rice field mapping tool using spaceborne SAR data. *The ERS-Envisat symposium*. Gothenburg, Germany.
- HUADONG, G., LIAO, J., CHUNMING, H., DONG, Q., ZHEN, L., LI, X., SHAO, Y., WANG, C., YUE, H. & FAN, X. (2006) Conceptual studies on RICESAT. *Asian Journal of Geoinformatics*, 6, 31-35.
- INOUE, Y., KUROSU, T., MAENO, H., URATSUKA, S., KOZU, T., DABROWSKA-ZIELINSKA, K. & QI, J. (2002) Season-long daily measurements of multifrequency (Ka, Ku, X, C, and L) and full-polarization

References

- backscatter signatures over paddy rice field and their relationship with biological variables. *Remote Sensing of Environment*, 81, 194-204.
- JAVIER MARCELLO, F. M., FRANCISCO EUGENIO (2004) Evaluation of thresholding techniques applied to oceanographic remote sensing imagery. *Image and Signal Processing for Remote Sensing X* Maspalomas, Gran Canaria, Spain.
- JENSEN, J. R. (1996) *Introductory digital image processing - A remote sensing perspective*, New Jersey, Prentice-Hall, Inc.
- JENSEN, J. R. (2007) *Remote sensing of the environment: an earth resource perspective*, Upper Saddle River, Prentice-Hall.
- KAJALAINEN, M., KUITTINEN, R., VESA, J., TUOMO, K., HIEU, N. M. & HA, T. T. T. (2000) Rice yield estimation using SAR images, meteorological data and GIS. *The ERS-Envisat symposium*. Gothenburg, Germany.
- KROPFF, M. J., LAAR, H. H. V. & MATTHEWS, R. B. (1994) ORYZA 1: An ecophysiological model for irrigated rice production. IN M.J., K., H.H., V. L. & R.B., M. (Eds.) *SARP Research*.
- KUROSU, T., FUJITA, M. & CHIBA, K. (1995) Monitoring of rice crop growth from space using the ERS-1 C-band SAR. *IEEE Trans. Geosci. Remote Sensing*, 33, 1092-1096.
- LAM-DAO, N., LE-TOAN, T. & FLOURY, N. (2005) The Use of SAR Data for Rice Crop Monitoring - A Case Study of Mekong River Delta – Vietnam. *The 26th Asian Conference on Remote Sensing*. Ha Noi, Vietnam.
- LE-TOAN, T. (2002) Guidelines for ground data collection for rice monitoring experiments using Radar data. Toulouse, Centre d'Etudes Spatiales de la Biosphere.
- LE-TOAN, T. & AL., E. (1999) RISAR project final report. MATRA SYSTEMS and CESBIO.
- LE-TOAN, T., BOUVET, A., TAN, B., ZENGYUAN, L., WEI, H., BINGBAI, L., PINGPING, Z. & BONDEAU, A. (2005) Rice monitoring in China - Mid-term report. *The 2005 Dragon Symposium "Mid-Term results"*. Santorini, Greece.
- LE-TOAN, T., FEURER, D. & FLORSCH, G. (2003) RISAR Validation report – Rice mapping in the Mekong delta, ESA contract No 13201/98/NL/SB CCN 002. CESBIO.
- LE-TOAN, T., LAUR, H., MOUGIN, E. & LOPES, A. (1989) Multitemporal and dual-polarization observations of agriculture vegetation covers by X-band SAR images. *IEEE Trans. Geosci. Remote Sensing*, 27, 709-717.
- LE-TOAN, T., RIBBES, F., WANG, L. F., FLOURY, N., DING, K. H., KONG, J. A., FUJITA, M. & KUROSU, T. (1997) Rice crop mapping and monitoring using ERS-1 data based on experiment and modelling results. *IEEE Trans. Geosci. Remote Sensing*, 35, 41-56.
- LI, Y., LIAO, Q., LI, X., LIAO, S., CHI, G. & PENG, S. (2003) Towards an operational system for regional-scale rice yield estimation using a time-series of Radarsat ScanSAR images. *International Journal of Remote Sensing*, 24, 4207-4220.
- LI, Z., SUN, G., WOODING, M., PANG, Y., DONG, Y., CHEN, E. & TAN, B. (2004) Rice monitoring using ENVISAT ASAR data in China. *The 2004 Envisat & ERS symposium*. Salzburg, Austria.
- LIEW, S. C., KAM, S. P., TUONG, T. P., CHEN, P., MINH, V. Q. & LIM, H. (1998) Application of multitemporal ERS-2 synthetic aperture radar in

References

- delineating rice cropping systems in the Mekong River Delta, Vietnam. *IEEE Trans. Geosci. Remote Sensing*, 36, 1412-1420.
- LILLESAND, T. M., KIEFER, R. W. & CHIPMAN, J. W. (2004) *Remote Sensing and Image Interpretation*, New York, John Wiley & Sons, Inc.
- LING, F., QINMIN, W. & XIAOQIN, W. (2005) Identification of rice crop using ENVISAT ASAR in Fuzhou, Fujian province, China. *The 2005 Dragon Symposium "Mid-Term results"*. Santorini, Greece.
- LOPES, A., TOUZI, R. & NEZRY, E. (1990) Adaptive speckle filters and scene heterogeneity. *IEEE Trans. Geosci. Remote Sensing*, 28, 992-1000.
- WEISSTEIN, ERIC W. (2009) Relative error. From MathWorld-A Wolfram Web resource. <http://mathworld.wolfram.com/RelativeError.html>.
- MATRA-SYSTEMS (2000) RISAR processing – reference manual, version 3.1. MATRA SYSTEMS and INFORMATION.
- MCCOY, R. M. (2005) *Field Methods in Remote Sensing*, New York, The Guilford Press.
- MENDOZA, T., BOUMAN, B., BURESH, R., GUMMERT, M., JOHNSON, D., LAMPAYAN, R. & SINGLETON, G. (2007) Tracing IRRC tracks in Vietnam. *Rice Research for Intensified Production and Prosperity in Lowland Ecosystems*.
- OGAWA, S., INOUE, Y., MINO, N. & TOMITA, A. (1998) Monitoring of rice field using SAR data and optical data. *The 2nd International Workshop on Retrieval of Bio- and Geo-physical Parameters from SAR Data for Land Applications*.
- OGURO, Y., IMAMOTO, C., SUGA, Y. & TAKEUCHI, S. (2001) Monitoring of rice field by Landsat-7 ETM+ and Landsat-5 TM data. *The 22nd Asian Conference on Remote Sensing*. Singapore.
- OUCHI, K., DAVIDSON, G., SAITO, G., ISHITSUKA, N., MOHRI, N. & URATSUKA, S. (2002) Automatic rice-crop mapping using maximum likelihood SAR segmentation and Gaussian expectation maximisation. *IEEE Trans. Geosci. Remote Sensing*, 475-477.
- PANIGRAHY, S., CHAKRABORTY, M. & PARIHAR, J. S. (1999) Radar remote sensing for inventory and monitoring of rice crop - Indian experience of 1990's. *The 20th Asian Conference on Remote Sensing*.
- PHOOMPANICH, S., ANAN, T. & POLNGAM, S. (2005) Multi-temporal Radarsat for crop monitoring. *The 26th Asian Conference on Remote Sensing*. Ha Noi, Vietnam.
- QUEGAN, S., HE, G., SANTUARI, M., XIAOQIN, W. & QINMIN, W. (2005) Land use/cover classification and rice mapping based on ENVISAT ASAR data. *The 2005 Dragon Symposium "Mid-Term results"*. Santorini, Greece.
- RIBBES, F. & LE-TOAN, T. (1998) Mapping and monitoring rice crop with Radarsat data. *IEEE Trans. Geosci. Remote Sensing*, 2749-2751.
- RIBBES, F. & LE-TOAN, T. (1999a) Coupling radar data and rice growth model for yield estimation. *IEEE Geosci. and Remote Sensing symposium IGARSS*.
- RIBBES, F. & LE-TOAN, T. (1999b) Rice field mapping and monitoring with Radarsat data. *International Journal of Remote Sensing*, 20, 745-765.
- RICHARDS, J. A. & JIA, X. (2006) *Remote sensing digital image analysis - An introduction*, Springer.
- ROSENQVIST, A. (1999) Temporal and spatial characteristics of irrigated rice in JERS-1 L-band SAR data. *International Journal of Remote Sensing*, 20, 1567-1587.

References

- SAKAMOTO, T., VAN NGUYEN, N., OHNO, H., ISHITSUKA, N. & YOKOZAWA, M. (2006) Spatio-temporal distribution of rice phenology and cropping systems in the Mekong Delta with special reference to the seasonal water flow of the Mekong and Bassac rivers. *Remote Sensing of Environment*, 100, 1-16.
- SHAO, Y., FAN, X., LIU, H., XIAO, J., ROSS, S., BRISCO, B., BROWN, R. & STAPLES, G. (2001) Rice monitoring and production estimation using multitemporal RADARSAT. *Remote Sensing of Environment*, 76, 310-325.
- SHAO, Y., LIAO, J., FAN, X. & WANG, Y. (2002) Analysis of temporal backscatter of rice: A comparison of RADARSAT observations with modelling results. *IEEE Geosci. and Remote Sensing symposium IGARSS*.
- SHAO, Y., LIU, H., DONG, X. F. J. X. Q., BRISCO, X. W. S. R. B., BROWN, R. & STAPLES, G. (1999) Radarsat data for operational rice monitoring and its potential for yield estimation. *The 20th Asian Conference on Remote Sensing*.
- SHI, Z. & FUNG, K. B. (1994) A Comparison of Digital Speckle Filters. *Geoscience and Remote Sensing Symposium, 1994. IGARSS '94. Surface and Atmospheric Remote Sensing: Technologies, Data Analysis and Interpretation., International*. Pasadena, CA, USA.
- STANKIEWICZ, K. A. (2006) The efficiency of crop recognition on ENVISAT ASAR images in two growing seasons. *IEEE Trans. Geosci. Remote Sensing*, 44, 806-814.
- TAKEUCHI, S., KONISHI, T., OGURO, Y. & SUZA, Y. (1999) Estimation of rice-planted areas in early stage using Radarsat data. *The 20th Asian Conference on Remote Sensing*.
- THIEL, C., REICHE, J., LEITERER, R. & SCHMULLIUS, C. (2007) Synergistic usage of ASAR WS and MERIS data for large scale water and vegetation monitoring in Africa - A science product of the aquifer project. *Envisat Symposium 2007*. Montreux, Switzerland.
- TUONG, T. P. (2007) Alternate wetting and drying irrigation (AWD): a technology for water saving in rice production. *The crop cutting ceremony, BADC farm*. Modhupur, Tangail.
- WANG, X., WANG, Q., LING, F., SHI, X., CHEN, Y. & ZHU, X. (2005) ENVISAT ASAR data for agriculture mapping in Zhangzhou, Fujian province, China. *The 2005 Dragon Symposium "Mid-Term results"*. Santorini, Greece.
- WOODING, M. & ZENGYUAN, L. (2000) Rice mapping using ERS SAR data in Guangdong province, China. *ESA-ENVISAT Symposium*. Gothenburg, Germany.
- XIAO, X., BOLES, S., FROLKING, S., LI, C., BABU, J. Y., SALAS, W. & III, B. M. (2006) Mapping paddy rice agriculture in South and Southeast Asia using multi-temporal MODIS images. *Remote Sensing of Environment*, 100, 95-113.
- YANG, S., SHEN, S., BINGBAI, L., LE-TOAN, T. & WEI, H. (2008) Rice mapping and monitoring using Envisat ASAR data. *IEEE Geoscience and Remote sensing Letters*, 5, 108-112.
- YOSHIDA, S. (1981) *Fundamentals of rice crop science*, Los Banos, Laguna, Philippines, The International Rice Research Institute.

APPENDICES

A. ASAR APP images used

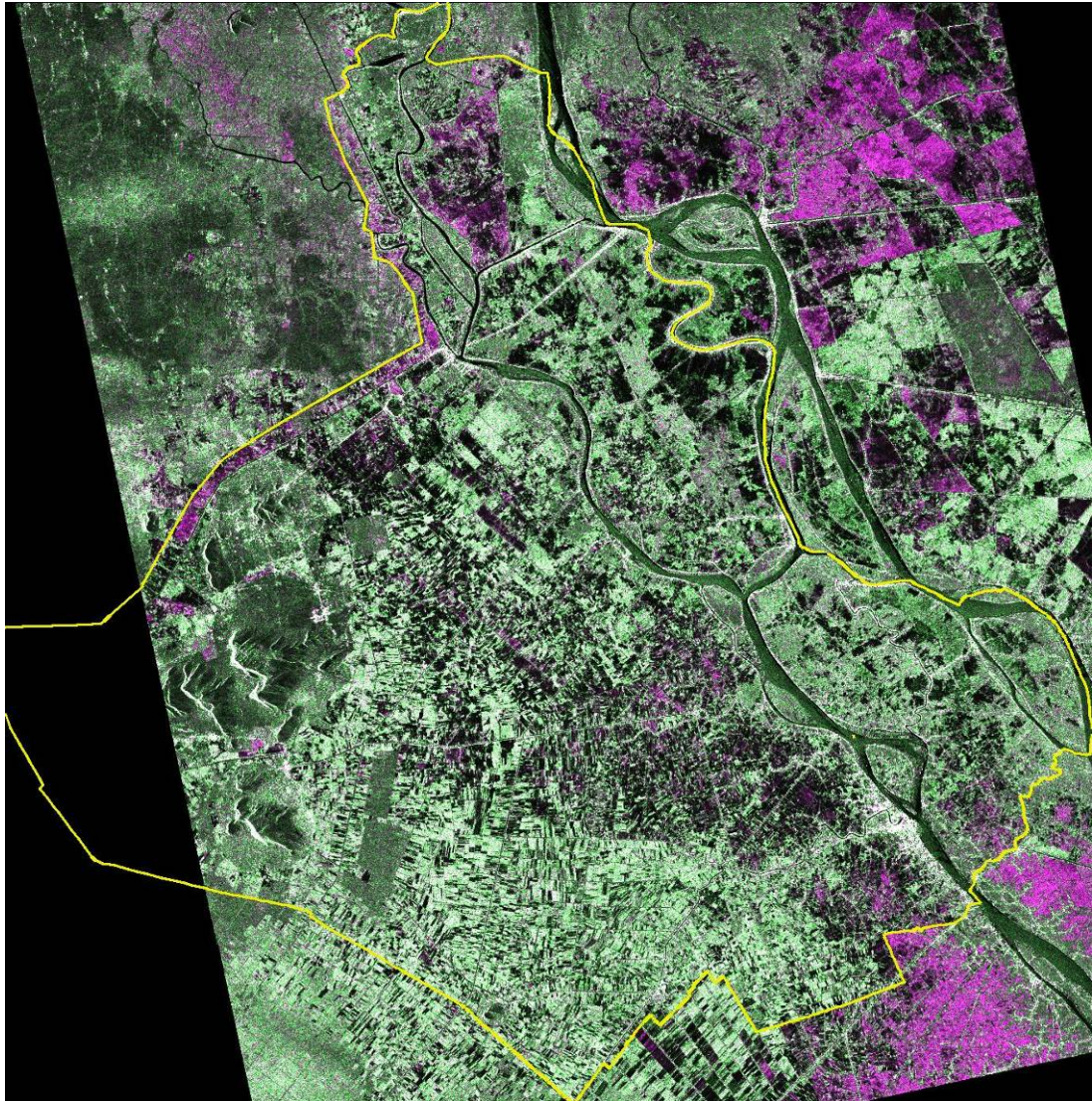


**Figure A.1. Colour composite ASAR APP image acquired on 28 Apr. 2007
(R=HH, G=VV, B=HH), provincial boundary in yellow polyline.**

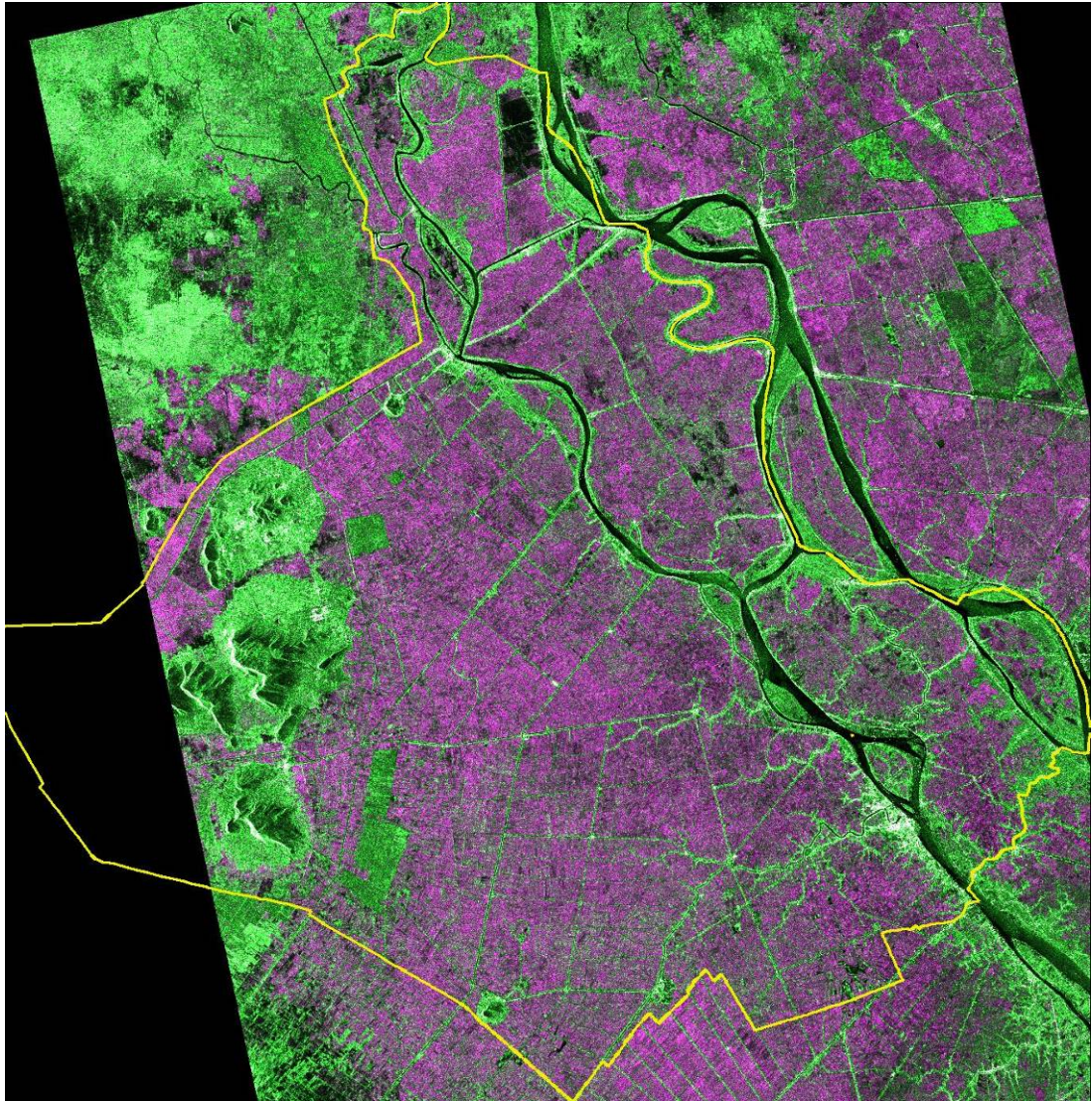


**Figure A.2. Colour composite ASAR APP image acquired on 02 Jun. 2007
(R=HH, G=VV, B=HH), provincial boundary in yellow polyline.**

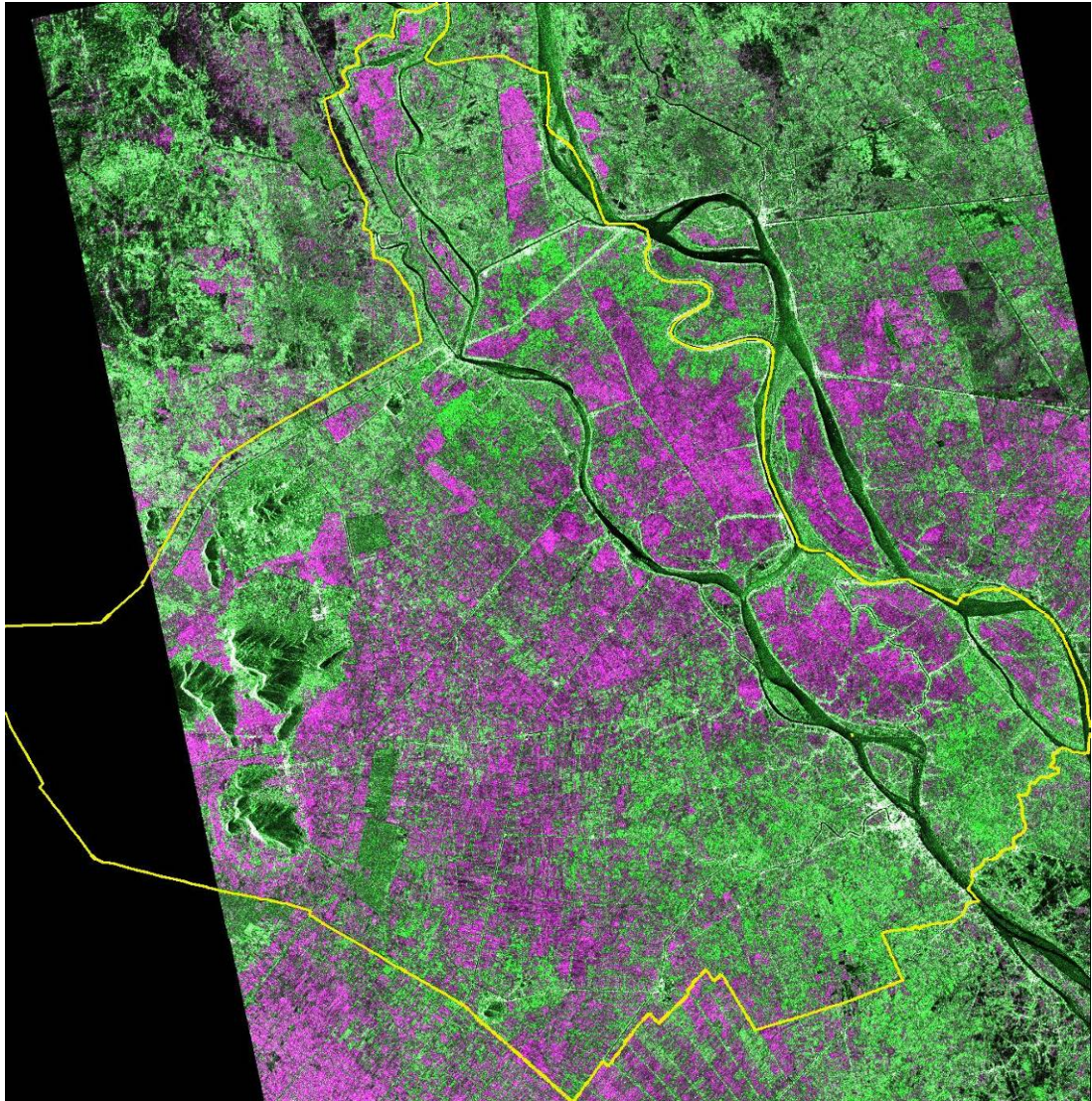
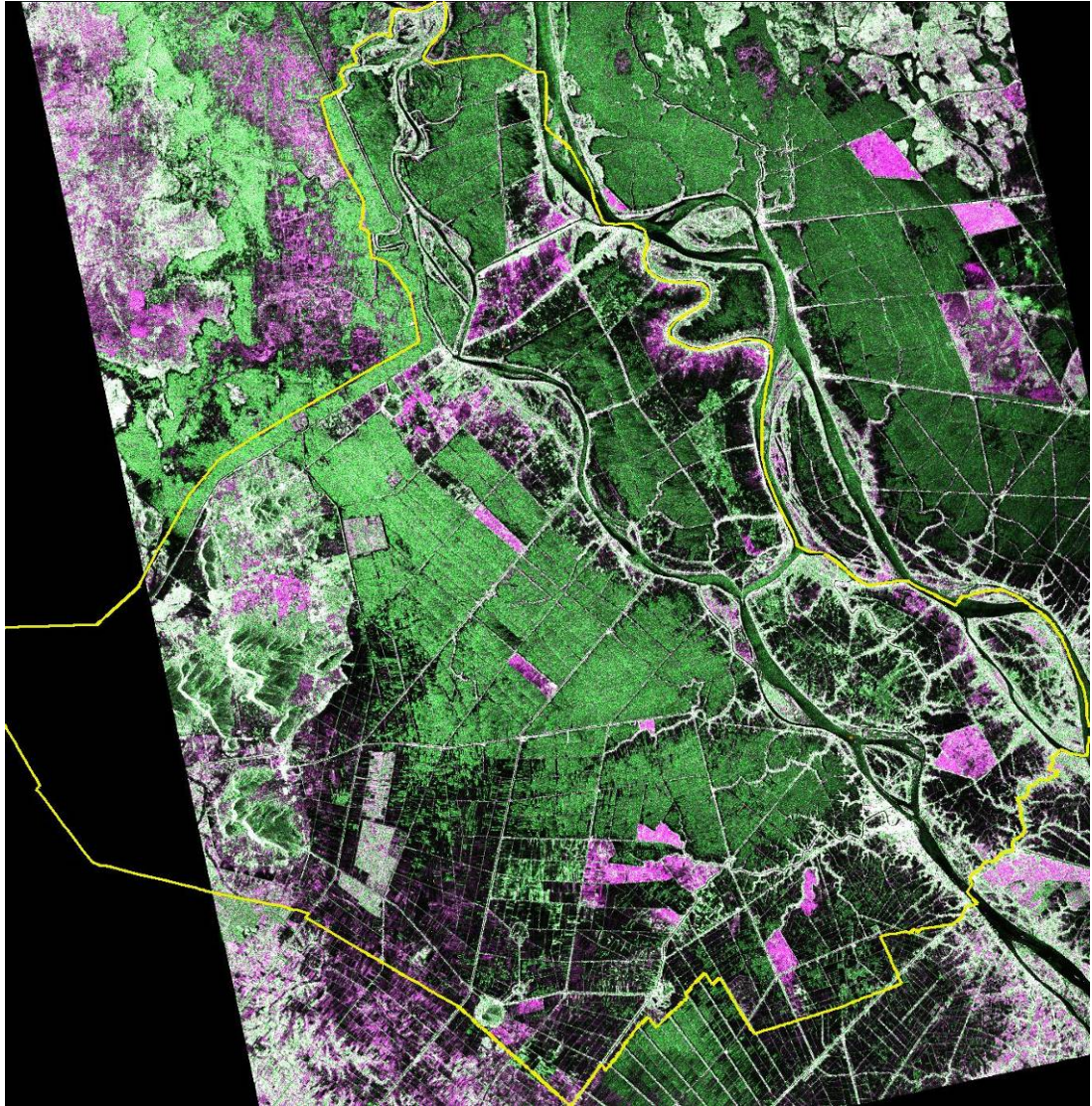
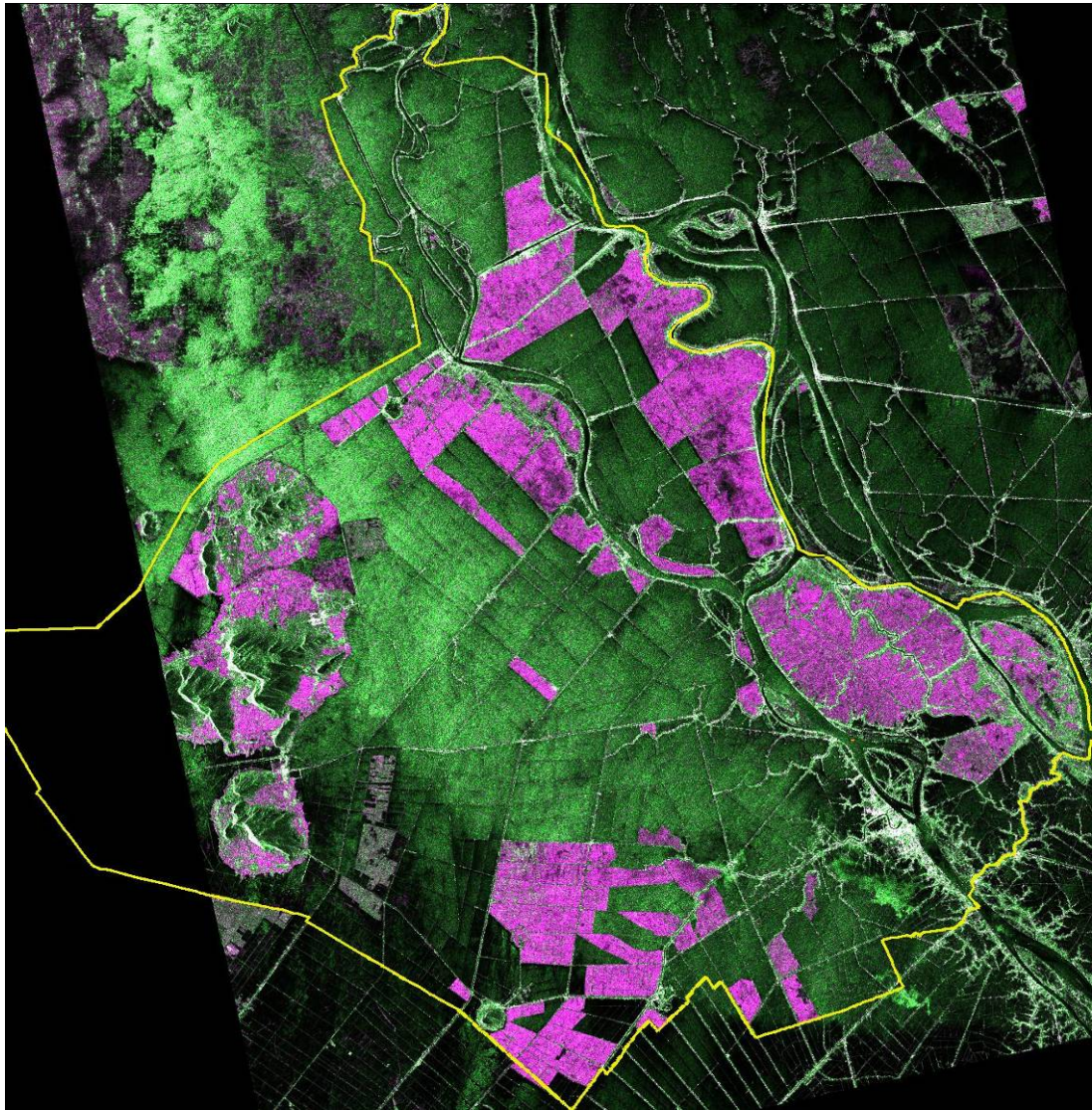


Figure A.3. Colour composite ASAR APP image acquired on 07 Jul. 2007 (R=HH, G=VV, B=HH), provincial boundary in yellow polyline.



**Figure A.4. Colour composite ASAR APP image acquired on 15 Sep. 2007
(R=HH, G=VV, B=HH), provincial boundary in yellow polyline.**



**Figure A.5. Colour composite ASAR APP image acquired on 20 Oct. 2007
(R=HH, G=VV, B=HH), provincial boundary in yellow polyline.**

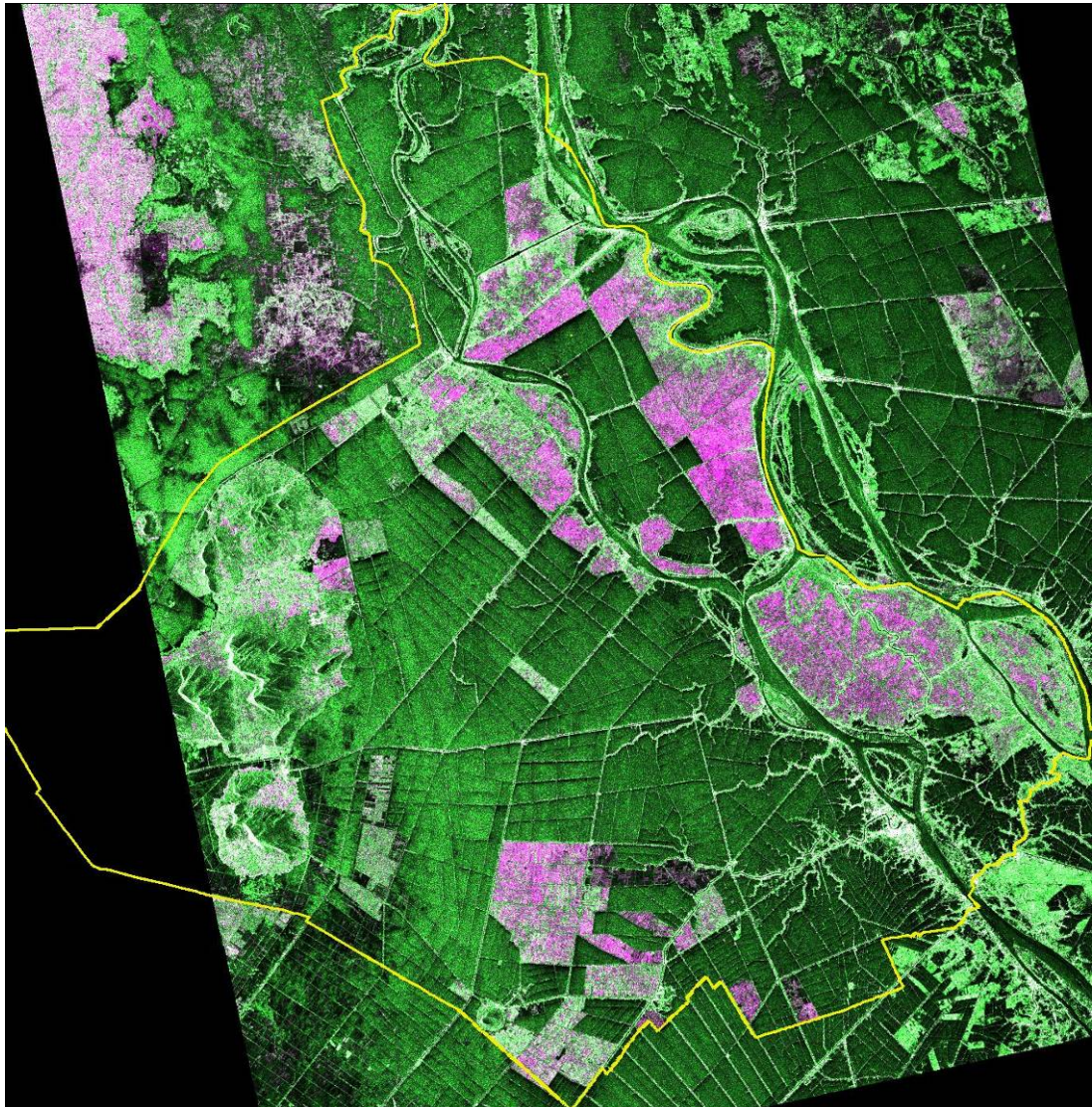


**Figure A.6. Colour composite ASAR APP image acquired on 24 Nov. 2007
(R=HH, G=VV, B=HH), provincial boundary in yellow polyline.**

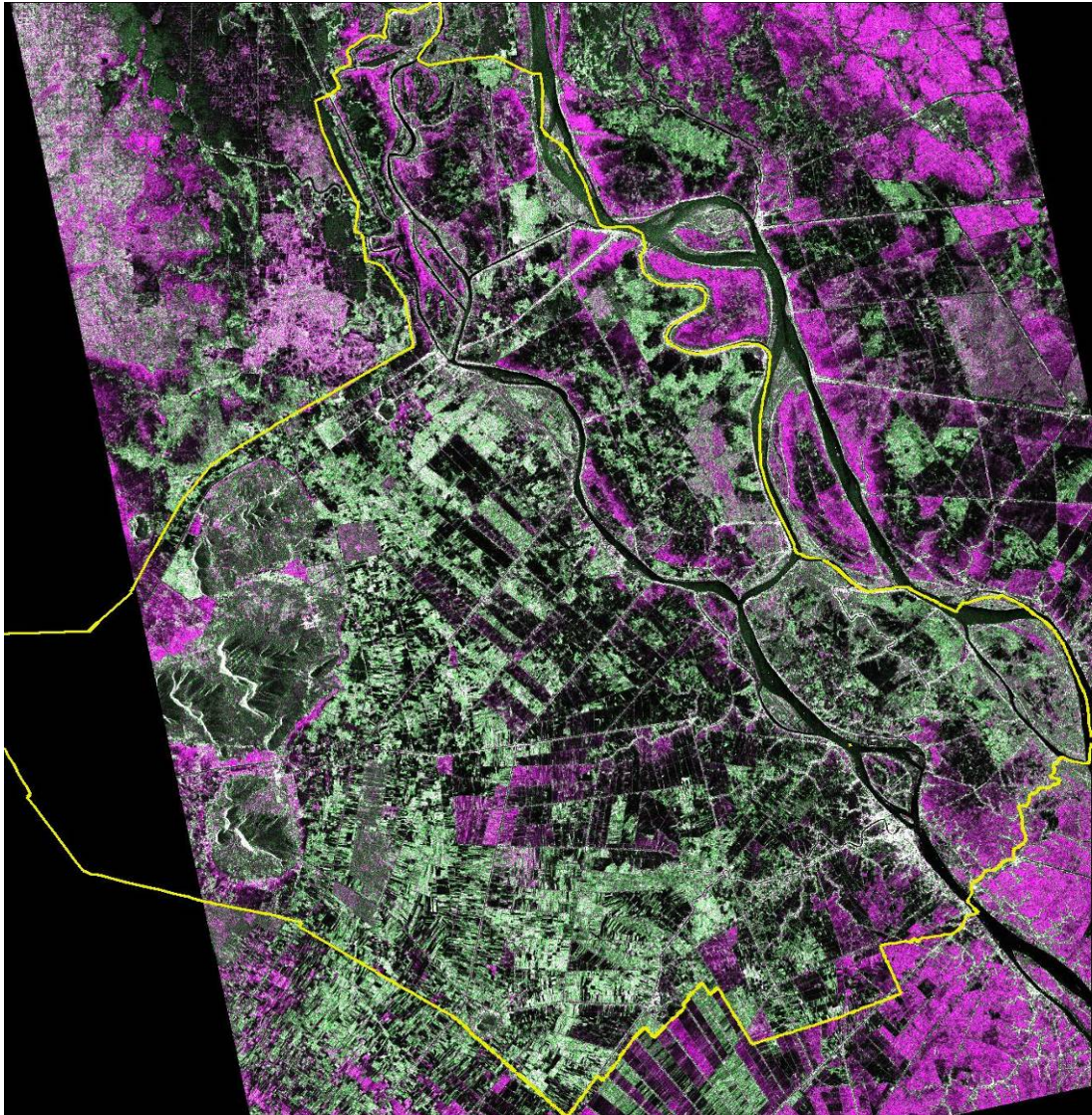


**Figure A.7. Colour composite ASAR APP image acquired on 29 Dec. 2007
(R=HH, G=VV, B=HH), provincial boundary in yellow polyline.**

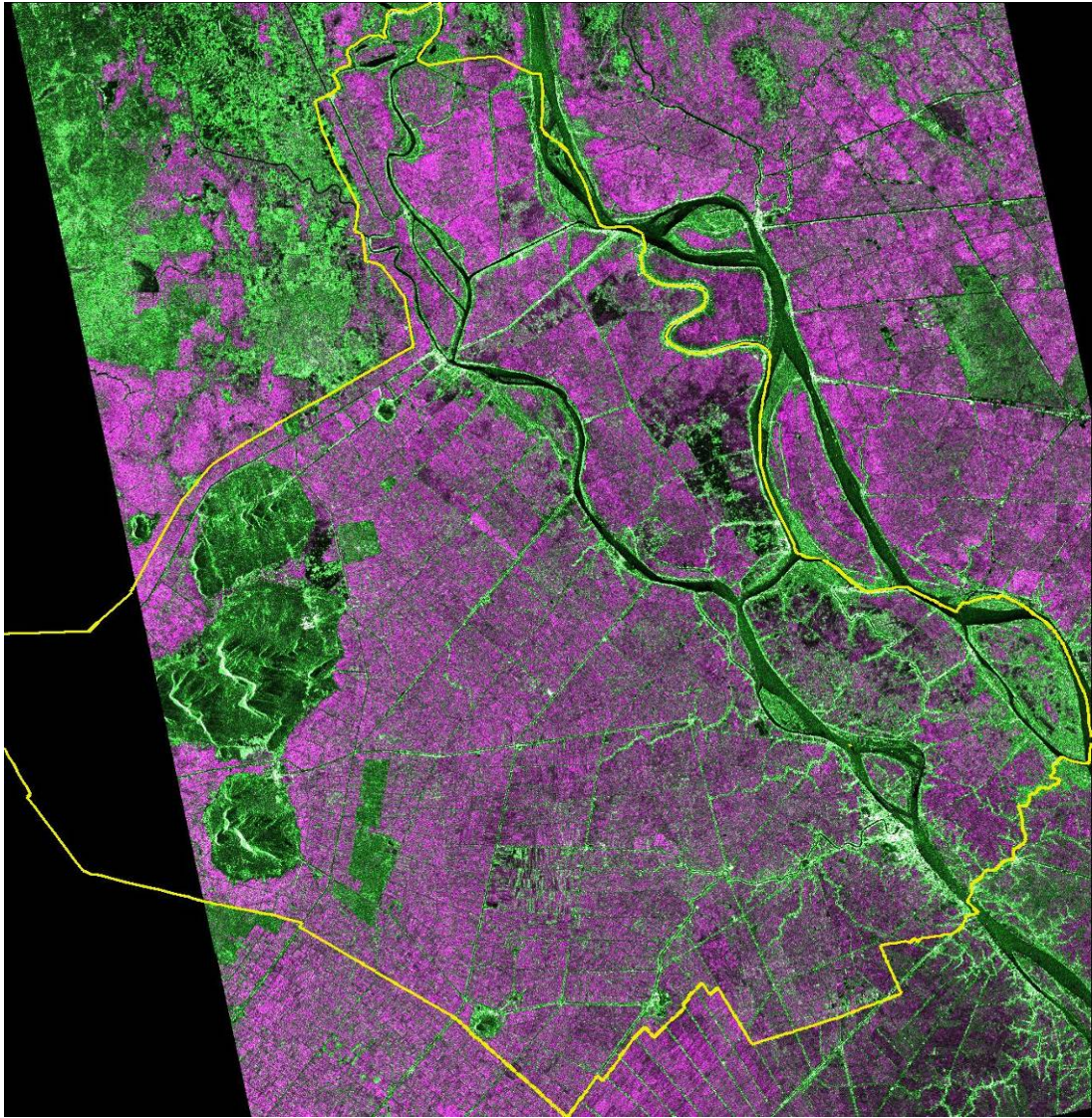


**Figure A.8. Colour composite ASAR APP image acquired on 02 Feb. 2008
(R=HH, G=VV, B=HH), provincial boundary in yellow polyline.**

B. Backscattering coefficient and yield of sampling fields, and their regression models

B.1 A case of Summer Autumn 2007 crop

Code	HH				VV				HH/VV			YIELD (kg/m ²)
	28/4/07	2/6/07	7/7/07		28/4/07	2/6/07	7/7/07		28/4/07	2/6/07	7/7/07	
BM1	0.431	0.443	0.346		0.454	0.156	0.069		0.951	2.837	5.019	0.432
BM2	0.720	0.387	0.313		1.188	0.099	0.138		0.606	3.888	2.272	0.525
BM3	0.337	0.410	0.356		0.363	0.092	0.238		0.927	4.460	1.499	0.432
BM4	0.708	0.645	0.645		0.537	0.241	0.150		1.319	2.671	4.309	0.417
BM5	0.294	0.361	0.438		0.376	0.135	0.143		0.783	2.680	3.056	0.540
VB1	0.149	0.602	0.246		0.109	0.224	0.264		1.365	2.692	0.931	0.617
VB2	0.089	0.608	0.321		0.094	0.119	0.276		0.952	5.101	1.164	0.617
VB3	0.056	0.670	0.593		0.043	0.139	0.178		1.311	4.823	3.323	0.586
VB4	0.165	1.093	0.254		0.082	0.127	0.189		2.013	8.612	1.346	0.556
VB5	0.035	0.692	0.294		0.044	0.131	0.127		0.795	5.304	2.312	0.540
BH1	0.438	1.332	0.685		0.451	0.142	0.119		0.970	9.372	5.773	0.586
BH2	0.110	0.457	0.802		0.151	0.156	0.098		0.728	2.930	8.212	0.540
BH3	0.409	0.660	0.551		0.533	0.110	0.186		0.768	6.015	2.970	0.556
BH4	0.293	1.187	0.333		0.254	0.147	0.102		1.155	8.061	3.264	0.556
BH5	0.211	0.627	0.519		0.395	0.160	0.280		0.533	3.920	1.853	0.617
VC1	0.048	0.560	0.304		0.094	0.113	0.398		0.516	4.972	0.765	0.617
VC2	0.031	0.595	0.306		0.024	0.151	0.244		1.296	3.947	1.255	0.571
VC3	0.091	0.700	0.261		0.171	0.096	0.581		0.533	7.255	0.449	0.386
VC4	0.109	0.365	0.248		0.113	0.137	0.296		0.964	2.671	0.837	0.540
VC5	0.044	0.708	0.283		0.067	0.149	0.397		0.660	4.760	0.713	0.571
PH1	0.452	0.446	0.486		0.776	0.065	0.228		0.582	6.894	2.130	0.617
PH2	0.423	0.791	0.738		0.497	0.114	0.218		0.852	6.929	3.380	0.710
PH3	0.393	0.498	0.281		0.566	0.148	0.314		0.694	3.359	0.896	0.602
PH4	0.602	0.655	0.328		0.562	0.137	0.222		1.072	4.771	1.478	0.602
PH5	0.326	0.901	0.502		0.462	0.117	0.197		0.704	7.718	2.541	0.710
LDB1	0.045	0.442	0.581		0.052	0.220	0.077		0.868	2.011	7.559	0.520
LDB2	0.141	0.333	0.742		0.184	0.222	0.098		0.763	1.498	7.607	0.520
LDB3	0.047	0.484	0.442		0.114	0.238	0.119		0.408	2.035	3.719	0.500
LDB4	0.125	0.509	0.364		0.274	0.187	0.184		0.454	2.724	1.977	0.480
LDB5	0.103	0.364	0.664		0.250	0.347	0.108		0.410	1.049	6.118	0.500
MHD1	0.384	0.547	0.573		0.366	0.162	0.162		1.050	3.377	3.546	0.500
MHD2	0.501	0.578	0.304		0.522	0.121	0.181		0.959	4.792	1.677	0.500
MHD3	0.403	0.443	0.466		0.447	0.141	0.121		0.901	3.143	3.849	0.500
MHD4	0.345	0.621	0.615		0.391	0.118	0.081		0.882	5.249	7.597	0.460
MHD5	0.207	0.597	0.649		0.463	0.190	0.127		0.447	3.150	5.101	0.460
Multiple regression analysis using LINEST function												
AG	-0.003	0.095	-0.017	0.493	-0.009	-0.353	-0.015	0.606	-0.005	0.011	-0.004	0.517
	0.076	0.056	0.065	0.051	0.136	0.273	0.057	0.070	0.006	0.006	0.038	0.047
	0.088	0.073	#N/A	#N/A	0.062	0.074	#N/A	#N/A	0.145	0.071	#N/A	#N/A
	0.968	30.000	#N/A	#N/A	0.664	30.000	#N/A	#N/A	1.689	30.000	#N/A	#N/A
	0.016	0.161	#N/A	#N/A	0.011	0.166	#N/A	#N/A	0.026	0.151	#N/A	#N/A

Appendices

BM (CP)	0.559	-1.127	0.207	0.637	-0.215	-0.479	0.046	0.543	-0.034	-0.075	-0.178	0.990
	0.137	0.185	0.056	0.036	0.855	0.865	0.143	0.257	0.012	0.020	0.040	0.103
	0.977	0.018	#N/A	#N/A	0.375	0.092	#N/A	#N/A	0.976	0.018	#N/A	#N/A
	14.264	1.000	#N/A	#N/A	0.200	1.000	#N/A	#N/A	13.524	1.000	#N/A	#N/A
	0.013	0.000	#N/A	#N/A	0.005	0.009	#N/A	#N/A	0.013	0.000	#N/A	#N/A
VB	0.084	-0.171	0.604	0.620	0.838	0.227	-0.908	0.444	-0.012	-0.013	0.018	0.648
	0.101	0.068	0.286	0.065	0.004	0.003	0.009	0.001	0.024	0.013	0.060	0.087
	0.882	0.024	#N/A	#N/A	1.000	0.000	#N/A	#N/A	0.588	0.045	#N/A	#N/A
	2.489	1.000	#N/A	#N/A	25857.609	1.000	#N/A	#N/A	0.475	1.000	#N/A	#N/A
	0.004	0.001	#N/A	#N/A	0.005	0.000	#N/A	#N/A	0.003	0.002	#N/A	#N/A
BH	-0.025	0.004	0.016	0.578	0.076	1.650	0.217	0.246	-0.004	0.010	-0.143	0.643
	0.182	0.109	0.291	0.152	0.054	0.252	0.038	0.043	0.007	0.012	0.130	0.066
	0.044	0.060	#N/A	#N/A	0.991	0.006	#N/A	#N/A	0.689	0.034	#N/A	#N/A
	0.015	1.000	#N/A	#N/A	36.335	1.000	#N/A	#N/A	0.740	1.000	#N/A	#N/A
	0.000	0.004	#N/A	#N/A	0.004	0.000	#N/A	#N/A	0.003	0.001	#N/A	#N/A
CT	-0.046	-0.036	0.054	0.616	0.345	0.251	0.022	0.473	-0.007	-0.003	-0.011	0.628
	0.070	0.055	0.118	0.051	0.091	0.209	0.035	0.033	0.005	0.005	0.029	0.040
	0.096	0.037	#N/A	#N/A	0.762	0.019	#N/A	#N/A	0.321	0.032	#N/A	#N/A
	0.212	6.000	#N/A	#N/A	6.416	6.000	#N/A	#N/A	0.946	6.000	#N/A	#N/A
	0.001	0.008	#N/A	#N/A	0.007	0.002	#N/A	#N/A	0.003	0.006	#N/A	#N/A
VC	-1.269	-0.553	-3.610	1.450	-0.327	-1.596	-1.211	0.982	0.492	-0.032	-0.425	0.631
	4.640	0.331	3.871	1.642	0.772	4.625	1.948	0.844	0.107	0.011	0.091	0.095
	0.839	0.071	#N/A	#N/A	0.659	0.104	#N/A	#N/A	0.977	0.027	#N/A	#N/A
	1.735	1.000	#N/A	#N/A	0.645	1.000	#N/A	#N/A	14.214	1.000	#N/A	#N/A
	0.027	0.005	#N/A	#N/A	0.021	0.011	#N/A	#N/A	0.031	0.001	#N/A	#N/A
PH	0.146	0.156	-0.156	0.546	0.341	-2.396	-0.741	1.270	0.050	0.001	-0.014	0.548
	0.008	0.008	0.013	0.009	0.164	0.313	0.075	0.052	0.060	0.033	0.164	0.196
	1.000	0.002	#N/A	#N/A	0.994	0.009	#N/A	#N/A	0.767	0.055	#N/A	#N/A
	702.792	1.000	#N/A	#N/A	54.132	1.000	#N/A	#N/A	1.099	1.000	#N/A	#N/A
	0.013	0.000	#N/A	#N/A	0.013	0.000	#N/A	#N/A	0.010	0.003	#N/A	#N/A
TS	0.369	-0.003	0.071	0.439	-0.621	-0.155	0.005	0.802	0.114	-0.034	-0.124	0.704
	0.221	0.184	0.145	0.104	0.234	0.985	0.118	0.197	0.027	0.016	0.093	0.123
	0.522	0.077	#N/A	#N/A	0.669	0.065	#N/A	#N/A	0.772	0.054	#N/A	#N/A
	2.182	6.000	#N/A	#N/A	4.033	6.000	#N/A	#N/A	6.768	6.000	#N/A	#N/A
	0.039	0.036	#N/A	#N/A	0.050	0.025	#N/A	#N/A	0.058	0.017	#N/A	#N/A
LD	0.387	0.637	0.006	0.016	-0.589	-0.143	0.081	0.594	0.016	0.030	-0.073	0.403
	0.201	0.439	0.163	0.311	0.046	0.022	0.020	0.007	0.024	0.062	0.195	0.131
	0.934	0.009	#N/A	#N/A	0.997	0.002	#N/A	#N/A	0.927	0.009	#N/A	#N/A
	4.734	1.000	#N/A	#N/A	112.404	1.000	#N/A	#N/A	4.244	1.000	#N/A	#N/A
	0.001	0.000	#N/A	#N/A	0.001	0.000	#N/A	#N/A	0.001	0.000	#N/A	#N/A

Appendices

MH	-0.006	-0.152	0.124	0.526	0.488	-0.261	-0.095	0.498	-0.005	-0.007	0.059	0.483
	0.139	0.137	0.181	0.154	0.373	0.438	0.236	0.119	0.002	0.004	0.017	0.017
	0.830	0.018	#N/A	#N/A	0.658	0.026	#N/A	#N/A	0.978	0.007	#N/A	#N/A
	1.631	1.000	#N/A	#N/A	0.642	1.000	#N/A	#N/A	14.764	1.000	#N/A	#N/A
	0.002	0.000	#N/A	#N/A	0.001	0.001	#N/A	#N/A	0.002	0.000	#N/A	#N/A
CM	-0.038	-0.204	0.023	0.610	0.095	0.002	-0.085	0.508	-0.002	-0.017	0.072	0.503
	0.040	0.063	0.037	0.041	0.210	0.132	0.062	0.044	0.002	0.003	0.017	0.014
	0.653	0.015	#N/A	#N/A	0.328	0.021	#N/A	#N/A	0.833	0.011	#N/A	#N/A
	3.769	6.000	#N/A	#N/A	0.974	6.000	#N/A	#N/A	9.972	6.000	#N/A	#N/A
	0.003	0.001	#N/A	#N/A	0.001	0.003	#N/A	#N/A	0.003	0.001	#N/A	#N/A
CM LOGEST	0.921	0.656	1.049	0.628	1.236	1.009	0.841	0.506	0.995	0.965	1.160	0.503
	0.081	0.129	0.075	0.083	0.431	0.270	0.128	0.090	0.003	0.007	0.035	0.028
	0.659	0.031	#N/A	#N/A	0.326	0.044	#N/A	#N/A	0.834	0.022	#N/A	#N/A
	3.872	6.000	#N/A	#N/A	0.966	6.000	#N/A	#N/A	10.029	6.000	#N/A	#N/A
	0.011	0.006	#N/A	#N/A	0.006	0.011	#N/A	#N/A	0.014	0.003	#N/A	#N/A

Note: Numbers in bold font are the coefficients of determination

B.2 A case of Winter Summer 2007 crop

Code	HH				VV				HH/VV			YIELD Kg/m ²
	13/1/07	17/2/07	24/3/07		13/1/07	17/2/07	24/3/07		13/1/07	17/2/07	24/3/07	
BM1	0.394	0.401	0.386		0.146	0.071	0.266		2.698	5.649	1.453	0.907
BM2	0.367	0.413	0.350		0.141	0.134	0.231		2.608	3.077	1.519	0.740
BM3	0.536	0.483	0.298		0.125	0.070	0.169		4.293	6.936	1.762	0.771
BM4	0.452	0.579	0.234		0.218	0.076	0.194		2.070	7.608	1.201	0.733
BM5	0.411	0.872	0.322		0.101	0.102	0.307		4.068	8.575	1.050	0.848
VB1	0.693	0.370	0.471		0.221	0.203	0.445		3.143	1.819	1.058	0.849
VB2	0.543	0.415	0.272		0.146	0.180	0.362		3.709	2.309	0.751	0.802
VB3	0.659	0.337	0.172		0.111	0.154	0.187		5.917	2.188	0.922	0.802
VB4	0.587	0.414	0.141		0.120	0.104	0.308		4.910	3.961	0.458	0.772
VB5	0.556	0.157	0.153		0.104	0.133	0.552		5.359	1.176	0.278	0.772
BH1	0.605	0.921	0.395		0.289	0.081	0.361		2.096	11.301	1.093	0.787
BH2	0.633	0.419	0.577		0.079	0.068	0.253		8.034	6.152	2.286	0.802
BH3	0.519	0.460	0.471		0.170	0.080	0.323		3.057	5.777	1.460	0.725
BH4	0.402	0.536	0.389		0.191	0.108	0.317		2.107	4.971	1.228	0.848
BH5	0.352	0.620	0.479		0.216	0.060	0.347		1.630	10.408	1.380	0.787
VC1	0.364	0.708	0.463		0.191	0.131	0.388		1.910	5.416	1.193	0.772
VC2	0.397	1.186	0.314		0.243	0.216	0.434		1.632	5.501	0.723	0.756
VC3	0.428	0.350	0.406		0.177	0.242	0.261		2.411	1.446	1.556	0.787
VC4	0.420	0.370	0.320		0.164	0.126	0.241		2.557	2.925	1.327	0.787
VC5	0.399	0.920	0.404		0.238	0.121	0.336		1.677	7.598	1.204	0.756
PH1	0.268	0.343	0.250		0.242	0.092	0.194		1.108	3.744	1.288	0.787
PH2	0.343	0.755	0.429		0.065	0.247	0.383		5.259	3.063	1.118	0.880
PH3	0.291	0.353	0.425		0.194	0.071	0.177		1.506	4.990	2.403	0.772
PH4	0.240	0.353	0.226		0.178	0.071	0.241		1.349	5.012	0.937	0.772

Appendices

PH5	0.376	0.862	0.295		0.081	0.113	0.305		4.620	7.623	0.970	0.880
LDB1	0.096	0.540	0.488		0.036	0.247	0.234		2.699	2.190	2.083	0.650
LDB2	0.068	0.798	0.373		0.032	0.168	0.217		2.133	4.760	1.720	0.650
LDB3	0.132	0.928	0.361		0.028	0.162	0.111		4.632	5.745	3.265	0.650
LDB4	0.109	0.775	0.340		0.035	0.181	0.264		3.097	4.283	1.291	0.600
LDB5	0.114	0.777	0.366		0.042	0.188	0.146		2.711	4.132	2.502	0.600
MHD1	0.243	0.713	0.288		0.087	0.108	0.115		2.806	6.588	2.509	0.700
MHD2	0.416	0.962	0.289		0.142	0.120	0.113		2.931	7.991	2.553	0.700
MHD3	0.199	0.739	0.244		0.102	0.081	0.171		1.950	9.094	1.422	0.760
MHD4	0.591	0.696	0.349		0.283	0.161	0.188		2.092	4.319	1.855	0.700
MHD5	0.537	0.776	0.454		0.183	0.132	0.399		2.940	5.871	1.140	0.760
Multiple regression analysis using LINEST function												
LD	0.840	0.323	-0.559	0.117	-0.119	0.479	-4.922	0.733	0.017	-0.002	-0.004	0.614
	0.234	0.103	0.326	0.158	0.222	0.449	2.729	0.098	0.047	0.023	0.042	0.099
	0.935	0.014	#N/A	#N/A	0.780	0.026	#N/A	#N/A	0.134	0.051	#N/A	#N/A
	4.773	1.000	#N/A	#N/A	1.181	1.000	#N/A	#N/A	0.051	1.000	#N/A	#N/A
	0.003	0.000	#N/A	#N/A	0.002	0.001	#N/A	#N/A	0.000	0.003	#N/A	#N/A
CM 9 Samples	-0.500	-0.158	0.098	0.940	0.053	-0.710	0.214	0.752	0.019	0.017	-0.033	0.628
	0.267	0.140	0.093	0.178	0.287	0.347	0.172	0.058	0.031	0.006	0.024	0.062
	0.575	0.043	#N/A	#N/A	0.661	0.038	#N/A	#N/A	0.675	0.038	#N/A	#N/A
	2.259	5.000	#N/A	#N/A	3.246	5.000	#N/A	#N/A	3.463	5.000	#N/A	#N/A
	0.013	0.009	#N/A	#N/A	0.014	0.007	#N/A	#N/A	0.015	0.007	#N/A	#N/A

Note: Numbers in bold font are the coefficients of determination